

SYNTHESIS OF STRAINED CARBON NANOTUBE FRAGMENTS AND A NEW
TOOL FOR MOLECULAR STRAIN ANALYSIS

by

CURTIS EUGENE COLWELL

A DISSERTATION

Presented to the Department of Chemistry and Biochemistry
and the Graduate School of the University of Oregon
in partial fulfillment of the requirements
for the degree of
Doctor of Philosophy

June 2020

DISSERTATION APPROVAL PAGE

Student: Curtis Eugene Colwell

Title: Synthesis of Strained Carbon Nanotube Fragments and a New Tool for Molecular Strain Analysis.

This dissertation has been accepted and approved in partial fulfillment of the requirements for the Doctor of Philosophy degree in the Department of Chemistry and Biochemistry by:

Michael M. Haley	Chairperson
Ramesh Jasti	Advisor
Michael Pluth	Core Member
Benjamín Alemán	Institutional Representative

and

Kate Mondloch	Interim Vice Provost and Dean of the Graduate School
---------------	--

Original approval signatures are on file with the University of Oregon Graduate School.

Degree awarded June 2020

© 2020 Curtis Eugene Colwell

DISSERTATION ABSTRACT

Curtis Eugene Colwell

Doctor of Philosophy

Department of Chemistry and Biochemistry

June 2020

Title: Synthesis of Strained Carbon Nanotube Fragments and a New Tool for Molecular Strain Analysis.

Cycloparaphenylene technology has advanced significantly in recent years. From the initial synthesis to today, laboratories around the world have made small improvements that have accumulated into an efficient synthesis of these strained nanohoops. This has allowed us to confirm theoretical hypotheses about the optoelectronic properties that are resultant from frontier molecular orbital symmetry. Furthermore, it facilitates cycloparaphenylene synthesis with functional groups that further expand the cycloparaphenylene π systems on the road to larger fragments of carbon nanotubes. These functionalized cycloparaphenylenes are useful not only for extending the π system, but also for polymer synthesis and further functional materials that exploit cycloparaphenylene properties. In addition to exploiting optoelectronic properties, the strain could also be exploited, however, it is not intuitive where strain is located in these molecules. A new computational technique is described that locates strain in strained macrocyclic molecules and helps to exploit strain productively. Together, these advances in cycloparaphenylene technology enable their wide and successful deployment. This dissertation includes previously published co-authored material.

CURRICULUM VITAE

NAME OF AUTHOR: Curtis Eugene Colwell

GRADUATE AND UNDERGRADUATE SCHOOLS ATTENDED:

University of Oregon, Eugene, Oregon
Memorial University of Newfoundland, St. John's, Newfoundland

DEGREES AWARDED:

Doctor of Philosophy, Chemistry, 2020, University of Oregon
Bachelor of Science with Honours, Chemistry, 2015, Memorial University of
Newfoundland

AREAS OF SPECIAL INTEREST:

Organic Chemistry
Computational Chemistry
Physical Organic Chemistry

PROFESSIONAL EXPERIENCE:

Research and Development Intern, Thermo Fisher Scientific, Eugene, Oregon,
2019

GRANTS, AWARDS, AND HONORS:

Special Opps Travel & Research Award, University of Oregon, 2019

Graduate Student Symposium Scholarship ACS New Orleans, University of
Florida, 2018

Undergraduate Student Research Award, Natural Sciences and Engineering
Research Council, 2015

Undergraduate Student Research Award, Natural Sciences and Engineering
Research Council, 2014

Research Internships in Science and Engineering, Deutscher Akademischer
Austauschdienst, 2014

Undergraduate Research Award, Memorial University of Newfoundland, 2013

PUBLICATIONS:

Colwell, C. E., [3.3.3]Cyclophanes as Pyrenophane Precursors. Honours Thesis, Memorial University of Newfoundland, St. John's, NFLD, 2015.

Golder, M. R.; Colwell, C. E.; Wong, B. M.; Zakharov, L. N.; Zhen, J.; Jasti, R. Iterative Reductive Aromatization/Ring-Closing Metathesis Strategy toward the Synthesis of Strained Aromatic Belts. *J. Am. Chem. Soc.* **2016**, *138* (20), 6577–6582.

Lovell, T. C.*; Colwell, C. E.*; Zakharov, L. N.; Jasti, R. Symmetry Breaking and the Turn-on Fluorescence of Small, Highly Strained Carbon Nanohoops. *Chem. Sci.* **2019**, *10*, 3786–3790.

Peters, G. M.; Grover, G.; Maust, R. L.; Colwell, C. E.; Bates, H.; Edgell, W. A.; Jasti, R.; Kertesz, M.; Tovar, J. D. Linear and Radial Conjugation in Extended π -Electron Systems. *J. Am. Chem. Soc.* **2020**, *142*, 2293–2300.

Colwell, C. E.; Price, T. W.; Stauch, T.; Jasti, R. Strain Visualization for Strained Macrocycles. *Chem. Sci.* **2020**, *11*, 3923–3930.

ACKNOWLEDGMENTS

First and foremost, I must thank my fiancé, Terri, for supporting me in this endeavor. There will never be a way to completely thank her for everything over these last five years not only as a life partner, but also an intelligent and determined scientific collaborator. I thank Prof. Ramesh Jasti for believing in me and welcoming a young bright-eyed and naïve student to Oregon and turning out a clear-eyed realist better equipped for the world. We have had many extremely inspirational late nights out on the town. His loose mentorship style allowed me to pursue numerous opportunities (not limited to being a biotech intern, financial analyst, and programmer) that were extremely formative for me. I am deeply grateful for my committee, Prof. Michael Haley, Prof. Michael Pluth, and Prof. Benjamín Alemán, that held my feet to the fire when necessary in order to develop me into a better scientist and communicator. A special thanks to Mike Haley for his enthusiasm for science and mentorship over the years. I would like to thank Prof. George Nazin and, again, Prof. Benjamín Alemán for allowing me to pursue an unconventional first year rotation process in which I toured through different labs learning skills for carbon nanotube growth and characterization.

A number of mentors were extremely helpful along the way including, but not limited to Prof. Matthew Golder, Dr. Evan Darzi, Dr. Penghao Li, Dr. Brittany White, Dr. Jeff Van Raden, Dr. Gabe Rudebusch, Dr. Ben Taber, Rudy Resch, and David Miller. Numerous students helped make this thesis possible, namely Alex Edgell, Tara Clayton, Thaís de Faria, and Tavis Price. Dr. Tobias Schaub was a crucial collaborator and mentor in the laboratory who additionally, along with Lisa, was an exceptional friend. I would like to thank all Jasti lab members past and present for their hard work and dedication.

Additionally, I must thank my collaborators Prof. Tim Stauch, Prof. Miklos Kertesz, Prof. J. D. Tovar, Dr. Garvin Peters, and Prof. J.-F. Morin for their work and support. There are a number of people that are crucial to the research facilities at University of Oregon. Most notably NMR specialists Dr. Mike Strain and Dr. Nanette Jarenwattananon, crystallography expert Dr. Lev Zakharov, stores clerk Jennifer Jess and everyone down at CAMCOR and the chemistry office, in particular Janet Macha. During my graduate career I had the opportunity to intern at Thermo Fisher Scientific for which I must thank Stacey York.

Prior to arriving at the University of Oregon, a number of important figures shaped my chemistry career, namely Prof. Graham Bodwell, Prof. Max von Delius, Prof. Yuming Zhao, and Mrs. Atkinson. Finally, I thank my family for supporting me with the non-scientific challenges that come with obtaining a graduate degree. In particular, my brother, Ian Colwell, for making StrainViz possible by writing parts of some scripts used for automating computations as well as software related technical and general support. Along this same vein I would like to thank the support team at Gaussian that has enthusiastically answered endless questions about their software.

Science is a worldwide team effort that requires the dedication of thousands of people over hundreds of years and I am honored to stand on the shoulders of giants in order to contribute this work.

Ramesh, this one's for you

TABLE OF CONTENTS

Chapter	Page
ADVANCING CYCLOPARAPHENYLENE SYNTHESIS	1
I.1. Background	1
I.2. Initial syntheses of cycloparaphenylenes	1
I.3. Syntheses of smaller cycloparaphenylenes	4
I.4. Advanced methodology for cycloparaphenylene synthesis	5
I.5. Scope of functionality allowed.....	7
I.6. Literature examples exploiting this new methodology	8
I.7. Co-authored content	10
I.8. Bridge to Chapter 2	11
TURNING ON FLUORESCENCE IN SMALL CYCLOPARAPHENYLENES	12
II.1. Background	12
II.2. Synthesis of <i>meta</i> -cycloparaphenylenes	14
II.3. Structural features	17
II.4. Photophysical properties	19
II.5. Conclusions	22
II.6. Co-authored content.....	23
II.7. Bridge to Chapter III	23
STRAIN VISUALIZATION FOR STRAINED MACROCYCLES.....	24
III.1. Introduction.....	24
III.2. Computational Methods.....	27
III.3. Results & Discussion.....	33

Chapter	Page
III.3.1. Fragments accurately represent the molecule.....	33
III.3.2. Energies are expectedly similar to previous results.	34
III.3.3. Local strain energy relates to reactivity.....	37
III.4. Unique strain analysis of macrocycles from the literature.	41
III.5. Conclusions.....	45
III.6. Co-authored content.....	45
III.7. Bridge to Chapter IV	46
RING CLOSING METATHESIS FOR CONVERSION OF NANOHOOPS INTO	
NANOBELTS.....	47
IV.1. Background.....	47
IV.2. Syntheses of partial belt cycloparaphenylenes	49
IV.3. Properties of partial belt cycloparaphenylenes.....	53
IV.4. Towards nanobelt synthesis using ring closing metathesis	57
IV.5. Chlorinated cycloparaphenylenes.....	59
IV.6. Co-authored content	61
IV.7. Bridge to Chapter V.....	62
REDUCING REQUIRED FUNCTIONALITY FOR NANOHOOP CONVERSION	
INTO A NANOBELT.....	63
V.1. Background.....	63
V.2. Alkyne cyclization	64
V.3. Highly alkyne functionalized intermediates	67
V.4. Cyclodehydrochlorination	70

Chapter	Page
V.5. Zipping up chlorinated oligophenylenes onto cycloparaphenylenes	71
V.6. Future outlook.....	73
V.7. Co-authored content.....	74
V.8. Bridge to Chapter VI.....	74
APPLICATIONS OF FUNCTIONALIZED CYCLOPARAPHENYLENES	75
VI.1. Background.....	75
VI.2. Producing conjugated polymers from cycloparaphenylenes	75
VI.3. Optoelectronic properties of cycloparaphenylene conjugated polymers.....	76
VI.4. Co-authored content	79
VI.5. Bridge to Conclusion	80
CONCLUSION.....	81
SUPPLEMENTARY INFORMATION FOR CHAPTER II.....	82
A.1. Experimental Details.....	82
A.2. Photophysical Characterization	119
A.3. Electrochemical Analysis	122
A.4. HOMO and LUMO Level Calculations.....	127
A.5. Calculated Absorption Spectra	127
A.6. Inherent Strain Calculation	134
A.7. X-ray Crystallography.	135
SUPPLEMENTARY INFORMATION FOR CHAPTER III	137
B.1. Experimental details.....	137
B.2. Comments on calculations	138

Chapter	Page
B.3. Instructions for running StrainViz	139
B.4. Specific Example	141
B.5. Fragments used for strain calculations.....	143
B.5.1. Fragments use for Figure III.4	143
B.5.2. Fragments used for Figure III.5	147
B.5.3. Fragments used for Figure III.6	151
B.5.4. Fragments used for Figure III.7	152
B.5.5. Fragments used for Figure III.8	152
B.5.6. Fragments used for Figure III.9	154
B.5.7. Fragments used for Figure III.10	155
SUPPLEMENTARY INFORMATION FOR CHAPTER IV	156
C.1. Experimental Details:.....	156
C.2. X-ray Crystallography.....	180
SUPPLEMENTARY INFORMATION FOR CHAPTER V	181
D.1. Experimental Details.....	181
D.2. X-ray Crystallography.	215
REFERENCES CITED.....	216

LIST OF FIGURES

Figure	Page
I.1. Initial syntheses of cycloparaphenylenes	2
I.2. [12]- to [5]CPP UV-vis absorption and emission	3
I.3. Syntheses of cycloparaphenylenes from common building blocks.	5
I.4. Triethylsilyl groups in cycloparaphenylene synthesis.....	7
II.1. Summary of cycloparaphenylenes as sub-units of carbon nanotubes and their orbital symmetry.....	13
II.2. Crystal structure of <i>m</i> [6]CPP and calculated strain of [<i>n</i>]CPPs and <i>m</i> [<i>n</i>]CPPs	18
II.3. Absorbance and emission spectra of <i>m</i> [<i>n</i>]CPPs, orbital symmetry comparison of [5]CPP and <i>m</i> [5]CPP, as well as the absorbance, extinction coefficient, emission, and quantum yield of <i>m</i> [5]- to <i>m</i> [8]-, <i>m</i> [10]-, and <i>m</i> [12]CPP	20
III.1. Comparison of typical strain determining calculations and StrainViz	26
III.2. An ideal experiment for computational strain determination and the approximation of this by StrainViz	29
III.3. Workflow for strain analysis.....	30
III.4. Strain analysis using fragments of [8]CPP having 2-7 phenylenes	35
III.5. Literature examples of strain energy determinations compared to StrainViz analysis.....	38
III.6. Torsional angles and total strain of [6]CPP and <i>m</i> [6]CPP	39
III.7. Strain release during bromination of [6]CPP	40

Figure	Page
III.8. Möbius molecules have more strain due to an internal twist when compared to a non-Möbius belt	42
III.9. Strain energy present in Yamago's nanoball	43
III.10. Strain energy in copper-free click reagents	44
IV.1. Templates for carbon nanotube growth	48
IV.2. Synthesis of carbon nanobelts by the Itami and Miao laboratories	49
IV.3. Deplanarization of the belt fragments in partial belt nanohoops	54
IV.4. UV-vis spectra of partial belt nanohoops IV.19 , IV.20 , IV.25 , and [9]CPP	55
IV.5. Strain map of molecules involved in synthesis of partial belt IV.25	58
IV.6. Size of R group dictates stereochemistry of the addition reaction	59
V.1. π system extending reactions and their ratio of minimum functional groups to phenylenes	63
V.2. Van der Waals radius models of desired macrocycles from Scheme V.4	69
V.3. Concept for zipping chlorinated oligophenylenes onto cycloparaphenylenes	72
VI.1. Reactions available to terminal alkyne	76
VI.2. UV-vis spectra of cycloparaphenylene polymers relative to poly(phenylene ethynylene) polymers and cycloparaphenylenes	77
VI.3. Frontier molecular orbitals for cycloparaphenylene oligomer	78
VI.4. Frontier molecular orbital levels of [8]CPP , octa- <i>p</i> -phenylene, and octa(<i>p</i> -phenylene ethylene)	79
A.1. Extinction coefficient determination of <i>m</i>[5]CPP	119
A.2. Extinction coefficient determination of <i>m</i>[6]CPP	119

Figure	Page
A.3. Extinction coefficient determination of <i>m</i>[7]CPP	120
A.4. Extinction coefficient determination of <i>m</i>[8]CPP	120
A.5. Extinction coefficient determination of <i>m</i>[10]CPP	121
A.6. Extinction coefficient determination of <i>m</i>[12]CPP	121
A.7. <i>m</i>[5]CPP cyclic voltammetry	123
A.8. <i>m</i>[6]CPP cyclic voltammetry	124
A.9. <i>m</i>[7]CPP cyclic voltammetry	124
A.10. <i>m</i>[8]CPP cyclic voltammetry	125
A.11. <i>m</i>[10]CPP cyclic voltammetry	125
A.12. <i>m</i>[12]CPP cyclic voltammetry	126
A.13. Comparison of HOMO and LUMO energy levels of [<i>n</i>]CPPs and <i>m</i>[<i>n</i>]CPPs	127
A.14. <i>m</i>[5]CPP Calculated and experimental absorption	128
A.15. <i>m</i>[6]CPP Calculated and experimental absorption	129
A.16. <i>m</i>[7]CPP Calculated and experimental absorption	130
A.17. <i>m</i>[8]CPP Calculated and experimental absorption	131
A.18. <i>m</i>[10]CPP Calculated and experimental absorption	132
A.19. <i>m</i>[12]CPP Calculated and experimental absorption	133
A.20. ORTEP representation of <i>m</i>[6]CPP	136
B.1. Workflow diagram for StrainViz method.	139
C.1. ORTEP representation of C.11	180
C.2. ORTEP representation of partially aromatized IV.29	180
D.1. ORTEP representation of <i>trans</i> isomer of D.17	215

LIST OF TABLES

Table	Page
I.1. Functional groups and their tolerance to aromatization conditions.....	9
III.1. Reported strain energies of [12]CPP	35
V.1. Catalysts for alkyne cyclization.	65
A.1. Triplicate quantum yield data, excited at the absorbance maxima.	121
A.2. Triplicate quantum yield data, excited at HOMO→LUMO transition.	122
A.3. HOMO→LUMO absorbance maxima and extinction coefficients.	122
A.4. Fluorescence lifetimes and calculated decay rates.....	122
A.5. Oxidation potentials of <i>m</i> [<i>n</i>]CPPs.....	123
A.6. First oxidation peak of <i>m</i> [<i>n</i>]CPPs.	123
A.7. Calculated HOMO→LUMO absorption for <i>m</i> [<i>n</i>]CPPs.....	127
A.8. Single point energies of compounds used in homodesmotic reactions and calculated strain.....	134
A.9. Calculated strain energy in <i>m</i> [<i>n</i>]CPPs, <i>ipso</i> carbon deviation, and dihedral angle.....	134
B.1. Fragments used for Figure III.4. Fragment size 2.	144
B.2. Fragments used for Figure III.4. Fragment size 3.	144
B.3. Fragments used for Figure III.4. Fragment size 4.	145
B.4. Fragments used for Figure III.4. Fragment size 5.	145
B.5. Fragments used for Figure III.4. Fragment size 6.	146
B.6. Fragments used for Figure III.4. Fragment size 7.	146
B.7. Fragments used for [10]CPP	147

Table	Page
B.8. Fragments used for [9]CPP	148
B.9. Fragments used for [8]CPP	149
B.10. Fragments used for [7]CPP	149
B.11. Fragments used for [6]CPP	150
B.12. Fragments used for [6]cyclophenacene.....	150
B.13. Fragments used for [2.2]paracyclophane.....	151
B.14. Fragments used for [2](6,1)naphthaleno[1]paracyclophane.....	151
B.15. Fragments used for <i>m</i> [6]CPP.....	151
B.16. Fragments used for dibromo[6]CPP.....	152
B.17. Fragments used for tetrabromo[6]CPP.....	152
B.18. Fragments used for the Tanaka belt.....	152
B.19. Fragments used for the Möbius Tanaka belt.....	153
B.20. Fragments used for the Vögtle belt.....	153
B.21. Fragments used for the Möbius Vögtle belt.....	154
B.22. Fragments used for the Yamago ball.....	154
B.23. Fragments used for the Yamago ball panel.....	154
B.24. Fragments used for cyclooctyne.....	155
B.25. Fragments used for <i>trans</i> -cyclooctene.....	155
B.26. Fragments used for <i>trans</i> -bicyclo[6.1.0]nonene.....	155

LIST OF SCHEMES

Scheme	Page
I.1. Facile syntheses of advanced building blocks	9
II.1. Building block synthetic approach to <i>m</i> [6]-, <i>m</i> [7]-, <i>m</i> [8]-, <i>m</i> [10]- and <i>m</i> [12]CPP. 16	16
II.2. Modified synthetic strategy for <i>m</i> [5]CPP.....	17
III.1. Bromination of <i>m</i> [6]CPP	39
IV.1. Synthesis of CPP precursors having vinyl functional groups.....	50
IV.2. Synthesis of vinyl functionalized CPP precursor macrocycles	51
IV.3. Synthesis of partial nanobelts	51
IV.4. Synthesis of an extremely strained partial nanobelt	53
IV.5. Strain energy changes during aromatization and ring closing metathesis.....	56
IV.6. Incorporation of chlorinated phenylenes and cyclohexadienes into CPP synthesis	61
V.1. Synthesis of CPP V.4 and alkyne cyclization to partial nanobelt V.5	65
V.2. Synthesis of CPP V.8 and alkyne cyclization to partial nanobelt V.9	66
V.3. Synthesis of V.14 and alkyne cyclization to partial nanobelt V.15	67
V.4. Macrocyclization attempts with highly functionalized precursors	69
V.5. 2-chlorophenylene functionalized CPP V.20 for testing cyclodehydrochlorination conditions to produce V.21	71
V.6. Planar molecule for testing multiple sequential cyclodehydrochlorination reactions	73
V.7. Future possible carbon nanobelt formation strategies.....	74
VI.1. Synthesis of polymers with cyclic and linear conjugation pathways	77

CHAPTER I

ADVANCING CYCLOPARAPHENYLENE SYNTHESIS

I.1. Background

Cycloparaphenylenes are becoming widely recognized for their unique properties as rare examples of perfectly circular, relatively stable, highly strained molecules¹ with high quantum yield,^{2,3} high absorption coefficients,³ fullerene hosting ability,^{4,5} and desirable mechanical properties.⁶⁻⁸ Study of these properties would not have been possible if not for efficient and scalable methods for their preparation. Since 2008, significant advancements have not only allowed larger quantities of cycloparaphenylenes to be produced, but also cycloparaphenylenes with diverse functional groups at any position on the macrocycle. These advancements have not been fully addressed in the publications for which they were used, therefore, this thesis introductory chapter will chronicle these seemingly small changes in synthetic methodology from original syntheses to today's hybrid methodology.

I.2. Initial syntheses of cycloparaphenylenes

The very first synthesis of a cycloparaphenylene was by Prof. Ramesh Jasti in 2008.⁹ This elegant synthesis produced cycloparaphenylenes in only four steps. (Figure I.1a) First, *cis*-diarylcyclohexadiene **I.1** was prepared from lithiation and addition of 1,4-diodobenzene to benzoquinone followed by methylation of the resulting alkoxide groups. This is then converted from the diiodide to the diboronate to serve as a Suzuki coupling partner. Suzuki coupling yields a mixture of macrocycles such as **I.2** that were separated at this stage. These macrocycles are then reduced to convert the dimethoxycyclohexadienes to phenylenes forming cycloparaphenylenes for the first time.

Using this synthesis [18]-, [12]-, and, [9]CPP were synthesized. Soon after, in 2009, the Itami laboratory published methods for making [12]CPP in a selective manner.¹⁰ (Figure I.1b) This synthesis used oxidation instead of reduction for converting macrocycles such as I.5 into cycloparaphenylenes and as a result is limited to [9]CPP and above.

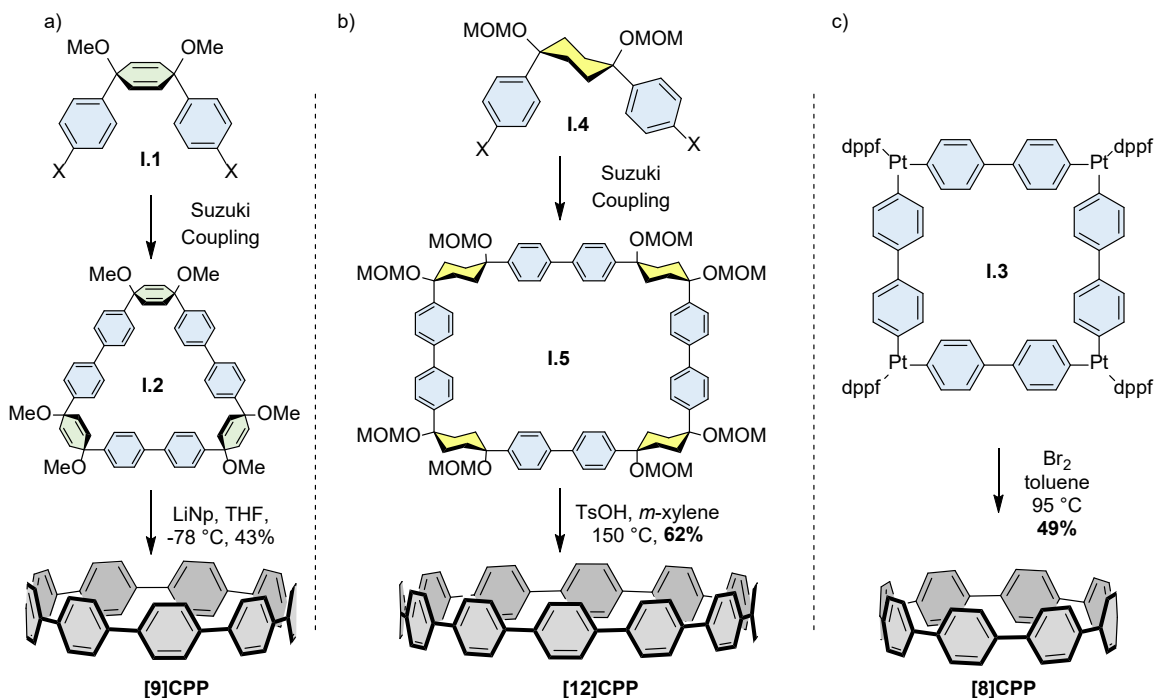


Figure I.1. Initial syntheses of cycloparaphenylenes. a) The initial synthesis by Jasti and Bertozzi used Suzuki macrocyclization followed by reductive aromatization. b) Itami synthesized [12]CPP selectively using Suzuki coupling and oxidative aromatization. c) Aryl-platinum macrocycle reductive aromatization by Yamago yielded [8]CPP.

From this launching point, the first ever cycloparaphenylenes were able to be studied. An initial remark is the decrease in fluorescence wavelength with increasing size contrary to linear conjugated molecules. Already with only three data points, cycloparaphenylenes were showing interesting properties.⁹ Adding more data points clarifies the picture. In 2010, a completely novel cycloparaphenylene preparation method was discovered in the Yamago laboratory.¹¹ First, platinum cornered macrocycles were

prepared via cross metalation of 4,4'-bis(trimethyltin)biphenyl. These macrocycles were converted directly to cycloparaphenylenes by reductive elimination. This allowed [8]CPP preparation for the first time. (Figure 1c) However, no smaller cycloparaphenylene could be prepared via this method. By mixing terphenyl with biphenyl macrocycle precursors, it was possible to make a statistical mixture of all cycloparaphenylenes from 8 to 12 phenylenes. This allowed for a more fine analysis of the structure/property relationship of the photophysical properties.¹² (Figure I.2)

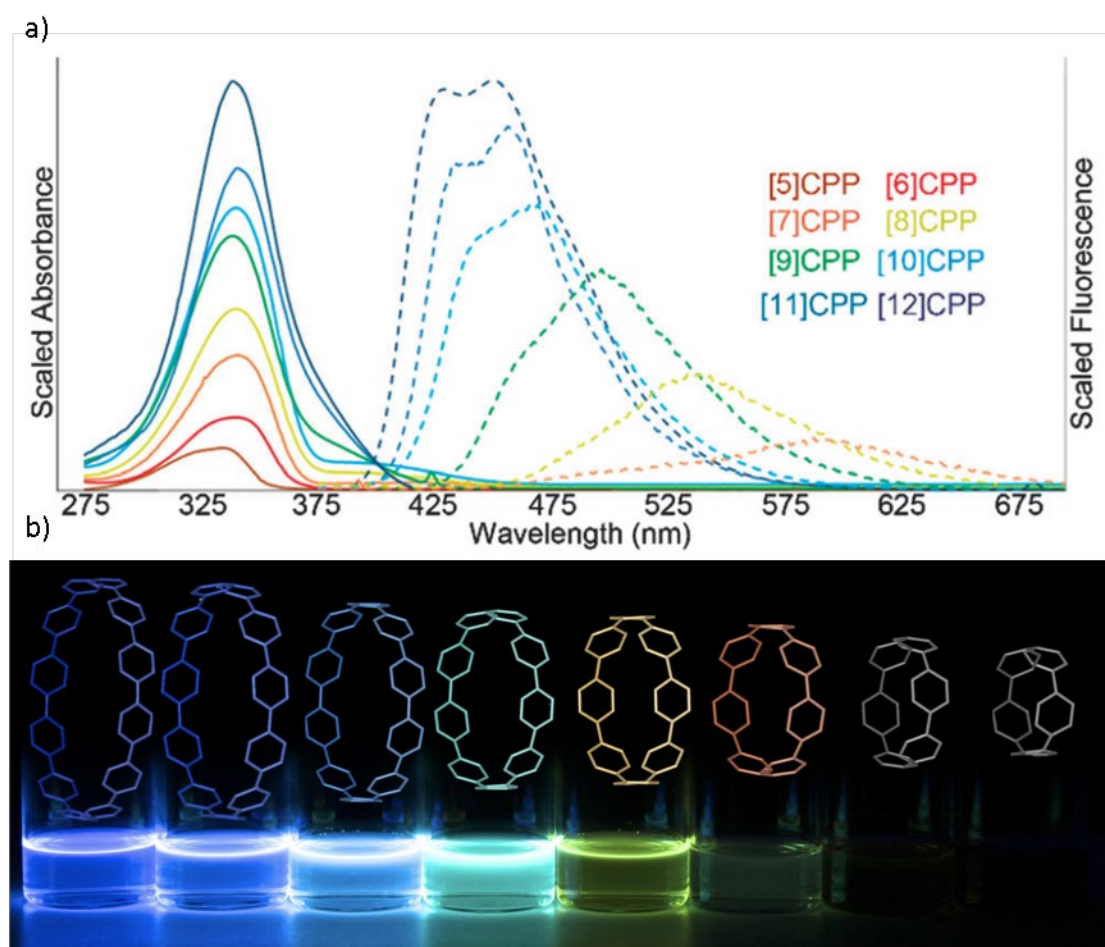


Figure I.2. [12]- to [5]CPP UV-vis absorption (solid) and emission (dotted) as spectra (a) and visual (b)

I.3. Syntheses of smaller cycloparaphenylenes

As with any synthesis, a selective synthesis intended to synthesize one cycloparaphenylene size at a time is most efficient. The newly formed Jasti laboratory modified the original cycloparaphenylene synthesis to synthesize 1,4-diarylcyclohexadienes that are no longer symmetric such as **I.6**. This allowed specific synthesis of [12]CPP down to [8]CPP and allowed reasonable amounts of these molecules to be prepared using sodium naphthalenide reduction as the final step.¹³ More importantly, it allowed the synthesis of [7]CPP for the first time using intermediate **I.7**.¹⁴ Shortly after, by adding a new building block to the synthetic arsenal shown in Figure I.3 having two cyclohexadienes separated by a single phenylene, **I.8**, [6]CPP was synthesized.¹⁵ Upon synthesis of [6]CPP a new phenomenon was discovered, this cycloparaphenylene was not fluorescent. (Figure I.2) Centrosymmetry of the molecule had finally taken over. All cycloparaphenylenes have a Laporte forbidden HOMO→LUMO transition, but not until [6]CPP does this cause the LUMO→HOMO transition to completely cease.²

Using the same building block **I.8** allowing the synthesis of [6]CPP, [10]CPP could now be easily prepared by Suzuki coupling to **I.9**. This is similar to the original cycloparaphenylene synthesis, but with more specificity.⁵ (Figure I.3) In the original cycloparaphenylene synthesis, the preparation of [9]CPP was quite unusual. If only Suzuki couplings were taking place, the macrocycle leading to [9]CPP is not possible. However, if an oxidant is present in the reaction, boronate homocoupling leads to a six ring building block akin to **I.7** *in situ* that allows [9]CPP preparation. A similar side product appeared during [10]CPP preparation. Boronate homocoupling of **I.9** yields a

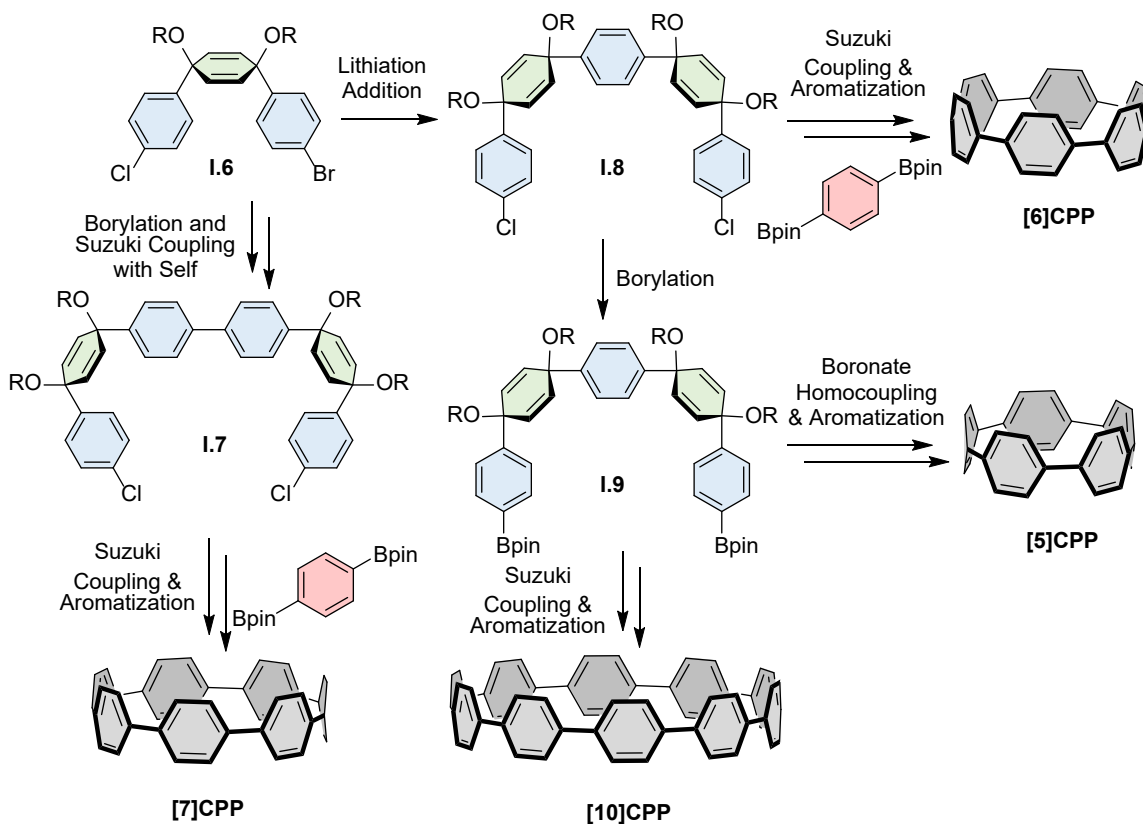


Figure 1.3. Syntheses of cycloparaphenylenes from common building blocks.

macrocycle leading to **[5]CPP**. This macrocycle, does not fully reduce when subjected to alkali naphthalenide. Fortunately, the partially reduced macrocycle is converted into **[5]CPP** via elimination with LDA.¹⁶ To date, no smaller cycloparaphenylene exists.

1.4. Advanced methodology for cycloparaphenylene synthesis

The synthesis of **[5]CPP** highlighted a problem with sodium naphthalenide reduction. Although extremely efficient for most bare cycloparaphenylenes, these extreme conditions may result in undesired outcomes. More importantly, this final step limits functionality incorporation in cycloparaphenylene synthesis. Using alkali naphthalenide reduction, no delicate functional groups survive the aromatization step. Only aryl,¹⁷⁻¹⁹ alkyl, and pyridyl^{20,21} functional groups could be brought through, although with little opportunity for further reactivity. This is highlighted in an attempt to

bring ester functionality through by the Tanaka laboratory that required careful optimization for maximum yield of just 24%.²² Alternatively, the Wang group developed a Diels-Alder based functionalization method that ultimately relies on oxidative aromatization with DDQ and produces ester functionalized cycloparaphenylenes in good yield.²³ In similar timing to the Jasti laboratory, the Yamago laboratory prepared **[5]CPP** using Yamamoto homocoupling instead of boronate homocoupling.²⁴ Using hydroxy instead of methoxy functionalized macrocycles, far milder tin reduction was used instead of alkali naphthalenide.²⁵

In addition to being a milder aromatization method, the synthetic sequence from the Yamago laboratory uses triethylsilyl protecting groups. We later discovered that these could direct lithiate addition to a cyclohexadienone. It was previously known that an alkoxide enhanced stereoselectivity (*cis/trans*, >19:1) over other functional groups such as a methoxy group (*cis/trans*, 3:1),²⁶ however, a triethylsiloxy group effectively blocks one face of the cyclohexadienone resulting in exclusively the *cis* diastereomer. (Figure I.4a) This allows production of the five ring piece quickly from triethylsilyl protected ketones and 1,4-dibromobenzene. Primarily, triethylsilyl protection increases cycloparaphenylene synthesis convergence. Take, for example, the construction of common cycloparaphenylene building block **I.8**. (Figure I.4b) Originally, **I.6** is lithiated and added into benzoquinone monomethyl ketal followed by acetal deprotection. Then, to ketone **I.12** is added another lithiate to yield **I.8**. However, using triethylsilyl protection, a triethylsilyl protected ketone **I.11** is directly added to the original lithiate of **I.6**. This increases the convergence and therefore scalability and efficiency of cycloparaphenylene syntheses.

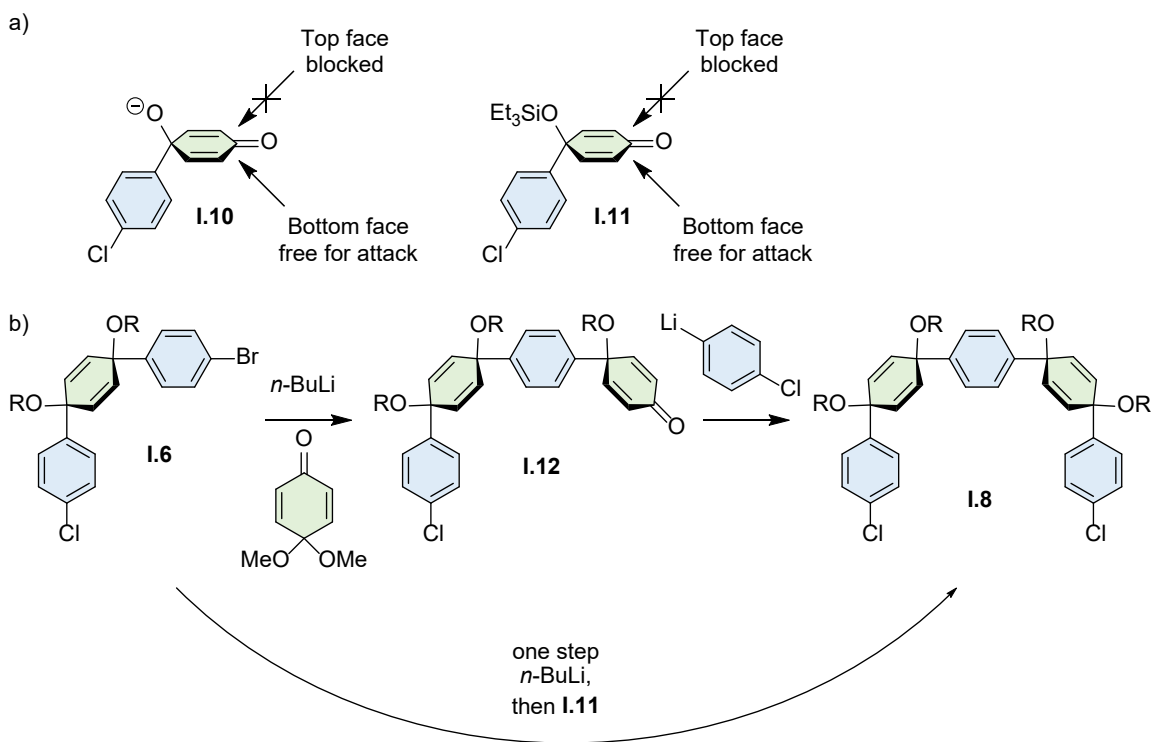


Figure I.4. Triethylsilyl groups in cycloparaphenylene synthesis. a) Triethylsilyl protecting groups effectively block one face of the ketone from lithiate addition. b) Triethylsilyl protected building blocks allow for more convergent syntheses when compared to previous methods.

I.5. Scope of functionality allowed

Not only could all cycloparaphenylenes be prepared using tin reduction, but now the general synthetic methods of the Jasti laboratory could produce functionalized cycloparaphenylenes. In the synthesis of partial belt nanohoops, two cycloparaphenylenes are prepared using previous reductive aromatization methods and one using the newer methods combining Yamago's tin reduction and the use of triethylsilyl protecting groups for stereocontrol.²⁷ The previous synthesis requires ring closing metathesis to occur prior to reductive aromatization to maintain the functional groups required for building the partial belt segment. However, using tin reduction, an alkene functionalized

cycloparaphenylene is synthesized and ring closing metathesis occurs after. This small change both preempts stereochemical issues²⁶ and allows the production of usefully, in this case alkene, functionalized cycloparaphenylenes.

Together, triethylsilyl protection and mild reductive aromatization methods were significant advancements in synthetic methodology for cycloparaphenylene synthesis. From this advancement, syntheses of cycloparaphenylenes having alcohols,²⁸ fluorines,^{29,30} azides,²⁸ and alkynes³¹ were made possible in addition to most work in this thesis. (Table I.1) Of the functional groups used, some have interesting anecdotes surrounding the aromatization step. For example, fluorinated cycloparaphenylenes were conceived of long before their first synthesis. However, aromatization using alkali naphthalenide stripped off the fluorine present and yielded an unfunctionalized cycloparaphenylene. Additionally, alkyne incorporated cycloparaphenylenes were synthesized using both alkali naphthalenide and tin reduction methods, however, when alkali naphthalenide was used, a mixture of the alkyne, alkene, and alkyl cycloparaphenylenes were produced.³¹ Another report from the Moore laboratory, however, does produce a cycloparaphenylene with three internal alkynes with sodium naphthalenide in high yields.³²

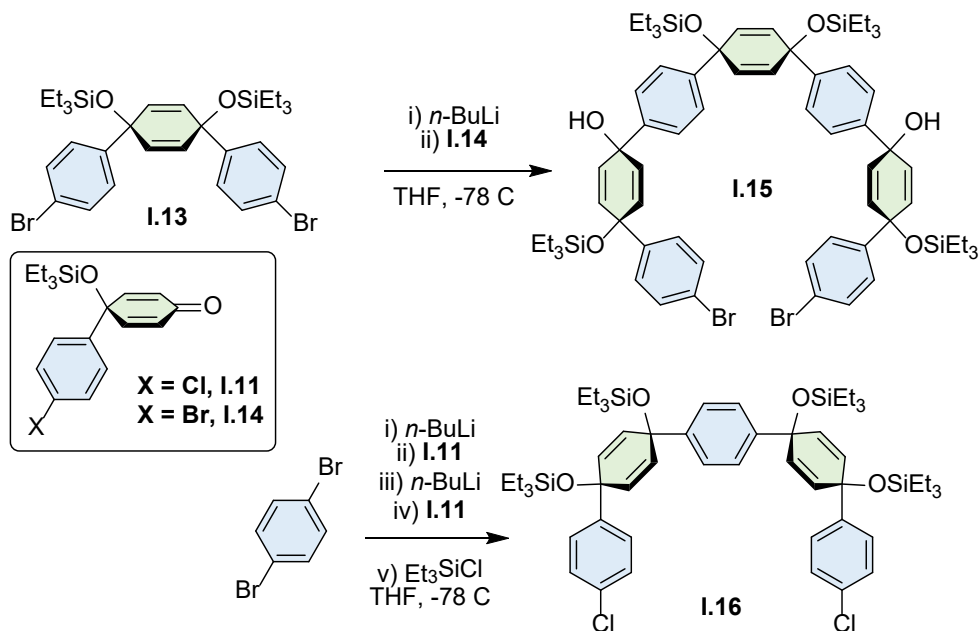
I.6. Literature examples exploiting this new methodology

The Jasti laboratory has been exploiting this methodology since 2015 to expedite cycloparaphenylene synthesis. The first example is **I.15** preparation for a perylene-containing cycloparaphenylene synthesis.³³ **I.13** was lithiated twice and added into two equivalents of **I.14**. This one crucial step makes a perylene-containing cycloparaphenylene synthesis far easier than ever before. The next impactful building

Functional Group	Alkali Naphthalenide	Tin Reduction
Fluorine	Removes Fluorine	Tolerated
Alkyne	May reduce alkyne	Tolerated
Azide	Unknown, likely reduced	Tolerated
Alcohols	Unknown	Tolerated
Alkene	Unknown, likely reduced	Tolerated

Table I.1. Functional groups and their tolerance to aromatization conditions.

block to be developed was **I.16** synthesized with allyl functionality not depicted for simplicity in Scheme I.1.²⁷ Two equivalents of **I.11** are added to a single dibromobenzene. This produces **I.16** quickly and in good yield. These are two excellent examples producing fundamental cycloparaphenylene building blocks.



Scheme I.1. Facile syntheses of advanced building blocks using the advantage of a triethylsilyl protecting and directing group.

The additional benefit of this new methodology is functional group tolerance as mentioned previously. Tolerance of alkene, alkyne, and 2-chlorophenyl groups allows new partial belt synthesis mentioned later in this thesis. Furthermore, toleration of hydroxymethyl groups allowed the first ever biocompatible cycloparaphenylene synthesis.²⁸ Incorporating an alkyne into the cycloparaphenylene backbone allowed the productive exploitation of the inherent strain.³¹ Fluorinated cycloparaphenylenes are the first examples of aligned cycloparaphenylene tubes.²⁹ We continue to create new highly functional cycloparaphenylenes with various utilities all made possible by this leap in methodology.^{34,35}

I.7. Co-authored content

This thesis contains co-authored material that was published in peer reviewed journals. The work in Chapter 2 was co-authored with Terri Lovell, Dr. Lev Zakharov, and Prof. Ramesh Jasti and published under the title “Symmetry breaking and the turn-on fluorescence of small, highly strained carbon nanohoops” in *Chemical Science*.³⁶ The work in Chapter 3 was co-authored with Tavis Price, Prof. Tim Stauch, and Prof. Ramesh Jasti and published under the title of “Strain Visualization for Strained Macrocycles” in *Chemical Science*.³⁷ The ring-closing metathesis work in Chapter 4 was co-authored with Prof. Matthew Golder, Prof. Bryan Wong, Dr. Lev Zakharov, Jingxin Zhen, and Prof. Ramesh Jasti and published under the title “Iterative Reductive Aromatization/Ring-Closing Metathesis Strategy toward the Synthesis of Strained Aromatic Belts” in the *Journal of the American Chemical Society*.²⁷ The polymer research in Chapter 5 was co-authored with Garvin Peters, Girishma Grover, Ruth Maust, Haley Bates, William Edgell, Prof. Ramesh Jasti, Prof. Miklos Kertesz, and Prof. John D. Tovar and published under

the title “Linear and Radial Conjugation in Extended pi-Electron Systems” in the *Journal of the American Chemical Society*.³⁸

I.8. Bridge to Chapter 2

This advanced methodology has been a key driver for quickly accessing new molecules in this field. It was indispensable for all work performed for this thesis. In the next chapter, it was used to quickly prepare a series of cycloparaphenylenes to test a hypothesis concerning their optoelectronic properties.

CHAPTER II

TURNING ON FLUORESCENCE IN SMALL CYCLOPARAPHENYLENES

II.1. Background

Carbon nanohoops possess size dependent optical properties that stand in stark contrast to related materials such as acyclic oligophenylenes or even semiconducting quantum dots. Whereas most materials show red-shifting fluorescence emission with increasing size, the cycloparaphenylenes have red-shifting fluorescence with decreasing size. For example, **[12]CPP** emits at 450 nm whereas **[8]CPP** emits at 533 nm.³⁹ Concomitant with this red-shifting fluorescence is a decreasing quantum yield as nanohoop size decreases. For example, **[12]CPP** has a quantum yield of 81% whereas the smallest cycloparaphenylenes, **[5]-** and **[6]CPP**, are completely non-emissive.⁴⁰⁻⁴² Another unique feature of cycloparaphenylene optics is that the major absorption is diameter independent with a maximum at 340 nm for all cycloparaphenylenes.^{43,44}

These unique photophysical properties spurred investigation into theoretical explanations of these phenomena. The absorption phenomena is explained by Yamago and co-workers⁴³ wherein the major absorption is dominated by transitions similar in energy (i.e. HOMO→LUMO+1 or LUMO+2 and HOMO-1 or HOMO-2→LUMO) amongst all sized cycloparaphenylenes and the HOMO→LUMO transition is symmetry forbidden. Similarly, detailed theoretical work by Tretiak and co-workers suggested that cycloparaphenylenes with more than seven phenyl rings are emissive due to exciton localization in an S_1' excited state in which the centrosymmetry is broken, seen in Figure II.1b for **[12]CPP**.²

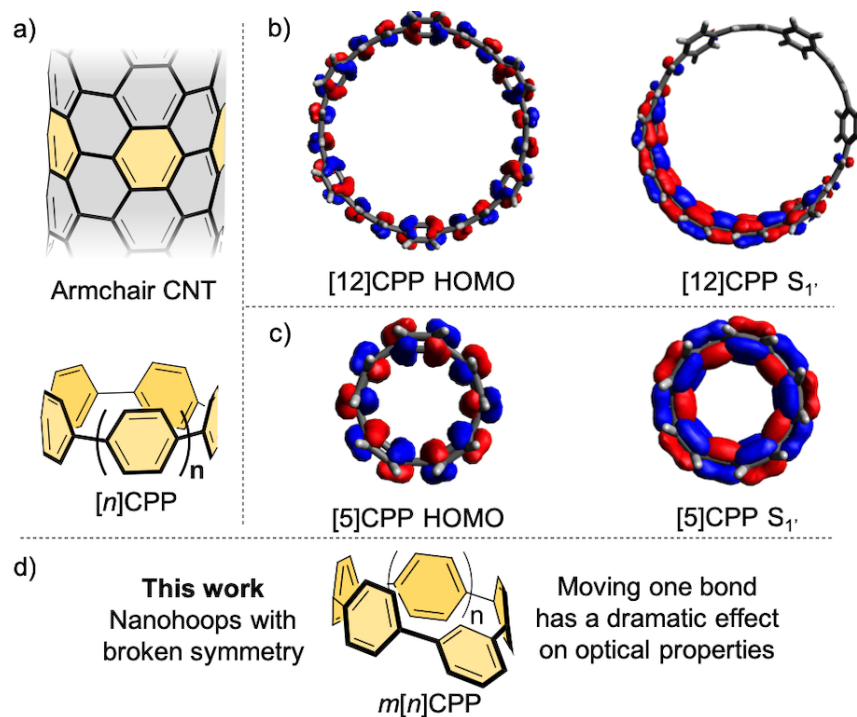


Figure II.1. a) Structure of an armchair carbon nanotube and its relation to $[n]$ CPPs; b) HOMO (left) and excited state (right) $S_{1'}$ orbitals of $[12]$ CPP and c) HOMO (left) and excited state (right) $S_{1'}$ orbitals of $[5]$ CPP. Orbitals have been calculated using CAM-B3LYP/STO-3G level of theory. d) $m[n]$ CPPs with broken symmetry in this work.

Since this localization and symmetry breaking does not happen in the smaller sizes (Figure II.1c), these structures become non-emissive as the transition is forbidden by symmetry. These works suggest that disrupting the centrosymmetric nature of the molecular orbitals is a strategy that could be employed to alter the photophysical properties of the nanohoops. This basic concept was theoretically explored by Tretiak wherein they postulated that inserting different acenes into the cycloparaphenylene backbone would break the excited state symmetry.⁴⁵

Inspired by these works, we report the synthesis, characterization, and analysis of a new class of carbon nanohoops wherein one phenyl ring is linked in the *meta*-position

(Figure II.1d). This minor change in linkage, or “kink”, acts to break nanohoop conjugation, therefore altering the molecular orbital symmetry without significantly decreasing the inherent strain. The *meta*-nanohoops, termed *meta*[*n*]CPPs (*m*[*n*]CPPs), are compared to the [*n*]CPP series to further understand what effect this small structural perturbation has on the photophysical properties and to provide experimental evidence corroborating Tretiak’s theoretical prediction.² Additionally, tuning the photophysical properties of this growing class of structures is critical for exploiting them as novel scaffolds in biological imaging,⁴⁶ supramolecular sensing^{47–49} as well as novel optoelectronic materials.^{50,51} Herein, we report the general synthesis of a *m*[*n*]CPPs series, carbon nanohoops with broken symmetry, and a detailed study of their photophysical properties.

II.2. Synthesis of *meta*-cycloparaphenylenes

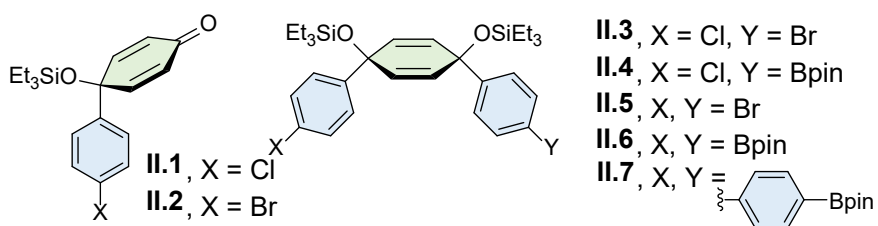
The preparation of these fully conjugated and highly bent macrocycles is a synthetic challenge due to the large intrinsic strain in the target molecules. The most strained target compound, *m*[5]CPP, is calculated to have 102 kcal/mol of strain (*vide infra*). Fortunately, methods for [*n*]CPP synthesis can be adapted, wherein the strain is incorporated using cyclohexadienes as curved masked phenylenes. Building blocks **II.1–7** are easily accessed on gram scale using previously developed methods (Scheme 1).^{52,53} By combining these building blocks through selective lithiation followed by diastereoselective addition, or Suzuki Miyaura cross coupling, advanced intermediates **II.8–12** were readily prepared (see Appendix A for more detail). Following this, relatively unstrained macrocycles **II.13–17** were prepared via Suzuki-Miyaura cross coupling of intermediates **II.8–12** and 1,3-dibromobenzene or 1,3-benzenediboronic acid

bis(pinacol) ester in moderate yields ranging from 10–45%. The triethylsilyl protecting groups were removed and the cyclohexadienes were unmasked via reductive aromatization to yield *m*[6]-, *m*[7]-, *m*[8]-, *m*[10]-, and *m*[12]CPP in fairly good yields.

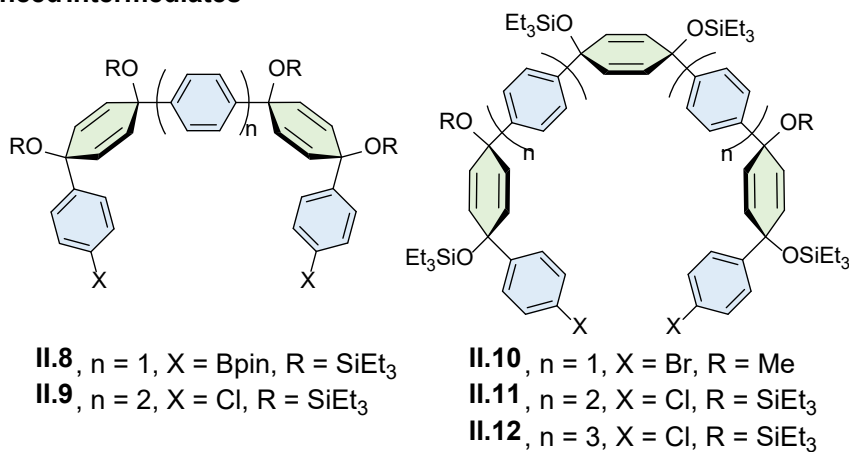
As proposed, upon synthesis of *m*[6]CPP, we immediately noticed bright green fluorescence, which is not observed in the parent [6]CPP. Characterization by NMR (¹H and ¹³C), IR, mass spectrometry, and X-ray crystallography (for *m*[6]CPP) confirmed structural assignment. A telling piece of characterization data for the product is the chemical shift of the inward pointing proton present on the *meta*-connected phenylene. As the nanohoop shrinks, the proton is forced further into the shielding cones of the flanking phenylenes. This results in the signal shifting upfield from 7.12 ppm for *m*[12]CPP to 5.62 ppm for *m*[6]CPP. Characterization by cyclic voltammetry resulted in redox chemistry similar to that of [*n*]CPPs.

The synthesis of the most strained *m*[5]CPP required a slightly different strategy (Scheme 2). Here, the *meta*-functionalized benzene was incorporated into ketone precursor **II.18**. Lithiation of **II.3** and addition to ketone **II.18**, followed by protection with triethylsilyl chloride affords advanced intermediate **II.19**. Miyaura borylation gives the bisboronate **II.20** in good yield. Oxidative homocoupling⁵² then smoothly transforms **II.20** to the challenging macrocycle **II.21** in 42% yield under mild conditions. Deprotection and reductive aromatization yielded *m*[5]CPP. Again, we noticed immediately that this very strained *meta*-nanohoop is fluorescent whereas the parent [5]CPP is non-emissive. With a series of these highly strained cycloparaphenylene analogues in hand, the property influence of symmetry breaking was explored.

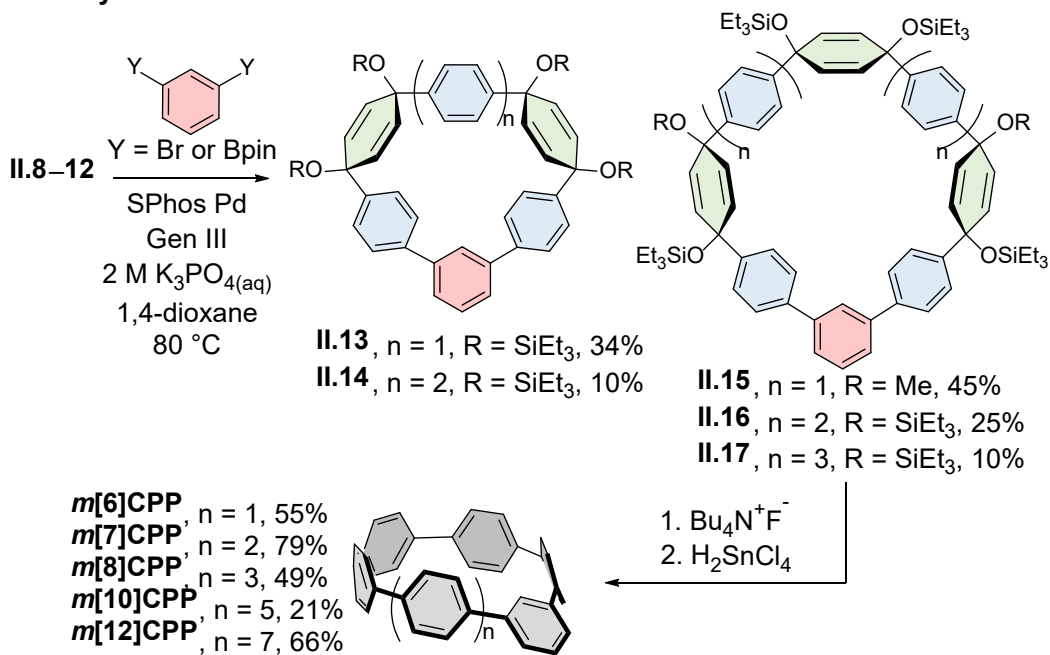
BuildingBlocks



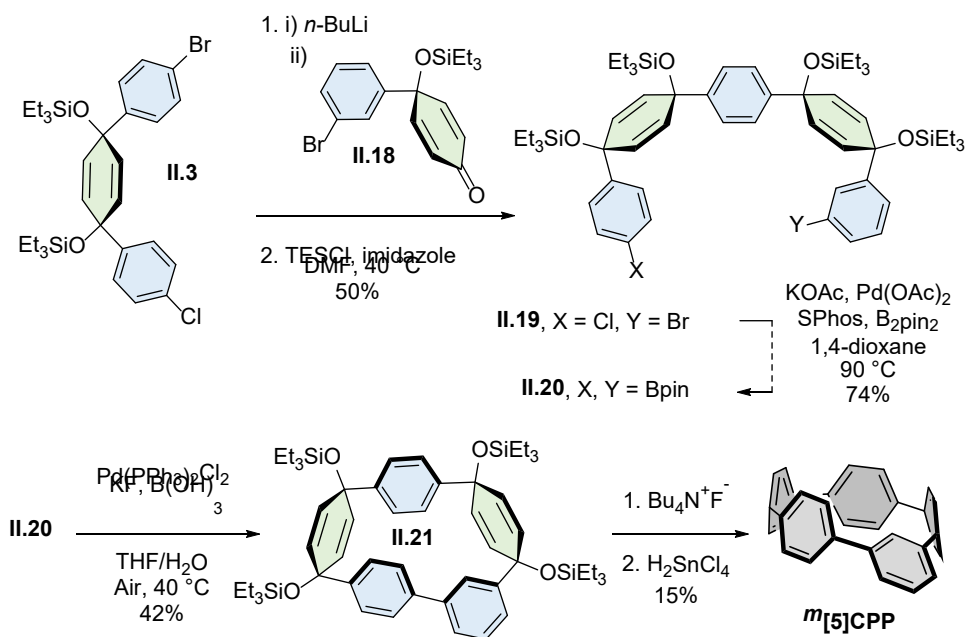
Advanced Intermediates



Macrocyclization and Reductive Aromatization



Scheme II.1. Building block synthetic approach to *m*[6]-, *m*[7]-, *m*[8]-, *m*[10]- and *m*[12]CPP.



Scheme II.2. Modified synthetic strategy for *m*[5]CPP.

II.3. Structural features

When discussing carbon nanohoops, strain is a critical quality that endows them with atypical optical properties^{44,54} and reactivity.^{55,56} As the diameter of these carbon nanohoops decreases, the inherent strain increases and changes the geometry and optical properties. To gain insight into the strain, single crystals of *m*[6]CPP were obtained by slow evaporation of dichloromethane solutions. From inspection of the crystal structure, the dihedral angle decreases from 49° at the *meta*-phenylene to 19° at the opposite side of the hoop, seen in Figure 2a. This suggests that the part of the nanohoop opposing the *meta*-phenyl unit has even more dihedral strain than [6]CPP, which has an average dihedral angle of 26°. ⁴⁰

In order to quantify the strain energy of the entire *m*[*n*]CPP series, theoretical homodesmotic reactions were performed at B3LYP/6-31G(d,p) level of

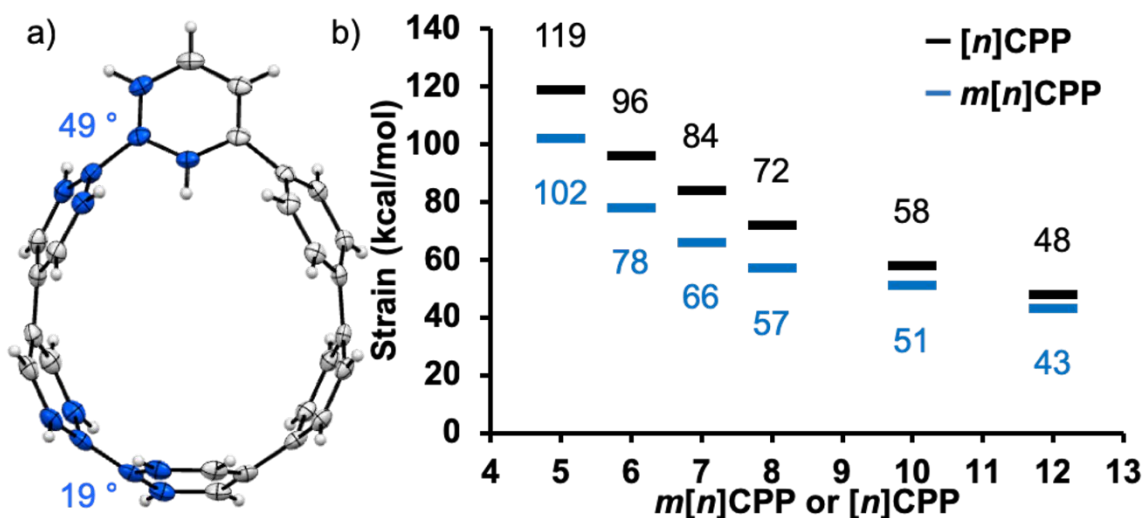


Figure II.2. a) Molecular structure of $m[6]CPP$ determined by X-ray crystallography (thermal ellipsoids shown at 50% probability). b) Calculated strain using homodesmotic reactions of $[n]CPPs$ (black) and $m[n]CPPs$ (blue) at B3LYP/6-31G(d,p) level of theory.⁵⁷ The inherent strain ranges from 43–102 kcal/mol. Compared to conventional cycloparaphenylenes with the same amount of phenylenes, $m[n]CPPs$ are less strained by about 20%, as seen in Figure 2b. The most strained macrocycle of our series, $m[5]CPP$, possesses 102 kcal/mol of strain. This places it below $[5]CPP$ (119 kcal/mol),⁴⁰ and above $[6]CPP$ (97 kcal/mol)⁴³ in terms of strain. The calculated structures show an expected gradual decrease in dihedral angle and increase in *ipso* carbon deviation from planarity as the nanohoop size decreases, similar to the parent $[n]CPPs$. (Table S9) Interestingly, the dihedral angle next to the *meta*-phenylene widens with increasing strain. Although the strain can only be inferred from dihedral angles between phenylenes and calculated homodesmotic reactions, it is clear the strain plays a central role in defining the properties.

II.4. Photophysical properties

The photophysical properties are particularly exciting. Similar to cycloparaphenylenes, the $m[n]$ CPPs have a common absorption maximum around 328 nm (Fig. 3a) from HOMO-1→LUMO and HOMO→LUMO+1 transitions (Fig. S13–S18). However, there is a red-shifting second absorption as the size of the hoop decreases (visible as a peak for $m[6]$ – $m[8]$ CPP and a shoulder to the main absorption at 328 nm for $m[10]$ - and $m[12]$ CPP), which is the HOMO→LUMO absorption. The extinction coefficient of the higher energy transition is larger than the lower energy transition in all cases (Fig. 3c and Table S3). The series shows decreasing, but never vanishing, fluorescence ranging from 429–534 nm and quantum yields ranging from 0.01 for $m[5]$ CPP to 0.77 for $m[12]$ CPP (Fig. 3a and b). Fluorescent lifetimes of all $m[n]$ CPPs are around 3 ns (Table S4), which is different than the $[n]$ CPP series with lifetimes ranging from 2–18 ns.

Density functional theory calculations and a comparison to the $[n]$ CPPs were used to explain the photophysical phenomena further. As mentioned earlier, HOMO→LUMO transition of $[n]$ CPPs is Laporte forbidden due to conservation of ground and excited state orbital symmetry. The cycloparaphenylenes are therefore excited through HOMO→LUMO+1 and HOMO→LUMO+2 or HOMO-1→LUMO and HOMO-2→LUMO. From these states, internal conversion to a spatially localized $S_{1'}$ state occurs. Here, the larger $[n]$ CPPs ($n \geq 8$) exhibit exciton localization over about seven of the phenylenes (Figure 1b). When exciton localization occurs, the symmetry is different than the ground state,

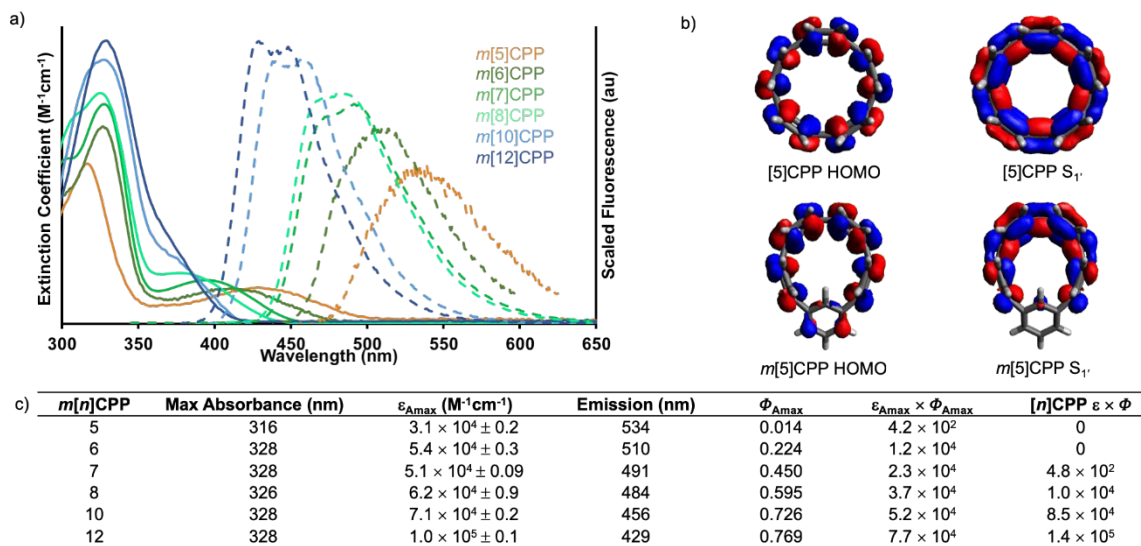


Figure II.3. a) Absorbance and emission spectra of $m[n]$ CPPs. b) HOMO (left) and $S_{1'}$ (right) orbital depiction of $[5]$ CPP and $m[5]$ CPP, demonstrating change in orbital symmetry. Calculated using CAM-B3LYP/6-31G(d) level of theory. c) Absorbance, extinction coefficient (ϵ), emission and quantum yield (Φ) of $m[5]$ – to $m[8]$ –, $m[10]$ –, and $m[12]$ CPP and $m[n]$ CPPs and $[n]$ CPPs brightness comparison.

allowing the $S_{1'} \rightarrow$ HOMO transition. When $n \leq 7$ there is complete orbital delocalization over the whole $S_{1'}$ excited state structure (Fig. 1c), therefore the ground state symmetry is conserved. In these cases, the $S_{1'} \rightarrow$ HOMO transition is Laporte forbidden, resulting in undetectable fluorescence for $[5]$ CPP and $[6]$ CPP and very weak fluorescence for $[7]$ CPP.

Our calculations show that changing a single phenylene from *para* to *meta* does in fact change the π -system orbital symmetry. Figure 3b demonstrates the difference in orbital symmetry between the HOMO and relaxed excited state of $m[5]$ CPP compared to $[5]$ CPP. The symmetry broken nano hoops show a dramatic

increase in intensity for both HOMO→LUMO and S₁'→HOMO transitions. This is apparent from a significant increase in the extinction coefficient and oscillator strength of the HOMO→LUMO transition when comparing **m[5]CPP** with an extinction coefficient of $6.0 \times 10^3 \text{ M}^{-1}\text{cm}^{-1}$ and oscillator strength of 0.1217 to **[5]CPP** possessing an extinction coefficient of $4.5 \times 10^2 \text{ M}^{-1}\text{cm}^{-1}$ and oscillator strength of 0.0015.⁴⁰ The change in orbital symmetry also results in a “turn on” in fluorescence for smaller sizes.

Like *[n]*CPPs, the *m[n]*CPPs quantum yield decreases with decreasing size. However, the transition is at no point forbidden by symmetry as is the case for *[n]*CPPs. As such, the reduction in quantum yield is attributed to strain effects. It was previously reported that curving a conjugated system, such as *p*-phenylenes⁵⁸ or pyrene,⁵⁹ reduces the quantum yield respective to increasing strain. For *m[n]*CPPs, the decrease in quantum yield indicates an increase in non-radiative decay rate (k_{nr}) as the fluorescence lifetime was relatively constant across all *m[n]*CPPs measured (Table S4). In cycloparaphenylenes, the lifetime increases as the diameter decreases and the S₁'→HOMO transition is forbidden due to centrosymmetry. In contrast, introducing a *meta* phenylene allows S₁'→HOMO transitions across the entire series of *m[n]*CPPs.

To truly assess the aptitude of the *m[n]*CPPs to serve as enhanced fluorophores compared to *[n]*CPPs analogues, we turn to their brightness, which is the product of the extinction coefficient and quantum yield. Nanohoops **m[5]**–**m[8]CPPs** have an obvious increase in brightness over their *para*-counterparts, seen in Figure 3c. For example, **[8]CPP** was previously used as a fluorescent probe with a brightness of $10,000 \text{ M}^{-1}\text{cm}^{-1}$.⁴⁶ Now, **m[6]CPP** has a comparable

brightness of $12,000 \text{ M}^{-1}\text{cm}^{-1}$, but is far easier to produce. This edge is lost at larger sizes where *m*[10]- and *m*[12]CPPs are still brighter than commercial fluorophores like DAPI,^{60–62} AMC,⁶³ and rhodamine 110,^{60,64,65} but not quite as bright as [10]-¹³ and [12]CPP.^{13,14} We anticipate this is relevant to nanohoops as new biocompatible fluorophores and novel fluorescent sensing materials.⁴⁶

II.5. Conclusions

The connectivity of carbon atoms, size, and symmetry all play critical roles in determining the properties of carbon nanomaterials. Rarely can these variables be systematically probed so precisely. Bottom-up synthetic strategies allow for the examination of these fundamental questions in an unambiguous manner. By rational design, a *m*[*n*]CPP series was prepared where a single carbon-carbon bond is moved over by one position from the parent carbon [*n*]CPPs. Shifting a phenylene in a cycloparaphenylene from *para* to *meta* was proven as an efficient means to activate the previously forbidden absorption and emission transitions by breaking orbital symmetry, resulting in a fluorescence turn-on of the smaller nanohoops. The fluorescence enhancement was accompanied by a blue-shift of these transitions proportional to a decrease in strain of about 20%.

Advantageously, smaller nanohoops, which are more easily accessed by synthesis, are rendered fluorescent. Moreover, the smaller binding pockets of the smaller nanohoops provide an opportunity for fluorescence sensing of analytes that are not possible with the larger hoops. In relation to this possible application, fortuitously, these *m*[*n*]CPPs have a C-H group directed to the interior of the structure which

could be exchanged in a second-generation design to a coordinating group. Further studies of these new nanohoop structures will be reported in due course.

II.6. Co-authored content

The work in Chapter 2 was co-authored with Terri Lovell, Dr. Lev Zakharov, and Prof. Ramesh Jasti and published under the title “Symmetry breaking and the turn-on fluorescence of small, highly strained carbon nanohoops” in *Chemical Science*.³⁶ Terri Lovell performed roughly half the synthesis and characterized the optoelectronic properties. I performed the remaining synthesis, grew crystals, and performed strain analysis. Dr. Lev Zakharov solved the crystal structure of **m[6]CPP**. Prof. Ramesh Jasti edited the manuscript.

II.7. Bridge to Chapter III

While analysing *m[n]CPP* strain we made inferences about the strain based on the crystal structure data available, however, a computational method that quantified strain location did not exist. Unlike conventional cycloparaphenylenes, these molecules are not symmetric and we would expect that strain is not spread symmetrically throughout the molecule. In the next chapter, I detail a computational method for locating exactly where strain is present in a strained macrocycle.

CHAPTER III

STRAIN VISUALIZATION FOR STRAINED MACROCYCLES

III.1. Introduction

Strain has a unique impact on molecular properties and reactivity. Macrocyclic strain is leveraged in chemical biology for bioorthogonal reactivity^{66,67} and in polymer chemistry for ring opening metathesis.^{68,69} Additionally, graphitic macrocycles, such as carbon nano hoops,³⁵ have enhanced solubility,⁷⁰ remarkable photophysical properties,^{3,12} and reactivity^{31,71-73} that all arise from strain. These attributes, and improvements in methods for their synthesis,^{13,22,25,74} have caused a renewed interest in strained macrocyclic molecules. While methods for probing solubility and photophysical properties are well established, macrocyclic strain is a challenging characteristic to analyze and quantify. The best known methods for calculating macrocyclic strain energy (the potential energy released upon breaking the macrocycle) compare heat of formation for strained and unstrained molecules in a theoretical strain releasing reaction.^{1,75,76} While combustion calorimetry can be used,^{77,78} computationally determined energies are now standard due to the quality of current computational methods and the challenge of obtaining accurate experimental results. It has become routine to report the calculated strain energy of new strained macrocycles with their synthesis due to the fundamental effects of this tension.

Total strain energies are commonly reported and the strain in specific parts of the molecule cannot be discerned. While the total strain energy does provide some information, it does not correlate perfectly to reactivity. For example, when

the same amount of strain energy is spread over more atoms, the molecule is more stable than when it is concentrated in fewer atoms. If this is corrected for by dividing by the total atoms, non-participating atoms artificially lower the strain energy per atom determined. Local strain can sometimes be inferred in highly symmetric molecules, such as strain per phenylene in a cycloparaphenylene. However, non-symmetric molecules have unevenly distributed strain energy leading to locations of higher reactivity that may be unintuitive. Some alternative metrics have been devised to measure local strain. For example, the deplanarization of an aromatic ring, torsional angle in a biphenyl segment, and bond lengths can be compared to an unstrained comparative molecule.^{16,74} For non-planar π -systems, a measure of pyramidalization was developed that estimates relative strain in non-planar aromatics such as corannulene and fullerene.^{79,80} However, these measurements are not quantitative and, therefore, cannot be compared across molecules which limits their utility. Even when combining total strain calculation with these other metrics, it results in an incomplete depiction of molecular strain energy.

A method that determines strain both quantitatively and locally is quite useful. Therefore, a computational method was developed that identifies the quantity of strain energy local to every coordinate (bond, angle, and torsional angle) in a molecule. This strain visualization software is called StrainViz and has been made freely available. A similar method was previously reported for mechanochemistry where unstrained molecules are stretched and the tension that conformational changes that induce stretching,^{82,83} however, the inherent strain

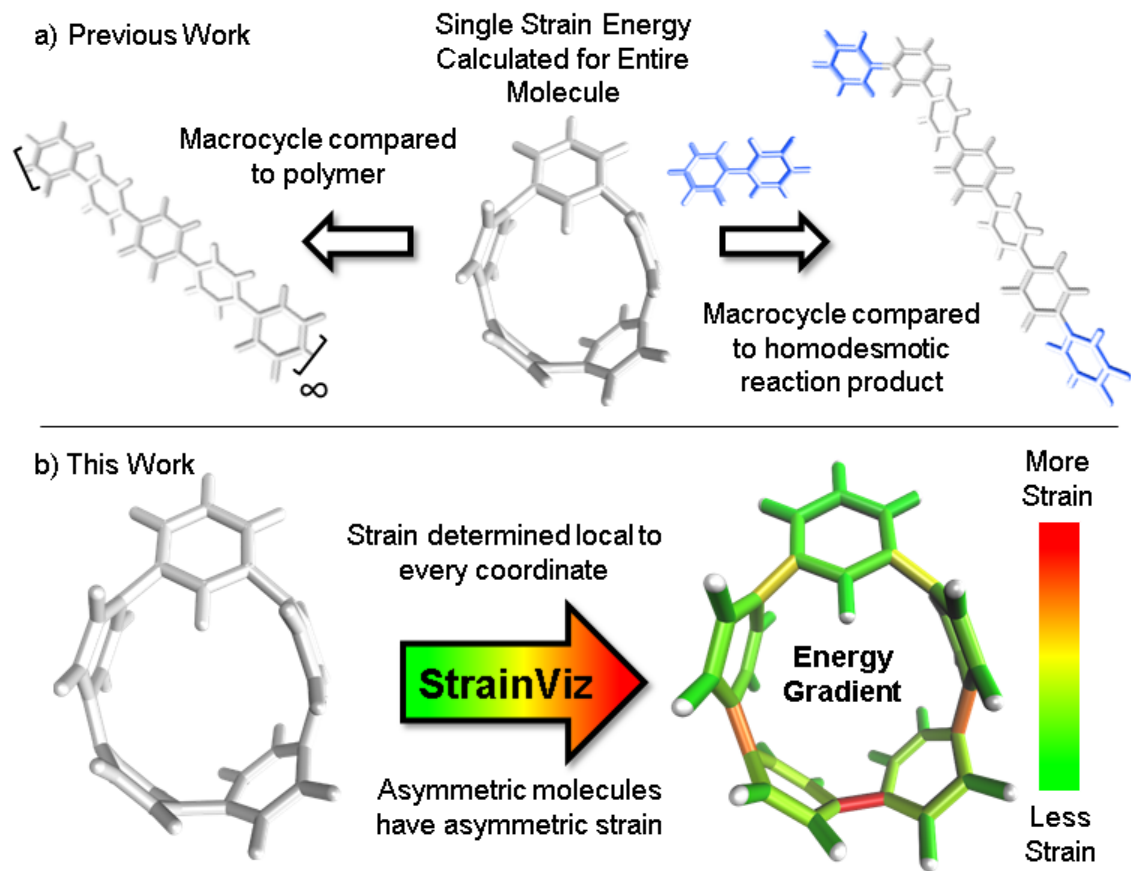


Figure III.1. a) Strain energy is calculated by comparing the strained molecule to an unstrained polymer or homodesmotic reaction product resulting in a single strain energy for the entire molecule. b) StrainViz determines strain energy local to every coordinate. was not addressed. StrainViz can find this elusive strain energy. Our new method was evaluated to establish its accuracy using prior calculated strain energies and experimental reaction results from the literature. It is freely available on GitHub.⁸⁴ The resulting computational method provides an interactive and insightful strain map. Knowledge of specific strain location facilitates and enhances synthetic efforts towards strained macrocycles by providing the exact and specific impact on strain of structural changes in a molecule. As is demonstrated herein with

StrainViz, it is now possible to make inferences about the local properties and reactivity in strained molecules.

III.2. Computational Methods

This new computational method is fundamentally an advancement on the use of a homodesmotic reaction to estimate strain energy (Figure III.1, previous work going right).⁸⁵ Here, the macrocyclic strain energy may be defined as the energy associated with deforming a linear molecular segment when included in a macrocycle. For example, the deformation of a phenylene when included in a cycloparaphenylene. To use a homodesmotic reaction to determine this quantity, the molecular geometry is optimized and the single point energy of the lowest energy conformation is determined ($E_{\text{macrocycle}}$). In this state, the molecule retains strain energy that cannot be realized until the molecule is broken so that tension is released. Breaking the molecule creates radicals at each side of the break that must be capped with a capping molecule that is similarly broken and placed at each end aiming to retain the local environment of the ends. Then, the lowest energy conformation of this strain released theoretical molecule (E_{linear}) is calculated and compared to the original molecule while accounting for the atoms added to cap the broken ends (E_{cap}) by determining the single point energy of the capping molecule shown in blue in Figure III.1. The difference in total energy between the starting materials and products of this theoretical homodesmotic reaction is the total strain energy (E_{strain}) in the macrocycle shown in Equation 1.

$$E_{\text{strain}} = (E_{\text{macrocycle}} + E_{\text{cap}}) - E_{\text{linear}} \text{ (Equation 1)}$$

This is an example of how a homodesmotic reaction may be used for estimating strain energy. The homodesmotic reaction has been rigorously defined elsewhere.⁸⁶

It is also possible to disassemble the molecule into an infinite polymer and compare the repeating unit energies in both the macrocycle and the unstrained polymer.^{9,87} If it were possible to connect these geometries by creating a trajectory between the strained and unstrained states, one could comment on how the energy of each atom changes to release strain energy as the trajectory proceeds. Ideally, the trajectory would begin in the optimized geometry of the strained molecule and descend to an unstrained infinite polymer (Figure III.2a). The macrocycle cannot be broken without changing the atomic environment and introducing additional strain into the analysis. A theoretical trajectory between the strained macrocycle and unstrained infinite polymer that isolates macrocyclic strain energy is therefore impossible.

It is, however, possible to fragment the molecule so that it may descend into an unstrained state without introducing new strain. By deleting certain atoms, the trajectory shown in Figure III.2b becomes possible and allows the initial geometry to share the location of its atoms (highlighted in the inset of Figure III.3) with the strained molecule while still relaxing to an unstrained state upon geometry optimization. The trajectory of each atom accurately represents the trajectory of atoms in the strained molecule to atoms in an unstrained state. This approximates an ideal strain energy determining experiment by averaging these trajectories for multiple fragments.

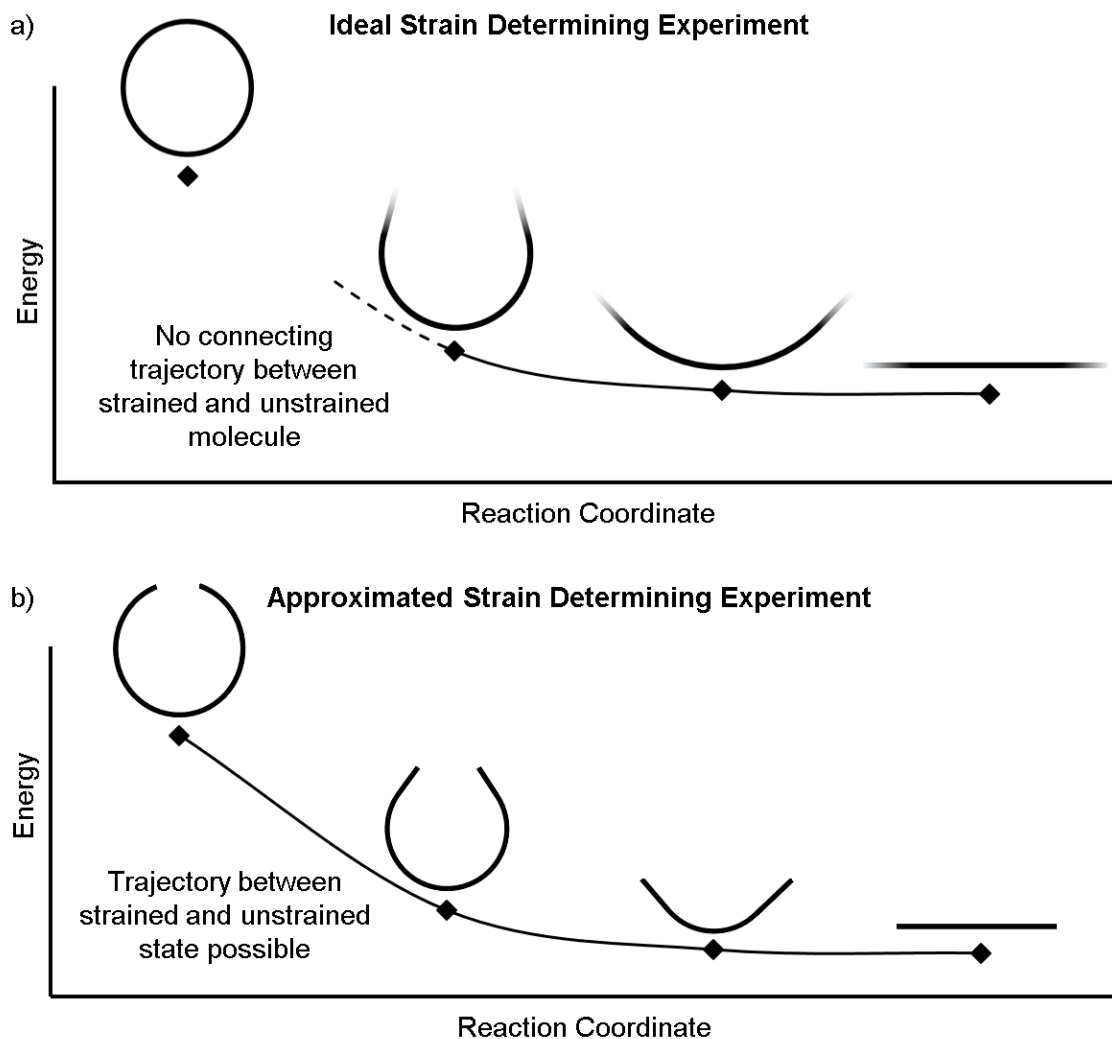


Figure III.2. a) This ideal experiment begins with the strained macrocycle and ends with an infinite polymer where the strain has been released. b) By removing part of the molecule, the beginning and end geometries can now be connected by a strain releasing trajectory. This allows the local trajectory of each atom to be determined.

In practice, a segment of the molecule is removed, such as a phenylene or ethylene, to create a fragment as shown in steps 1 and 2 of Figure III.3. The choice of fragments does not appear to significantly impact overall strain energy determination, however, it can impact strain distribution. Therefore, obtaining accurate results requires as many symmetrically created fragments as possible. For

example, when analyzing cycloparaphenylenes, there should be as many fragments as there are phenylenes to be removed. Once a fragment is removed the ends are capped with hydrogen atoms. This requires the segment removed to be at least two atoms (e.g. ethylene) to accommodate replacement with hydrogens. These capping hydrogen atoms are optimized by freezing all atoms in the fragment that match the initial geometry. This ensures they do not add additional strain to the fragment when the fragment is optimized. All fragments created for the analyses in this paper are in the supplementary information to remove any ambiguity.

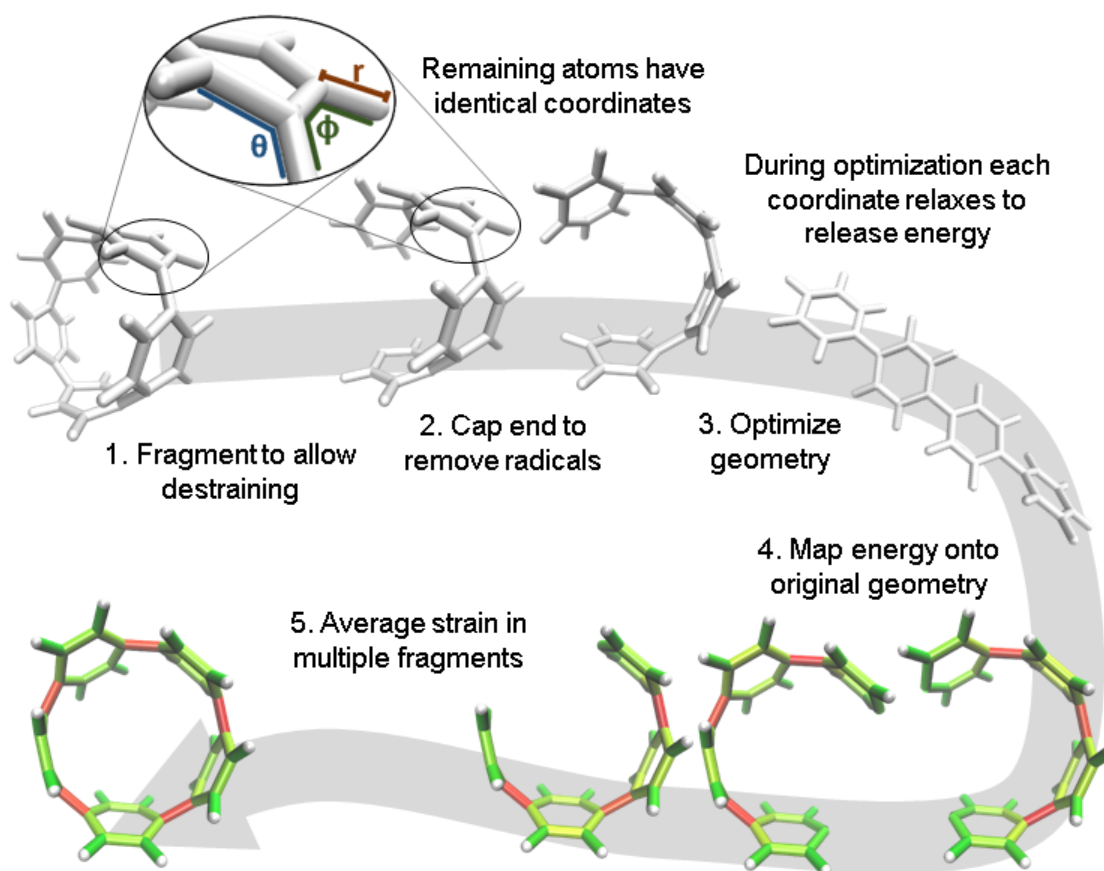


Figure III.3. Workflow for strain analysis. The coordinates in each molecule fragment relax to release strain energy that is quantified per coordinate (r : bond length, θ : angle, ϕ : torsional angle).

The trajectory of each individual atom during this process follows the optimization algorithm given by the program used. In these studies, Gaussian09⁸⁸ was used with the quasi-Newton rational function optimization (RFO) method that is the default for Gaussian03 due to it converging more smoothly than the newer direct inversion in the iterative subspace (DIIS) method.⁸⁹ StrainViz can also be used with Orca, delivering similar results and being free for academic users.^{90,91} The energy of each atom is given by its relationship to other atoms via internal coordinates. The internal coordinates describe the distances and angles between atoms shown in a zoomed in image in Figure III.3. There are three coordinates that together describe the position of every atom relative to each other: the distance between two atoms, the angle between three atoms, and the torsional angle between four atoms. The optimization algorithm minimizes the energy of the geometry by interrogating these internal coordinates and adjusting them to release energy. The algorithm estimates a force for each coordinate (F) and, depending on step size, assigns a displacement (Δx). It is also possible to define “strain” as the force and “strain energy” as the total energy associated with that force. Multiplying the force by the displacement, as shown in Equation 2, identifies the change in energy ($\Delta E_{\text{coord est}}$) each coordinate experiences in each step.

$$F\Delta x = \Delta E_{\text{coord est}} \text{ (Equation 2)}$$

The energy determined from this specific calculation is only an estimate. The algorithm overestimates the total energy released for each displacement due to the necessary use of redundant internal coordinates.⁹² Therefore, each step is

scaled relative to the actual change in the single point energy calculated ($\Delta E_{\text{step actual}}$ in Equation 3) at each step.

$$\Delta E_{\text{coord actual}} \approx \Delta E_{\text{coord est}} (\Delta E_{\text{step actual}} / \Delta E_{\text{step est}}) \text{ (Equation 3)}$$

Where $\Delta E_{\text{step est}}$ is the sum of all $\Delta E_{\text{coord est}}$ present. As the optimization proceeds, these energies become smaller until the relaxed geometry is found and ΔE approaches zero for all coordinates. For a given coordinate, summing the energy determined for each optimization step gives the total amount of energy stored in that internal coordinate.

After symmetrically fragmenting the molecule, optimizing the fragments, and analyzing the trajectory of the internal coordinates, this data must be displayed in a way that effectively communicates the information gathered. The effective color mapping scheme used for analyzing mechanical force was adopted.⁸¹ The bond strain energy associated is simple to display because there is a single value per bond and the bonds are colored accordingly. For the energy associated with the angle between three atoms, the energy is divided in half among the two contributing bonds. Finally, for the torsional angle between four atoms, the energy is split evenly among the three bonds connecting the four contributing atoms. These maps are produced for bond, angle, and torsional strain energy in each fragment. Then the energies per bond are averaged among every fragment containing that bond and a single map for each type of strain energy. Finally, the three types are summed and a total strain map is produced.

It is important to note that almost none of the above mentioned processes are done manually. A package of freely available scripts on GitHub automate

Gaussian input file creation, job submission, and VMD script generation.⁸⁴ Each analysis only requires the manual generation of an optimized geometry and appropriate fragments, StrainViz does the rest.

III.3. Results & Discussion

With a framework in place for analyzing strained molecules, it is important to check the assumptions made when creating this method. There are three main assumptions that underpin the validity of this computational method: 1. The fragments chosen accurately represent the base molecule. 2. The sum of all energies for all internal coordinates total to an energy that is corroborated by previous methods. 3. The local strain energy determined relates to reactivity. If these three assumptions are proven valid, then StrainViz is useful for determining strain energy.

III.3.1. Fragments accurately represent the molecule.

By using fragments to calculate strain energy in the molecule we lose the information provided by the portion omitted. Although it is not possible to compare the fragment directly with the base molecule, it is possible to identify differences when varying the fragment size. **[8]CPP** was analyzed using fragments of increasing size (Figure III.4). From this analysis we will see how much information is lost dependent on the size of the omitted portion.

When molecule fragments are being analyzed, the fragment size must be judiciously chosen to reduce the impact of edge effects where the molecule is cut. It has been previously seen, in the strain-induced retro-Huisgen cycloaddition of triazoles,⁹³ that when the edge atoms are connected to the triazole by coordinates

(torsional angle across an ethyl or propyl group), results do not match expectations. Therefore, the program does not include any coordinates that contain the end capping atoms or the atoms attached to them. This trims away forces at the ends of the geometry that are most susceptible to these edge effects. By doing so, the results become more relevant regardless of fragment size, but limits how small the fragments may be made. Despite this consideration, the chosen fragment size does still have an impact on the accuracy. Within each fragment, the variability of strain energy measurement for each bond from the analysis also increases with decreasing fragment size. The four largest **[8]CPP** fragment sizes, shown in Figure III.4, all determine strain energies within 3% of their mean. These fragments also are internally consistent. Each individual strain energy determined for each bond is also within 3% of the mean. This consistency shows that when the fragments used are at least half the original molecule edge effects are minimal.

III.3.2. Energies are expectedly similar to previous results.

A relevant computational technique must deliver results that are relatively consistent with previously described techniques while providing new insight. Unfortunately, there is no computational benchmark or easily obtainable experimental data for strain and the amount determined can vary depending on the technique used. For example, **[12]CPP** has a range of strain energies depending on the computational technique (summarized in Table III.1). Given this relatively wide range in the literature, there is significant room for error in any new computational method. However, when using a similar computational technique, (entries 1-4) the range narrows significantly even when using different levels of

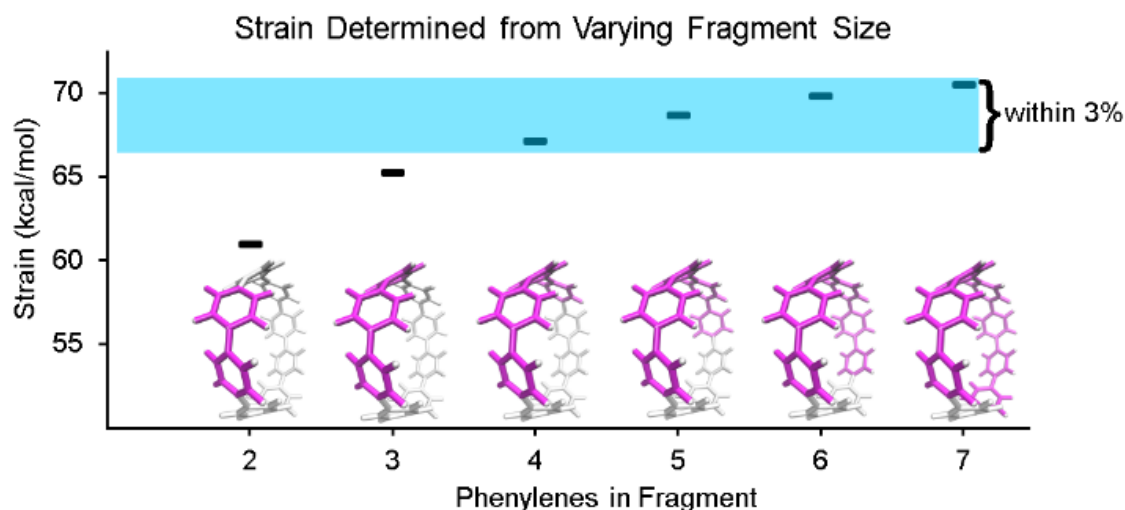


Figure III.4. Fragments of [8]CPP having 2-7 phenylenes (highlighted in pink) were used in the strain analysis. Fragments retaining 50% or more of the molecule all determined strain energies within 3% of each other. All calculations were performed at the B3LYP/6-31G(d) level of theory unless otherwise noted.

theory. Therefore, StrainViz will be compared directly to known examples using the homodesmotic reaction at the same level of theory. Values similar to previous reports should be expected.

Strain Energy	Theory	Reference
50 kcal/mol	B3LYP/6-31G(d)	11
48.1 kcal/mol	B3LYP/6-31G(d)	1
49.0 kcal/mol	B3LYP/6-31G(d)	94
50.2 kcal/mol	M06-2X/6-31G(d)	94
42 kcal/mol	Gaussian Pseudopotentials	87
48.3 kcal/mol	B3LYP/6-31G(d)	This work

Table III.1. Reported strain energies of [12]CPP.

A variety of molecules with macrocyclic strain energy were used in this analysis (Figure III.5). Given that cycloparaphenylenes are well studied in this respect, cycloparaphenylenes having six to ten phenylenes were analyzed and compared to an analysis using homodesmotic reactions (Figure III.5a).¹ Comparing these two analyses, we can see that the results are most similar at larger cycloparaphenylene sizes. This is consistent with the aforementioned accuracy of the StrainViz analysis where larger cycloparaphenylene fragments result in more accurate strain energy determinations. Analyzing Itami's carbon nanobelt resulted in even better matching with previous efforts (Figure III.5b).⁹⁵ The high accuracy may be owed to the fragment optimization trajectory quality. See supplementary information for further comments. A recently synthesized highly strained small cyclophane from the Bodwell group⁹⁶ and [2.2]paracyclophane⁹⁷ were also analyzed and confirm that StrainViz is consistent with prior computational efforts (Figure III.5c).

The literature report of [2.2]paracyclophane does attempt to quantify the strain energy present in the phenylene and ethylene segments.⁹⁷ This was done in a similar manner to our method. The molecule was broken up and the strain energy in each fragment was determined by comparing single point energies of the strained and unstrained states. Their analysis, however, found different amounts of strain than their homodesmotic reaction; 10.2 kcal/mol per phenylene and 5.6 kcal/mol per ethylene summing to 31.6 kcal/mol, but 30.8 kcal/mol from a homodesmotic reaction using the ω B97X-D functional. This begs the question

which analysis is more accurate. With our method, the local strain adds up to the total strain by definition.

By corroborating results found in the literature, we establish that StrainViz determines total strain energies that are reasonable. This shows that generating a map of local strain does not compromise the total strain analysis quality. More importantly, we see exactly where in the structure the strain is distributed. We hope to confirm that local strain is more instructive than total strain for reactivity.

III.3.3. Local strain energy relates to reactivity.

In a previous paper, we described the synthesis of cycloparaphenylenes having one phenylene switched from being *para* to *meta* connected.³⁶ We described the strain using homodesmotic reactions and concluded that the *meta*-cycloparaphenylenes are less strained than cycloparaphenylenes with an equal amount of phenylenes (Figure III.6). A structural strain parameter from the crystal structure, the torsional angle between adjacent phenylenes, had values above and below comparable cycloparaphenylenes which hinted that strain may not be evenly distributed. Lacking a tool to directly locate and quantify strain at specific locations on the molecule, we could not at that time make any further claims about strain in these molecules. Now, StrainViz locates the strain and predicts the reactivity of *meta*-cycloparaphenylenes.

Analysis using StrainViz in Figure III.6 shows that strain is concentrated across from the *meta* phenylene. Changing a phenylene in a cycloparaphenylene from being *para* to *meta* connected relieves strain at that end of the molecule, but adds strain at the opposite end. If this program provides a meaningful molecular

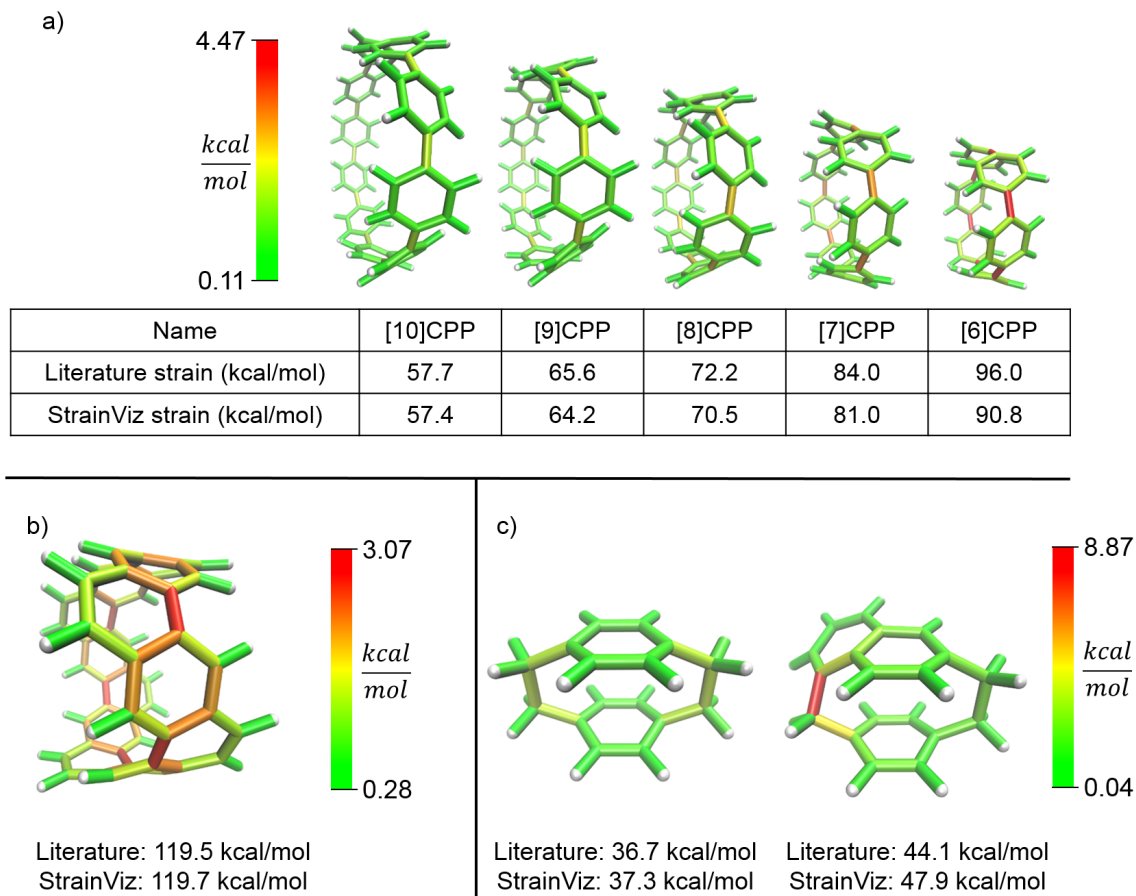


Figure III.5. Literature examples of strain energy determinations compared to StrainViz analysis. a) Cycloparaphenylene strain determined by homodesmotic reactions.¹ b) Carbon nanobelt strain energy extrapolated from increasing size belts.⁹⁵ c) [2.2]paracyclophane strain and Bodwell's more strained analogue determined by isodesmotic reaction B3LYP/6-31G(d,p)⁹⁷ and M06-2X/Def2TZVP⁹⁶ respectively. strain analysis, then this high strain area should react faster in a strain relieving reaction. For example, bromination of a *meta*-cycloparaphenylene should occur exactly across from the meta phenylene where the majority of the strain is located. Indeed, upon bromination of a *m*[6]CPP, bromination occurs exactly where predicted by our calculations (Scheme III.1).

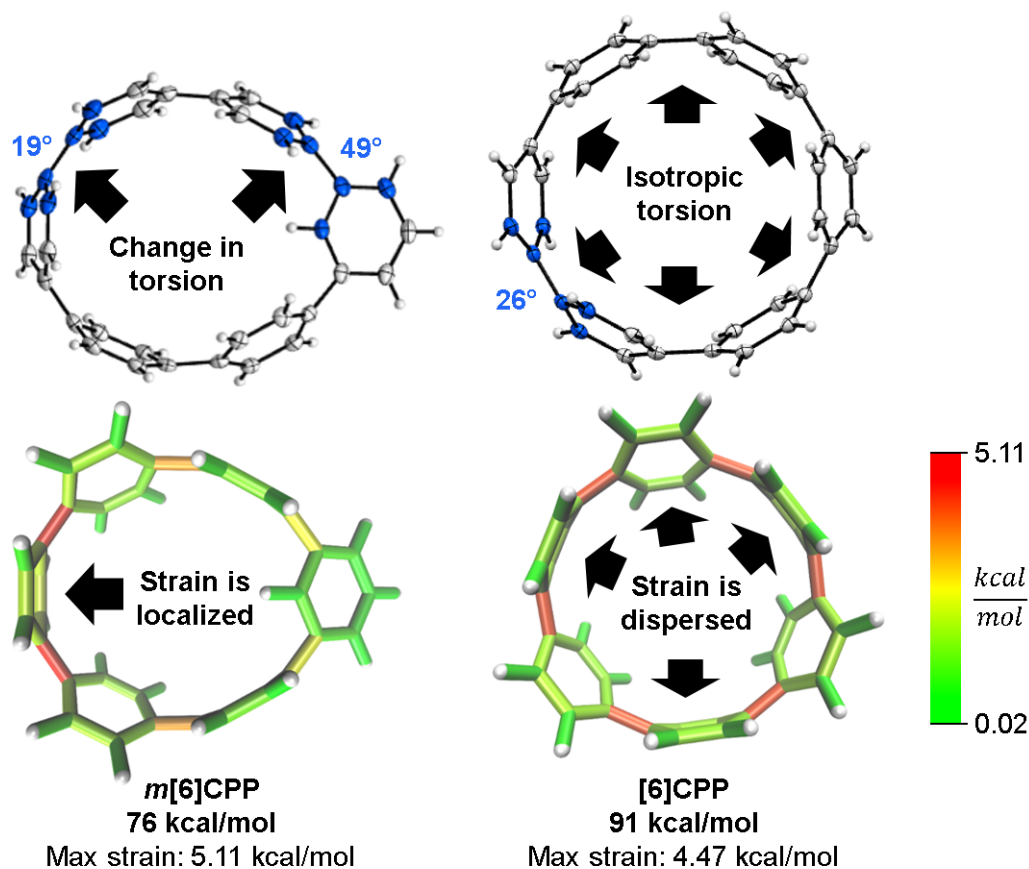
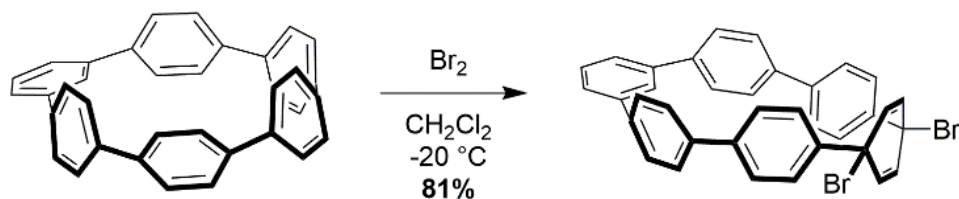


Figure III.6. Torsional angles and total strain of [6]CPP and *m*[6]CPP. Changing connectivity from *para* to *meta* decreases total strain, but increases local strain energy.



Scheme III.1. Bromination of *m*[6]CPP.

Even more striking from the analysis is that despite *meta*-cycloparaphenylenes being less strained in total, they should be more reactive due to a higher amount of local strain relative to a cycloparaphenylene where strain is spread equally over the molecule. This phenomenon is seen clearly in the

aforementioned publications by Yamago. In the case of either bromination⁷¹ or C-C bond activation by platinum,⁷² a reaction at one phenylene is followed by a faster second reaction. This is not consistent with the total quantity of strain present in each reacting molecule. A homodesmotic reaction of the starting cycloparaphenylene and singly brominated cycloparaphenylene shows that the second has much less strain energy. However, when analyzed using StrainViz as shown in Figure III.7, it is clear that the singly brominated intermediate has more strain across from the first site of bromination and that the molecule has been activated to brominate the second time at a faster rate.

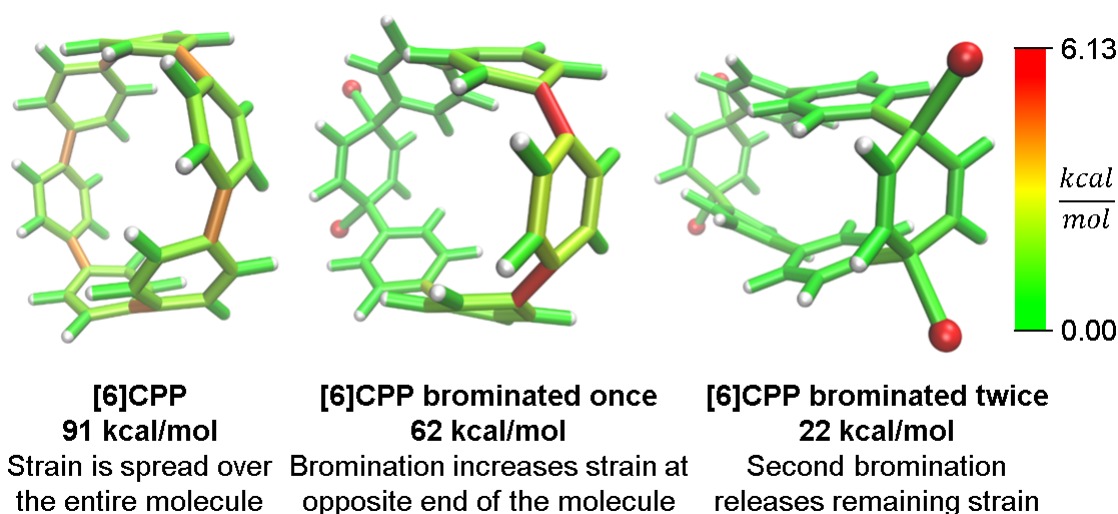


Figure III.7. Strain release during bromination of [6]CPP. First bromination activates molecule to be more reactive in the second step.

Despite these specific examples of reactivity correlating extremely well to the strain energy present at certain locations in the molecule, it is important to note that the specific reaction taking place is being aided by relief of strain to effect the transformation. This is why it is not the bond with the highest determined strain energy

that is broken during the reaction, but that the chemical reactivity occurring is preferred when in proximity to higher strain energy.

III.4. Unique strain analysis of macrocycles from the literature.

In addition to validating the method, we thought it instructive to provide use cases for StrainViz. Additional molecules from the literature were analyzed using this method to determine strain energies and the location of it as a heat map. The Tanaka group recently reported two strained nanobelt structures where one has a turn in it so that it forms a Möbius loop shown in Figure III.8a.⁹⁸ This geometry is intriguing in that the turn introduces additional strain energy to the molecule. The non-Möbius geometry is strained similarly to the corresponding cycloparaphenylene, however, the Möbius geometry is quite different. Despite having five repeating units instead of four, it is more strained overall. The additional strain is introduced at the entry points to the turn. This is similar to a polymer knot where strain is mostly located at a choke point at the knot entry.^{99,100} Within the turn there is higher strain and outside of the turn there is significantly less. The symmetry of this Möbius molecule prevents direct comparison to a non-Möbius molecule, however, it is possible to instead study molecules with higher symmetry (Figure III.8b). A Vögtle belt¹⁰¹ has high enough symmetry to directly compare molecularly degenerate molecules with and without a Möbius turn. The Vögtle belt has evenly distributed strain resulting in relatively little at any single point. Adding a Möbius twist places extreme strain (four times as much) on two symmetrically separated bonds at the entrance and exit of the twist. In total, strain

increases from 105 kcal/mol to 238 kcal/mol. This speaks to the challenge of synthesizing rigid Möbius molecules that are of fundamental interest.¹⁰²

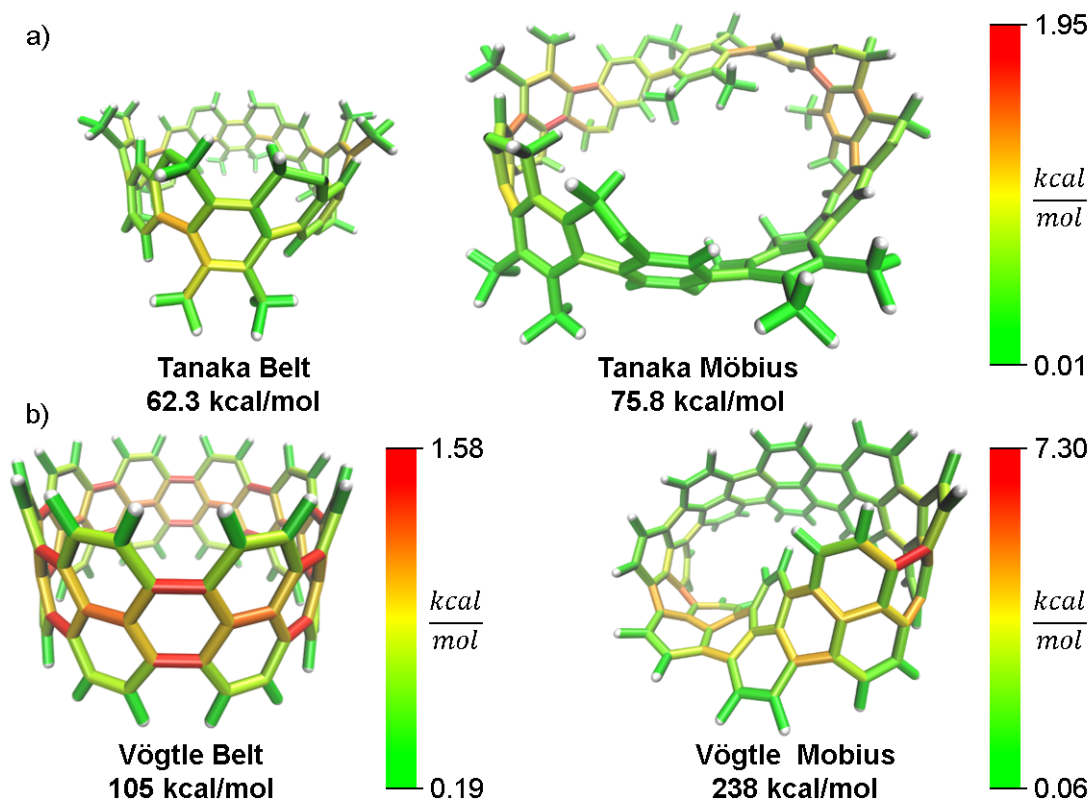


Figure III.8. Möbius molecules have more strain due to an internal twist when compared to a non-Möbius belt. a) The Möbius molecule synthesized in the Tanaka group is more strained than the non-Möbius despite being a larger size. b) In a symmetric Möbius molecule, strain is centered at the twist entry point.

In addition to macrocyclic molecules, multimacrocyclic molecules can be analyzed as long as each fragment fully releases all strain present. The Yamago group has reported a highly symmetric nanoball with multiple macrocyclic connections (Figure III.9).¹⁰³ Analyzing a single panel shows that strain is spread relatively evenly around the periphery aside from some anisotropy induced by the

C_2 symmetry of this lowest energy conformation. In the ball, however, it appears that there is more strain at the corners as opposed to the edges. This indicates that the three additional macrocycles in the ball add strain where they attach at the corners of a panel. As they do not apply force directly in the direction of any edges, the force is split between the edges and concentrates at the corners. This unique multimacrocylic strain contribution is easily apparent using this analysis.

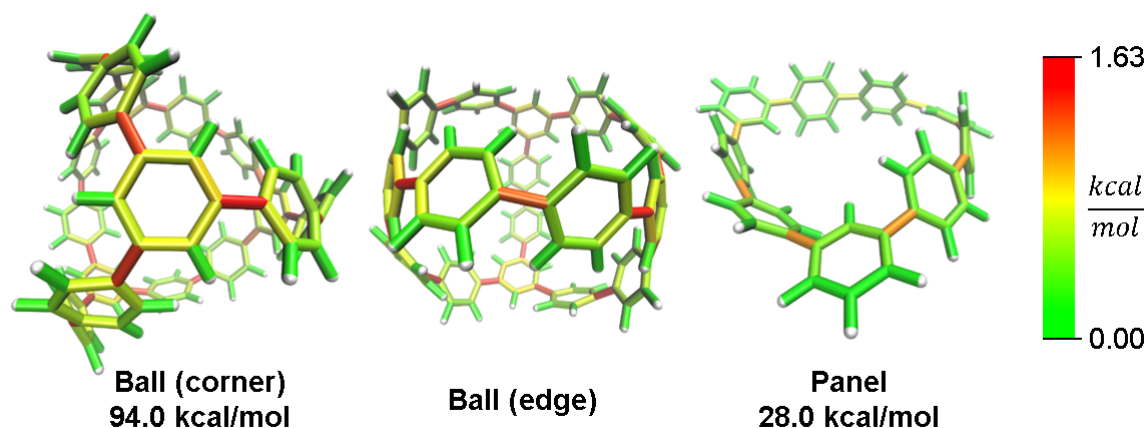


Figure III.9. Strain energy present in Yamago's nanoball. More strain at the ball corners relative to the edge.

While this analysis was designed for analyzing curved aromatic molecules, it applies widely in the analysis of strained molecules. For example, strained hydrocarbons play a very important role as bioorthogonal reagents. Specifically, cyclooctynes and *trans*-cyclooctenes are used as reactive reagents for copper-free click reactivity in biological media. A previous Houk group analysis¹⁰⁴ noted that a strain energy based analysis fails to accurately predict molecular reactivity and instead used a distortion/interaction model¹⁰⁵ to accurately predict reactivity. However, our novel analysis can correctly order the reactivity of these strained reagents using a local strain analysis. The analysis of cyclooctyne in Figure III.10

reveals 13.7 kcal/mol of strain whereas *trans*-cyclooctene has 17.4 kcal/mol both have nearly the same proportion (42% and 41%) located at the reactive site. This is in agreement with the relative rate of reaction with a tetrazine of 30 and 13,000 M⁻¹s⁻¹ respectively. Furthermore, when comparing the more reactive *trans*-bicyclo[6.1.0]nonene to *trans*-cyclooctene in Figure III.10, the total strain energy increases only slightly to 18.9 kcal/mol, however, the reaction rate increases 160 fold.¹⁰⁶ By increasing the macrocycle rigidity, the strain is shifted to the reactive alkene. The *trans*-cyclooctene has 7.2 kcal/mol of strain energy located in the alkene, whereas *trans*-bicyclo[6.1.0]nonene has 9.3 kcal/mol. This increases the reactivity more than would be predicted by total strain energy. Again, the StrainViz analysis provides the missing information that previous strain analyses lack. While this analysis does not provide accurate prediction of rates as the distortion/interaction model of the Houk group does,¹⁰⁵ it may be put to good use in informing the design of new strained bioorthogonal reagents by evaluating strain local to the reactive site.

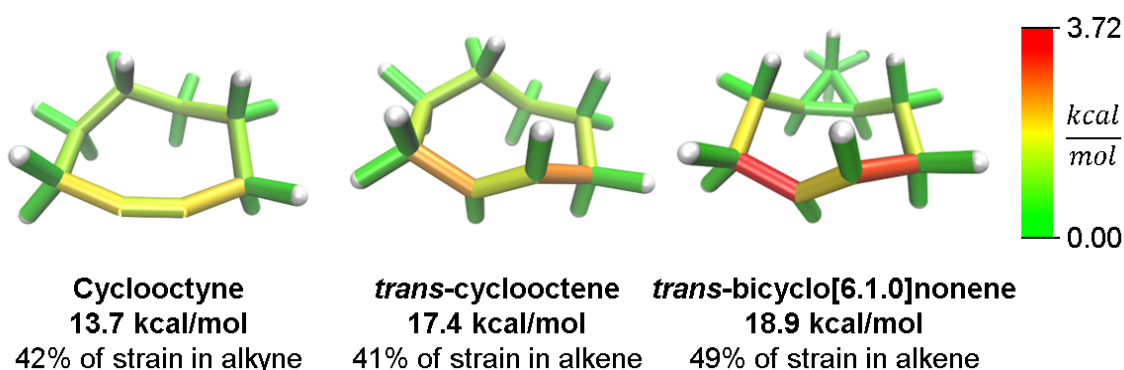


Figure III.10. Strain energy in copper-free click reagents. *Trans*-cyclooctene is more strained than cyclooctyne, but has similar strain distribution. Increasing rigidity by addition of a cyclopropyl fusion increases strain energy and shifts it to the reactive site.

III.5. Conclusions

A new computational method is reported for the determination of strain energy in macrocycles. This method improves on the current standard of using homodesmotic reactions to determine strain energy by locating contributions to the total strain. The robustness of the method was tested to show that fragment sizes of at least more than half of the molecule give accurate results. The method is accurate in that it delivers reasonable total strain energy relative to previous computational results. It is effective in strain promoted reaction prediction by successfully locating the site of bromination in unsymmetric molecules. Finally, a sampling of literature examples were analyzed with new insight gathered including design considerations for new strained bioorthogonal reagents. This new computational strain determination method is, therefore, broadly useful for the research of strained macrocycles.

III.6. Co-authored content

The work in Chapter 3 was co-authored with Tavis Price, Prof. Tim Stauch, and Prof. Ramesh Jasti and published under the title of “Strain Visualization for Strained Macrocycles” in *Chemical Science*.³⁷ I wrote the manuscript, performed all computational analyses, and wrote the StrainViz software. Tavis Price performed the synthesis and bromination of **m[6]CPP**. Prof. Tim Stauch provided crucial mentorship and edited the manuscript. Prof. Ramesh Jasti edited the manuscript.

III.7. Bridge to Chapter IV

The final frontier of carbon nanohoop research is their conversion into carbon nanotubes. With advanced synthetic methods we are better prepared for this challenge than ever before. Attempts have been made to grow carbon nanotubes directly from nanohoops and nanobowls with some success. However, the extension of nanohoops into nanobelts and finally into short nanotubes with precise structure requires a method to effect these transformations. In the next chapters, our attempts are documented.

CHAPTER IV
RING CLOSING METATHESIS FOR CONVERSION OF NANOHOOPS INTO
NANOBELTS

IV.1. Background

Attempts to grow carbon nanotubes from cycloparaphenylenes have been unsuccessful likely due to their being held together with single carbon-carbon bonds. It is possible to extend existing carbon nanotubes,¹⁰⁷ however, when these conditions are applied to cycloparaphenylenes¹⁰⁸ or small carbon bowls¹⁰⁹ carbon nanotubes of an exclusive size are not produced. Therefore, synthesis of slightly larger carbon nanotube fragments for use as seeds is proposed as a solution. The only successful growth of single type carbon nanotubes comes from platinum surface fused carbon bowls that grew into (6,6) carbon nanotubes.¹¹⁰ (Figure IV.1) Synthesis of larger carbon nanotube fragments, such as carbon nanobelts, and their attachment to surfaces are challenges restricting the use of cycloparaphenylenes as carbon nanotube templates.

Work in the Itami laboratory has prepared some carbon nanobelts,^{95,111} however, not from cycloparaphenylenes and, therefore, not in a way that generally extends a carbon nanotube edge. The Miao laboratory converted cycloparaphenylenes into carbon nanobelts using the Scholl reaction, however, only for [12]CPP and larger.¹¹² (Figure IV.2) Their key innovation was using two electron donating propoxy functional groups on each phenylene to facilitate oxidation of these functional groups. If these electron donating groups are not present the reaction does not proceed.^{18,113,114} These initial advancements into

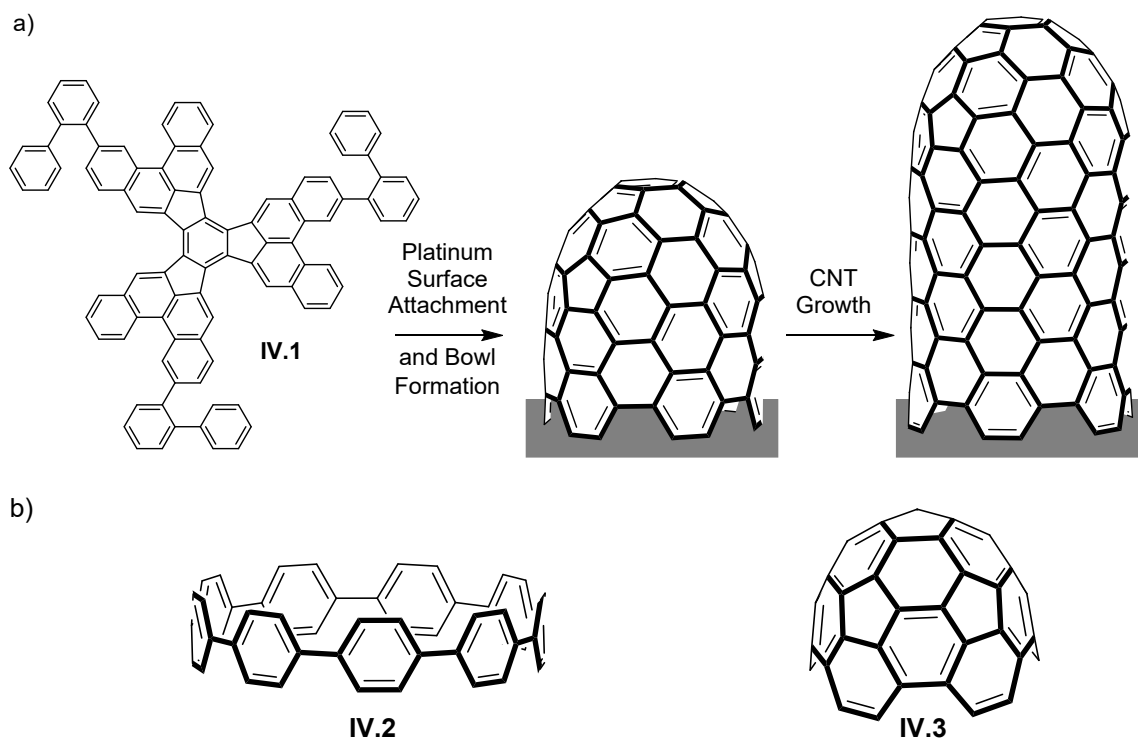


Figure IV.1. a) Exclusively (6,6) carbon nanotubes can be grown from a platinum surface bound carbon bowl. b) Other carbon nanotube seeds produce carbon nanotube mixtures centered around the template diameter.

carbon nanobelt synthesis are significant, but do not provide a general solution for carbon nanotube edge extension for all cycloparaphenylene sizes. Therefore, our laboratory seeks a general method for extending even small cycloparaphenylenes into carbon nanobelts.

Former laboratory members Dr. Tom Sisto and Prof. Matt Golder made progress toward this goal during their graduate work. Dr. Tom Sisto discovered how small cycloparaphenylenes could decompose in the presence of acidic or oxidizing conditions when attempting the Scholl reaction on a phenyl functionalized [8]CPP.¹⁸ Prof. Matt Golder was using ring closing metathesis to add new benzo fusions to a cycloparaphenylene.²⁷ Ring closing metathesis requires

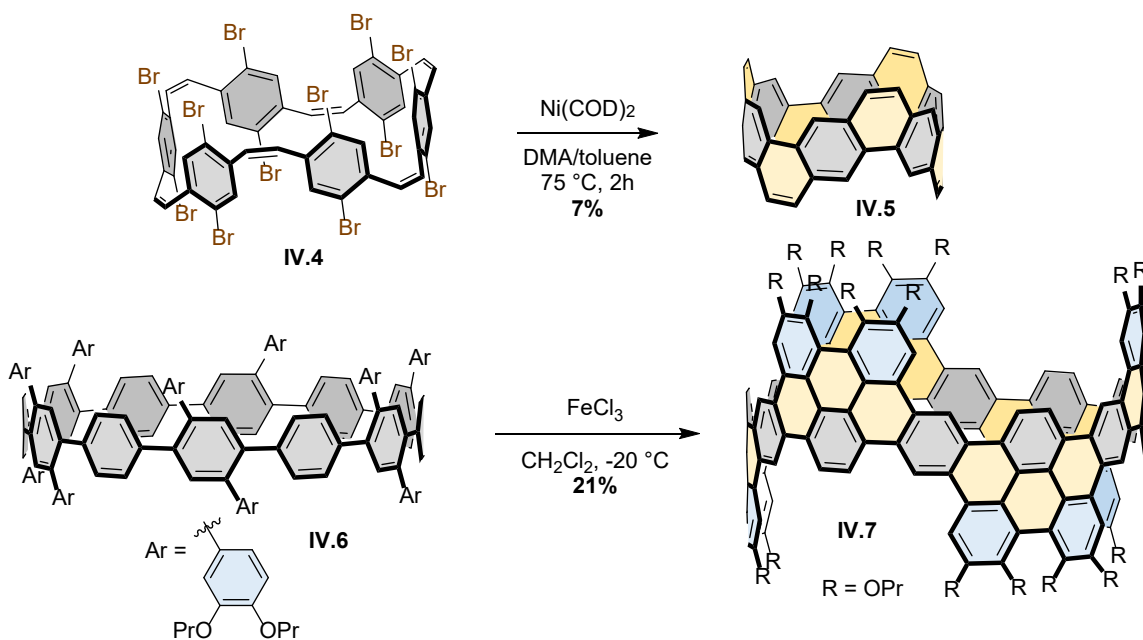


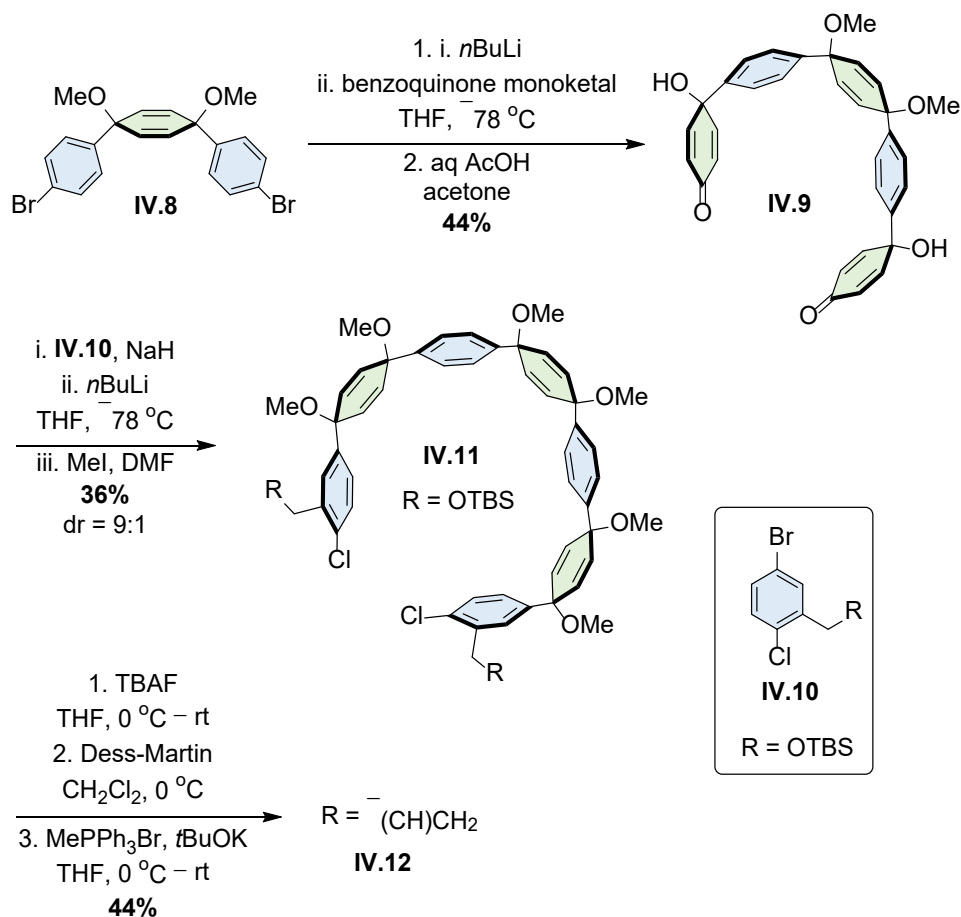
Figure IV.2. Synthesis of carbon nanobelts by the Itami and Miao laboratories.

extremely mild reaction conditions and therefore could be effective. Although problems arose when attempting to add significant quantities of functionalization,²⁶ [8]- and [9]CPP could be produced with significantly large belt fragments within them.

IV.2. Syntheses of partial belt cycloparaphenylenes

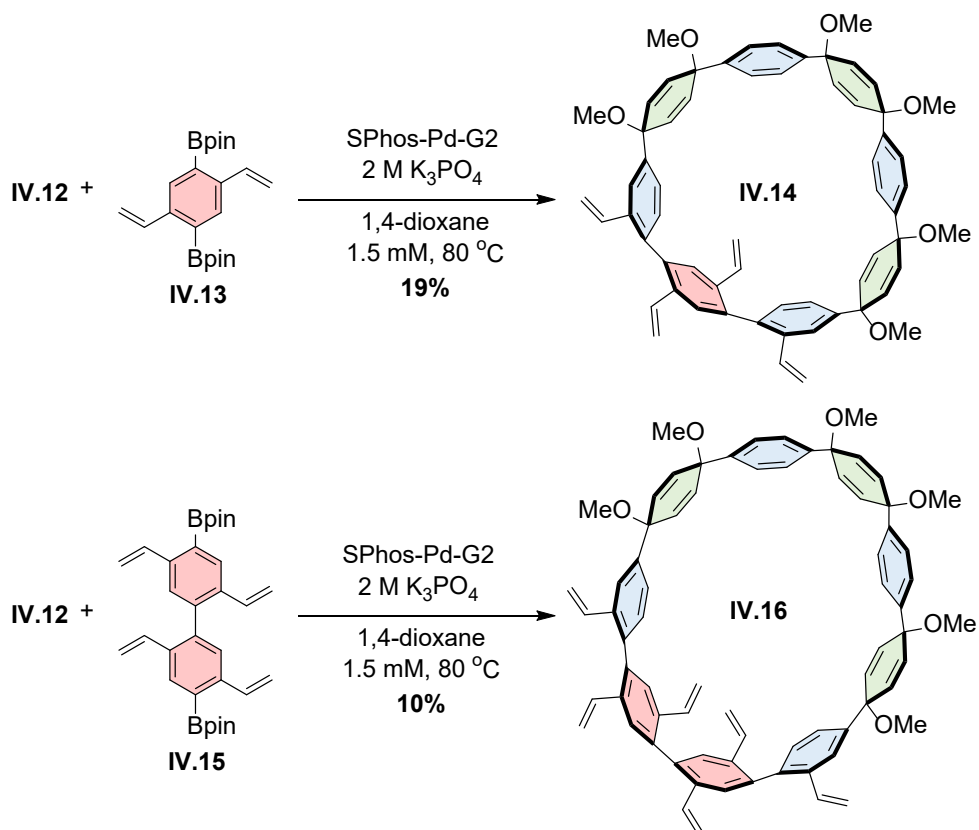
These cycloparaphenylenes were prepared by first synthesizing a protected benzyl alcohol functionalized macrocycle precursor. (Scheme IV.1) The benzyl alcohols were deprotected, oxidized to aldehydes, and reacted in a Wittig reaction to form vinyl groups. Then this vinyl functionalized macrocycle precursor underwent the macrocyclization reaction with coupling partners bearing even more vinyl functionality. (Scheme IV.2) Once the macrocycle is formed, the vinyl groups are converted by ring closing metathesis into new benzo fusions forming a large polycyclic aromatic hydrocarbon in the macrocycle. (Scheme IV.3) As the

conditions for this transformation are mild, the macrocycle does not risk decomposition. Finally, the macrocycle is converted into a cycloparaphenylene via reductive aromatization.

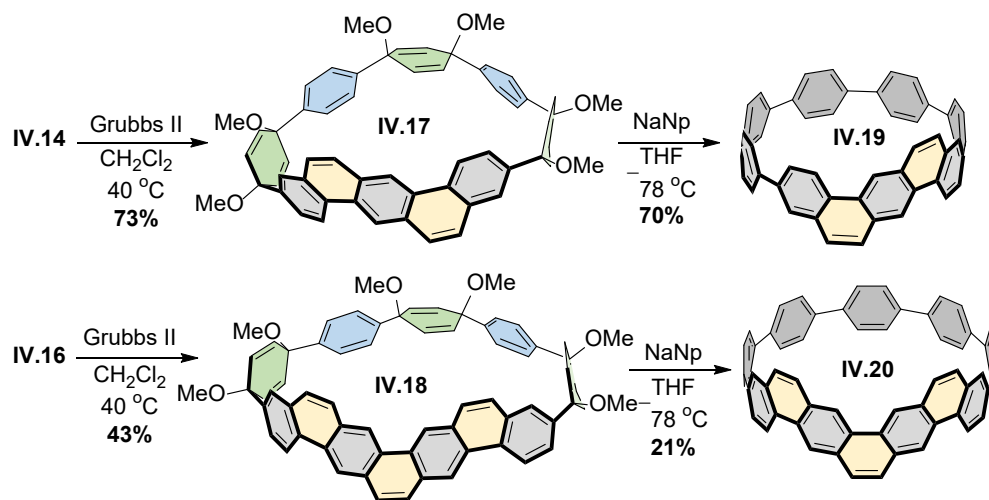


Scheme IV.1. Synthesis of cycloparaphenylene precursors having vinyl functional groups.

Although the [8]CPP and [9]CPP partial belt syntheses validated the basic ring closing metathesis/reductive aromatization approach, this strategy has limitations. First, the use of protected alcohols as vinyl surrogates is a cumbersome approach to the requisite alkenes. Furthermore, when the synthesis of [n]cyclophenacenes is considered, it was noted that functionalization is required on the cyclohexadiene rings,



Scheme IV.2. Synthesis of vinyl functionalized cycloparaphenylene precursor macrocycles.

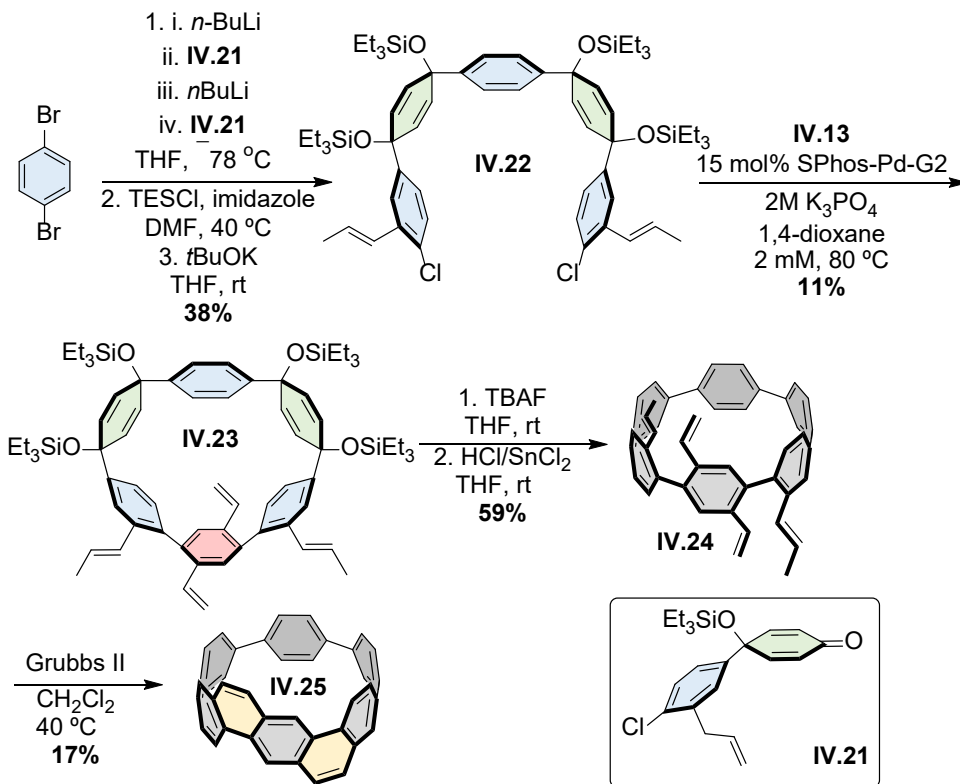


Scheme IV.3. Synthesis of partial nanobelts

leading to macrocyclic intermediates possessing multiple stereocenters.²⁶ In these cases, it is desirable to execute reductive aromatization prior to ring closing metathesis, thereby eliminating potential mismatched chirality between functionalized cyclohexadiene rings during the metathesis events. In addition to these points, we were curious if smaller, more highly strained belts could be accessed through this combination of reductive aromatization and ring-closing metathesis methodology.

A [6]CPP partial belt was targeted to investigate a second-generation methodology addressing these challenges. First, allyl groups were incorporated to **IV.21** as vinyl surrogates for the ring closing metathesis reaction (Scheme IV.4). Monolithiation of 1,4-dibromobenzene followed by subsequent addition of ketone **IV.21** yields an aryl bromide that undergoes a second lithiation followed by addition to a second equivalent ketone **IV.21** to rapidly provide a five-ring macrocycle precursor in one pot isolated as a single diastereomer. The crude diol is then protected using triethylsilyl chloride, followed by base catalyzed olefin isomerization to yield precursor **IV.22** in 38% yield over three steps.

Dichloride **IV.22** and bisboronate **IV.13** undergo Suzuki coupling under standard conditions to deliver macrocycle **IV.23** in 11% yield. The subsequent silyl deprotection followed by reductive aromatization under mild conditions recently reported by Yamago yields **IV.24**, with no evidence of styrene decomposition. Ring-closing metathesis then afforded **IV.25** in an unoptimized 17% yield. This second-generation approach, in which reductive aromatization is carried out prior to the ring closing metathesis reaction, provides a concise



Scheme IV.4. Synthesis of an extremely strained partial nanobelt

synthesis of the most strained of the three partial belt targets accessed.

Furthermore, the synthesis of **IV.24** addresses a longstanding problem with the functionalization of [n]CPPs by offering four substituents along the backbone with precise regiochemistry.

IV.3. Properties of partial belt cycloparaphenylenes

Together, these three partial belt cycloparaphenylenes represented, at the time, the largest belt segments synthesized in a cycloparaphenylene. When analysing the degree of bending that occurs for the large polycyclic aromatic hydrocarbons contained within these molecules by either X-ray crystallography or density functional theory, one may see that the **[8]-** and **[6]CPP** represent the most bent benzo[k]tetrapienes ever produced. (Figure IV.3) Only the Bodwell

laboratory's teropyrenophanes¹¹⁵ had similarly curved large polycyclic hydrocarbons prior to this report.

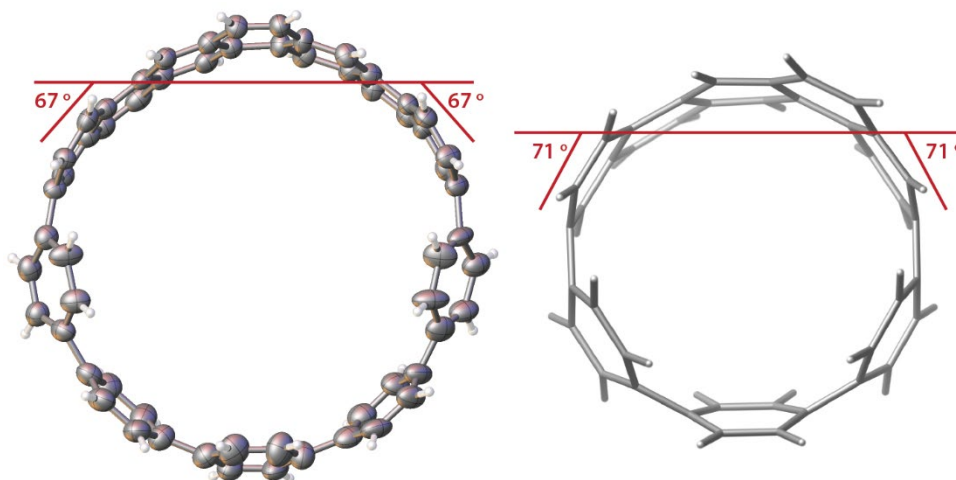


Figure IV.3. Deplanarization of the belt fragments in partial belt nanohoops.

The optical and electronic properties were surprisingly identical to the parent cycloparaphenylenes of each partial belt cycloparaphenylene synthesized. As is typical of cycloparaphenylenes, the properties do not match expectations. When adding additional conjugation one might expect that absorption and emission should red shift. However, these molecules display nearly identical absorption and emission as their parent cycloparaphenylenes. Analysis of frontier orbitals via density functional theory describe reasonably well why this is. Orbital density for the HOMO and LUMO resides primarily on the cycloparaphenylene core and not on the benzo fusions. For this reason, the levels of the HOMO and LUMO remain nearly identical. Therefore, the fluorescent emission and the redox potentials remain consistent. Only in the absorption spectrum are there minor differences. (Figure IV.4) This is due to the major absorption consisting of

transitions between non-frontier molecular orbitals which do have asymmetry and localization due to additional benzo fusions.

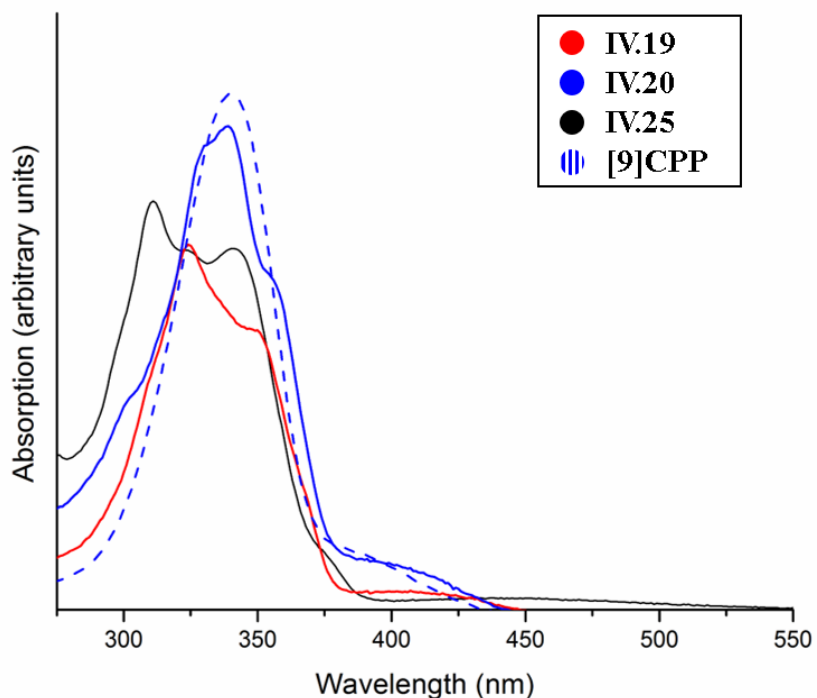
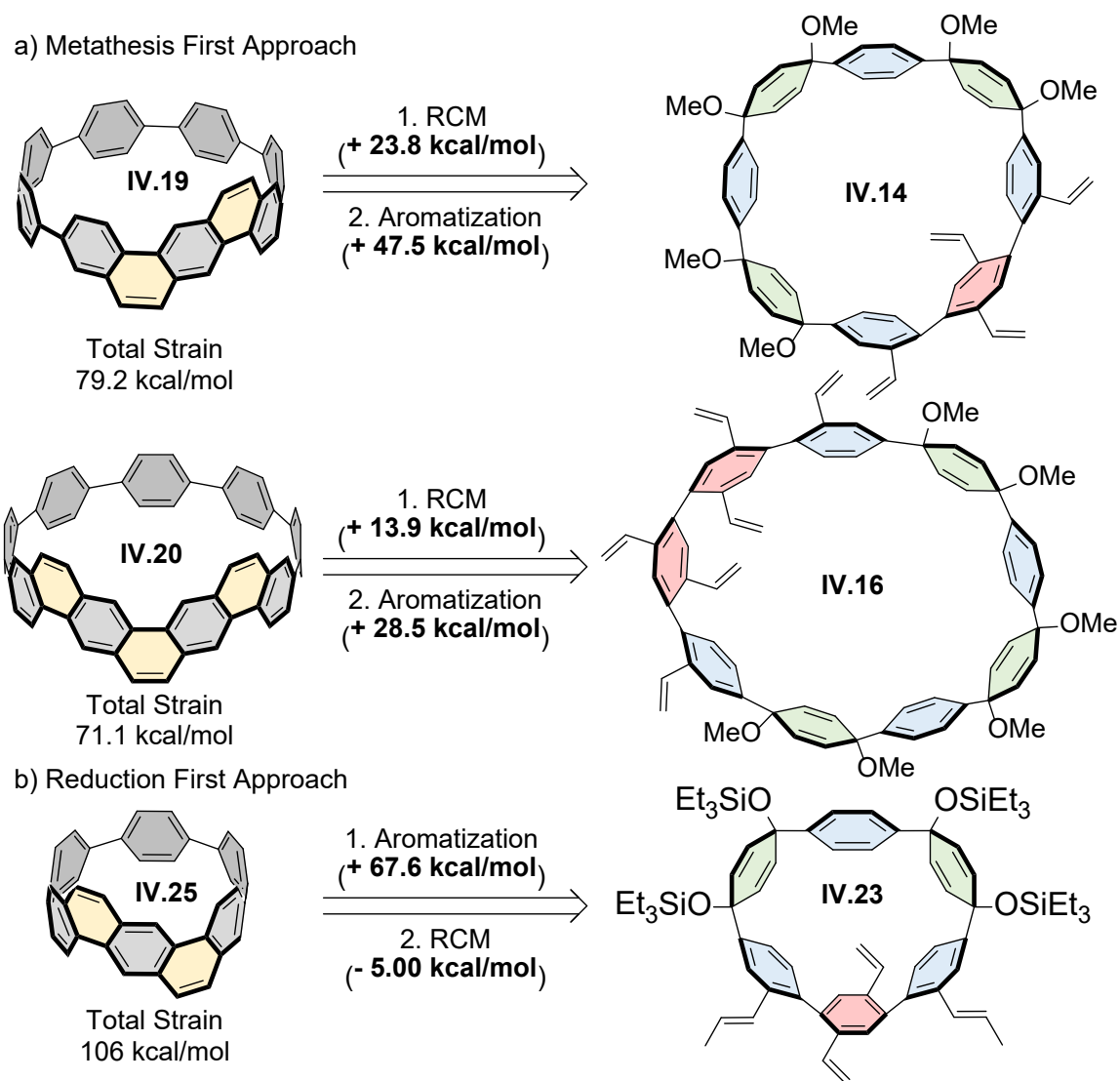


Figure IV.4. UV-vis spectra of partial belt nano hoops **IV.19**, **IV.20**, **IV.25**, and **[9]CPP**.

Strain is incorporated into these molecules in a fascinating way throughout the synthesis. We evaluated the strain energies of **IV.19**, **IV.20**, **IV.25**, and corresponding precursors computationally using homodesmotic reactions.

Gaussian09⁸⁸ at the ω B97D/6-31G(d) level of theory was used. (Scheme IV.5) We first determined that **IV.19** has 79.2 kcal/mol of strain energy, while **IV.20** has 71.1 kcal/mol of strain energy relative to acyclic counterparts. The smallest of our belt fragments, **IV.25**, has a strain energy of 106 kcal/mol. Interestingly, these values are only 5–9 kcal/mol higher than their parent [8]-, [9]-, and **[6]CPP** analogues which have 72, 66, and 97 kcal/mol of strain energy, respectively.



Scheme IV.5. Strain energy changes during aromatization and ring closing metathesis.

Evaluation of penultimate macrocycles **IV.17** and **IV.18** indicates that the powerful reductive aromatization step builds in 47.5 kcal/mol of strain (31.5 kcal/mol \rightarrow 79 kcal/mol) and 28.5 kcal/mol of strain (42.6 kcal/mol \rightarrow 71.1 kcal/mol) in the formation of **IV.19** and **IV.20**, respectively. More importantly, however, ring closing metathesis is able to build in 23.8 kcal/mol (7.75 kcal/mol \rightarrow 31.5 kcal/mol) and 13.9 kcal/mol (28.7 kcal/mol \rightarrow 42.6 kcal/mol) of strain energy during the transformations of **IV.14** \rightarrow **IV.17** and **IV.16** \rightarrow **IV.18**,

respectively. Hence, in these cases, ring-closing metathesis acts in conjunction with the Suzuki–Miyaura macrocyclization and sodium naphthalenide promoted reductive aromatization to allow for a gradual increase in strain energy. We next evaluated the energy landscape of our second-generation approach. Interestingly, in this case, the ring-closing metathesis event is a strain relieving process rather than a strain building process. Upon building in 43.4 kcal/mol during the macrocyclization step in the synthesis of **IV.23**, reductive aromatization afforded **IV.24**, a molecule with almost as much strain energy as **[5]CPP** (111 kcal/mol versus 119 kcal/mol).

We attribute the high strain energy of **IV.24** to unfavourable steric interactions between *ortho*–*ortho* groups forced into close proximity with one another due to the rigid geometry of such a small macrocycle. Finally, ring closing metathesis of **IV.24** afforded **IV.25**, which is 5 kcal/mol less strained than its penultimate intermediate (111 kcal/mol → 106 kcal/mol). Now that we have StrainViz, it is possible to locate this strain. (Figure IV.5) Using this tool, we can see that the strain in the tetra functionalized cycloparaphenylene is localized on the side with the additional functional groups. Once the ring closing metathesis is performed, the opposite occurs where now the strain is spread across the polycyclic aromatic hydrocarbon and more localized in the opposite side.

IV.4. Towards nanobelt synthesis using ring closing metathesis

These partial belt molecules are stepping stones towards the eventual goal of converting cycloparaphenylenes into nanobelts. In these first molecules, we incorporated the functional groups strategically. The alkene groups are

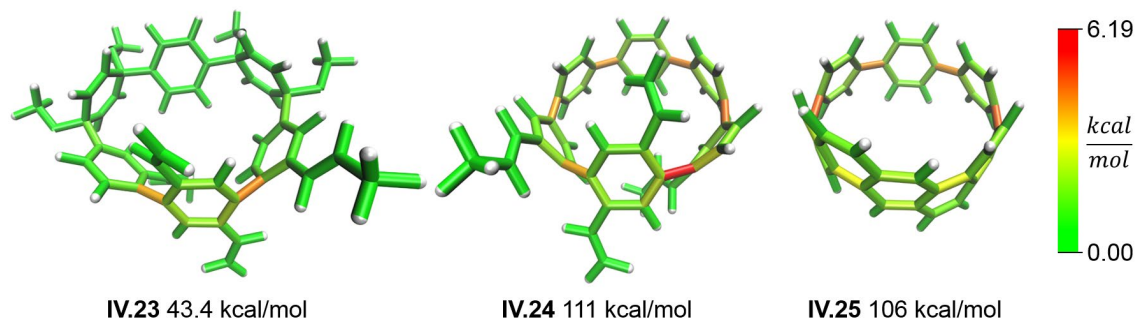


Figure IV.5. Strain map of molecules involved in synthesis of partial belt **IV.25**.

incorporated onto the ends of the coupling partner with cyclohexadienes and the Suzuki coupling partner. These positions are the easiest to functionalize, whereas closer to the cyclohexadienes is far more challenging to functionalize. Adding functional groups near the cyclohexadiene is a long standing challenge. Nanobelt synthesis using ring closing metathesis requires two functional groups per phenylene in a cycloparaphenylene. A typical cycloparaphenylene synthesis requires benzoquinone, lithiate, and Suzuki coupling partners. Using the new methodology prepared for the synthesis of **IV.25**, it is certainly possible to add two allyl groups to each of these starting materials. However, there are significant problems that arise the least of which being the massive synthetic undertaking required.

Adding an additional two or three steps at the outset of an already long cycloparaphenylene synthesis results in a ballooning of synthetic effort required. Furthermore, the formation of *cis*-diarylcyclohexadienes is hampered by steric bulk on the lithiate. The *trans*-diarylcyclohexadiene is instead preferred resulting in a maximum yield of 50% in a 1:1 mixture of *cis* and *trans*.²⁶ (Figure IV.6) Even if *cis*-diarylcyclohexadienes are obtained, coupling to any other *cis*-

diarylcyclohexadiene results in a diastereomeric mixture that significantly complicates characterization of intermediates. This is only if the coupling occurs efficiently. Steric bulk adds an additional challenge to the Suzuki couplings required, especially the macrocyclization where the molecule must adopt a conformation that is even less preferred with the addition of steric bulk. For these reasons, an alternative method for introducing the necessary functional groups would greatly facilitate the realization of the intended targets.

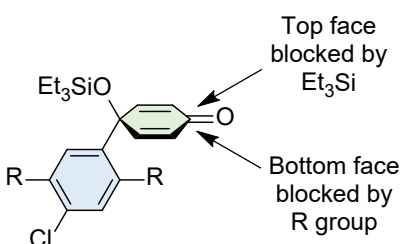


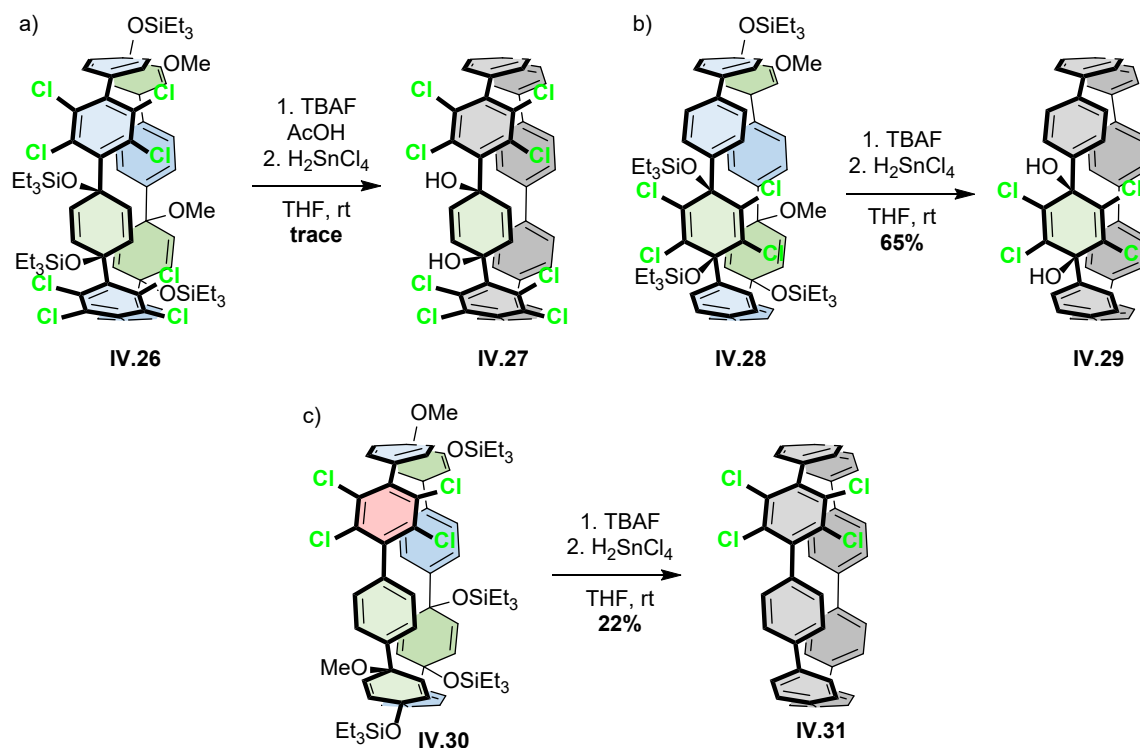
Figure IV.6. Size of R group dictates stereochemistry of the addition reaction.

IV.5. Chlorinated cycloparaphenylenes

If one were to imagine the smallest possible masked functional group, the eventual arrival at chloride is inevitable. No other functional group combines the requisite stability, reactivity, and steric size. For this reason, chloride functionalized cycloparaphenylenes were targeted with the intent to use palladium catalysed reactions to convert chlorinated cycloparaphenylenes into whatever functional group desired. Not only do chlorides meet stringent requirements as masked functionality, but also all building blocks required for chlorinated cycloparaphenylene synthesis are commercially available or produced in a single step. Therefore, a number of cycloparaphenylene building blocks were prepared with significant chlorination.

Using these building blocks, a series of [8]CPP precursor macrocycles were prepared with distinct molecular motifs. When tetrachlorobenzene was used in place of 1,4-dibromobenzene to produce octochlorinated precursors, the aromatization resulted in decomposition of the macrocycle due to the ability of the tetrachlorophenylene to act as a leaving group. (Scheme IV.6a) During synthesis of this building block, macrocycle deprotection, and this aromatization step, this was a problem. In the aromatization, the molecule has a choice between the hydroxide or the tetrachlorophenylidene group and in this case chooses the tetrachlorophenylidene. When chloranil was substituted for benzoquinone, the aromatization reaction proceeded with each cyclohexadiene except for the chlorinated cyclohexadiene. (Scheme IV.6a) This was confirmed by X-ray crystallography of the partially aromatized macrocycle. Finally, when the tetrachlorophenylene is Suzuki coupled into the macrocycle, the aromatization works. (Scheme IV.6c)

From this, we can at least see that producing chlorinated cycloparaphenylenes is not trivial. Years after this work, the Yamago laboratory had similar trouble with the aromatization of a tetrafluorinated cyclohexadiene and developed more potent aromatization conditions that presumably would also reduce tetrachlorinated cyclohexadienes.¹¹⁶ However, even if this reductive aromatization were possible, using polychlorinated cycloparaphenylenes as precursors to polyalkene functionalized cycloparaphenylenes is not currently possible, as the ring closing metathesis strategy requires functional groups on every single phenylene. Despite these results, producing chlorinated



Scheme IV.6. Incorporating chlorinated phenylenes and cyclohexadienes into cycloparaphenylene synthesis. a) Perchlorinated lithiate. b) Perchlorinated benzoquinone. c) Perchlorinated Suzuki coupling partner.

cycloparaphenylenes may still be a solution for both the ring closing metathesis strategy and as a potential method to fix cycloparaphenylenes to surfaces for carbon nanotube growth. By substituting tetra- for dichlorinated precursors it may be possible that dichlorination will have a lesser effect on the electronics of the precursors and allow formation of the required cycloparaphenylenes.

IV.6. Co-authored content

The ring-closing metathesis work in Chapter 4 was co-authored with Prof. Matthew Golder, Prof. Bryan Wong, Dr. Lev Zakharov, Jingxin Zhen, and Prof. Ramesh Jasti and published under the title “Iterative Reductive Aromatization/Ring-Closing Metathesis Strategy toward the Synthesis of Strained

Aromatic Belts” in the *Journal of the American Chemical Society*.²⁷ Prof. Matthew Golder performed the synthesis and characterization of molecules **IV.19** and **IV.20**, wrote the manuscript and coordinated all parties. I synthesized and characterized molecule **IV.25**. Prof. Bryan Wong provided computational analysis. Dr. Lev Zakharov solved the crystal structures. Jingxin Zhen synthesized molecular precursors. Prof. Ramesh Jasti edited the manuscript.

IV.7. Bridge to Chapter V

The challenges of using ring closing metathesis are primarily prohibitive due to the required quantity of functional groups. A potential solution is the discovery of reactions that require fewer functional groups to effect the same transformation. This concept is explored in the following chapter.

CHAPTER V

REDUCING REQUIRED FUNCTIONALITY FOR NANOHOOP CONVERSION INTO A NANOBELT

V.1. Background

In order to reduce the required number of functional groups, the functional groups that are attached must be able to react with the neighbouring unfunctionalized phenylenes. For example, when the Scholl reaction is used, it fuses an appended phenylene to a neighbouring unfunctionalized phenylene in the cycloparaphenylene. If ring closing metathesis is used, it requires a functional group to phenylene ratio of 2:1 whereas the Scholl reaction requires a 1:1 ratio. (Figure V.1) Conversion of cycloparaphenylenes into nanobelts would be made easier by discovering reactions that require less than a 1:1 ratio and occur under conditions amenable to even small cycloparaphenylenes.

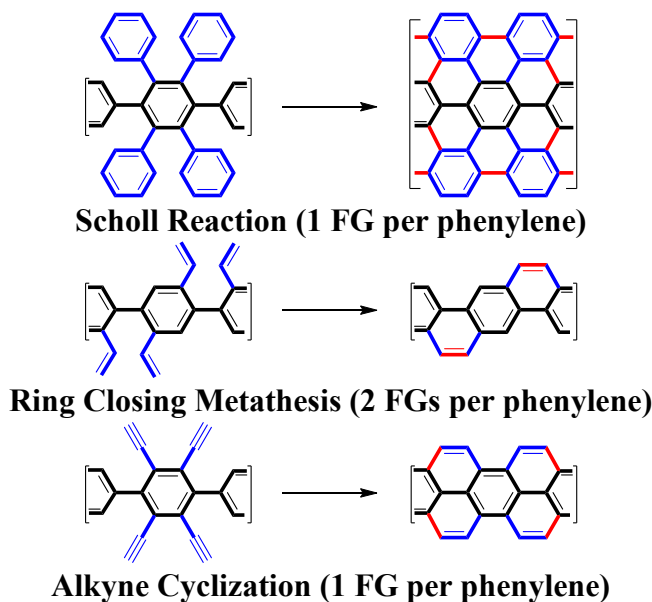


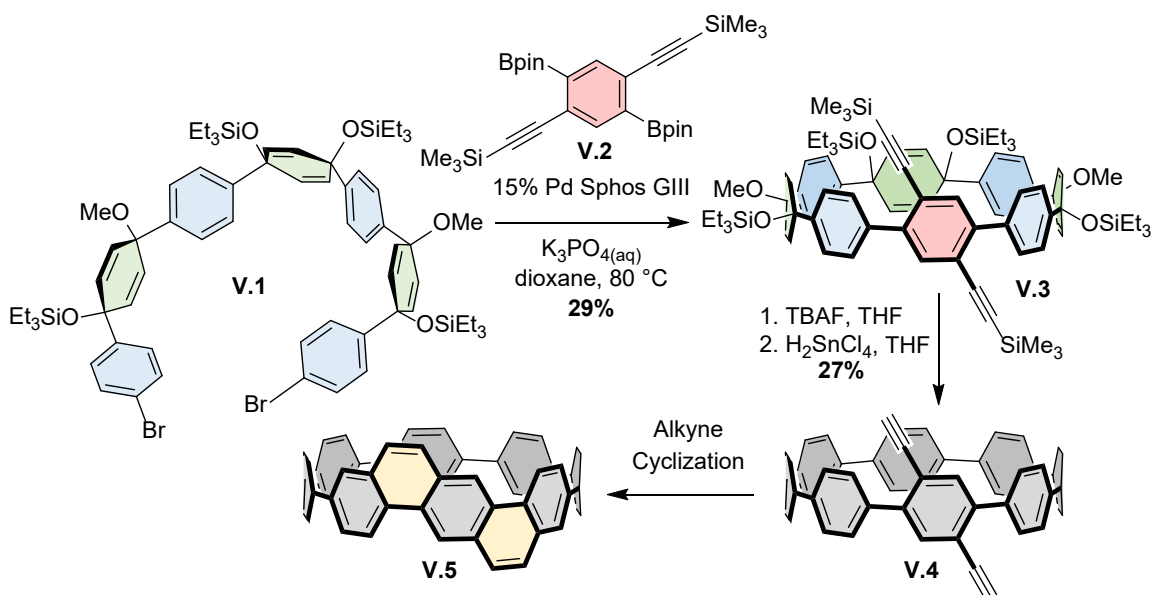
Figure V.1. π system extending reactions and their ratio of minimum functional groups to phenylenes.

In the Scholl reaction, the neighbouring phenylene acts as a nucleophile leading to carbocationic character and therefore decomposition for smaller strained cycloparaphenylenes¹⁸ and only works when highly activated pendant phenylenes are used on **[12]CPP** and larger.¹¹² If C-H activation could occur in place of this, it may be milder. Alkyne cyclization may proceed via noble metal catalysis to isomerize a terminal alkyne into a new benzo fusion. This requires no change in unsaturation which is highly desirable for mild benzo fusion.

V.2. Alkyne cyclization

The dibenzo-fused **[8]CPP** previously prepared using ring closing metathesis is a good known target.²⁷ To prepare this molecule, a diethynyl **[8]CPP** is prepared and alkyne cyclization converts it to the target molecule. First, a macrocycle was prepared via Suzuki cross coupling of **V.1** with **V.2**. (Scheme V.1) Then, deprotection and aromatization of macrocycle **V.3** yields the diethynyl **[8]CPP V.4**. Alkyne cyclization conditions were tested on this substrate. (Table V.1) Recently, acid catalyzed acylation proved effective on a functionalized **[9]CPP**,¹¹⁷ however, in our case only decomposition was observed using these and milder conditions. As an alternative, platinum(II) chloride was attempted as it has been effective for this transformation with planar substrates.¹¹⁸ Gratifyingly, platinum(II) chloride worked efficiently to deliver the dibenzo-fused **[8]CPP**. Unfortunately, this reaction is quite sluggish. Therefore, more exotic ruthenium catalysts^{119–121} were used to deliver the alkyne cyclized cycloparaphenylene at a much quicker rate. It should be noted that increasing the temperature expedites the reaction, however, at a certain point decomposes the cycloparaphenylene

dependent on the inherent strain. With appropriate alkyne cyclization conditions in hand, more complicated systems were targeted to push the methodology.



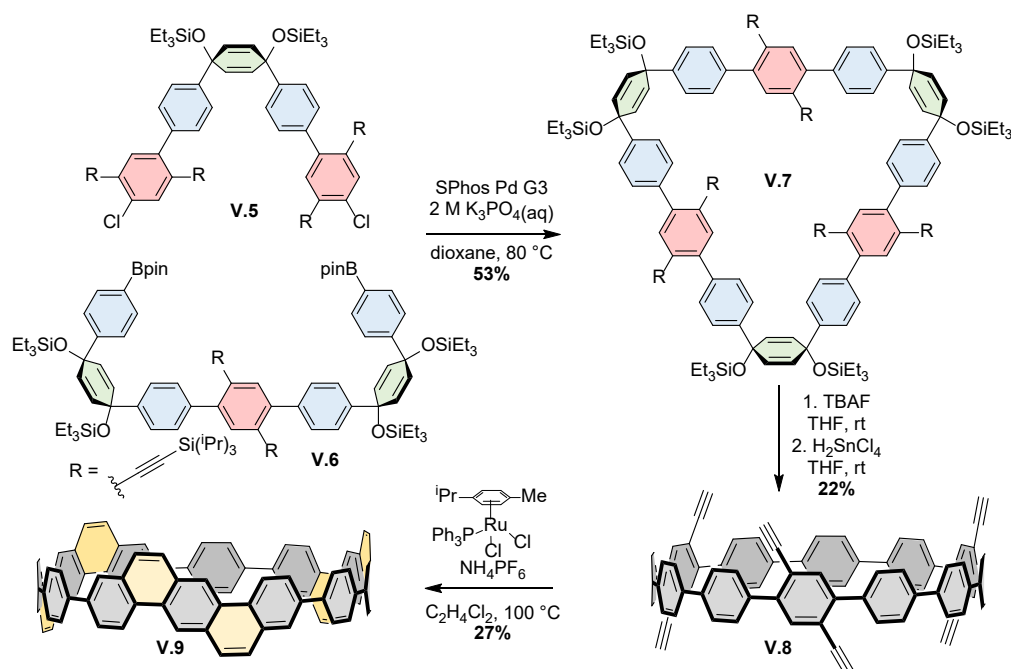
Scheme V.1. Synthesis of cycloparaphenylene **V.4** and alkyne cyclization to partial nanobelt **V.5**.

Catalyst	Solvent	Temperature	Time	Yield
Triflic acid	CH_2Cl_2	25 °C	1 h	0%
Trifluoroacetic acid	CH_2Cl_2	25 °C	1 h	0%
(cymene)Ru(PPh ₃)Cl ₂	$C_2H_4Cl_2$	100 °C	18 h	75%
TpRu(PPh ₃)(MeCN) ₂ PF ₆	$C_2H_4Cl_2$	100 °C	6 h	80%
PtCl ₂	toluene	85 °C	2 days	64%

Table V.1. Catalysts for alkyne cyclization.

Using the conditions optimized for diethynyl [8]CPP **V.4**, a cycloparaphenylene having a large amount of alkynes was targeted. A [12]CPP having six alkynes has half the required functional groups to make a carbon nanobelt. (Scheme V.2) The resulting molecule **V.9** consists of three benzo[k]tetraphene units separated by phenylenes in the macrocycle. To realize this

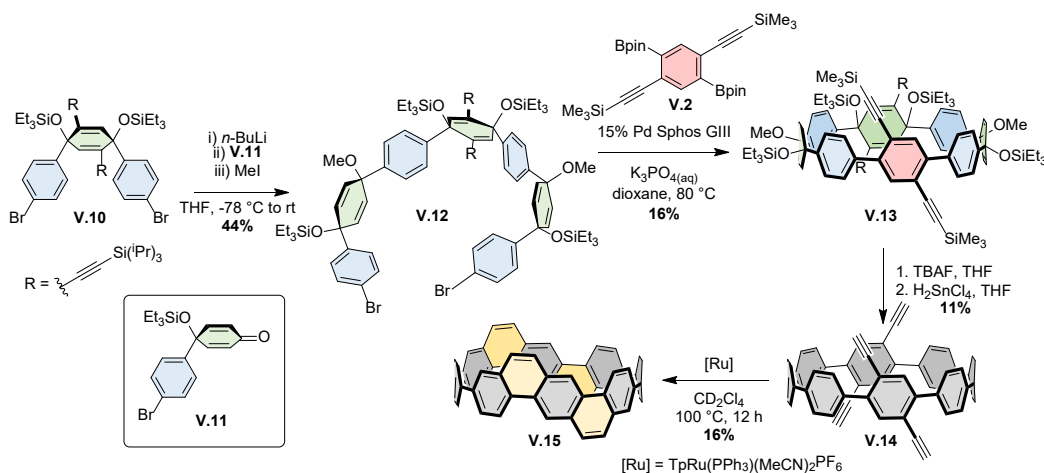
target, a modular synthesis was employed where corner pieces **II.4** and **II.5** are coupled to alkyne functionalized pieces **D.1** and **D.4** to create precursors **V.5** and **V.6** with the desired functional groups. Macrocyclization yielded **V.7** that was deprotected and aromatized to yield **V.8**, a **[12]CPP** bearing six alkynes. The optimized ruthenium catalyzed alkyne cyclization conditions then afforded **V.9**, half nanobelt, half nanohoop.



Scheme V.2. Synthesis of cycloparaphenylene **V.8** and alkyne cyclization to partial nanobelt **V.9**.

Unfortunately, using current methodology it is not possible to completely fuse every phenylene in the cycloparaphenylene to make an aromatic belt. The previously described methods incorporated functionality only at positions far from the cyclohexadiene in the precursors. To synthesize an aromatic belt, it must be possible to functionalize other positions on the cycloparaphenylene. Therefore, our next target to push the methodology further is an **[8]CPP** bearing four ethynyl

functional groups. (Scheme V.3) When looking back at our previous functionalized **[8]CPP**, incorporating two more ethynyl groups symmetrically requires functionalizing the central cyclohexadiene of **V.1**. To this end, a TIPS ethynyl functionalized benzoquinone equivalent was synthesized and after two lithiation addition reactions produced **V.10**. After alcohol protection, this dibromide was lithiated using *n*-BuLi and ketone **V.11** was added to each end followed by *in situ* methylation. This molecule is now nearly identical to **V.1** with the exception of two protected alkynes. Suzuki macrocyclization with ethynyl functionalized diboronate **V.2** afforded macrocycle **V.13** which has the four necessary protected ethynyl groups. Deprotection and aromatization yielded tetraethynyl functionalized **[8]CPP** **V.14**. Alkyne cyclization yields a second, more strained, half nanohoop half nanobelt **V.15**.



Scheme V.3. Synthesis of **V.14** and alkyne cyclization to partial nanobelt **V.15**.

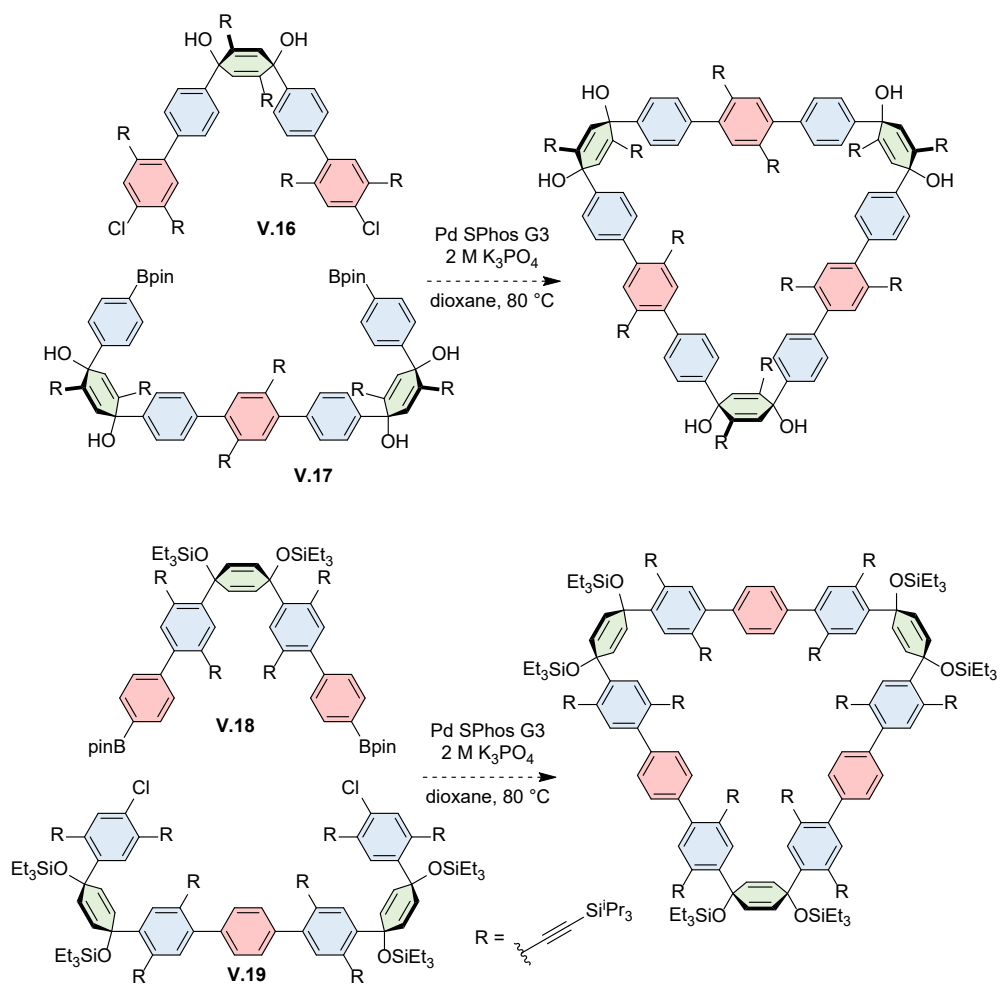
V.3. Highly alkyne functionalized intermediates

As alluded to previously, it was not possible to incorporate enough functional groups onto the cycloparaphenylene to convert it into a nanobelt. Highly functionalized precursors were prepared, however, macrocyclization could never

provide any material that resembled the desired product. Two strategies were tested, one where 1,4-dibromobenzene was alkyne functionalized and one where both the benzoquinone and Suzuki coupling partners were alkyne functionalized.

Using benzoquinone functionalization as developed for **V.15**, the requisite coupling partners **V.16** and **V.17** were produced, however, the macrocyclization did not occur. (Scheme V.4) Functionalizing lithiates (coloured blue) with alkynes added an additional challenge in that the lithiate addition to ketone **D.14** favours the *trans*- over the *cis*-diarylcyclohexadiene. Therefore, the reactions were performed at room temperature to get the maximum 50% yield for the reaction. The lithiate was prepared at -78 °C and transferred by cannula into a solution of ketone **D.14** at room temperature. The *cis* isomer was then separated by column chromatography as the more polar compound in the mixture. This prepared the requisite coupling partners **V.18** and **V.19** to prepare a [12]CPP with twelve alkynes, however, upon macrocyclization, no product could be isolated. These results indicate that these protected alkynes are too sterically large to accommodate formation of a macrocycle. Examination of a van der Waals radius representation reveals the extreme steric requirements of the alkyne protecting groups. (Figure V.2) Unfortunately, a compromise between alkyne stability and protecting group size was not found where the alkynes could survive to the macrocyclization step and the macrocyclization could proceed.

However, internal alkynes (propynyl, phenylethynyl, etc.) are far too unreactive. This is likely due to a change in mechanism. The terminal alkyne forms a ruthenium vinylidene intermediate that then performs an isomerization reaction



Scheme V.4. Macrocyclization attempts with highly functionalized precursors.

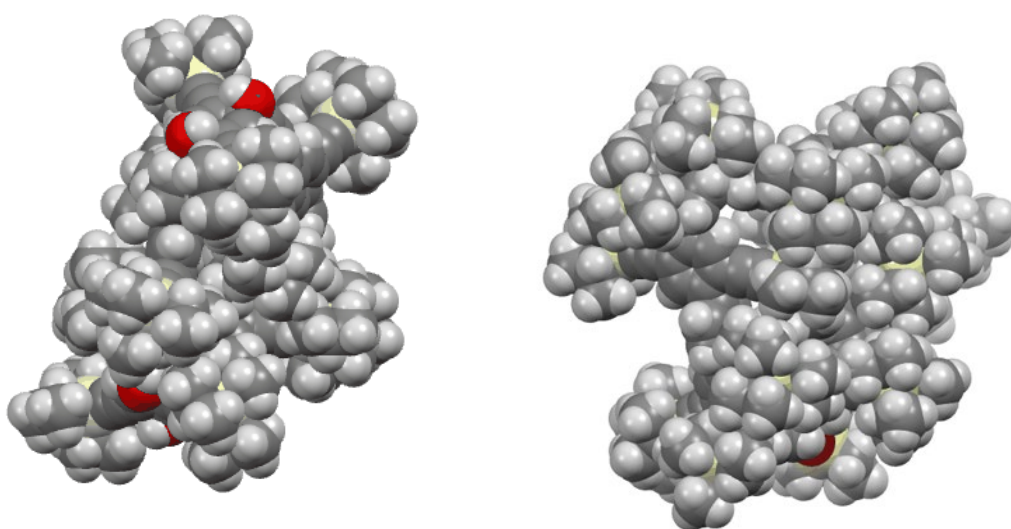


Figure V.2. Van der Waals radius models of desired macrocycles from Scheme V.4.

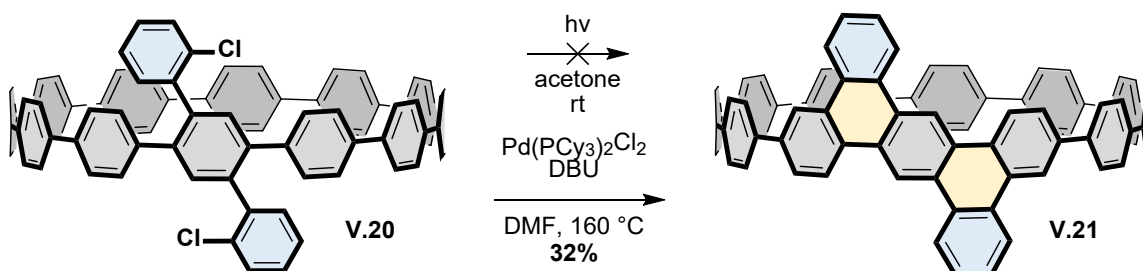
transferring a hydride from the adjacent phenylene to the ruthenium. This pathway is not available to internal alkynes and instead the metal simply complexes with the alkyne to activate it requiring higher temperatures to cross this higher energy transition state where the adjacent phenylene acts as a nucleophile similar to the Scholl reaction strategy.

V.4. Cyclodehydrochlorination

In 2016, the Morin laboratory discovered a highly efficient photoinitiated cyclodehydrochlorination reaction for the synthesis of nanographenes.¹²² Using chlorinated polymers, this reaction formed graphene nanoribbons with high efficiency.¹²³ If applied to cycloparaphenylenes, these highly efficient reactions would convert cycloparaphenylenes into nanobelts in high yields. Incorporating 2-chlorophenyl groups would require a phenylene to functional group 1:1 ratio as the protected alkynes do, however, with smaller steric size.

A test system **V.20** with just two 2-chlorophenyl groups was synthesized via similar methodology used for alkyne functionalized cycloparaphenylenes. A 1,4-dibromobenzene was functionalized with 2-chlorophenyl groups and incorporated into a **[12]CPP** synthesis. Even though the reaction was performed with a **[12]CPP** which is relatively unstrained, the reaction does not occur under the conditions used for planar systems. (Scheme V.5) This could be due to either the low lying LUMO providing a route for photoexcitation to be radiated away or the rigidity of the required transition state being enthalpically forbidden. In either case, heating the reaction to 110 °C allowed the reaction to likely take place forming the large aromatic hydrocarbon, however, with a commensurate decomposition releasing the strain present. Decomposition may be due to a

necessary carbocationic intermediate following electrocyclization, however, research is underway to find milder methods for effecting this transformation in the Morin group and may yet effect this transformation.



Scheme V.5. 2-chlorophenylene functionalized cycloparaphenylene **V.20** for testing cyclodehydrochlorination conditions to produce **V.21**.

Alternatively, one may consider palladium catalysed cyclodehydrochlorination. In this case, palladium undergoes oxidative addition followed by C-H insertion and reductive elimination of HCl to yield a seven membered palladacycle. Reductive elimination yields the desired transformation. Using this method, the 2-chlorophenyl functional group was converted into the desired product at 160 °C. Due to the strain in the cycloparaphenylene, the reaction proceeded slower than for planar systems requiring longer times and higher temperatures. This is in stark contrast to what was hoped for with cyclodehydrochlorination, a high yielding reaction proceeding at room temperature. However, the reaction can be added to a short list of cycloparaphenylene amenable reactions.

V.5. Zipping up chlorinated oligophenylenes onto cycloparaphenylenes

In addition to fusing to the adjacent phenylene, cyclodehydrochlorination could go further. Fusing the next phenylene simply requires adding additional

chlorinated phenylenes to the end of the appended functional group. The first cyclodehydrochlorination reaction sets up the additional cyclodehydrochlorination reactions. Theoretically, a single long chlorinated oligophenylene could undergo many cyclodehydrochlorination reactions and directly synthesize nanobelts from singly functionalized cycloparaphenylenes. (Figure V.3)

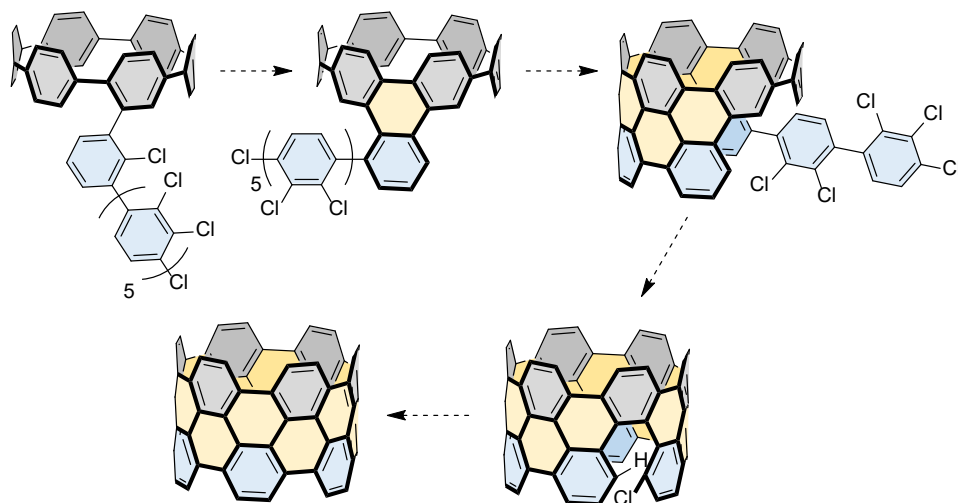
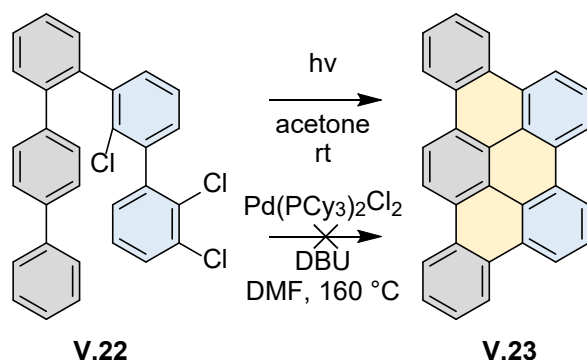


Figure V.3. Concept for zipping chlorinated oligophenylenes onto cycloparaphenylenes.

To test this concept, chlorinated oligophenylenes are required. 2,2',3,3'-trichlorobiphenyl-3-boronic pinacol ester was prepared and Suzuki coupled with 2-bromoterphenyl. Using the photoinitiated cyclodehydrochlorination conditions, this test system could be converted into nanographene **V.23**. (Scheme V.6)

However, palladium catalysis does not perform the same transformation. Instead, a complex mixture is produced. Unfortunately, the conditions that perform multiple sequential cyclodehydrochlorination reactions do not work with cycloparaphenylenes and the conditions that work with cycloparaphenylenes do not perform multiple sequential cyclodehydrochlorination reactions. Therefore, in collaboration with the Morin laboratory, we are testing milder reaction conditions

amenable to fusing chlorinated oligophenylenes to realize our goal of synthesizing nanobelts from singly functionalized cycloparaphenylenes.

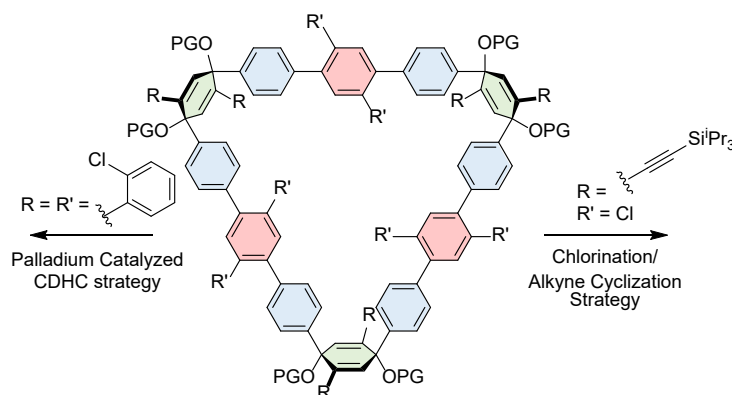


Scheme V.6. Planar molecule for testing multiple sequential cyclodehydrochlorination reactions.

V.6. Future outlook

By combining all the research performed one may arrive at strategies that combine the partially successful tactics. We established methods to functionalize every position on a cycloparaphenylene precursor macrocycle and have a reasonably sized arsenal of phenylene fusing reactions. Although extremely efficient and mild, ring closing metathesis is not immediately on the table due to the extreme functional group requirements. However, two reasonable strategies do come to mind. Simply replacing the bulky protected alkynes in section V.3 with 2-chlorophenyl groups could deliver carbon nanobelts by palladium catalyzed cyclodehydrochlorination. This would be a slightly milder method than the Scholl reaction used in the Miao laboratory¹¹² and deliver a totally unfunctionalized carbon nanobelt. The second reasonable strategy involves combining chlorination and alkyne cyclization. It is possible to functionalize the cyclohexadienes with alkynes and the Suzuki coupling partners with chlorides to deliver the required quantity of functional groups following Sonogashira coupling of the

remaining alkynes. This circumnavigates the steric problems seen earlier. Exploring functionalization via alkyne cyclization and chlorination in addition to discovering the cyclodehydrochlorination tactic has enabled new strategies for carbon nanobelt synthesis.



Scheme V.7. Future possible carbon nanobelt formation strategies.

V.7. Co-authored content

This chapter includes unpublished content that involved inputs from others. William A. Edgell and Tara Clayton help synthesize alkyne functionalized cycloparaphenylenes. Thaís de Faria helped synthesize **V.20**. Prof. Tobias Schaub developed and performed synthesis of **V.22**.

V.8. Bridge to Chapter VI

Synthesis of these cycloparaphenylenes did not yield a route converting cycloparaphenylenes into nanobelts. However, the methodology developed allows the synthesis of highly functionalized cycloparaphenylenes. These functionalized cycloparaphenylenes are useful for more than just nanobelt synthesis. The next chapter will detail uses for alkyne functionalized cycloparaphenylenes.

CHAPTER VI

APPLICATIONS OF FUNCTIONALIZED CYCLOPARAPHENYLENES

VI.1. Background

Alkyne functionality is highly useful due to its relative stability despite high reactivity in certain reactions. For example, alkynes are used in azide-alkyne cycloaddition reactions in biology due to both coupling partners reacting orthogonally to endogenous chemistry found in biology.^{67,124–126} This reaction falls under the category of “Click” reactions due to its high yield, wide scope, and synthetic ease.^{127,128} Additionally, alkynes are used in conjugated polymers due to available p orbitals.^{129,130} For these reasons, alkyne functionalized cycloparaphenylenes are highly useful for application into new areas.

There are numerous reactions available to alkynes some of which are shown in Figure VI.1. As mentioned above, the azide-alkyne cycloaddition is used. There are now multiple examples of cycloparaphenylenes in which phenylenes are replaced with alkynes in order to form a strained alkyne.^{31,32} Depending on the cycloparaphenylene size, and therefore strain on the alkyne, these molecules undergo reaction with azides without the need of a catalyst. Terminal alkynes could also be involved in Diels-Alder reactions^{131–133} or deprotonated and added into electrophiles.¹³⁴

VI.2. Producing conjugated polymers from cycloparaphenylenes

Conjugated polymers can be produced by reacting diethynyl monomers with dihalogenated monomers.¹³⁰ Therefore, the diethynyl cycloparaphenylenes from the previous chapter can be retooled to act as monomers. In collaboration

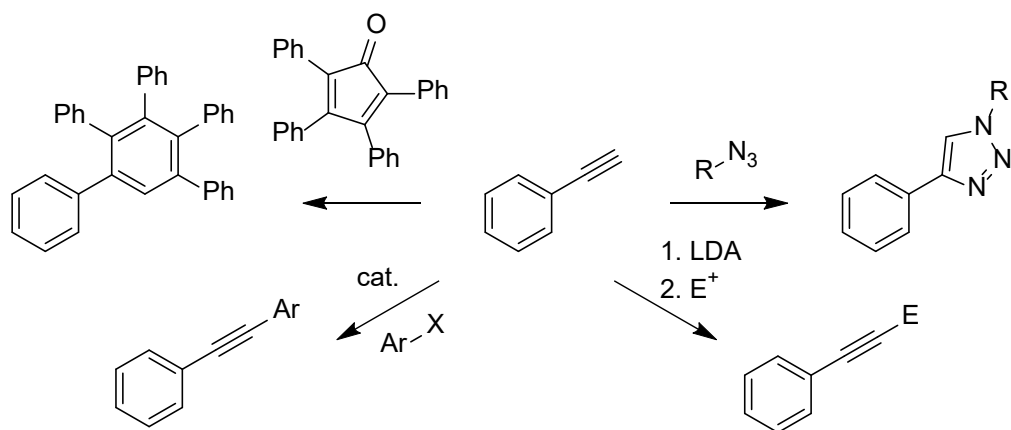
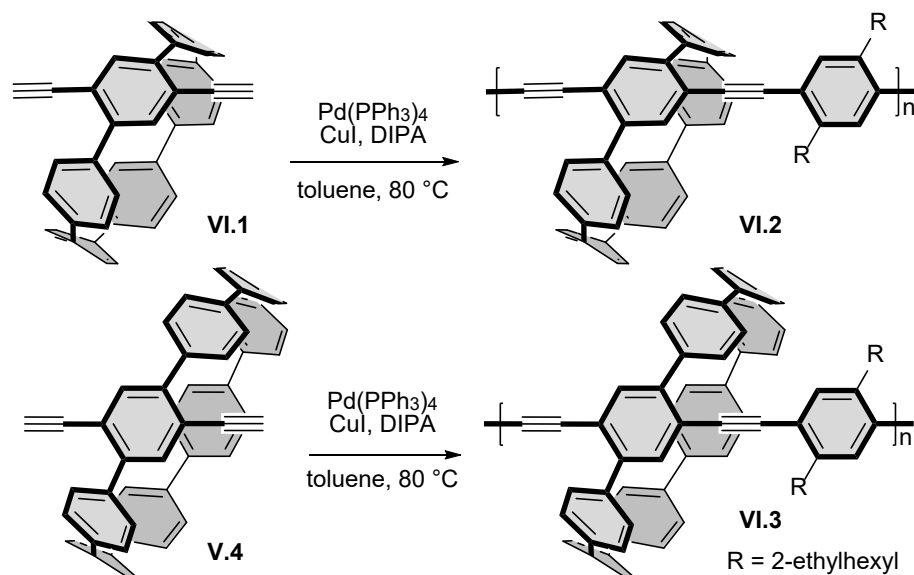


Figure VI.1. Reactions available to terminal alkynes

with laboratory member Ruth Maust and the Tovar laboratory, **VI.1** and **V.4** were synthesized and incorporated into conjugated polymers **VI.2** and **VI.3**. (Scheme VI.1) These polymers are unique in that they have both a path of linear conjugation, as all conjugated polymers do, and a path of cyclic conjugation. Polymers were prepared with thiophene and phenylene cross coupling partners via Sonogashira cross coupling.

VI.3. Optoelectronic properties of cycloparaphenylene conjugated polymers

Study of cycloparaphenylene polymers by UV-vis spectroscopy demonstrated properties unlike either cycloparaphenylenes or poly(phenylene ethynylene). (Figure VI.2) Overlaying these three spectra, one clearly sees absorption by cycloparaphenylene polymers further into the red than either monomers or non-cycloparaphenylene polymers. This is true for every polymer containing **[6]-** or **[8]CPP** and phenylene or thiophene monomers. This indicates conjugation between cyclic cycloparaphenylenes and the linear polymer. A poly(phenylene ethynylene) appears necessary as, simultaneously, cycloparaphenylene polymers consisting of a polyphenylene backbone synthesized



Scheme VI.1. Synthesis of polymers with cyclic and linear conjugation pathways.

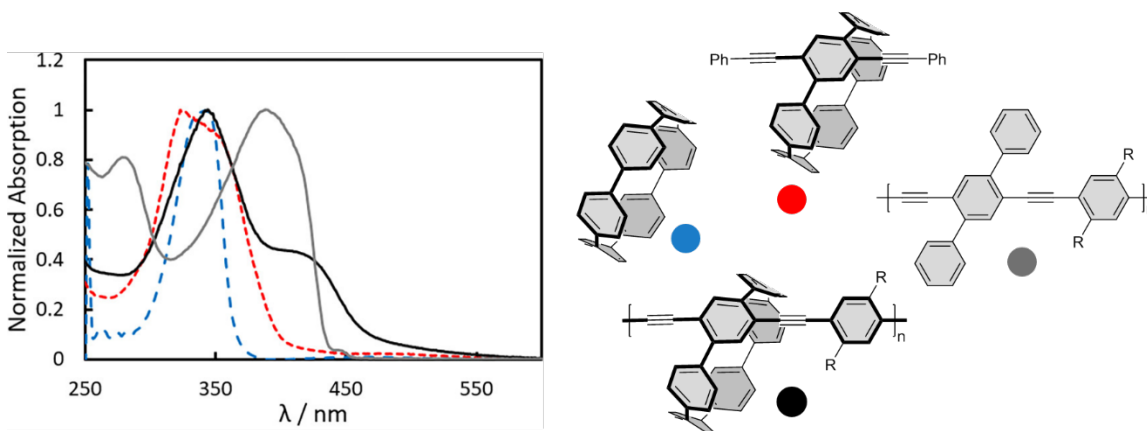


Figure VI.2. UV-vis spectra of cycloparaphenylene polymers relative to poly(phenylene ethynylene) polymers and cycloparaphenylenes.

in the Du laboratory had nearly identical photophysical properties to cycloparaphenylenes.¹³⁵

In collaboration with the Kertesz laboratory, we investigated why this was occurring in our polymers and not in polyphenylene polymers. The ethylene spacers are clearly causing the effect, but why? It appears that the ethynylene

spacers both allow better conjugated π system planarization and are at a higher oxidation state than the phenylenes resulting in a lower lying LUMO. From a frontier molecular orbital analysis of the polymers, we see that the HOMO resides primarily within individual appended cycloparaphenylenes, whereas the LUMO is primarily on the linear polymer. (Figure VI.3) This highlights an important feature of using strain to tune properties of a molecule. Whereas electron withdrawing or donating groups lower the LUMO or raise the HOMO respectively, introducing strain brings the two orbitals together simultaneously.

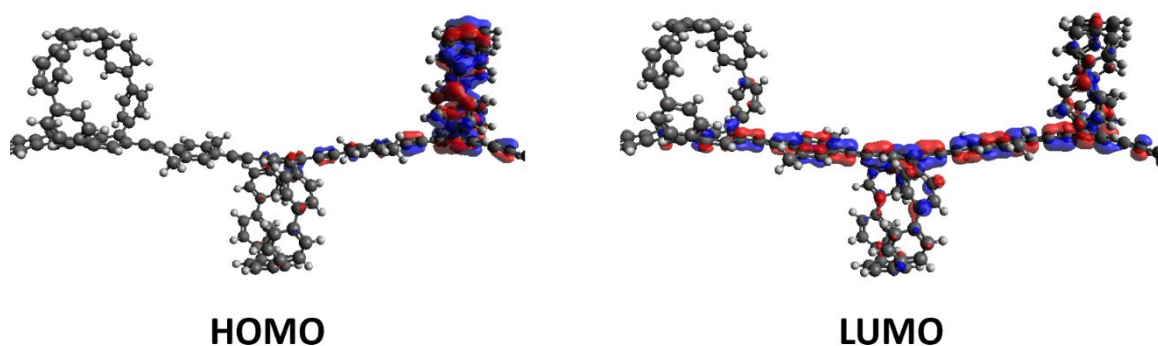


Figure VI.3. Frontier molecular orbitals for cycloparaphenylene oligomer.

From this alone, it is apparent why the polyphenylene cycloparaphenylene polymers do not exhibit novel photophysical properties. A cycloparaphenylene can be thought of as an infinite polyphenylene and behaves surprisingly very similar to one at large cycloparaphenylene sizes. As the size of the cycloparaphenylene decreases the strain increases and the HOMO raises while the LUMO lowers to meet it resulting in the emblematic red shifting emissive properties. If the HOMO and LUMO energies of a cycloparaphenylene and polyphenylene are overlaid, it is clear that the combined frontier molecular orbitals have properties nearly identical to the cycloparaphenylene monomer used. (Figure VI.4) However, when the

HOMO and LUMO energies of a cycloparaphenylene and poly(phenylene ethynylene) are overlaid, it is clear that the HOMO should centre on the cycloparaphenylene and the LUMO should centre on the polymer.

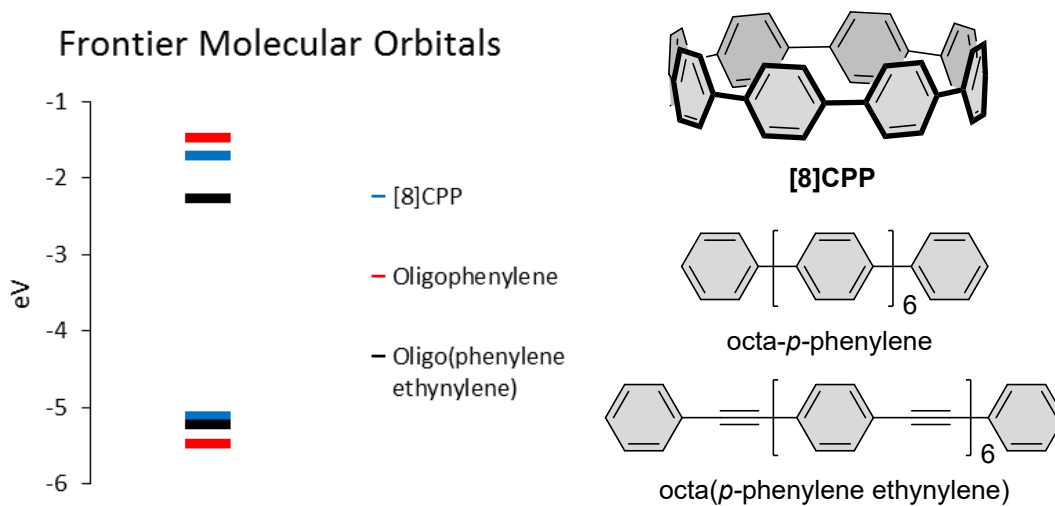


Figure VI.4. Frontier molecular orbital levels of [8]CPP, octa-*p*-phenylene, and octa(*p*-phenylene ethylene)

VI.4. Co-authored content

The polymer research in Chapter 5 was co-authored with Garvin Peters, Girishma Grover, Ruth Maust, Haley Bates, William A. Edgell, Prof. Ramesh Jasti, Prof. Miklos Kertesz, and Prof. John D. Tovar and published under the title “Linear and Radial Conjugation in Extended pi-Electron Systems” in the *Journal of the American Chemical Society*.³⁸ Garvin Peters performed polymerizations and characterized the polymers. Girishma Grover performed calculations on these polymers. Ruth Maust and William A. Edgell synthesized cycloparaphenylene monomers. Prof. Ramesh Jasti edited the manuscript. Prof. Miklos Kertesz edited the manuscript. Prof. John D. Tovar wrote the manuscript and coordinated the project.

VI.5. Bridge to Conclusion

These unique emergent properties upon cycloparaphenylene application in conjugated polymers highlight the urgency to apply them in various contexts. cycloparaphenylene functionalization is, therefore, very important for applying them. Advancing our methods for incorporating ethynyl groups developed in Chapter V facilitates this application.

CHAPTER VII

CONCLUSION

The current state of cycloparaphenylene technology has allowed significant application of cycloparaphenylene properties. Key innovations have allowed new functionality targeting significant challenges. This has enabled quick synthesis of the series of *meta*-cycloparaphenylenes that applied optoelectronic theory to provide new fluorophores. It has allowed the preparation of a host of cycloparaphenylenes with functionality that may convert them into nanobelts. These new functional cycloparaphenylenes can further apply cycloparaphenylene properties widely. Analysing their strain has enabled the productive exploitation of strain in all strained molecules. With this thesis, and our other works, there are significant advances in cycloparaphenylene technology that will apply them widely and successfully.

APPENDIX A

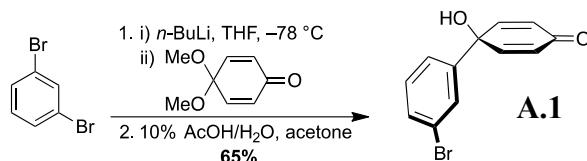
SUPPLEMENTARY INFORMATION FOR CHAPTER II

A.1. Experimental Details.

All glassware was flame dried and cooled under an inert atmosphere of nitrogen unless otherwise noted. Moisture sensitive reactions were carried out under nitrogen atmosphere using Schlenk and standard syringe/septa techniques. Tetrahydrofuran, dichloromethane, dimethylformamide and 1,4-dioxane were dried by filtration through alumina according to the methods describes by Grubbs.¹³⁶ Silica column chromatography was conducted with Zeochem Zeoprep 60 Eco 40-63 μm silica gel. Automated flash chromatography was performed using a Biotage Isolera One. Recycling gel permeation chromatography (GPC) was performed using a Japan Analytical Industry LC-9101 preparative HPLC with JAIGEL-1H/JAIGEL-2H columns in series using CHCl_3 . Thin Layer Chromatography (TLC) was performed using Sorbent Technologies Silica Gel XHT TLC plates.

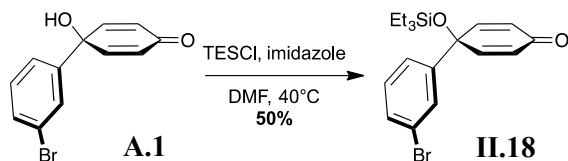
Developed plates were visualized using UV light at wavelengths of 254 and 365 nm. ^1H NMR spectra were recorded at 500 MHz or 600 MHz on a Bruker Advance-III-HD NMR spectrometer. ^{13}C NMR spectra were recorded 150 MHz on a Bruker Advance-III-HD NMR spectrometer. All ^1H NMR spectra were taken in CDCl_3 (referenced to TMS, δ 0.00 ppm) or $\text{DMSO}-d_6$ (referenced to residual DMSO, δ 2.50 ppm). All ^{13}C NMR spectra were taken in CDCl_3 (referenced to chloroform, δ 77.16 ppm) or $\text{DMSO}-d_6$ (referenced to DMSO, δ 39.52 ppm). Mass spectra were obtained from the University of Illinois at Urbana-Champaign Mass Spectrometry Lab using EI, ESI, ASAP, or MALDI or from University of Oregon CAMCOR using ASAP. HRMS was attempted for all

compounds, but when not successful, LRMS is reported. Absorbance and fluorescence spectra were obtained in a 1 cm Quartz cuvette with dichloromethane using an Agilent Cary 100 UV-Vis spectrometer and a Horiba Jobin Yvon Fluoromax-4 Fluorimeter. Fluorescent quantum yield was measured in dichloromethane at room temperature using a Hamamatsu absolute PL quantum yield measurement system. Fluorescence lifetimes were measured in dichloromethane using a Horiba Jobin Yvon TempPro Fluorescence Lifetime System. A LUDOX® prompt was used and decay curves were fit to a single exponential function. Electrochemical experiments were performed using a Biologic SP-50 potentiostat with a Ag wire reference electrode, Pt wire counter electrode, and glassy carbon working electrode under nitrogen atmosphere in 100 mM solutions of Bu₄NPF₆ in dichloromethane with ferrocene as a reference. All reagents were obtained commercially unless otherwise noted. Compounds *para*-benzoquinone mono-methyl ketal¹³⁷, **II.1**⁵², **II.2**⁵³, PPh₃ Pd G3 and SPhos Pd G3¹³⁸ were prepared according to literature procedure.



A.1. 1,3-dibromobenzene (4.3 mL, 35.7 mmol, 1.1 eq) was added to a 500 mL round bottom flask equipped with a stir bar. The reaction flask was capped with a septa, evacuated and refilled with nitrogen. Tetrahydrofuran (51 mL) was cannulated to the reaction flask, which was cooled to $-78\text{ }^\circ\text{C}$ over 30 min. *n*-BuLi (13.6 mL, 34.1 mmol, 1.05 eq, 2.5 M in hexanes) was added to the reaction mixture dropwise over 10 min. This was followed by the dropwise addition of *para*-benzoquinone monomethyl ketal (4.6 mL, 32.4 mmol, 1 eq) and the reaction stirred at $-78\text{ }^\circ\text{C}$ for 1 h. The reaction was quenched

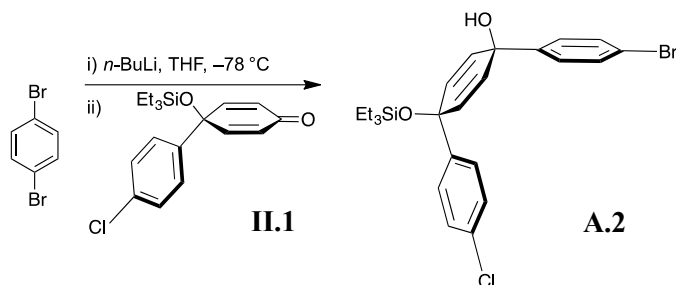
with deionized water (20 mL) at $-78\text{ }^{\circ}\text{C}$ and warmed to room temperature. The product was extracted with EtOAc (3 x 20 mL) and washed with brine (30 mL). The organic layers were dried over sodium sulfate, decanted and concentrated to yield the protected product as a slightly yellow solid. The protected product was dissolved in a minimal amount of acetone (20 mL) and a 10% acetic acid solution in water (20 mL) was added. This was stirred at room temperature for 1 h. The reaction was quenched with a saturated solution of sodium bicarbonate (50 mL). The product was extracted with EtOAc (3 x 20 mL), washed with brine (20 mL), dried over sodium sulfate and concentrated to yield the crude product as an orange solid. The product was purified by trituration with hexanes and ethanol to give **A.1** as an off white solid (5.588 g, 65% over 2 Steps). IR (neat) $1659, 1610\text{ cm}^{-1}$; $^1\text{H NMR}$ (600 MHz, Chloroform-*d*) δ 7.67 (t, $J = 1.9\text{ Hz}$, 1H), 7.46 (d, $J = 7.9\text{ Hz}$, 1H), 7.37 (d, $J = 7.9\text{ Hz}$, 1H), 7.25 (t, $J = 7.9\text{ Hz}$, 1H), 6.87 (d, $J = 10.0\text{ Hz}$, 2H), 6.23 (d, $J = 10.0\text{ Hz}$, 2H), 3.04 (s, 1H). $^{13}\text{C NMR}$ (151 MHz, Chloroform-*d*) δ 185.60, 150.34, 140.99, 131.53, 130.45, 128.54, 127.19, 124.04, 123.09, 70.58. HRMS (ESI-TOF) (m/z): $[\text{M}+\text{H}]^+$ calculated for $\text{C}_{12}\text{H}_{10}\text{BrO}_2$, 264.9864; found, 264.9871.



II.18. **A.1** (5.588 g, 26.7 mmol, 1 eq) and imidazole (5.74 g, 84.3 mmol, 4 eq) were added to a 250 mL round bottom flask equipped with a stir bar and septum.

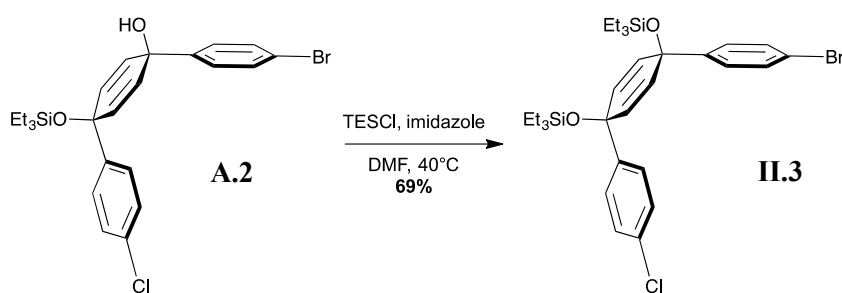
Dimethylformamide (105 mL) was added to the flask followed by triethylsilyl chloride

(4.2 mL, 89.8 mmol, 1.2 eq). The reaction mixture was heated to 40 °C in an oil bath and stirred overnight. The reaction mixture was cooled to room temperature and quenched with a saturated solution of sodium bicarbonate (30 mL). The product was extracted with EtOAc (3 x 100 mL) and washed with 5% lithium chloride solution in water (3 x 100 mL). The organic layers were dried over sodium sulfate and concentrated to yield the crude product as a yellow oil. The product was purified by automated flash silica gel chromatography (0% to 10% EtOAc in hexanes) to give **II.18** as a slightly yellow oil (4.0 g, 50%). IR (neat) 2954, 2875, 1670, 1631 cm⁻¹; ¹H NMR (600 MHz, Chloroform-*d*) δ 7.60 (t, *J* = 1.9 Hz, 1H), 7.42 (ddd, *J* = 7.9, 2.0, 1.0 Hz, 1H), 7.34 (ddd, *J* = 7.9, 1.8, 1.1 Hz, 1H), 7.21 (t, *J* = 7.9 Hz, 1H), 6.79 (d, *J* = 10.0 Hz, 2H), 6.24 (d, *J* = 10.0 Hz, 2H), 0.98 (t, *J* = 8.0 Hz, 9H), 0.66 (q, *J* = 7.9 Hz, 6H). ¹³C NMR (151 MHz, CDCl₃) δ 185.59, 151.35, 142.46, 131.10, 130.25, 128.60, 126.93, 124.08, 122.88, 72.70, 6.90, 6.22. HRMS (ESI-TOF) (*m/z*): [M+H]⁺ calculated for C₁₈H₂₄BrO₂Si, 379.0729; found, 379.0732.



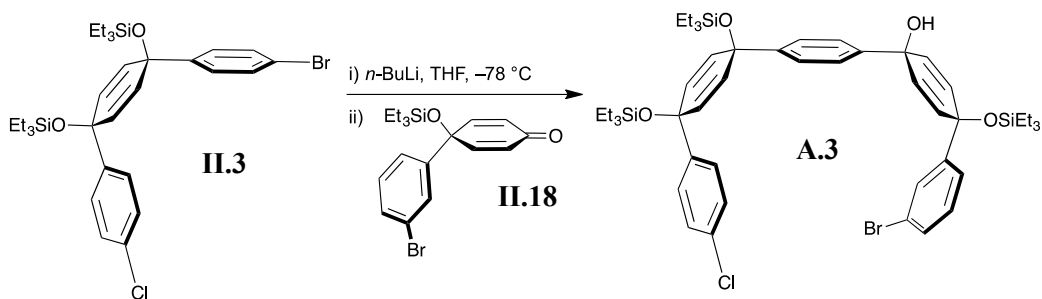
A.2. 1,4-dibromobenzene (3.9 g, 16 mmol, 1.1 eq) was added to a 100 mL round bottom flask equipped with a stir bar and septa. The flask was evacuated and filled with nitrogen. Tetrahydrofuran (23 mL) was added to the flask and this was cooled for 30 min at -78 °C. *n*-BuLi (6.5 mL, 16 mmol, 1.05 eq, 2.4 M in hexanes) was added dropwise over 5

min. **II.1** (4.6 mL, 15 mmol, 1 eq) was added to the reaction flask dropwise and the reaction was stirred for 1 h at $-78\text{ }^{\circ}\text{C}$. The reaction was quenched with deionized water (40 mL) while at $-78\text{ }^{\circ}\text{C}$ and warmed to room temperature. The product was extracted with EtOAc (3 x 70 mL) and washed with brine (3 x 40). The organic layers were dried over sodium sulfate, decanted and concentrated to yield the crude product **A.2** as a yellow oil. The product was used as is for the next reaction.

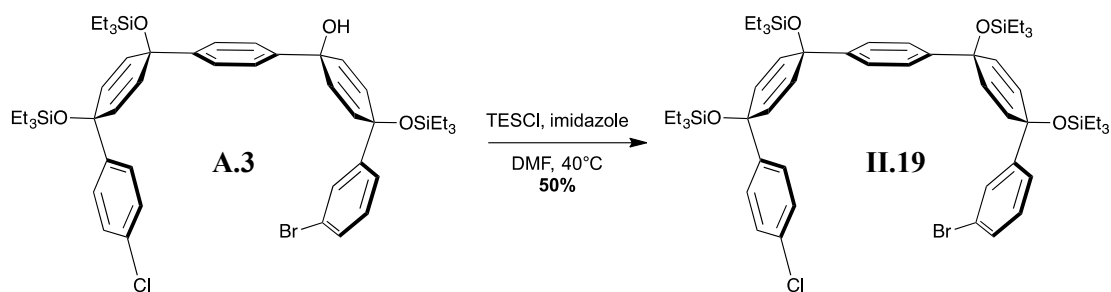


II.3. Crude **A.2** and imidazole (2.3 g, 25 mmol, 4 eq) were added to a 250 mL round bottom flask equipped with a stir bar and septum. Dimethylformamide (75 mL) was added to the flask followed by triethylsilyl chloride (3.0 mL, 18 mmol, 1.2 eq). The reaction mixture was heated to $40\text{ }^{\circ}\text{C}$ in an oil bath and stirred overnight. The reaction mixture was cooled to room temperature and quenched with a saturated solution of sodium bicarbonate (30 mL). The product was extracted with EtOAc (3 x 60 mL) and washed with 5% lithium chloride solution in water (30 mL) and brine (30 mL). The organic layers were dried over sodium sulfate and concentrated to yield the crude product as a yellow oil. The product was purified by automated flash silica gel chromatography (0% to 3% EtOAc in hexanes) to give **II.3** as a white solid (6.3 g, 69% over 2 steps). IR (neat) $2952, 2871, 1483, 1401\text{ cm}^{-1}$; $^1\text{H NMR}$ (600 MHz, Chloroform-*d*) δ 7.38 (d, $J = 8.3\text{ Hz}$, 2H), 7.23 (d, $J = 0.9\text{ Hz}$, 4H), 7.17 (d, $J = 8.3\text{ Hz}$, 2H), 5.95 (s, 4H), 0.95 – 0.89

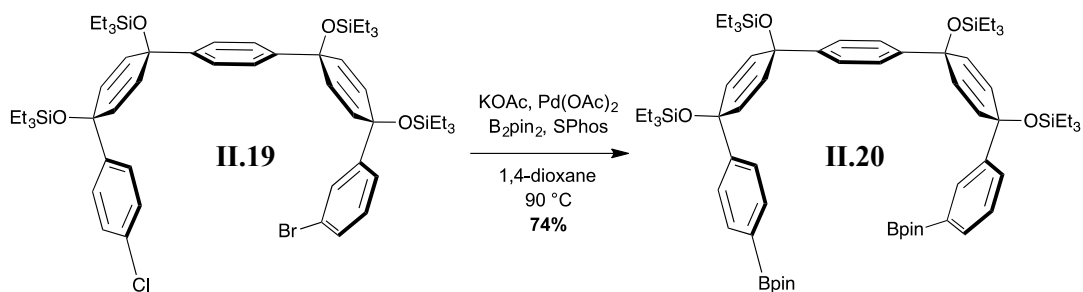
(m, 18H), 0.59 (qd, $J = 8.0, 2.5$ Hz, 12H). ^{13}C NMR (151 MHz, Chloroform- d) δ 144.97, 144.41, 133.11, 131.46, 131.37, 131.25, 128.31, 127.60, 127.24, 121.29, 71.10, 71.04, 7.02, 6.41. HRMS (EI) (m/z): $[\text{M}]^+$ calculated for $\text{C}_{30}\text{H}_{42}\text{BrClO}_2\text{Si}_2$, 604.1595; found, 604.1594.



A.3. **II.3** (1.5 g, 2.5 mmol, 1.1 eq) was added to a 25 mL one-neck round bottom flask equipped with a stir bar and septa. The flask was evacuated and filled with nitrogen. Tetrahydrofuran (27 mL) was added to the flask and it was cooled for 30 min at -78 °C. n -BuLi (1.0 mL, 2.6 mmol, 1.05 eq, 2.5 M in hexanes) was added dropwise over 3 min. **II.18** (0.72 mL, 2.5 mmol, 1 eq) was added to the reaction flask dropwise and the reaction was stirred for 1 h at -78 °C. The reaction was quenched with deionized water (10 mL) while at -78 °C and deionized water (5 mL) was added again when the ice bath was removed. The product was extracted with EtOAc (3 x 20 mL) and washed with brine (3 x 20 mL). The organic layers were dried over sodium sulfate and concentrated to yield the crude product **A.3** as a colorless oil. The product was not purified.

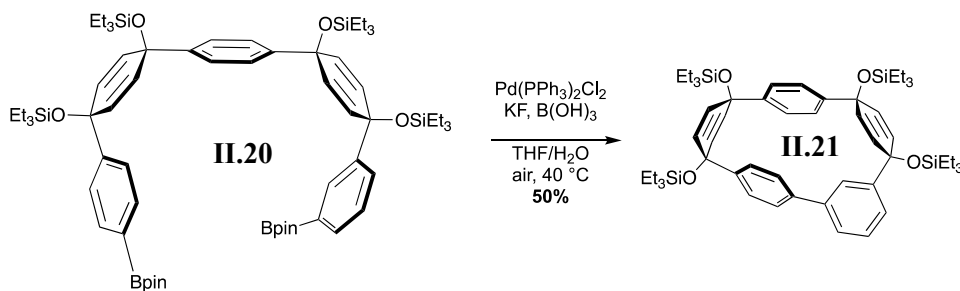


II.19. Crude **A.3** and imidazole (0.67 g, 9.9 mmol, 4 eq) were added to a 100 mL round bottom flask equipped with a stir bar and septum. Dimethylformamide (10 mL) was added to the flask followed by triethylsilyl chloride (0.5 mL, 3.0 mmol, 1.2 eq). The reaction mixture was heated to 40 °C in an oil bath and stirred overnight. The reaction mixture was cooled to room temperature and quenched with a saturated solution of sodium bicarbonate (20 mL). The product was extracted with EtOAc (3 x 100 mL) and washed with 5% lithium chloride solution in water (3 x 50 mL). The organic layers were dried over sodium sulfate and concentrated to yield the crude product as a yellow oil. The product was purified by automated flash silica gel chromatography (0% to 5% EtOAc in hexanes) to give **II.19** as a white solid (1.25 g, 50% over 2 steps). IR (neat) 2953, 2874, 1457, 1405 cm^{-1} ; ^1H NMR (600 MHz, Chloroform-*d*) δ 7.47 (dd, $J = 1.5$ Hz, 1H), 7.34 (dd, $J = 7.9, 1.9$ Hz, 1H), 7.25 – 7.22 (m, 6H), 7.21 – 7.17 (m, 3H), 7.08 (t, $J = 7.9$ Hz, 1H), 6.02 (d, $J = 10.9$ Hz, 2H), 6.00 (d, $J = 9.9$ Hz, 2H), 5.91 (d, $J = 3.9$ Hz, 2H), 5.90 (d, $J = 3.5$ Hz, 2H), 0.97 – 0.89 (m, 38H), 0.66 – 0.60 (m, 12H), 0.57 (q, $J = 7.8$ Hz, 13H). ^{13}C NMR (151 MHz, Chloroform-*d*) δ 148.41, 144.95, 144.83, 144.70, 131.91, 131.77, 131.06, 130.98, 130.14, 129.60, 129.14, 128.18, 127.28, 125.76, 125.70, 124.29, 122.35, 71.23, 71.15, 7.05, 7.03, 6.46, 6.41. HRMS (ESI-TOF) (m/z): $[\text{M}+\text{Na}]^+$ calculated for $\text{C}_{54}\text{H}_{80}\text{BrClNaO}_4\text{Si}_4$, 1041.3903; found, 1041.3909.



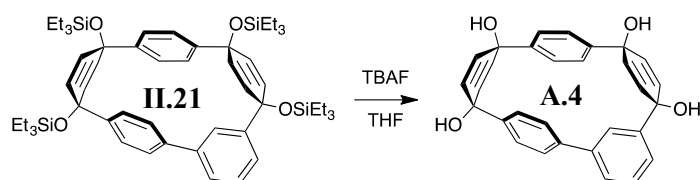
II.20. Oven dried KOAc (634.8 mg, 6.5 mmol, 6.6 eq) was added to a 25 mL round bottom flask equipped with a stir bar. **NOTE:** KOAc is extremely hygroscopic and the reaction is water sensitive, therefore it must be dried in an oven and weighed quickly while hot. The KOAc and flask were flame-dried again under vacuum until all apparent moisture was removed. Palladium(II) acetate (1.1 mg, 0.0049 mmol, 0.05 eq), SPhos (50.3 mg, 0.12 mmol, 0.125 eq), bis(pinacolato)diboron (994.8 mg, 3.9 mmol, 4 eq) and **II.19** (1.0 g, 0.98 mmol, 1 eq) were added to the flask, which was placed under vacuum for 1 h with stirring. The flask was purged with nitrogen and evacuated 3 times. 1,4-dioxane (3.3 mL) was purged with nitrogen for 1 h prior and added to the round bottom flask at room temperature. The round bottom flask was placed in an oil bath while it heated up to 90 °C. The reaction mixture changed from yellow to orange to red to a very dark red. The reaction was stirred at 90 °C overnight. EtOAc was added to the reaction mixture, which was filtered through a fritted suction funnel with 2 cm Celite[®]. The flask was rinsed several times with EtOAc and sonicated. The filtrate was transferred to a 250 mL flask and concentrated to yield a white waxy solid. This was rinsed with ethanol and suctioned through a Büchner funnel to yield **II.20** as a white solid (843.1 mg, 74%). IR (neat) 2953, 2875, 1357, 1317 cm⁻¹; ¹H NMR (600 MHz, Chloroform-*d*) δ 8.01 (s, 1H), 7.70 (d, *J* = 8.0 Hz, 2H), 7.68 (d, *J* = 8.4 Hz, 1H), 7.33 (d, *J* = 7.7 Hz, 2H), 7.29 (d, *J* = 7.9 Hz, 1H), 7.25 – 7.22 (m, 3H), 7.20 (d, *J* = 8.3 Hz, 2H), 6.02 (d, *J* = 9.8 Hz, 2H), 5.95

(d, $J = 10.0$ Hz, 2H), 5.93 (s, 4H), 1.34 (s, 12H), 1.30 (s, 12H), 0.96 – 0.88 (m, 36H), 0.65 – 0.54 (m, 24H). ^{13}C NMR (151 MHz, CDCl_3) δ 149.19, 145.31, 145.06, 144.72, 134.69, 133.60, 132.55, 131.64, 131.58, 131.37, 131.13, 128.62, 127.43, 125.61, 125.54, 125.15, 83.72, 83.61, 71.53, 71.36, 71.29, 71.25, 24.90, 24.88, 7.10, 7.06, 6.47, 6.45, 6.43. HRMS (ESI-TOF) (m/z): $[\text{M}+\text{Na}]^+$ calculated for $\text{C}_{66}\text{H}_{104}\text{B}_2\text{NaO}_8\text{Si}_4$, 1181.6892; found, 1181.6926.

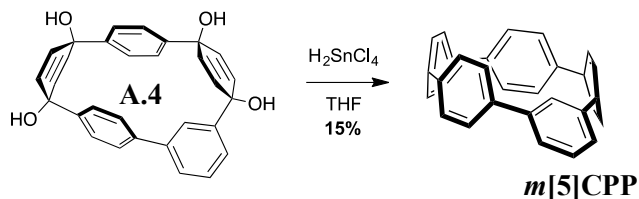


II.21. Diboronate ester **II.20** (400 mg, 0.417 mmol, 1.00 eq) was added to a round bottom flask followed by Pd(PPh₃)₂Cl₂ (59 mg, 0.083 mmol, 0.2 eq) and boric acid (129 mg, 2.09 mmol, 5.00 eq). The solids were dissolved in tetrahydrofuran (200 mL) and the mixture was stirred vigorously for 10 min. Potassium fluoride (24 mg, 0.417 mmol, 1.00 eq) dissolved in water (20 mL) was added to the mixture. The reaction was stirred at 40 °C open to the atmosphere overnight. The next day, the mixture was filtered through Celite[®] washing with EtOAc, dried over sodium sulfate, and concentrated to give the crude product as an orange oil. The product was purified by automated flash silica gel chromatography (0% to 30% dichloro in hexanes) to yield **II.21** as a white solid (190 mg, 50%). IR (neat) 2953, 2874, 1457, 1412 cm^{-1} ; ^1H NMR (500 MHz, Chloroform-*d*) δ 7.65 (d, $J = 6.6$ Hz, 1H), 7.43 – 7.35 (m, 2H), 7.12 (d, $J = 6.7$ Hz, 2H), 6.92 (d, $J = 6.7$ Hz, 2H), 6.88 (d, $J = 6.8$ Hz, 2H), 6.58 (d, $J = 6.9$ Hz, 2H), 6.47 (s, 1H), 6.40 (d, $J = 8.3$ Hz, 2H), 6.12 (d, $J = 8.3$ Hz, 2H), 5.96 (d, $J = 8.5$ Hz, 2H), 5.86 (d, $J = 8.5$ Hz, 2H), 1.01 (t, J

= 7.9 Hz, 9H), 0.97 (t, $J = 7.9$ Hz, 9H), 0.87 (t, $J = 8.0$ Hz, 9H), 0.84 (t, $J = 7.9$ Hz, 9H), 0.72 (q, $J = 7.9$ Hz, 6H), 0.64 (q, $J = 7.9$ Hz, 6H), 0.50 (q, $J = 7.9$ Hz, 6H), 0.46 (q, $J = 7.9$ Hz, 6H). ^{13}C NMR (126 MHz, CDCl_3) δ 145.63, 143.99, 143.87, 143.13, 141.22, 141.11, 134.02, 132.79, 132.74, 131.05, 130.66, 128.60, 126.93, 126.75, 125.79, 125.61, 123.22, 122.78, 72.88, 72.53, 72.02, 71.46, 7.12, 7.03, 6.96, 6.95, 6.46, 6.44, 6.41, 6.40. HRMS (ESI-TOF) (m/z): $[\text{M}+\text{Na}]^+$ calculated for $\text{C}_{54}\text{H}_{80}\text{NaO}_4\text{Si}_4$, 927.5031; found, 927.5050.

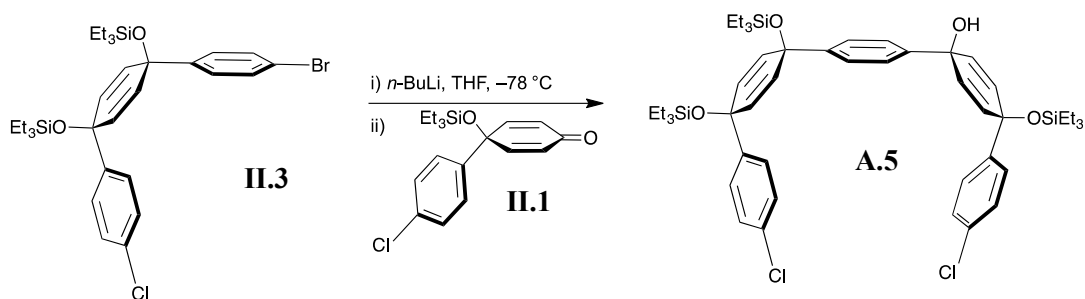


A.4. **II.21** (33 mg, 0.036 mmol, 1 eq) was dissolved in tetrahydrofuran (0.9 mL). Tetra-*n*-butylammonium fluoride (0.22 mL, 0.22 mmol, 6 eq, 1 M in tetrahydrofuran) was added and the reaction was stirred for 1 h. The reaction was quenched with water (1 mL) and the tetrahydrofuran was removed by distillation. The resulting mixture was filtered to afford **A.4** as a white solid that was rinsed with water and dichloromethane. The product was not purified further.

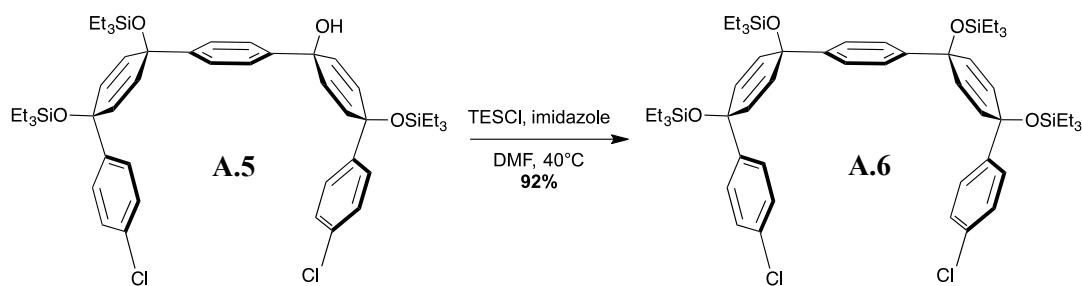


***m*[5]CPP.** Crude **A.4** was dissolved in tetrahydrofuran (0.36 mL). A solution of tin(II) dichloride dihydrate (18 mg, 79 μmol , 2.2 eq) and concentrated hydrochloric acid (12 μL , 150 μmol , 4.2 eq) in tetrahydrofuran (710 μL) was added and the reaction was stirred for 1 h at room temperature. A 1 M concentrated solution of NaOH (1 mL) was added and

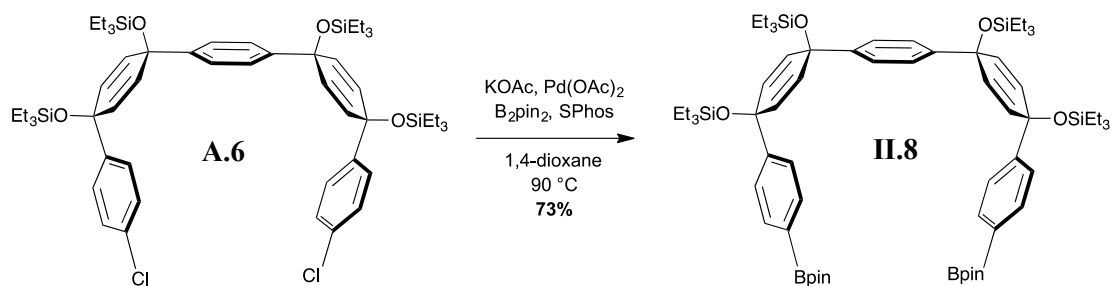
the mixture was extracted with dichloromethane (3 x 3 mL). The organic layers were concentrated and the product. The product was purified by preparative thin layer chromatography on alumina (50% dichloromethane in hexanes) to yield **m[5]CPP** as a yellow solid (2.0 mg, 15% over 2 steps). ^1H NMR (500 MHz, Chloroform-*d*) δ 7.40 – 7.31 (m, 15H), 7.06 (d, J = 8.7 Hz, 4H), 4.80 (s, 1H). ^{13}C NMR (151 MHz, Chloroform-*d*) δ 145.23, 142.82, 140.79, 139.05, 136.69, 135.38, 129.88, 128.64, 128.33, 127.54, 126.71, 121.18. HRMS (ASAP) (m/z): $[\text{M}+\text{H}]^+$ calculated for $\text{C}_{30}\text{H}_{21}$, 381.1643; found, 381.1642.



A.5. II.3 (6.0972 g, 10.1 mmol, 1.1 eq) was added to a 100 mL round bottom flask equipped with a stir bar and septa. The flask was evacuated and filled with nitrogen. Tetrahydrofuran (15 mL) was added to the round bottom flask and was cooled for 30 min at $-78\text{ }^\circ\text{C}$. $n\text{-BuLi}$ (4.2 mL, 10.6 mmol, 1.05 eq, 2.5 M in hexanes) was added dropwise. **II.1** (3.12 mL, 10.1 mmol, 1 eq) was added to the reaction flask dropwise and the reaction was stirred for 1 h at $-78\text{ }^\circ\text{C}$. The reaction was quenched with deionized water (15 mL) at $-78\text{ }^\circ\text{C}$ and warmed to room temperature. The product was extracted with ethyl acetate (3 x 40 mL) and washed with brine (30 mL). The organic layers were dried over sodium sulfate and concentrated to yield the crude product **A.5** as a colorless oil. The product was not purified.



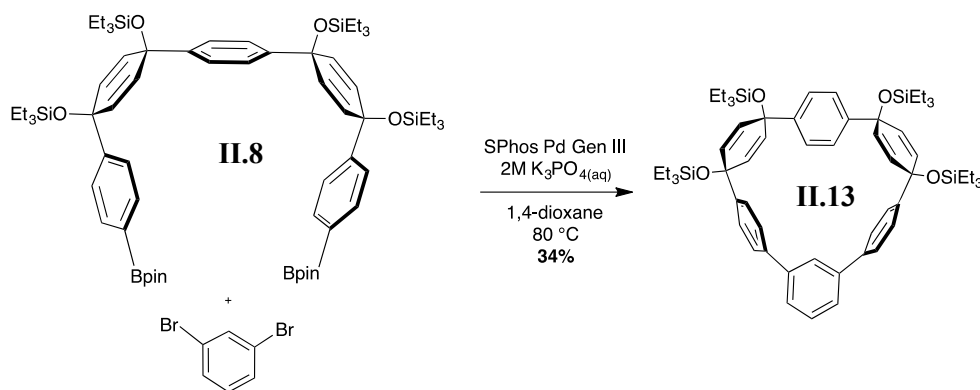
A.6. Crude **A.5** (8.67 g, 10.1 mmol, 1 eq) and imidazole (2.74 g, 40.2 mmol, 4 eq) were added to a 250 mL round bottom flask and was equipped with a stir bar and septum. Dimethylformamide (50 mL) was added to the flask followed by triethylsilyl chloride (2.0 mL, 12.1 mmol, 1.2 eq). The reaction mixture was heated to 40 °C in an oil bath and stirred overnight. The reaction mixture was cooled to room temperature and quenched with a saturated solution of sodium bicarbonate (50 mL). The product was extracted with ethyl acetate (3 x 100 mL) and washed with 5% lithium chloride solution in water (3 x 100 mL). The organic layers were dried over sodium sulfate and concentrated to yield the crude product as a yellow oil. The product was purified by automated flash silica gel chromatography (0% to 15% ethyl acetate in hexanes) to give **A.6** as a white solid (9.0 g, 92% over 2 steps). IR (neat) 2952, 2874, 1481, 1456, 1405 cm^{-1} ; ^1H NMR (600 MHz, Chloroform-*d*) δ 7.24 (s, 4H), 7.22 (d, $J = 8.4$ Hz, 4H), 7.19 (d, $J = 8.4$ Hz, 4H), 6.01 (d, $J = 10.1$ Hz, 4H), 5.91 (d, $J = 10.1$ Hz, 4H), 0.94 (t, $J = 7.9$ Hz, 18H), 0.91 (t, $J = 7.9$ Hz, 18H), 0.62 (q, $J = 7.9$ Hz, 12H), 0.57 (q, $J = 8.0$ Hz, 12H). ^{13}C NMR (151 MHz, Chloroform-*d*) δ 144.98, 144.63, 132.91, 131.68, 131.17, 128.15, 127.31, 127.23, 125.73, 71.18, 71.13, 7.05, 7.03, 6.46, 6.40. HRMS (ESI-TOF) (m/z): $[\text{M}+\text{Na}]^+$ calculated for $\text{C}_{54}\text{H}_{80}\text{Cl}_2\text{NaO}_4\text{Si}_4$, 997.4409; found, 997.4455.



II.8. Potassium acetate (KOAc) (1.1 g, 12 mmol, 6.6 eq) that had been stored in an oven was added to a 25 mL round bottom flask equipped with a stir bar. **NOTE:** KOAc is extremely hygroscopic and it is important to have none or very little moisture in the reaction, therefore it must be weighed very quickly while it is warm. The KOAc and flask were flame-dried again under vacuum until all apparent moisture was removed.

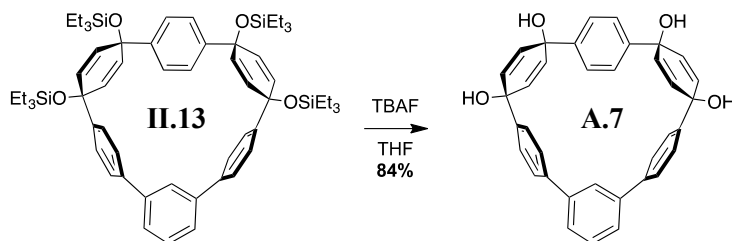
Palladium(II) acetate (20 mg, 0.09 mmol, 0.05 eq), SPhos (91 mg, 0.2 mmol, 0.13 eq), bis(pinacolato)diboron (1.8 g, 7 mmol, 4 eq) and **A.6** (1.7 g, 1.2 mmol, 1 eq) were added to the flask and was put under vacuum for 1 h with stirring. The flask was purged with nitrogen and evacuated 3 times. 1,4-dioxane (6 mL) was purged with nitrogen for 1 h, added to the round bottom flask at room temperature and the mixture was stirred for 5 min. The flask was placed in an oil bath and heated to 90 °C. The color of the reaction mixture changed from yellow to orange to red to a very dark red. The reaction was stirred at 90 °C over 2 nights. EtOAc was added to the reaction mixture. This was filtered through Celite[®] in a fritted suction funnel. The reaction flask was rinsed several times with EtOAc with sonication. The filtrate was transferred to a 250 mL round bottom flask and concentrated to yield a white waxy solid. This was rinsed with ethanol and filtered using a Büchner funnel to yield **II.8** as a white solid (1.51 g, 73%). IR (neat) 2954, 2876, 1610, 1361 cm^{-1} ; ^1H NMR (600 MHz, Chloroform-*d*) δ 7.69 (d, $J = 8.2$ Hz, 4H), 7.32 (d, $J = 8.2$ Hz, 4H), 7.22 (s, 4H), 5.98 (d, $J = 10.2$ Hz, 4H), 5.94 (d, $J = 10.2$ Hz, 4H), 1.33

(s, 24H), 0.95 – 0.90 (m, 36H), 0.63 – 0.56 (m, 24H). ^{13}C NMR (151 MHz, Chloroform-*d*) δ 149.17, 144.91, 134.65, 131.61, 131.22, 125.68, 125.16, 83.68, 71.60, 71.25, 24.88, 7.07, 6.45. HRMS (ESI-TOF) (*m/z*): $[\text{M}+\text{Na}]^+$ calculated for $\text{C}_{66}\text{H}_{104}\text{B}_2\text{NaO}_8\text{Si}_4$, 1181.6892; found, 1181.6871.



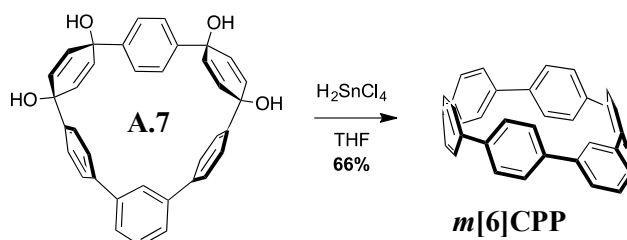
II.13. *m*-dibromobenzene (0.06 mL, 0.08 mmol, 1 eq), **II.8** (666.5 mg, 0.058 mmol, 1.2 eq) and SPhos Pd G3 (38.1 mg, 0.0048 mmol, 0.1 eq) were added to a 50 mL round bottom flask equipped with a stir bar. The flask was evacuated for 5 min and purged with nitrogen 5 times. 1,4-dioxane and a solution of 2 M K_3PO_4 were purged with nitrogen for over 1 h prior to use. The round bottom flask was equipped with a septa and 1,4-dioxane (160 mL) was added to the round bottom flask and the solution was purged for 20 min. The round bottom flask was heated to 80 °C for 10 min and K_3PO_4 (16 mL, 2 M in deionized water) was added. The reaction was stirred at 80 °C overnight. The reaction mixture was cooled to room temperature. It was filtered through a fritted suction funnel filled with Celite[®]. The round bottom flask was rinsed with dichloromethane and filtered through the Celite[®] plug. The filtrate was added to a separatory funnel along with deionized water (10 mL) and the product was extracted (3 x 30) with dichloromethane. The organic layer was washed with brine (20 mL), dried over sodium sulfate and

concentrated to yield an orange oil. The product was purified by automated flash silica gel chromatography (5% to 45% dichloromethane in hexanes) to yield the product **II.13** as a white solid (193 mg, 34%). IR (neat) 2952, 2874, 1457, 1403, 1237 cm^{-1} ; ^1H NMR (600 MHz, Chloroform-*d*) δ 7.55 (dd, $J = 7.5, 1.9$ Hz, 2H), 7.48 – 7.44 (m, 5H), 7.30 (d, $J = 8.3$ Hz, 4H), 6.93 (s, 4H), 6.24 (t, $J = 1.9$ Hz, 1H), 6.13 (d, $J = 10.1$ Hz, 4H), 5.72 (d, $J = 10.1$ Hz, 4H), 0.97 (t, $J = 7.9$ Hz, 18H), 0.93 (t, $J = 7.9$ Hz, 18H), 0.69 (q, $J = 7.9$ Hz, 12H), 0.58 (q, $J = 7.9$ Hz, 12H). ^{13}C NMR (151 MHz, CDCl_3) δ 144.92, 144.77, 143.15, 142.47, 141.76, 131.48, 131.43, 128.80, 128.69, 128.06, 125.99, 125.81, 125.73, 125.35, 122.39, 71.19, 70.58, 7.15, 7.04, 6.97, 6.80, 6.61, 6.50, 6.48, 6.42. HRMS (ESI-TOF) (m/z): $[\text{M}+\text{Na}]^+$ calculated for $\text{C}_{60}\text{H}_{84}\text{NaO}_4\text{Si}_4$, 1003.5344; found, 1003.5375.

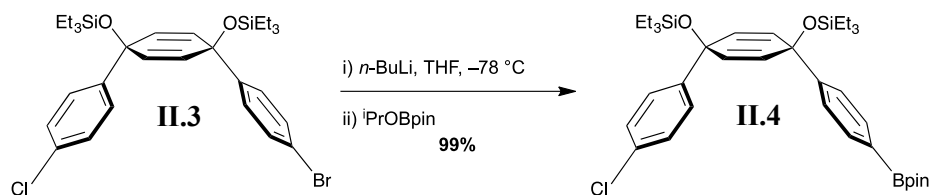


A.7. Tetrahydrofuran (1.05 mL) was added to **II.13** (102.9 mg, 0.1 mmol, 1 eq) and the vial was equipped with a stir bar and septa. Tetra-*n*-butylammonium fluoride (1.05 mL, 1 mmol, 10 eq, 1 M in tetrahydrofuran) was added to the reaction flask and this was stirred for 2 h at room temperature. The reaction was quenched with deionized water (5 mL), filtered in a Büchner funnel and washed with deionized water and dichloromethane to yield **A.7** as a white solid (46 mg, 84%). IR (neat) 3370, 3187, 1408 cm^{-1} ; ^1H NMR (600 MHz, $\text{DMSO-}d_6$) δ 7.60 (dd, $J = 7.6, 1.9$ Hz, 2H), 7.51 (t, $J = 7.6$ Hz, 1H), 7.47 (d, $J = 8.0$ Hz, 4H), 7.33 (d, $J = 7.9$ Hz, 4H), 6.88 (s, 4H), 6.17 (t, $J = 2.0$ Hz, 1H), 6.07 (d, $J = 9.9$ Hz, 4H), 5.65 (d, $J = 9.8$ Hz, 4H). ^{13}C NMR (151 MHz, DMSO) δ 145.94, 144.97,

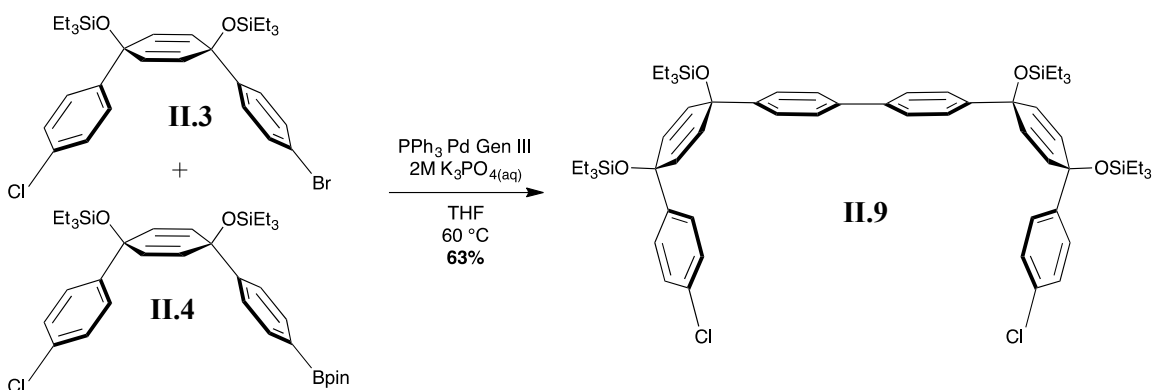
142.45, 142.38, 131.85, 131.53, 129.54, 128.78, 126.26, 125.54, 122.79, 68.63, 68.09, 23.53, 19.70, 13.98. HRMS (ESI-TOF) (m/z): $[M+Na]^+$ calculated for $C_{36}H_{28}NaO_4$, 547.1885; found, 547.1869.



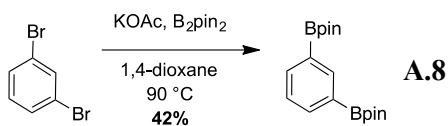
m[6]CPP. $SnCl_2 \cdot H_2O$ (180.6 mg, 0.80 mmol) was added to a 100 mL round bottom flask equipped with a stir bar and septum. Tetrahydrofuran (20 mL) was added to the flask followed by hydrochloric acid (0.13 mL, 1.6 mmol, 12 M). This was stirred at room temperature for 30 min. H_2SnCl_2 solution (2.1 mL, 0.09 mmol, 2.2 eq, 0.04 M) was added to the scintillation vial containing **A.7** (20.3 mg, 0.04 mmol, 1 eq) and was stirred for 1 h at room temperature. The reaction was quenched with saturated sodium bicarbonate (5 mL). The filtrate was transferred to a separatory funnel and the product was extracted with dichloromethane (5 x 7 mL). The organic layers were washed with brine (10 mL), dried over sodium sulfate and concentrated to give the crude product as a green solid. The product was purified by automated flash alumina column chromatography (10% to 45% dichloromethane in hexanes) to yield **m[6]CPP** as a green solid (12 mg, 66%). IR (neat) 2921, 2851, 1661, 1261 cm^{-1} ; 1H NMR (600 MHz, Chloroform-*d*) δ 7.45 – 7.38 (m, 19H), 7.15 (d, $J = 8.6$ Hz, 4H), 5.62 (t, $J = 1.9$ Hz, 1H). ^{13}C NMR (151 MHz, $CDCl_3$) δ 142.79, 139.53, 139.04, 137.43, 136.42, 136.38, 129.45, 128.99, 128.08, 127.85, 127.58, 127.20, 122.20, 77.25, 77.03, 76.82. HRMS (ASAP-TOF) (m/z): $[M+H]^+$ calculated for $C_{36}H_{25}$, 457.1956; found, 457.1956.



II.4. II.3 (5 g, 8.25 mmol, 1.0 eq) was added to a 100 mL round bottom flask equipped with a stir bar. The reaction flask was capped with a septa and the flask was evacuated and refilled with nitrogen. Tetrahydrofuran (48 mL) was added to the reaction flask and the mixture was cooled for 30 min at $-78\text{ }^{\circ}\text{C}$. *n*-BuLi (3.5 mL, 8.7 mmol, 1.05 eq, 2.5 M in hexanes) was added to the reaction mixture dropwise. This was followed by the dropwise addition of 2-Isopropoxy-4,4,5,5-tetramethyl-1,3,2-dioxaborolane (3.4 mL, 16.5 mmol, 2 eq) and the reaction was stirred at $-78\text{ }^{\circ}\text{C}$ for 1 h. The reaction was quenched with deionized water (30 mL) at $-78\text{ }^{\circ}\text{C}$ and the reaction mixture was warmed to room temperature. The product was extracted with ethyl acetate (3 x 50 mL) and washed with brine (3 x 20 mL). The organic layers were dried over sodium sulfate, decanted into a round bottom flask and concentrated to yield a slightly yellow oil. Ethanol (20 mL) was added to the oil and was sonicated, producing a white precipitate. The product **II.4** was isolated by suction filtration to yield a white solid (5.3 g, 99%). IR (neat) 2955, 2874, 1399, 1359, 1321 cm^{-1} ; ^1H NMR (500 MHz, Chloroform-*d*) δ 7.72 (d, $J = 7.8$ Hz, 2H), 7.32 (d, $J = 7.9$ Hz, 2H), 7.24 (d, $J = 8.8$ Hz, 2H), 7.22 (d, $J = 8.7$ Hz, 2H), 5.99 (d, $J = 10.0$ Hz, 2H), 5.92 (d, $J = 10.0$ Hz, 2H), 1.34 (s, 12H), 0.93 (t, $J = 8.0$ Hz, 9H), 0.91 (t, $J = 7.9$ Hz, 9H), 0.61 (q, $J = 8.0$ Hz, 6H), 0.57 (q, $J = 7.7$ Hz, 6H). ^{13}C NMR (126 MHz, CDCl_3) δ 148.90, 144.59, 134.73, 132.91, 131.60, 131.24, 128.21, 127.27, 125.15, 83.79, 71.45, 71.15, 24.88, 7.03, 6.45, 6.41. HRMS (ESI-TOF) (m/z): $[\text{M}+\text{Na}]^+$ calculated for $\text{C}_{36}\text{H}_{54}\text{BClNaO}_4\text{Si}_2$, 675.3240; found, 675.3246.

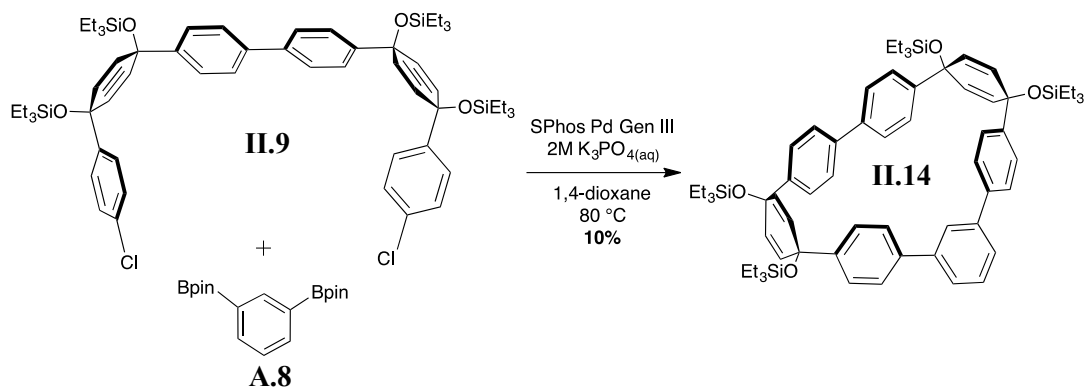


II.9. **II.3** (1.00 g, 1.65 mmol, 1 eq), **II.4** (1.18 g, 1.82 mmol, 1.1 eq) and PPh₃ Pd G3 (31 mg, 0.050 mmol, 0.03 eq) dissolved in tetrahydrofuran (16 mL) and warmed to 60 °C. K₃PO₄ (1.6 mL, 2 M in deionized water) was added and the reaction was left overnight. The next day, the reaction was filtered through Celite[®], dried over sodium sulfate and the solvent was removed under reduced pressure to yield an oil. The product was purified by automated flash silica column chromatography (0% to 30% dichloromethane in hexanes) to yield **II.9** as a white solid (1.1 g, 63%). IR (neat) 2951, 2873, 1490, 1456, 1401 cm⁻¹; ¹H NMR (500 MHz, Chloroform-d) δ 7.50 (d, J = 8.2 Hz, 4H), 7.37 (d, J = 8.5 Hz, 4H), 7.28 (d, J = 8.3 Hz, 4H), 7.23 (d, J = 8.5 Hz, 4H), 6.03 (d, J = 10.0 Hz, 4H), 5.96 (d, J = 9.8 Hz, 4H), 0.94 (t, J = 7.9 Hz, 36H), 0.61 (q, J = 8.1 Hz, 24H). ¹³C NMR (126 MHz, CDCl₃) δ 144.90, 144.66, 139.59, 132.97, 131.78, 131.16, 128.23, 127.33, 126.76, 126.24, 71.27, 71.16, 7.05, 7.04, 6.47, 6.43. HRMS (ESI-TOF) (m/z): [M+Na]⁺ calculated for C₆₀H₈₄Cl₂NaO₄Si₄, 1073.4722; found, 1073.4722.



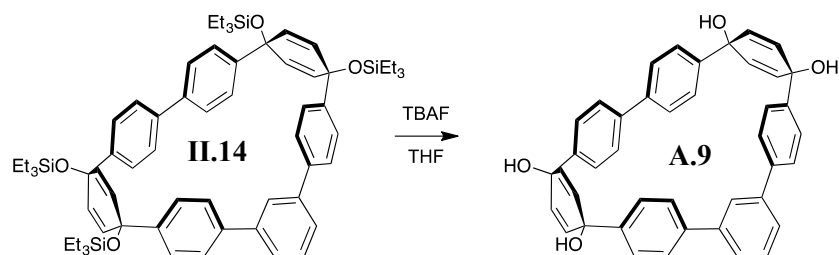
A.8. 1,3-dibromobenzene (5.0 mL, 9.8 g, 41 mmol, 1 equiv), Pd(dppf)₂Cl₂ (169 mg, 0.21 mmol, 0.005 equiv) and bis(pinacolato)diboron (25 g, 99 mmol, 2.4 eq) were added to a

round bottomed flask. Oven dried hot KOAc (27 g, 270 mmol, 6.6 eq) was added and the solids were placed under vacuum. The flask was refilled with nitrogen, 1,4-dioxane (40 mL) was added, and the reaction was warmed from room temperature to 90 °C. The reaction was stirred at this temperature overnight. The next day, the reaction was filtered through Celite[®] washing with ethyl acetate (80 mL) and the solvent of the filtrate was removed under reduced pressure until crystallization occurred. The crystals were collected by filtration and washed with cold ethanol to yield **A.8** as a white solid (5.8 g, 42%). IR (neat) 2977, 1602, 1303 cm⁻¹; ¹H NMR (500 MHz, Chloroform-*d*) δ 8.28 (s, 1H), 7.90 (d, *J* = 7.4 Hz, 2H), 7.37 (t, *J* = 7.4 Hz, 1H), 1.34 (s, 24H). ¹³C NMR (126 MHz, CDCl₃) δ 141.23, 137.62, 127.04, 83.73, 24.88. HRMS (ESI-TOF) (*m/z*): [M+H]⁺ calculated for C₁₈H₂₉B₂O₄, 331.2252; found, 331.2244.

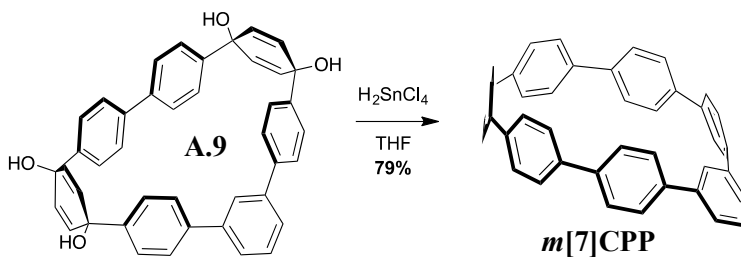


II.14. **II.9** (157 mg, 0.475 mmol, 1 eq), **A.8** (500 mg, 0.475 mmol, 1 eq), and SPhos Pd G3 (37 mg, 0.048 mmol, 0.1 eq) were dissolved in 1,4-dioxane (240 mL) and heated to 80 °C. K₃PO₄ (24 mL, 2 M in deionized water) was added and the reaction was stirred overnight. The reaction mixture was filtered through Celite[®] and the solvent was removed under reduced pressure to yield a golden oil. The product was purified by automated flash silica column chromatography (0% to 100% dichloromethane in hexanes) to yield a white solid. The solid was purified by recycling gel permeation

chromatography to yield **II.14** as a white solid (50 mg, 10%). IR (neat) 2954, 2875, 1085 cm^{-1} ; ^1H NMR (600 MHz, Chloroform- d) δ 7.58 (dd, $J = 7.5, 1.8$ Hz, 2H), 7.50 (m, 2H), 7.40 (d, $J = 8.4$ Hz, 4H), 7.26 (d, $J = 8.4$ Hz, 4H), 7.23 (d, $J = 8.3$ Hz, 4H), 7.04 (d, $J = 8.3$ Hz, 4H), 6.15 (d, $J = 10.0$ Hz, 4H), 6.07 (d, $J = 10.0$ Hz, 4H), 0.99 (t, $J = 7.9$ Hz, 18H), 0.98 (t, $J = 7.9$ Hz, 18H), 0.68 (q, $J = 7.9$ Hz, 12H), 0.66 (q, $J = 7.9$ Hz, 12H). ^{13}C NMR (151 MHz, CDCl_3) δ 143.56, 142.92, 141.63, 140.33, 140.10, 132.46, 131.98, 129.16, 128.78, 127.09, 126.80, 126.68, 126.57, 124.89, 72.54, 72.35, 7.08, 7.06, 6.49. HRMS (ESI-TOF) (m/z): $[\text{M}+\text{H}]^+$ calculated for $\text{C}_{66}\text{H}_{89}\text{O}_4\text{Si}_4$, 1057.5838; found, 1057.5869.

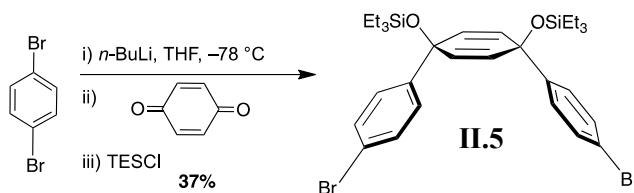


A.9. **II.14** (50 mg, 0.047 mmol, 1 eq) was dissolved in tetrahydrofuran (1.2 mL) and a Tetra-*n*-butylammonium fluoride (0.21 mL, 0.28 mmol, 6 eq, 1 M in tetrahydrofuran) was added. The reaction was stirred for 1 h at room temperature and quenched with water. Solvent was removed from this mixture under reduced pressure. Filtration afforded **A.9** as a white solid, which was washed with dichloromethane.



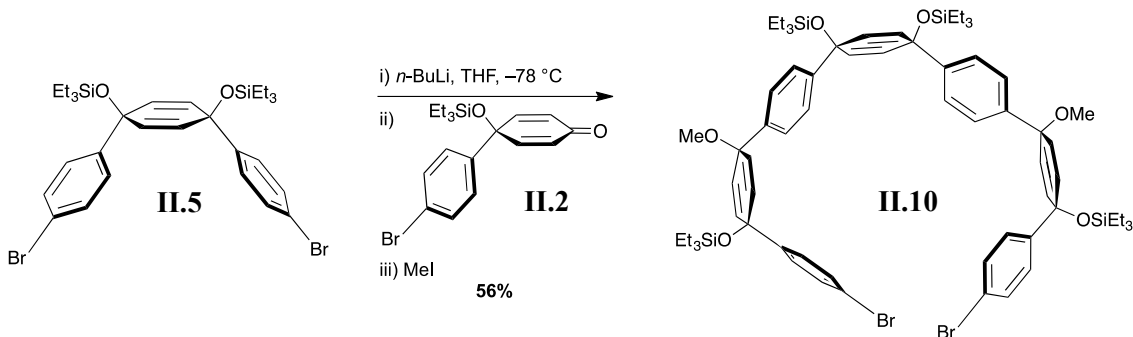
***m*[7]CPP**. Crude **A.9** was dissolved in minimal tetrahydrofuran and to it was added a solution of tin(II) dichloride monohydrate (23 mg, 100 μmol , 2.1 eq) and concentrated

aqueous hydrochloric acid (17 μ L, 200 μ mol, 4.2 eq) in tetrahydrofuran (1 mL). The reaction was stirred at room temperature for 1 h and quenched with a 1 M aqueous solution of NaOH. This mixture was extracted with dichloromethane and the combined extracts were dried over anhydrous sodium sulfate. The solvent was removed under reduced pressure and the material was purified by preparative thin layer chromatography on alumina (25% dichloromethane in hexanes) to yield **m[7]CPP** as a yellow fluorescent solid. (20 mg, 79%). IR (neat) 3020, 2922, 2850, 1581, 1480, 1261 cm^{-1} ; ^1H NMR (600 MHz, Chloroform- d) δ 7.51 – 7.43 (m, 19H), 7.42 (d, J = 8.5 Hz, 4H), 7.21 (d, J = 8.4 Hz, 4H), 6.08 (t, J = 1.9 Hz, 1H). ^{13}C NMR (151 MHz, CDCl_3) δ 142.54, 141.91, 138.78, 137.57, 137.37, 137.30, 137.24, 136.58, 129.08, 128.90, 127.69, 127.51, 127.48, 127.43, 127.02, 123.02. HRMS (ASAP-TOF) (m/z): $[\text{M}+\text{H}]^+$ calculated for $\text{C}_{42}\text{H}_{29}$, 533.2269; found, 533.2278.



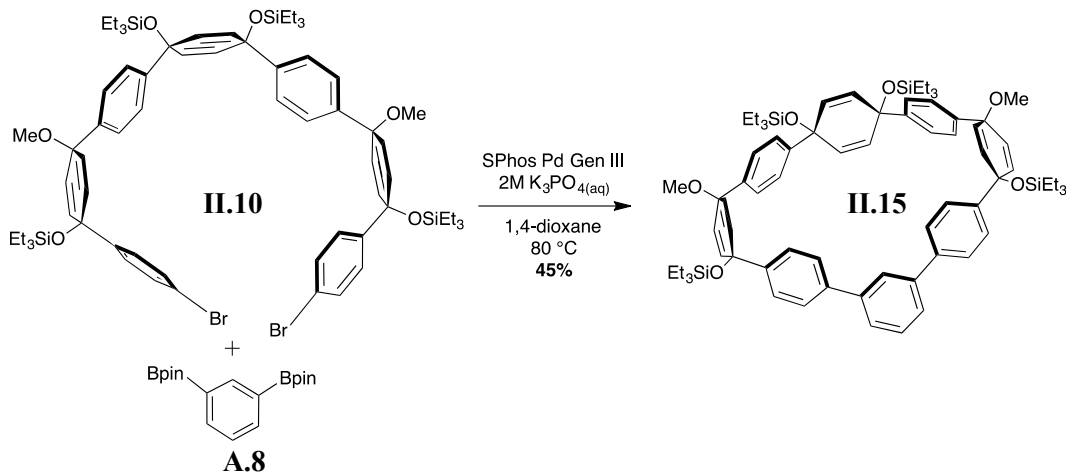
II.5. 1,4-dibromobenzene (5.00 g, 21.2 mmol, 2.8 eq) was dissolved in tetrahydrofuran (125 mL) and cooled to $-78\text{ }^\circ\text{C}$. $n\text{-BuLi}$ (8.2 mL, 20.4 mmol, 2.7 eq, 2.5 M in hexanes) was added followed by 1,4-benzoquinone (818 mg, 7.57 mmol, 1 eq), which was added in fifths. After each fifth, the reaction turned blue and the next fifth was not added until the reaction became yellow. When the last fifth was added, the reaction was stirred for 1 h, triethylsilyl chloride (4.4 mL, 4.0 g, 26 mmol, 3.5 eq) was added and the reaction was warmed to room temperature overnight. The next day, the reaction was quenched with water (60 mL) and extracted with ethyl acetate (3 x 60 mL). The combined extracts were

washed with brine (60 mL), dried over anhydrous sodium sulfate and solvent was removed to yield an oil. The product was purified by automated flash silica column chromatography (0% to 20% dichloromethane in hexanes) to yield a clear colorless oil. This was mixed with an equal amount of ethanol and let sit to yield large crystals, which were filtered and washed with ethanol, to yield **II.5** as a white solid (1.80 mg, 37%). IR (neat) 2952, 2871, 1477, 1400 cm^{-1} ; ^1H NMR (500 MHz, Chloroform-*d*) δ 7.38 (d, $J = 8.3$ Hz, 4H), 7.17 (d, $J = 8.3$ Hz, 4H), 5.95 (s, 4H), 0.92 (t, $J = 7.9$ Hz, 18H), 0.59 (q, $J = 8.0$ Hz, 12H). ^{13}C NMR (126 MHz, CDCl_3) δ 144.94, 131.39, 131.25, 127.60, 121.30, 71.09, 7.01, 6.41. HRMS (EI) (m/z): $[\text{M}]^+$ calculated for $\text{C}_{30}\text{H}_{42}\text{Br}_2\text{O}_2\text{Si}_2$, 648.1090; found, 648.1081.



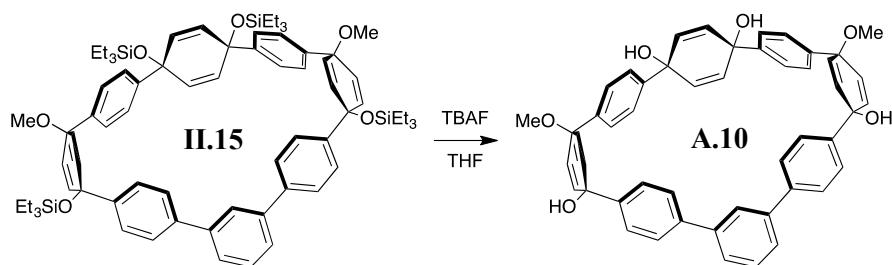
II.10. **II.5** (1.63 g, 2.50 mmol, 1 eq) was dissolved in tetrahydrofuran (50 mL, 100 mM) and cooled to -78°C . $n\text{-BuLi}$ (2.0 mL, 5.0 mmol, 2 eq, 2.5 M in hexanes) was added followed immediately by **II.2** (1.5 mL, 1.9 g, 5 mmol, 2 eq) and the reaction was stirred for 1 h at -78°C . It was quenched with methyl iodide (470 μL , 1.1 g, 7.5 mmol, 3 eq), warmed to room temperature and stirred overnight. The next day, water (20 mL) was added and the product was extracted with ethyl acetate (3 x 20 mL). The combined extracts were washed with brine (20 mL) and dried over anhydrous sodium sulfate. Solvent was removed under reduced pressure to yield an oil. The product was purified by

automated flash silica column chromatography (20% to 80% dichloromethane in hexanes) to yield **II.10** as a white solid (1.8 g, 56%). ¹H NMR (600 MHz, Chloroform-*d*) δ 7.34 (d, *J* = 8.6 Hz, 4H), 7.30 (d, *J* = 8.5 Hz, 4H), 7.26 (d, *J* = 8.5 Hz, 4H), 7.16 (d, *J* = 8.6 Hz, 4H), 6.09 (d, *J* = 10.2 Hz, 4H), 5.99 (d, *J* = 10.2 Hz, 4H), 5.96 (s, 4H), 3.33 (s, 6H), 0.96 (t, *J* = 7.9 Hz, 18H), 0.92 (t, *J* = 7.9 Hz, 18H), 0.66 (q, *J* = 7.9 Hz, 12H), 0.60 (q, *J* = 7.9 Hz, 12H). ¹³C NMR (151 MHz, CDCl₃) δ 145.68, 144.93, 141.99, 135.06, 131.40, 131.11, 129.35, 127.51, 126.02, 125.95, 121.07, 74.30, 71.68, 71.18, 52.06, 7.05, 6.49, 6.44. HRMS (ESI-TOF) (*m/z*): [M+Na]⁺ calculated for C₆₈H₉₄Br₂NaO₆Si₄, 1299.4392; found, 1299.4379.

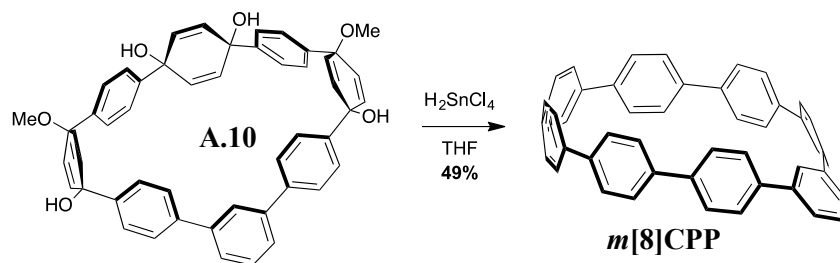


II.15. **A.8** (206 mg, 0.63 mmol, 1 eq), **II.10** (800 mg, 0.63 mmol, 1 eq), and SPhos Pd G3 (49 mg, 0.063 mmol, 0.1 eq) were dissolved in 1,4-dioxane (125 mL) and heated to 80 °C. K₃PO₄ (12.5 mL, 2 M in deionized water) was added and the reaction was stirred overnight. The reaction mixture was filtered through Celite[®], dried over sodium sulfate, and the solvent was removed under reduced pressure to yield a golden oil. The product was purified by automated flash silica column chromatography (20% to 80% dichloromethane in hexanes) to yield **II.15** as a white solid (340 mg, 45%). IR (neat)

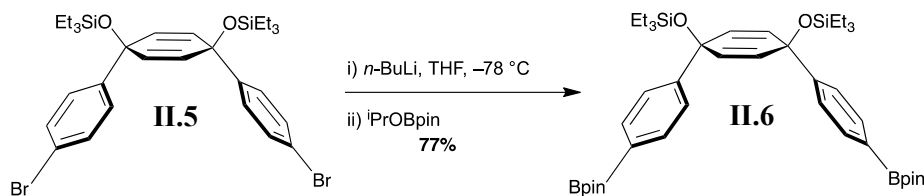
2951, 2874, 1457, 1406 cm^{-1} ; ^1H NMR (600 MHz, Chloroform-*d*) δ 7.65 (s, 1H), 7.58 (dd, $J = 7.6, 1.8$ Hz, 2H), 7.53 (d, $J = 8.4$ Hz, 4H), 7.51 (d, $J = 8.4$ Hz, 4H), 7.48 (d, $J = 7.5$ Hz, 1H), 7.45 (d, $J = 8.5$ Hz, 4H), 7.42 (d, $J = 8.3$ Hz, 4H), 6.15 (s, 4H), 6.12 (d, $J = 10.1$ Hz, 4H), 6.01 (d, $J = 10.2$ Hz, 4H), 3.29 (s, 6H), 1.01 (t, $J = 7.9$ Hz, 18H), 0.89 (t, $J = 8.0$ Hz, 18H), 0.72 (q, $J = 8.0$ Hz, 12H), 0.53 (q, $J = 8.0$ Hz, 12H). ^{13}C NMR (126 MHz, CDCl_3) δ 146.21, 145.04, 142.66, 141.06, 139.60, 135.49, 132.44, 131.12, 128.16, 127.82, 126.87, 126.31, 126.22, 125.87, 124.78, 73.80, 72.04, 69.76, 51.42, 7.12, 6.53. HRMS (ESI-TOF) (m/z): $[\text{M}+\text{Na}]^+$ calculated for $\text{C}_{74}\text{H}_{98}\text{NaO}_6\text{Si}_4$, 1217.6338; found, 1217.6381.



A.10. **II.15** (100 mg, 0.084 mmol, 1 eq) was dissolved in tetrahydrofuran (2.1 mL) and Tetra-*n*-butylammonium fluoride (0.50 mL, 0.50 mmol, 6 eq, 1 M in tetrahydrofuran) was added. The reaction was stirred for 1 h at room temperature and was quenched with water. Tetrahydrofuran was removed from this mixture under reduced pressure and filtration afforded **A.10** as a white solid, which was washed with dichloromethane. This crude material was used as is for the next reaction.

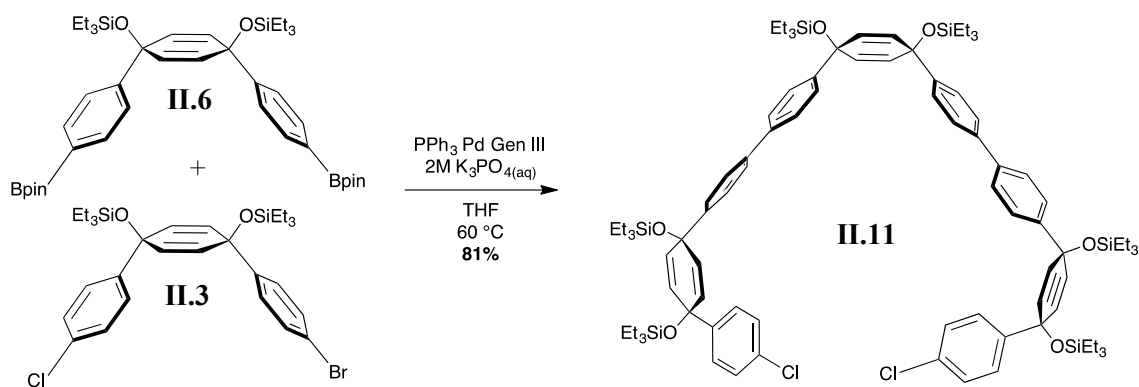


***m*[8]CPP**. Crude **A.10** was dissolved in minimal tetrahydrofuran and to it was added a solution of tin(II) dichloride monohydrate (62 mg, 280 μmol , 3.3 eq) and concentrated aqueous hydrochloric acid (44 μL , 530 μmol , 6.3 eq) in tetrahydrofuran (2.1 mL). The reaction was stirred at room temperature for 1 h and quenched with a 1 M aqueous solution of NaOH (1 mL). This mixture was extracted with dichloromethane (3 x 3 mL) and the combined extracts were dried over anhydrous sodium sulfate. The solvent was removed under reduced pressure and the product was purified by automated flash silica column chromatography (0% to 100% dichloromethane in hexanes) to yield ***m*[8]CPP** as a yellow solid (25 mg, 49%). IR (neat) 3022, 1586, 1481, 1388 cm^{-1} ; ^1H NMR (600 MHz, Chloroform-*d*) δ 7.56 (dt, $J = 7.7, 1.8$ Hz, 2H), 7.52 – 7.44 (m, 17H), 7.40 – 7.36 (m, 8H), 7.32 (d, $J = 8.2$ Hz, 4H), 6.36 (t, $J = 1.8$ Hz, 1H). ^{13}C NMR (151 MHz, CDCl_3) δ 142.42, 141.12, 139.45, 138.47, 138.00, 137.83, 137.57, 137.23, 135.86, 128.93, 128.51, 127.52, 127.49, 127.27, 127.24, 127.14, 123.24. HRMS (ASAP-TOF) (m/z): $[\text{M}+\text{H}]^+$ calculated for $\text{C}_{48}\text{H}_{33}$, 608.2582; found, 609.2585.



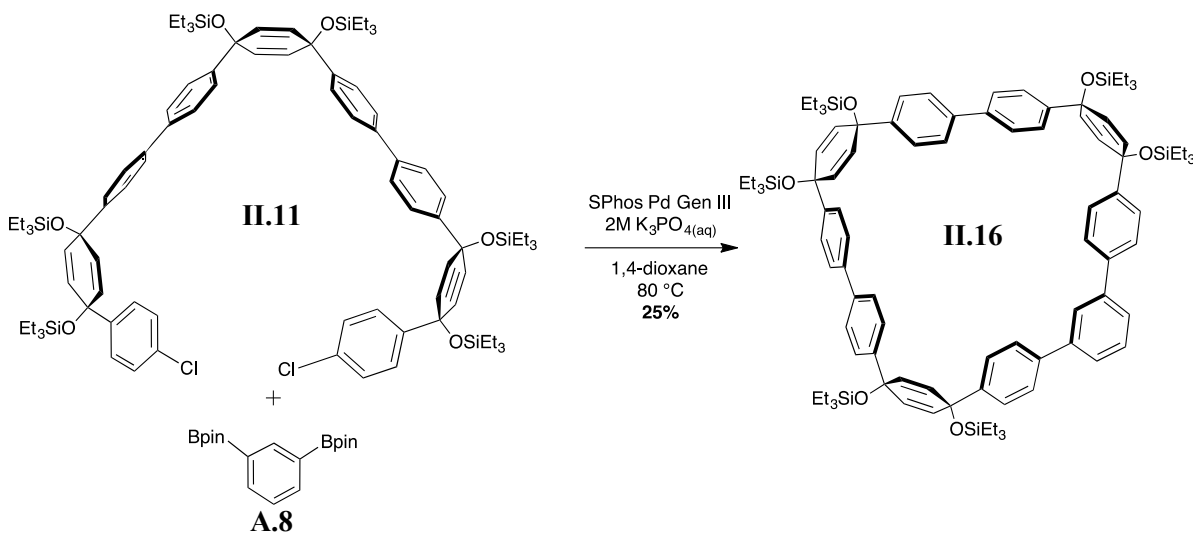
II.6. **II.5** (3.00 g, 4.61 mmol, 1 eq) was dissolved in tetrahydrofuran (50 mL) and cooled to -78 $^{\circ}\text{C}$. *n*-BuLi (3.9 mL, 9.7 mmol, 2.1 eq, 2.5 M in hexanes) was added followed

immediately by 2-isopropoxy-4,4,5,5-tetramethyl-1,3,2-dioxaborolane (2.1 mL, 1.9 g, 10 mmol, 2.2 eq). The reaction was stirred for 30 min and warmed to room temperature. The reaction was quenched with water (20 mL) and extracted with ethyl acetate (3 x 20 mL). The combined extracts were washed with brine (20 mL), dried over anhydrous sodium sulfate, and solvent was removed under reduced pressure to yield an oil. The oil was mixed with an equal amount of ethanol and placed in the freezer until crystals formed, which was filtered to yield **II.6** as a white crystalline powder (2.65 g, 77%). IR (neat) 2949, 2872, 1607, 1355 cm^{-1} ; ^1H NMR (500 MHz, Chloroform-*d*) δ 7.73 (d, $J = 7.6$ Hz, 4H), 7.37 (d, $J = 7.7$ Hz, 4H), 5.99 (s, 4H), 1.37 (s, 24H), 0.95 (t, $J = 7.8$ Hz, 18H), 0.62 (q, $J = 7.8$ Hz, 12H). ^{13}C NMR (126 MHz, CDCl_3) δ 149.08, 134.69, 131.41, 125.18, 83.72, 71.56, 24.89, 7.04, 6.45. HRMS (ESI-TOF) (m/z): $[\text{M}+\text{Na}]^+$ calculated for $\text{C}_{42}\text{H}_{66}\text{B}_2\text{NaO}_6\text{Si}_2$, 767.4482; found, 767.4514.



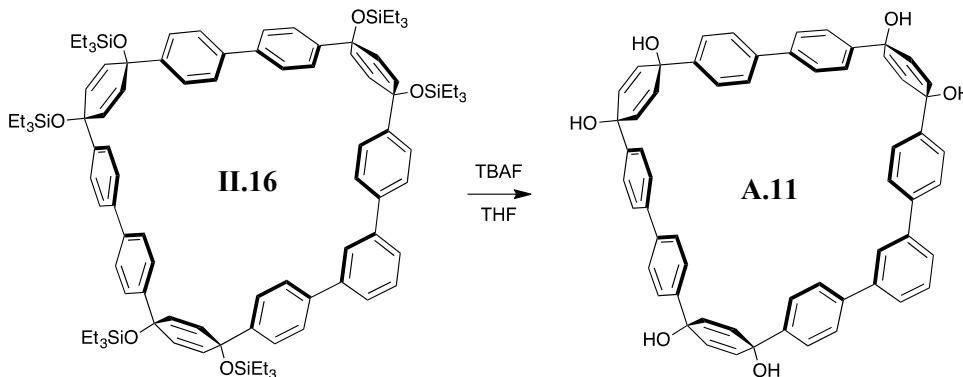
II.11. **II.6** (250 mg, 0.34 mmol, 1 eq), **II.3** (407 mg, 0.67 mmol, 2 eq), and PPh_3 Pd G3 (11 mg, 0.017 mmol, 0.05 eq) were dissolved in tetrahydrofuran (6.7 mL) and heated to 60°C . K_3PO_4 (0.67 mL, 2 M in deionized water) was added and the reaction was left overnight. The next day, the reaction was cooled to room temperature, filtered through Celite[®] while rinsing with ethyl acetate (15 mL), and dried over anhydrous sodium

sulfate. The solvent was removed under reduced pressure and the product was purified by automated flash silica column chromatography (0% to 50% dichloromethane in hexanes) to yield **II.11** as a white solid (421 mg, 81%). IR (neat) 2952, 2874, 1489, 1458, 1238 cm^{-1} ; ^1H NMR (500 MHz, Chloroform- d) δ 7.50 (d, $J = 8.2$ Hz, 8H), 7.42 (d, $J = 8.0$ Hz, 4H), 7.36 (d, $J = 7.9$ Hz, 4H), 7.28 (d, 4H), 7.22 (d, $J = 7.8$ Hz, 4H), 6.04 (s, 4H), 6.03 (d, $J = 8.8$ Hz, 4H), 5.95 (d, $J = 9.7$ Hz, 4H), 0.94 (q, $J = 8.3$ Hz, 54H), 0.67 – 0.57 (m, 36H). ^{13}C NMR (126 MHz, CDCl_3) δ 145.18, 144.83, 144.66, 139.70, 139.48, 132.99, 131.80, 131.52, 131.16, 128.23, 127.33, 126.78, 126.74, 126.33, 126.22, 71.38, 71.28, 71.18, 7.09, 7.06, 7.05, 6.51, 6.49, 6.45. HRMS (ESI-TOF) (m/z): $[\text{M}+\text{Na}]^+$ calculated for $\text{C}_{90}\text{H}_{126}\text{Cl}_2\text{NaO}_6\text{Si}_6$, 1563.7445; found, 1563.7485.

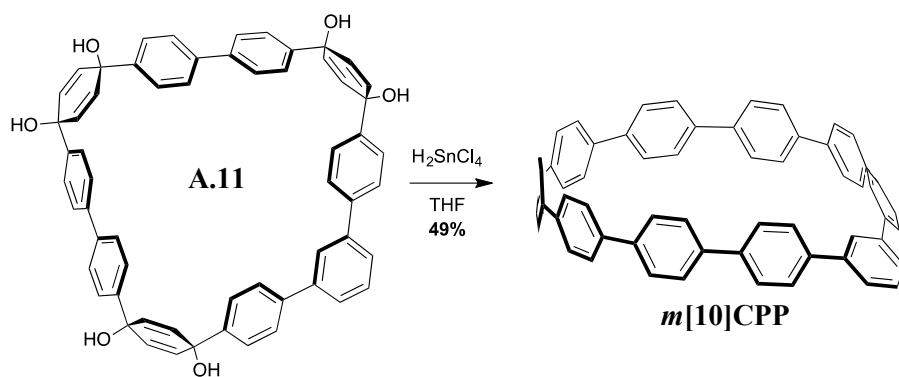


II.16. **II.11** (245 mg, 0.16 mmol, 1 eq), **A.8** (52 mg, 0.16 mmol, 1 eq), and SPhos Pd G3 (12 mg, 0.016 mmol, 0.1 eq) were dissolved in 1,4-dioxane (80 mL) and heated to 80 °C. K_3PO_4 (8 mL, 2M in deionized water) was added and the reaction was stirred for 3 h. The reaction mixture was filtered through Celite[®] and dried over anhydrous sodium sulfate. Solvent was removed to yield a brown oil, which was purified by automated flash silica column chromatography (0% to 100% dichloromethane in hexanes) to yield a white

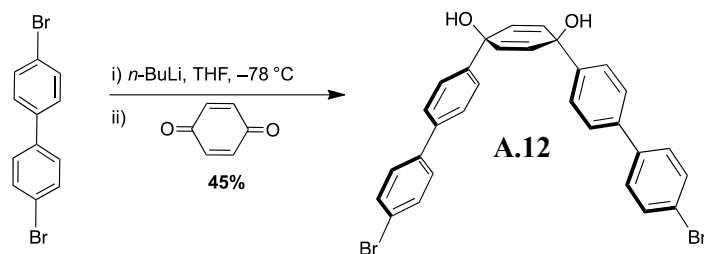
solid. The product was purified by recycling gel permeation chromatography (chloroform) to yield **II.16** as a white solid (62 mg, 25%). ^1H NMR (500 MHz, Chloroform-*d*) δ 7.74 (s, 1H), 7.58 – 7.52 (m, 6H), 7.52 – 7.46 (m, 9H), 7.46 – 7.39 (m, 8H), 7.35 (d, J = 8.3 Hz, 4H), 6.11 (d, J = 9.8 Hz, 4H), 6.04 – 5.97 (m, 7H), 1.03 – 0.87 (m, 54H), 0.71 – 0.53 (m, 36H). ^{13}C NMR (126 MHz, CDCl_3) δ 145.29, 145.22, 144.93, 141.64, 140.39, 139.46, 139.42, 131.80, 131.51, 131.36, 131.24, 129.12, 127.25, 126.75, 126.64, 126.51, 126.38, 126.13, 126.10, 71.57, 71.15, 71.11, 7.10, 7.07, 7.05, 6.49, 6.45. HRMS (ESI-TOF) (m/z): $[\text{M}+\text{Na}]^+$ calculated for $\text{C}_{96}\text{H}_{130}\text{NaO}_6\text{Si}_6$, 1569.8381; found, 1569.8341.



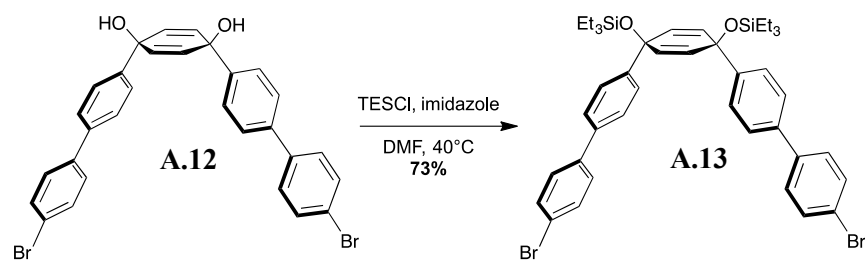
A.11. Tetrahydrofuran (1.3 mL) was added to **II.16** (20 mg, 13 μmol , 1 eq) and the vial was equipped with a stir bar and septa. Tetra-*n*-butylammonium fluoride (120 μL , 1 mmol, 9 eq, 1 M in tetrahydrofuran) was added to the reaction flask and stirred for 1 h at room temperature. The reaction was quenched with deionized water (1 mL) and the tetrahydrofuran was removed under reduced pressure. This mixture was filtered through a Büchner funnel, washed with deionized water and dichloromethane yielding **A.11** as a white solid. This solid was used as is for the next reaction.



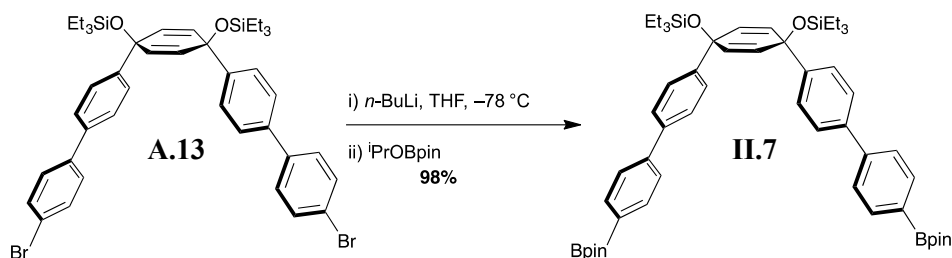
***m*[10]CPP.** Crude **A.11** (11 mg, 17 μmol , 1 eq) was dissolved in tetrahydrofuran (300 μL) and to it was added a solution of tin(II) dichloride monohydrate (9.5 mg, 42 μmol , 3.3 eq) and concentrated aqueous hydrochloric acid (6.7 μL , 80 μmol , 6.3 eq) in tetrahydrofuran (320 μL). The reaction was stirred at room temperature for 1 h and quenched with a 1 M aqueous solution of NaOH (1 mL). This mixture was extracted with dichloromethane (3 x 3 mL) and the combined extracts were dried over anhydrous sodium sulfate. The solvent was removed under reduced pressure and the product was purified by preparative thin layer chromatography on alumina (50% dichloromethane in hexanes) to yield ***m*[10]CPP** as a white solid (2 mg, 21%). IR (neat) 2918, 2849, 1672, 1480, 1463 cm^{-1} ; ^1H NMR (600 MHz, Chloroform-*d*) δ 7.62 (d, $J = 8.3$ Hz, 8H), 7.60 – 7.56 (m, 19H), 7.55 – 7.50 (m, 8H), 7.43 (d, $J = 7.9$ Hz, 4H), 6.86 (s, 1H). ^{13}C NMR (151 MHz, CDCl_3) δ 142.37, 141.12, 139.51, 139.22, 138.49, 138.32, 138.20, 138.13, 138.00, 137.93, 133.39, 129.03, 128.54, 127.65, 127.53, 127.49, 127.45, 127.44, 127.33, 127.24, 127.12, 124.26. LRMS (MALDI) (m/z): $[\text{M}]^+$ calculated for $\text{C}_{60}\text{H}_{40}$, 760.3125; found, 760.244.



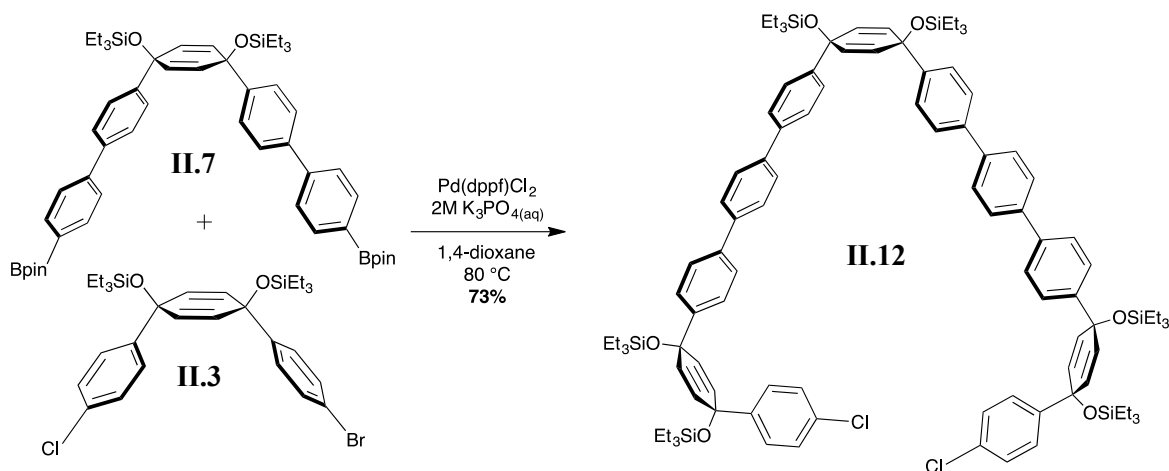
A.12. 4,4'-Dibromobiphenyl (19 g, 0.061 mol, 3.3 eq) was added to a 1000 mL round bottom flask equipped with a stir bar. The reaction flask was capped with a septa and the round bottom flask was evacuated and purged with nitrogen. Tetrahydrofuran (370 mL) was added to the reaction flask and cooled for 30 min at $-78\text{ }^{\circ}\text{C}$. *n*-BuLi (24.1 mL, 0.11 mol, 1.05 eq, 2.3 M in hexanes) was added to the reaction mixture dropwise over 25 min. The light brown solution was stirred for 15 min producing a white precipitate in a brown solution. *p*-benzoquinone (14.5 mL, 0.10 mol, 1 eq) was added to a 9 mL test tube and capped with a septa in order to weigh due to pungent odor. This was added portion-wise by removing the septa from the reaction flask (while a large flow of nitrogen was still flowing into the flask). As the benzoquinone was added, the reaction mixture turns blue momentarily before returning to brown. Benzoquinone was added until the blue color remained (2.3 g total). The reaction was stirred at $-78\text{ }^{\circ}\text{C}$ for 3 h. The reaction was quenched with deionized water (160 mL) at $-78\text{ }^{\circ}\text{C}$. The reaction mixture was warmed to room temperature. The product was extracted with ethyl acetate (3 x 200 mL) and washed with brine (3 x 100 mL). The organic layers were dried over sodium sulfate, decanted and concentrated to yield the crude product as a dark orange solid. This was purified by automated flash silica gel chromatography (10% to 60% ethyl acetate in hexanes). The crude product **A.12** was used as is for the next reaction.



A.13. **A.12** (4.0 g, 7.0 mmol, 1 eq) and imidazole (1.9 g, 28 mmol, 4 eq) were added to a 250 mL round bottom flask equipped with a stir bar and septum. Dimethylformamide (35 mL) was added to the flask followed by triethylsilyl chloride (3.8 mL, 23 mmol, 1.2 eq). The reaction mixture was heated to 40 °C in an oil bath and stirred overnight. The reaction mixture was cooled to room temperature and quenched with a saturated solution of sodium bicarbonate (30 mL). The product was extracted with ethyl acetate (3 x 100 mL) and washed with 5% lithium chloride solution in water (5 x 60 mL). The organic layers were dried over sodium sulfate and concentrated to yield the crude product as a brown solid. The product was purified by automated flash silica gel chromatography (0% to 10% ethyl acetate in hexanes) to give **A.13** as a pale yellow solid (4.10 g, 39% over 2 steps). IR (neat) 2952, 2874, 1481, 1458 cm^{-1} ; ^1H NMR (600 MHz, Chloroform- d) δ 7.53 (d, $J = 8.4$ Hz, 4H), 7.47 – 7.41 (m, 12H), 6.04 (s, 4H), 0.95 (t, $J = 7.9$ Hz, 18H), 0.63 (q, $J = 7.9$ Hz, 12H). ^{13}C NMR (151 MHz, CDCl_3) δ 145.55, 139.66, 138.79, 131.83, 131.51, 128.62, 126.65, 126.45, 121.50, 71.32, 7.07, 6.46. LRMS (MALDI) (m/z): $[\text{M}]^+$ calculated for $\text{C}_{42}\text{H}_{50}\text{Br}_2\text{O}_2\text{Si}_2$, 802.17; found, 802.24.

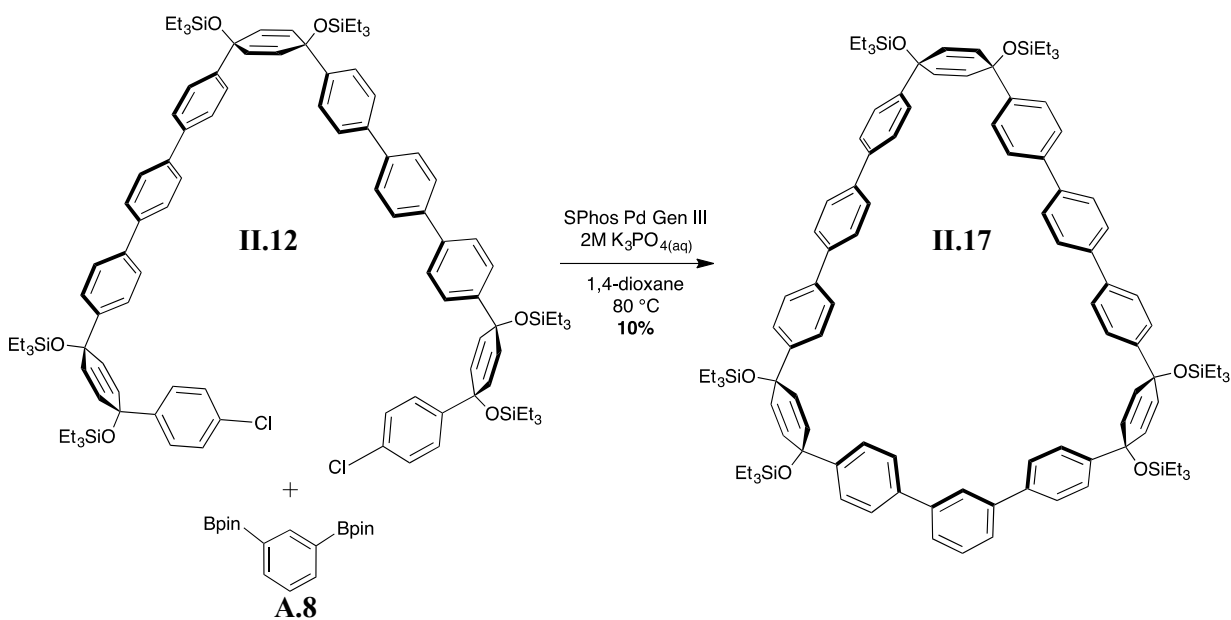


II.7. **A.13** (3.0 g, 3.74 mmol, 1.0 equiv) was added to a 100 mL round bottom flask equipped with a stir bar. The reaction flask was capped with a septa evacuated and refilled with nitrogen. Tetrahydrofuran (19 mL) was added to the reaction flask and the mixture was cooled for 30 min at $-78\text{ }^{\circ}\text{C}$. *n*-BuLi (3.4 mL, 8.2 mmol, 2.2 eq, 2.4 M in hexanes) was added to the reaction mixture dropwise, followed by the dropwise addition of 2-Isopropoxy-4,4,5,5-tetramethyl-1,3,2-dioxaborolane (3.0 mL, 14.9 mmol, 4 eq) and the reaction was stirred at $-78\text{ }^{\circ}\text{C}$ for 1 h. The reaction was quenched with deionized water (30 mL) at $-78\text{ }^{\circ}\text{C}$ and warmed to room temperature. The product was extracted with ethyl acetate (3 x 50 mL) and washed with brine (3 x 20 mL). The organic layers were dried over sodium sulfate and concentrated to yield **II.7** as a yellow solid (3.3 g, 98%). IR (neat) 2954, 2875, 1609, 1359 cm^{-1} ; ^1H NMR (600 MHz, Chloroform-*d*) δ 7.87 (d, $J = 7.7\text{ Hz}$, 4H), 7.63 – 7.41 (m, 12H), 6.04 (s, 4H), 0.96 (t, $J = 7.8\text{ Hz}$, 18H), 0.64 (q, $J = 8.1\text{ Hz}$, 12H). ^{13}C NMR (151 MHz, CDCl_3) δ 145.52, 143.50, 139.86, 135.33, 131.59, 127.02, 126.41, 83.84, 71.43, 24.94, 24.88, 7.17, 6.56. HRMS (ESI-TOF) (m/z): $[\text{M}+\text{Na}]^+$ calculated for $\text{C}_{54}\text{H}_{74}\text{B}_2\text{O}_6\text{Si}_2$, 919.5108; found, 919.5129.



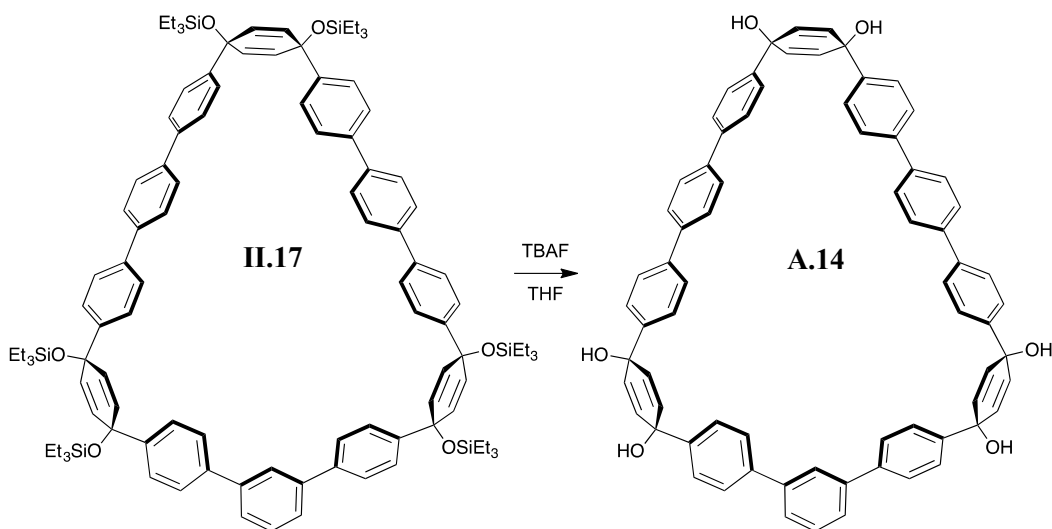
II.12. **II.7** (85.8 mg, 0.22 mmol, 1 eq), **II.3** (270.3 mg, 0.45 mmol, 2 eq) and Pd(dppf)₂Cl₂ (25.5 mg, 0.031 mmol, 0.07 eq) were added to a 10 mL round bottom flask equipped with a stir bar. The flask was evacuated (5 min) and purged with nitrogen 5 times. 1,4-dioxane and 2 M aqueous K₃PO₄ were purged with nitrogen for at least 1 h prior to use. The round bottom flask was equipped with a septa and 1,4-dioxane (2.2 mL) was added to the round bottom flask. The round bottom flask was heated to 80 °C over 5 min and K₃PO₄ (0.22 mL, 2 M in deionized water) was added. The reaction was stirred at 80 °C overnight. The reaction mixture was cooled to room temperature and filtered through a fritted suction funnel filled with Celite[®]. The round bottom flask was rinsed with dichloromethane, which was filtered through the Celite[®] plug. The filtrate was added to a separatory funnel along with deionized water (20 mL) and the product was extracted (3 x 20 mL) with dichloromethane. The organic layer was washed with brine (20 mL), dried over sodium sulfate and concentrated to yield the crude product as a brown solid. The product was purified by automated flash silica gel chromatography (5% to 25% dichloromethane in hexanes) to yield **II.12** as a white solid (277 mg, 73%). IR (neat) 2952, 2874, 1485, 1457, 1401 cm⁻¹; ¹H NMR (600 MHz, Chloroform-*d*) δ 7.65 (s,

8H), 7.55 (t, $J = 7.7$ Hz, 8H), 7.46 (d, $J = 8.1$ Hz, 4H), 7.39 (d, $J = 8.1$ Hz, 4H), 7.30 (s, 4H), 7.23 (d, $J = 8.4$ Hz, 4H), 6.09 – 6.02 (m, 8H), 5.97 (d, $J = 9.9$ Hz, 4H), 0.99 – 0.92 (m, 54H), 0.67 – 0.59 (m, 36H). ^{13}C NMR (151 MHz, CDCl_3) δ 145.26, 144.97, 144.68, 139.72, 139.61, 139.57, 139.48, 133.02, 131.82, 131.58, 131.21, 128.76, 128.28, 127.41, 127.38, 126.78, 126.76, 126.43, 126.32, 71.44, 71.32, 71.19, 18.66, 11.28, 7.14, 7.11, 7.09, 6.53, 6.51, 6.47, 6.34. LRMS (MALDI) (m/z): $[\text{M}]^+$ calculated for $\text{C}_{102}\text{H}_{134}\text{Cl}_2\text{O}_6\text{Si}_6$, 1693.82; found, 1694.838.

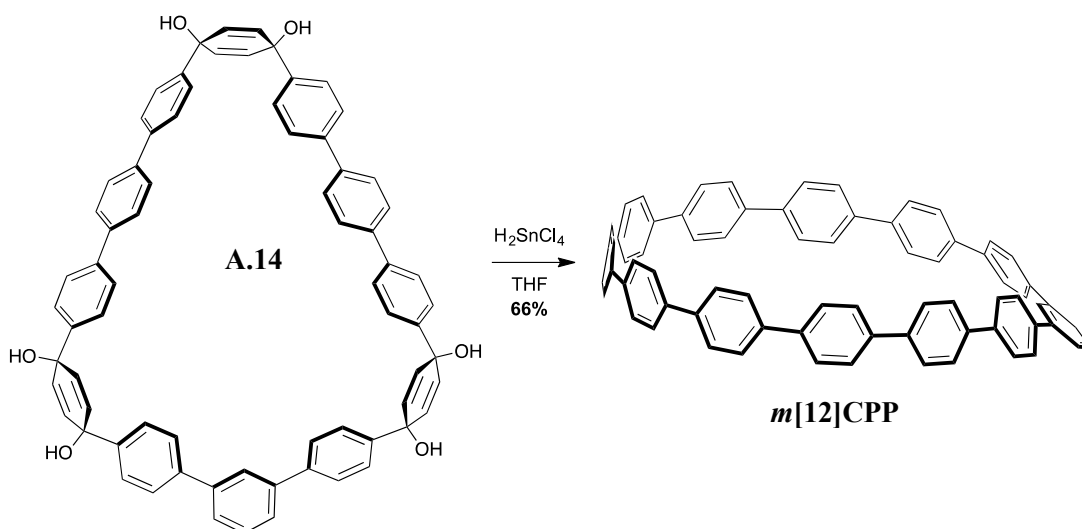


II.17. **A.8** (34.7 mg, 0.11 mmol, 1 eq), **II.12** (101.3 mg, 0.054 mmol, 1.05 eq) and SPhos Pd G3 3.6 mg, 0.0045 mmol, 0.1 eq) were added to a 100 mL round bottom flask equipped with a stir bar. The flask was evacuated (5 min) and purged with nitrogen 5 times. 1,4-dioxane and aqueous 2 M K_3PO_4 were purged for at least 1 h prior to use. The round bottom flask was equipped with a septum and 1,4-dioxane (33 mL) was added to the round bottom flask and the solution was purged for 30 min. The round bottom flask was heated to 80 °C over 10 min and K_3PO_4 (0.33 mL, 2 M in deionized water) was

added. The reaction was stirred at 80 °C overnight. The reaction mixture was cooled to room temperature and filtered through a fritted suction funnel filled with Celite[®]. The round bottom flask was rinsed with dichloromethane, which was also filtered through the Celite[®] plug. The filtrate was added to a separatory funnel along with deionized water (30 mL) and the product was extracted (3 x 30 mL) with dichloromethane. The organic layer was washed with brine (40 mL), dried over sodium sulfate and concentrated to yield a brown oil. The product was purified by flash silica column chromatography (0% to 30% dichloromethane in hexanes) followed by recycling gel permeation chromatography yielding **II.17** as a white solid (18 mg, 10%). ¹H NMR (600 MHz, Chloroform-d) δ 7.77 (t, J = 1.7 Hz, 1H), 7.65 (d, J = 3.5 Hz, 2H), 7.62 – 7.45 (m, 25H), 7.36 (d, J = 8.1 Hz, 8H), 6.16 (d, J = 9.7 Hz, 4H), 6.05 (s, 4H), 6.00 (d, J = 9.8 Hz, 4H), 1.00 (t, J = 7.9 Hz, 18H), 0.97 (t, J = 7.9 Hz, 18H), 0.92 (t, J = 7.9 Hz, 18H), 0.71 (q, J = 7.9 Hz, 12H), 0.65 (q, J = 7.9 Hz, 12H), 0.57 (q, J = 7.9 Hz, 12H). ¹³C NMR (151 MHz, CDCl₃) δ 145.33, 145.06, 144.75, 141.82, 140.68, 139.63, 139.48, 139.42, 139.27, 132.07, 131.64, 131.10, 127.39, 127.37, 127.30, 127.28, 126.74, 126.61, 126.56, 126.53, 126.18, 71.80, 71.72, 71.01, 7.14, 7.10, 7.05, 6.50, 6.48. LRMS (MALDI) (m/z): [M+H]⁺ calculated for C₁₀₈H₁₃₉O₆Si₆, 1699.919; found, 1699.904.



A.14. Tetrahydrofuran (0.11 mL) was added to **II.17** (18.2 mg, 0.01 mmol, 1 eq) and the vial was equipped with a stir bar and septa. Tetra-*n*-butylammonium fluoride (0.11 mL, 0.1 mmol, 10 eq, 1 M in tetrahydrofuran) was added to the reaction flask and this was stirred for 2 h at room temperature. The reaction was quenched with deionized water (5 mL) causing the product to precipitate. The resulting solution was filtered in a Büchner funnel, washed with deionized water and dichloromethane yielding **A.14** as a white solid. The crude product was used as is for the following reaction.



m[12]CPP. SnCl₂•H₂O (180.6 mg, 0.80 mmol) was added to a 100 mL round bottom flask equipped with a stir bar and septum. Tetrahydrofuran (20 mL) was added to the flask followed by hydrochloric acid (0.13 mL, 1.6 mmol, 12 M). This was stirred at room temperature for 30 min. H₂SnCl₂ solution (0.9 mL, 0.04 mmol, 3.3 eq, 0.04 M) was added to the scintillation vial containing **A.14** (11.1 mg, 0.01 mmol, 1 eq) and was stirred for 1 h at room temperature. The reaction was quenched with saturated sodium bicarbonate (5 mL). The filtrate was transferred to a separatory funnel and the product was extracted with ethyl acetate (3 x 7 mL). The organic layers were washed with brine (10 mL), dried over sodium sulfate and concentrated to give the crude product as a yellow solid. The product was purified by preparative thin layer chromatography on alumina (50% dichloromethane in hexanes) and recycling gel permeation chromatography to give **m[12]CPP** as a pale yellow solid (0.5 mg, 5% over 2 steps).

m[12]CPP was insoluble in CDCl₃ and a ¹³C spectrum was not recorded. IR (neat) 2924, 2853, 1483 cm⁻¹; ¹H NMR (600 MHz, Chloroform-d) δ 7.68 – 7.56 (m, 40H), 7.56 – 7.53 (m, 3H), 7.51 (d, J = 8.4 Hz, 4H), 7.12 (t, J = 1.8 Hz, 1H). LRMS (MALDI) (m/z): [M]⁺ calculated for C₇₂H₄₈, 912.3751; found, 912.329.

A.2. Photophysical Characterization

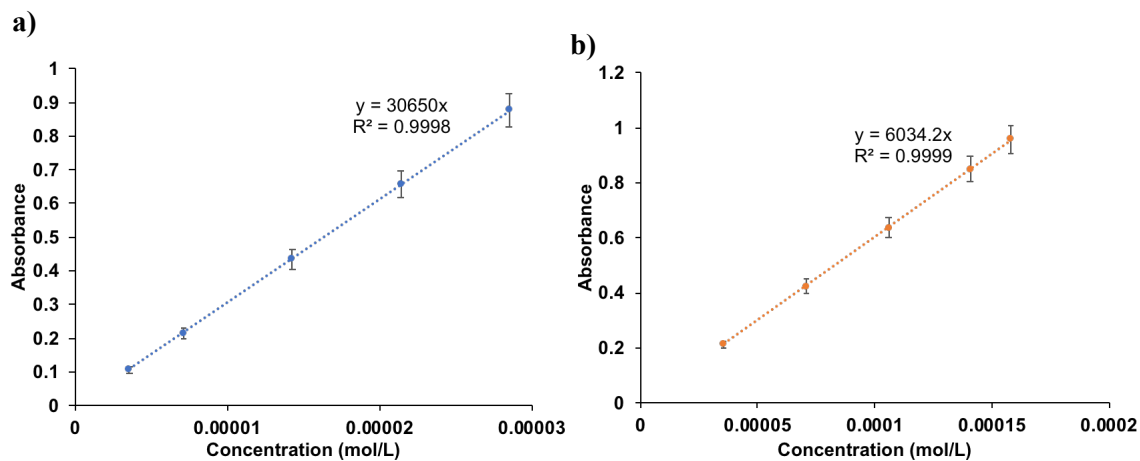


Figure A.1. Extinction coefficient determination of *m*[5]CPP at the a) absorbance maxima and b) HOMO→LUMO transition.

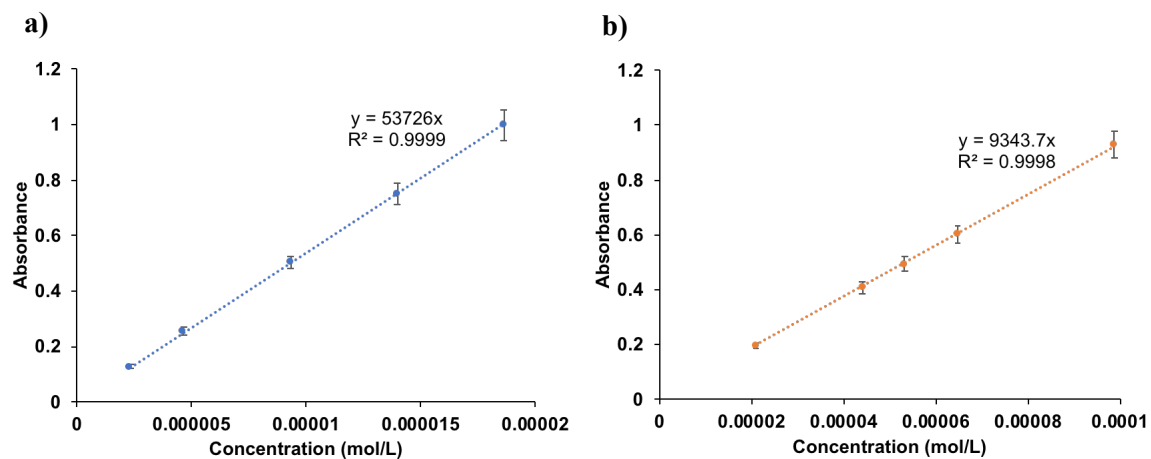


Figure A.2. Extinction coefficient determination of *m*[6]CPP at the a) absorbance maxima and b) HOMO→LUMO transition.

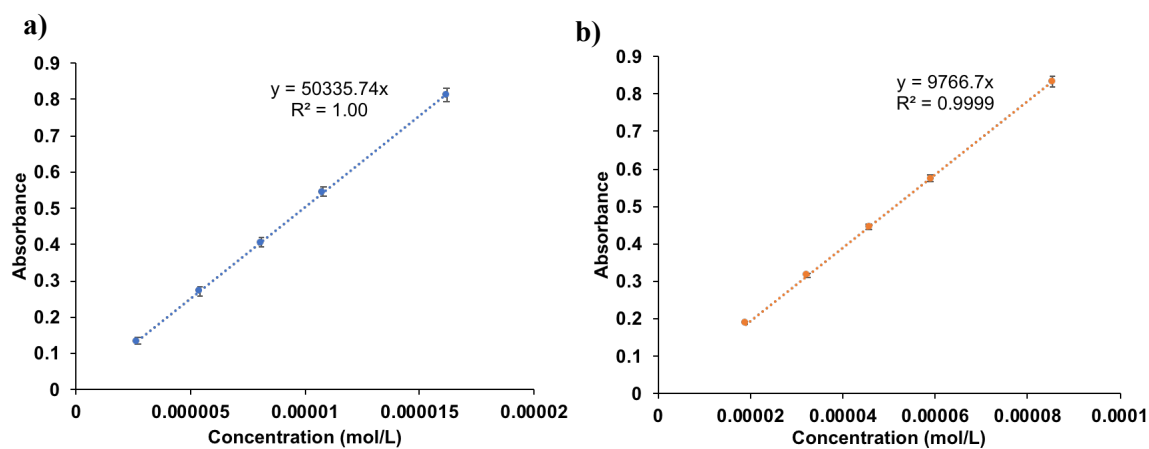


Figure A.3. Extinction coefficient determination of *m*[7]CPP at the a) absorbance maxima and b) HOMO→LUMO transition.

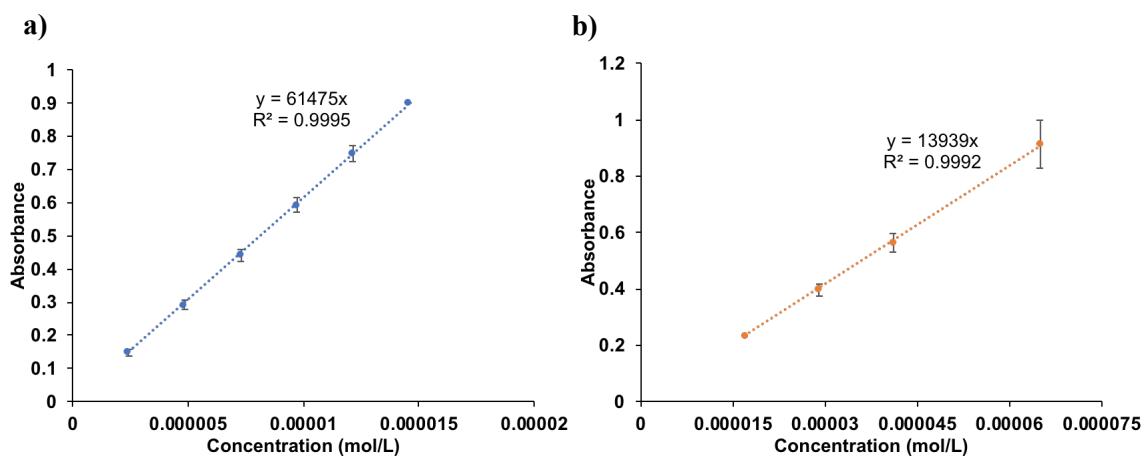


Figure A.4. Extinction coefficient determination of *m*[8]CPP at the a) absorbance maxima and b) HOMO→LUMO transition.

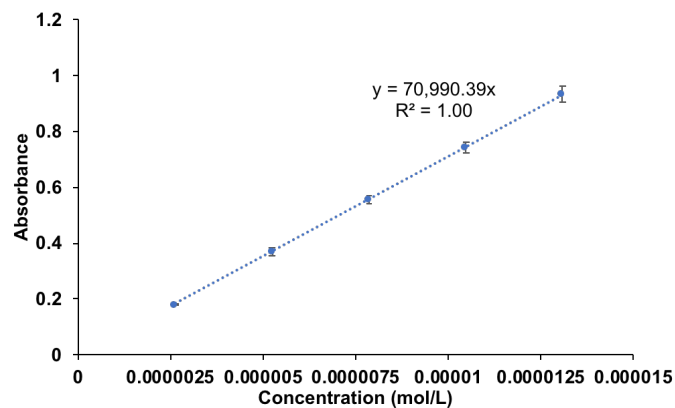


Figure A.5. Extinction coefficient determination of *m*[10]CPP at the absorbance maxima.

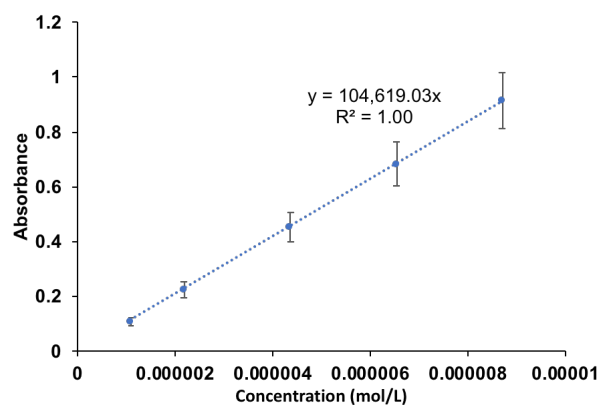


Figure A.6. Extinction coefficient determination of *m*[12]CPP at the absorbance maxima.

<i>m</i> [<i>n</i>]CPP	Trial 1	Trial 2	Trial 3	Φ Aver.
5	0.013	0.014	0.014	0.014 ± 0.001
6	0.225	0.224	0.224	0.224 ± 0.001
7	0.453	0.445	0.451	0.450 ± 0.004
8	0.592	0.598	0.595	0.595 ± 0.003
10	0.726	0.729	0.722	0.726 ± 0.004
12	0.77	0.772	0.766	0.769 ± 0.003

Table A.1. Triplicate quantum yield data, excited at the absorbance maxima.

$m[n]$ CPP	Trial 1	Trial 2	Trial 3	$\Phi_{\text{Aver.}}$
5	0.015	0.015	0.014	0.015 ± 0.001
6	0.246	0.232	0.234	0.237 ± 0.008
7	0.47	0.471	0.474	0.472 ± 0.002
8	0.608	0.612	0.608	0.609 ± 0.002

Table A.2. Triplicate quantum yield data, excited at HOMO→LUMO transition.

$m[n]$ CPP	H→L Absorbance (nm)	$\epsilon_{\text{H→L}}$ (M ⁻¹ cm ⁻¹)
5	428	$6.0 \times 10^3 \pm 0.3$
6	410	$9.4 \times 10^3 \pm 0.5$
7	394	$9.9 \times 10^3 \pm 0.08$
8	376	$1.4 \times 10^4 \pm 0.1$

Table A.3. HOMO→LUMO absorbance maxima and extinction coefficients.

$m[n]$ CPP	Lifetime (ns)	Rate of radiative decay (10^8 s^{-1})	Rate of non-radiative decay (10^8 s^{-1})
5	1.05	0.133	9.36
6	2.68	0.834	2.89
7	3.56	1.26	1.54
8	3.41	1.45	1.48
10	2.45	2.96	1.12
12	1.78	4.32	1.30

Table A.4. Fluorescence lifetimes and calculated decay rates.

A.3. Electrochemical Analysis

The oxidation of these molecules proceeds similar to that of CPPs with a decreasing oxidation potential with decreasing size. Two reversible oxidations are observed in the electrochemical window of dichloromethane except for **$m[5]$ CPP** which had a single irreversible oxidation event. As the size of the $m[n]$ CPP increases, the separation between the oxidations becomes smaller and both oxidations shift to higher potential.

$m[n]$ CPP	1 st Oxidation (V)	2 nd Oxidation (V)	Difference (V)
6	0.50	0.68	0.18
7	0.65	0.82	0.17
8	0.70	0.85	0.15
10	0.79	0.90	0.11
12	0.86	0.94	0.08

Table A.5. Oxidation potentials of $m[n]$ CPPs.

$m[n]$ CPP	1 st Oxidation Peak (V)
5	0.47
6	0.53
7	0.67
8	0.74
10	0.81
12	0.88

Table A.6. First oxidation peak of $m[n]$ CPPs.

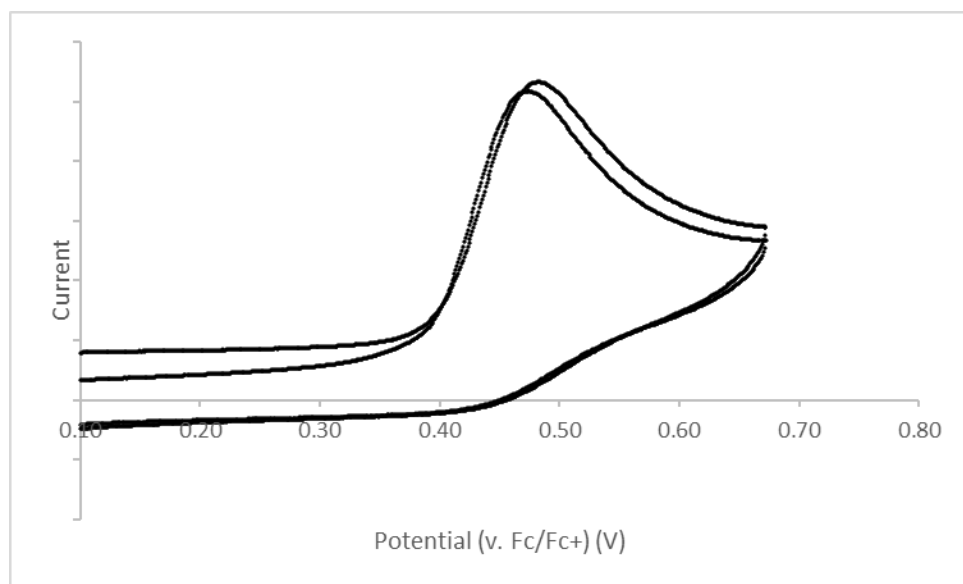


Figure A.7. $m[5]$ CPP Single irreversible oxidation (dichloromethane) $E = 0.47$ V.

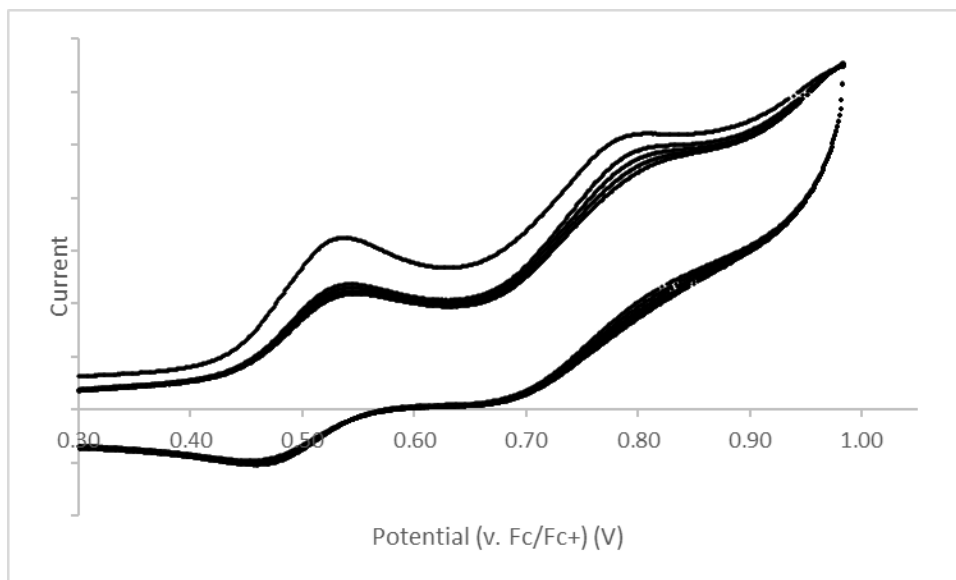


Figure A.8. *m*[6]CPP Oxidation (dichloromethane) $E_{1/2} = 0.50$ V and 0.68 V.

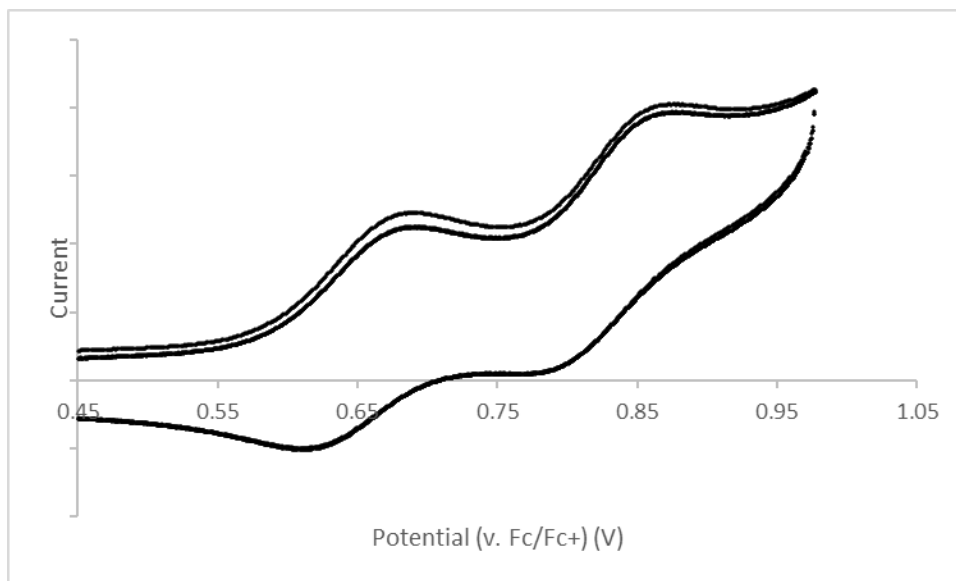


Figure A.9. *m*[7]CPP Oxidation (dichloromethane) $E_{1/2} = 0.65$ V and 0.81 V.

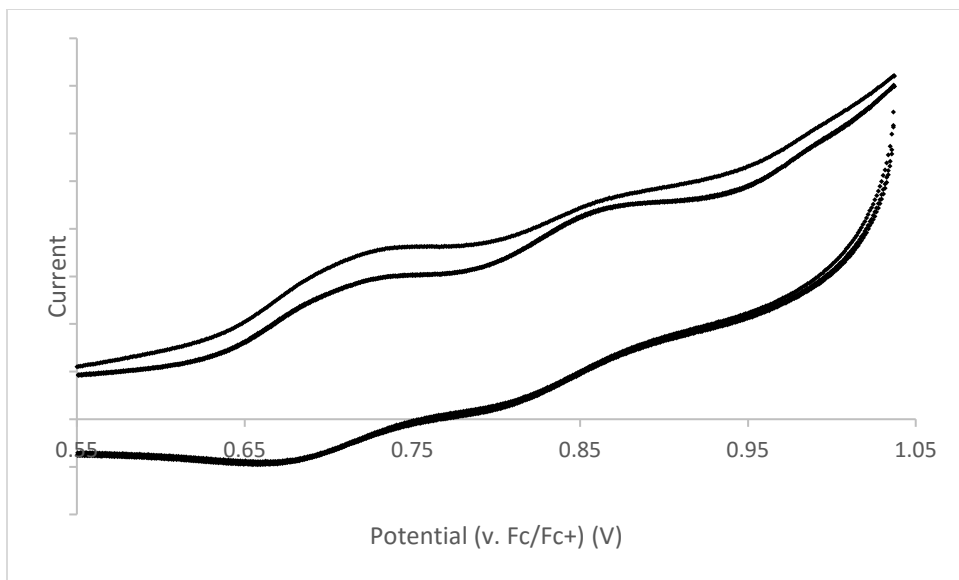


Figure A.10. *m*[8]CPP Oxidation (dichloromethane) $E_{1/2} = 0.69$ V and 0.85 V.

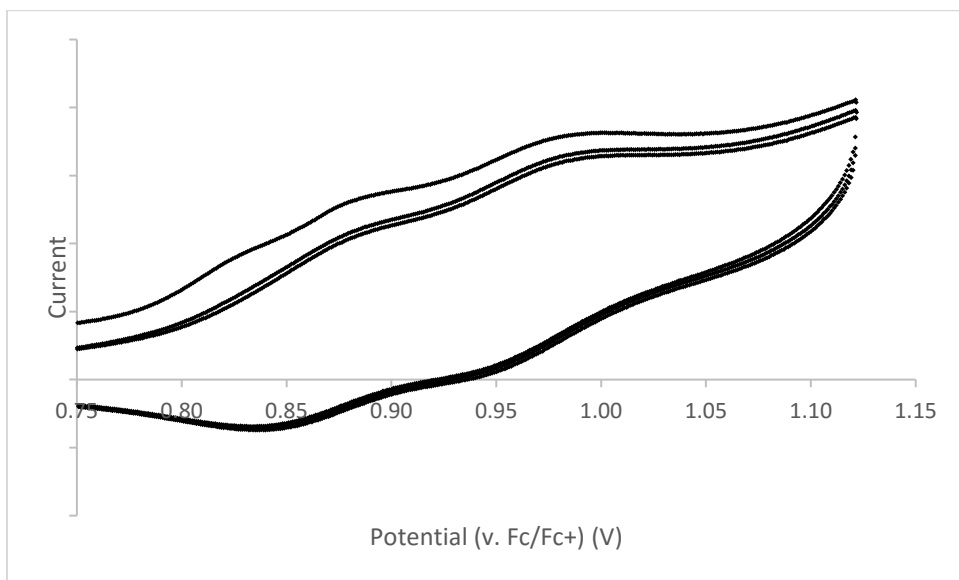


Figure A.11. *m*[10]CPP Oxidation (dichloromethane) $E_{1/2} = 0.80$ V and 0.91 V.

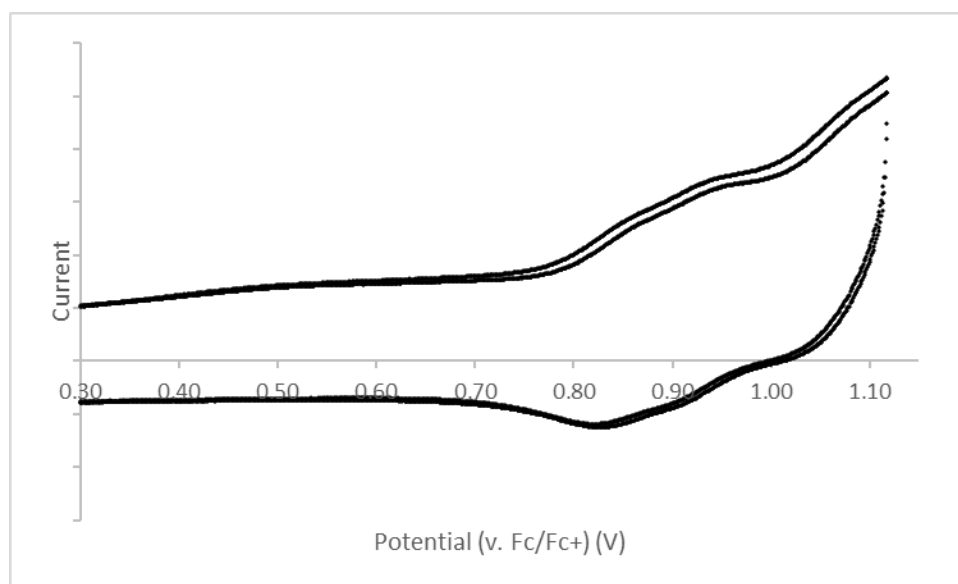


Figure A.12. *m*[12]CPP Oxidation (dichloromethane) $E_{1/2} = 0.86$ V and 0.95 V.

A.4. HOMO and LUMO Level Calculations

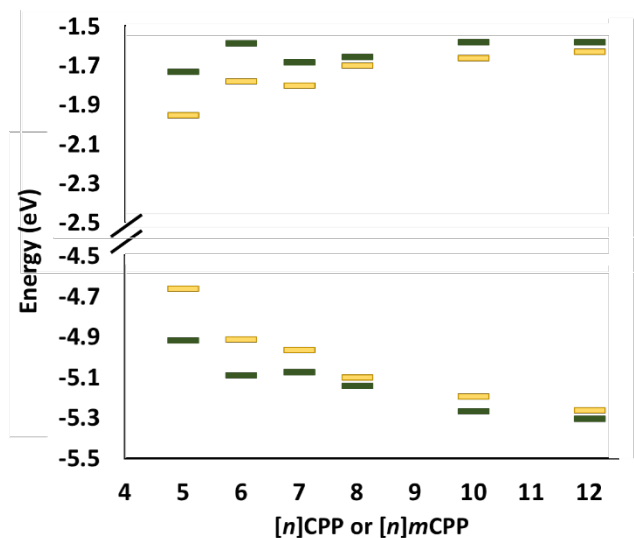


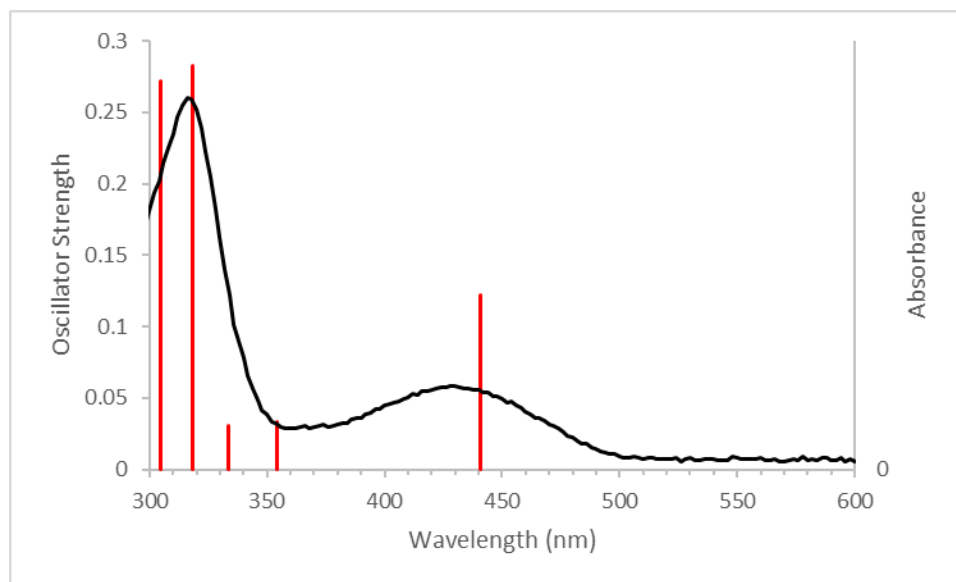
Figure A.13. Comparison of HOMO and LUMO energy levels of $[n]$ CPPs (yellow) and $m[n]$ CPPs (green). Calculated using B3LYP/6-31G(d,p) level of theory.

A.5. Calculated Absorption Spectra

Geometries optimized using Gaussian 09⁸⁸ with B3LYP/6-31G(d,p), then using the same basis, a time dependent calculation of 12 states was performed. The results were analyzed using GaussSum.

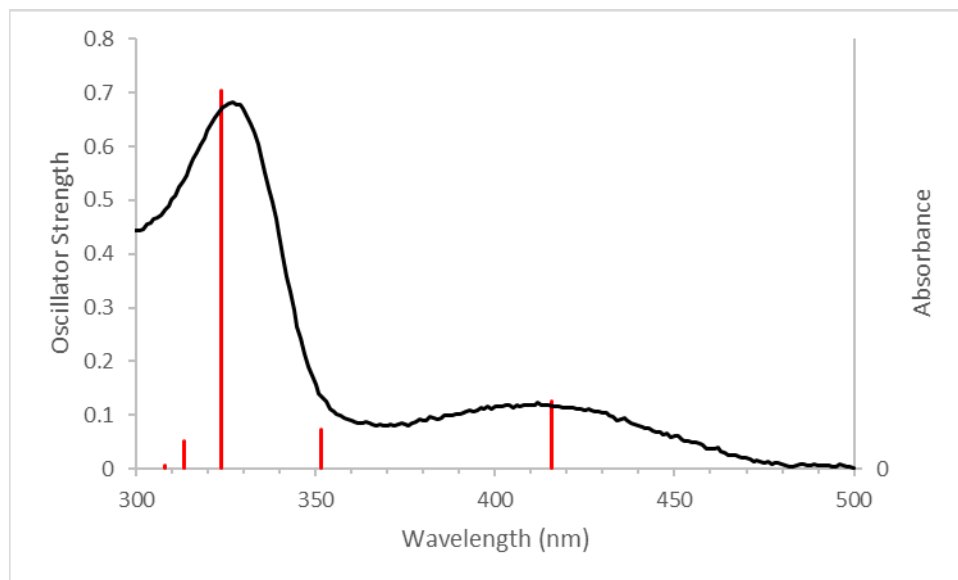
$m[n]$ CPP	λ_{max} (nm)	Oscillator strength	H→L Contribution (%)
5	441	0.122	98
6	416	0.126	97
7	404	0.172	97
8	397	0.176	95
10	388	0.227	91
12	383	0.281	86

Table A.7. Calculated HOMO→LUMO absorption for $m[n]$ CPPs.



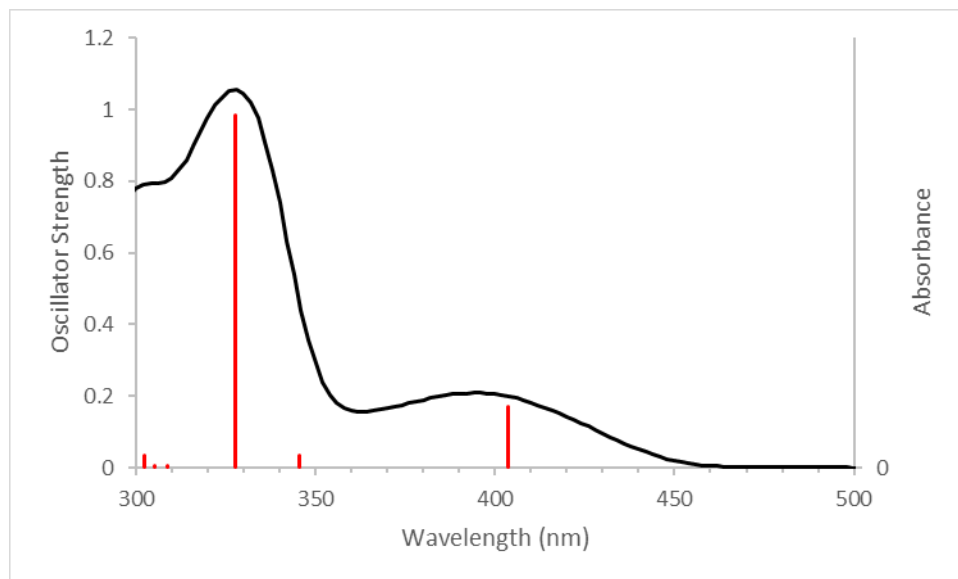
No.	Energy (cm-1)	Wavelength (nm)	Osc. Strength	Symmetry	Major contributing transitions
1	22677.08	440.9738	0.1217	Singlet-A	HOMO->LUMO (98%)
2	28232.63	354.2001	0.033	Singlet-A	H-1->LUMO (27%), HOMO->L+1 (71%)
3	29990.92	333.4343	0.0309	Singlet-A	H-1->LUMO (15%), HOMO->L+2 (70%)
4	31409.65	318.3735	0.2824	Singlet-A	H-1->LUMO (38%), HOMO->L+1 (17%), HOMO->L+2 (13%), HOMO->L+3 (24%)
5	32829.18	304.607	0.272	Singlet-A	H-1->LUMO (17%), HOMO->L+3 (51%)
6	34168.07	292.6709	0.0064	Singlet-A	H-2->LUMO (73%), H-1->L+1 (16%)
7	34314.05	291.4258	0.0007	Singlet-A	H-1->L+1 (37%), HOMO->L+4 (51%)
8	34995.59	285.7503	0.0523	Singlet-A	H-4->LUMO (10%), H-2->LUMO (12%), H-1->L+1 (20%), HOMO->L+4 (30%)
9	35145.61	284.5306	0.002	Singlet-A	H-4->LUMO (12%), H-3->LUMO (12%), HOMO->L+5 (33%), HOMO->L+6 (10%)
10	35563.4	281.1879	0.0103	Singlet-A	H-4->LUMO (23%), H-3->LUMO (14%), HOMO->L+6 (21%)
11	35806.18	279.2814	0.0019	Singlet-A	H-3->LUMO (37%), HOMO->L+6 (15%)
12	36343.34	275.1536	0.0588	Singlet-A	H-7->LUMO (23%), H-4->LUMO (23%), HOMO->L+8 (13%)

Figure A.14. *m*[5]CPP Calculated absorption (red lines) compared to experimental absorption (black trace) results and table of calculated transitions.



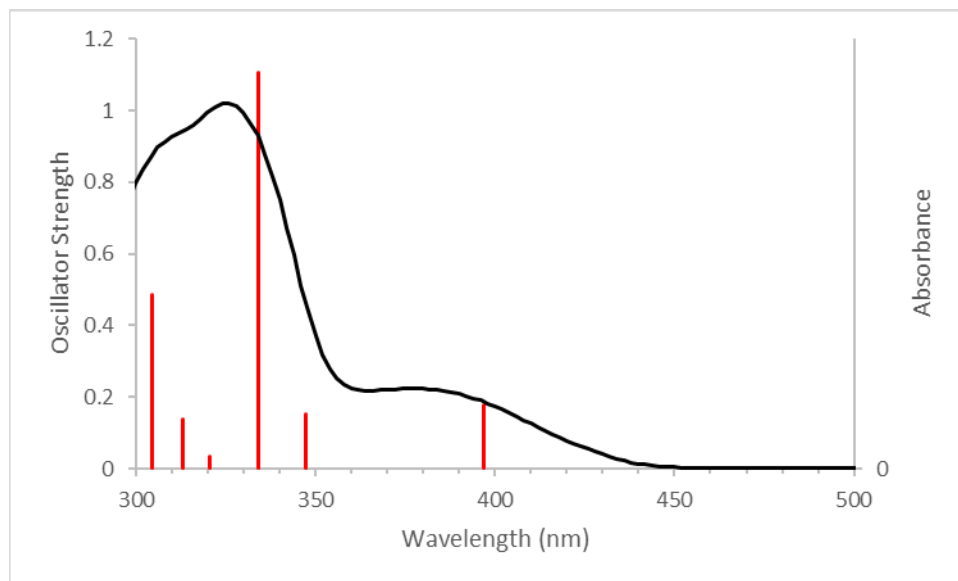
No.	Energy (cm-1)	Wavelength (nm)	Osc. Strength	Symmetry	Major contributing transitions
1	24054.68	415.7195	0.126	Singlet-A	HOMO->LUMO (97%)
2	28438.3	351.6384	0.0731	Singlet-A	H-1->LUMO (25%), HOMO->L+1 (74%)
3	30893.45	323.6932	0.7042	Singlet-A	H-1->LUMO (70%), HOMO->L+1 (22%)
4	31889.55	313.5824	0.0502	Singlet-A	HOMO->L+2 (79%)
5	32471.07	307.9664	0.0069	Singlet-A	H-2->LUMO (15%), H-1->L+1 (80%)
6	33162.29	301.5473	0.0005	Singlet-A	H-2->LUMO (30%), HOMO->L+3 (58%)
7	33675.26	296.9539	0.1059	Singlet-A	H-2->LUMO (36%), HOMO->L+4 (31%)
8	35029.47	285.474	0.2921	Singlet-A	H-2->LUMO (15%), HOMO->L+3 (27%), HOMO->L+4 (40%)
9	35264.17	283.5739	0.0218	Singlet-A	H-6->LUMO (18%), HOMO->L+5 (23%), HOMO->L+6 (37%)
10	36278.82	275.6429	0.0251	Singlet-A	H-3->LUMO (23%), HOMO->L+5 (40%), HOMO->L+6 (13%)
11	36550.63	273.5931	0.0082	Singlet-A	H-7->LUMO (27%), HOMO->L+7 (32%), HOMO->L+8 (21%)
12	36911.96	270.9149	0.0143	Singlet-A	H-8->LUMO (17%), H-3->LUMO (15%), H-2->L+1 (36%), HOMO->L+9 (13%)

Figure A.15. *m*[6]CPP Calculated absorption (red lines) compared to experimental absorption (black trace) results and table of calculated transitions.



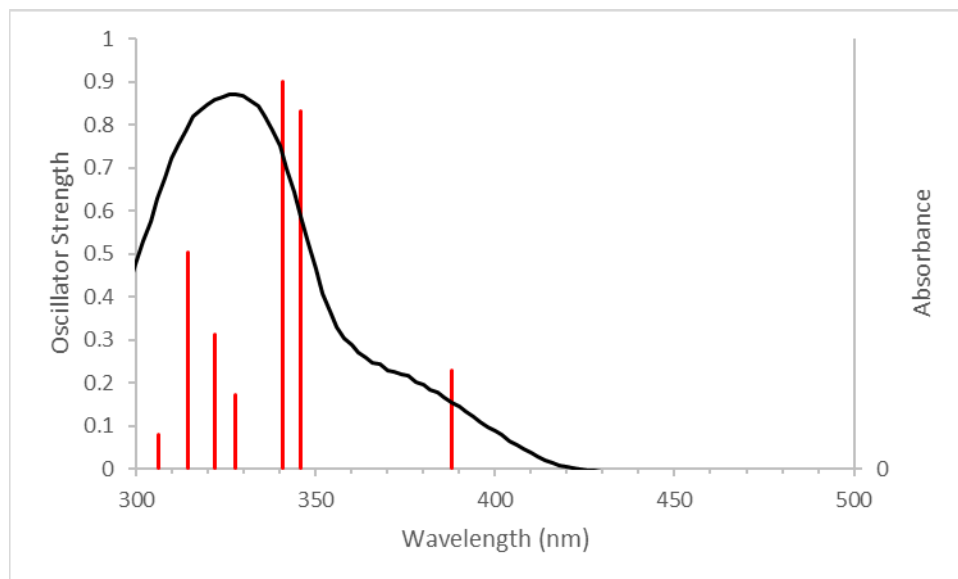
No.	Energy (cm-1)	Wavelength (nm)	Osc. Strength	Symmetry	Major contributing transitions
1	24781.38	403.5287	0.1718	Singlet-A	HOMO->LUMO (97%)
2	28944.01	345.4946	0.0342	Singlet-A	H-1->LUMO (32%), HOMO->L+1 (66%)
3	30529.7	327.5499	0.9834	Singlet-A	H-1->LUMO (66%), HOMO->L+1 (31%)
4	32396.87	308.6718	0.0062	Singlet-A	H-2->LUMO (12%), H-1->L+1 (83%)
5	32745.3	305.3873	0.0071	Singlet-A	H-2->LUMO (48%), HOMO->L+2 (45%)
6	33070.34	302.3857	0.0326	Singlet-A	H-4->LUMO (10%), HOMO->L+4 (74%)
7	33687.36	296.8473	0.2207	Singlet-A	H-2->LUMO (23%), HOMO->L+2 (23%), HOMO->L+3 (25%)
8	34174.52	292.6157	0.1759	Singlet-A	H-2->LUMO (12%), HOMO->L+2 (22%), HOMO->L+3 (44%)
9	35339.18	282.972	0.079	Singlet-A	HOMO->L+5 (43%)
10	35952.16	278.1474	0.0225	Singlet-A	H-2->L+1 (59%), H-1->L+2 (24%)
11	36171.55	276.4604	0.0569	Singlet-A	H-3->LUMO (24%), H-2->L+1 (10%), HOMO->L+3 (16%), HOMO->L+6 (12%)
12	36332.86	275.233	0.014	Singlet-A	H-10->LUMO (12%), H-3->LUMO (20%), HOMO->L+8 (20%)

Figure A.16. *m*[7]CPP Calculated absorption (red lines) compared to experimental absorption (black trace) results and table of calculated transitions.



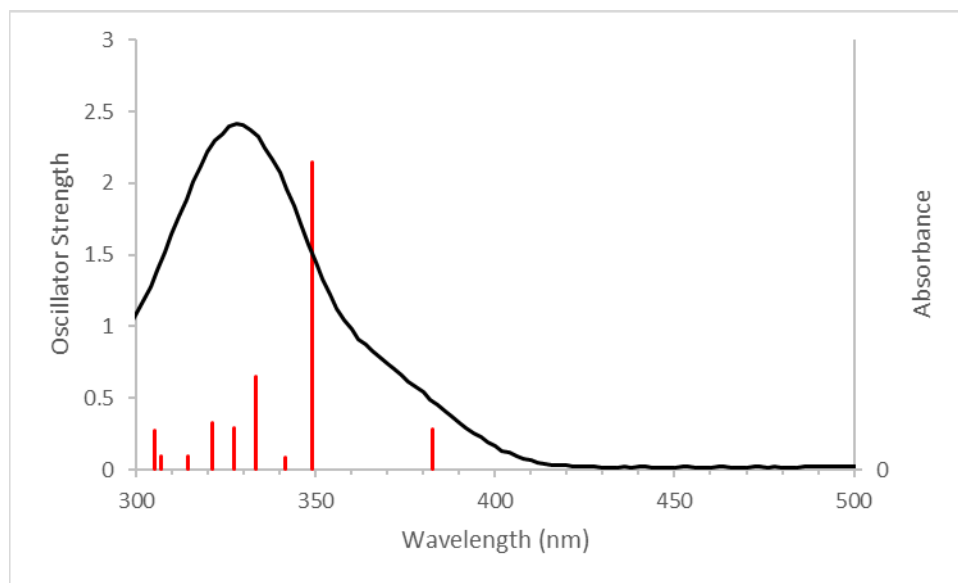
No.	Energy (cm-1)	Wavelength (nm)	Osc. Strength	Symmetry	Major contributing transitions
1	25186.28	397.0416	0.1764	Singlet-A	HOMO->LUMO (95%)
2	28785.12	347.4017	0.1531	Singlet-A	H-1->LUMO (18%), HOMO->L+1 (81%)
3	29923.98	334.1802	1.1065	Singlet-A	H-1->LUMO (80%), HOMO->L+1 (18%)
4	31187.85	320.6377	0.0351	Singlet-A	H-1->L+1 (85%)
5	31941.17	313.0756	0.1391	Singlet-A	H-2->LUMO (76%), HOMO->L+2 (14%)
6	32853.38	304.3827	0.4857	Singlet-A	H-2->LUMO (12%), HOMO->L+2 (78%)
7	33596.22	297.6525	0.0011	Singlet-A	H-5->LUMO (13%), HOMO->L+3 (19%), HOMO->L+4 (52%)
8	34197.1	292.4224	0.086	Singlet-A	H-2->L+1 (88%)
9	34645.55	288.6374	0.0318	Singlet-A	H-3->LUMO (12%), HOMO->L+3 (59%), HOMO->L+4 (18%)
10	34857.67	286.8809	0.0563	Singlet-A	HOMO->L+5 (55%)
11	35451.29	282.0772	0.0355	Singlet-A	H-3->LUMO (13%), H-1->L+2 (14%), HOMO->L+6 (29%)
12	35921.51	278.3847	0.2387	Singlet-A	H-3->LUMO (28%), H-1->L+2 (60%)

Figure A.17. *m*[8]CPP Calculated absorption (red lines) compared to experimental absorption (black trace) results and table of calculated transitions.



No.	Energy (cm-1)	Wavelength (nm)	Osc. Strength	Symmetry	Major contributing transitions
1	25783.93	387.8384	0.2275	Singlet-A	HOMO->LUMO (91%)
2	28917.4	345.8126	0.8323	Singlet-A	HOMO->L+1 (98%)
3	29329.55	340.9531	0.9001	Singlet-A	H-1->LUMO (98%)
4	30510.34	327.7577	0.1709	Singlet-A	H-1->L+1 (88%)
5	31057.99	321.9783	0.3116	Singlet-A	H-2->LUMO (94%)
6	31807.28	314.3934	0.5032	Singlet-A	HOMO->L+2 (93%)
7	32663.84	306.1489	0.0805	Singlet-A	H-2->L+1 (89%)
8	33421.2	299.2113	0.0744	Singlet-A	H-3->LUMO (13%), HOMO->L+3 (78%)
9	33980.14	294.2896	0.2859	Singlet-A	H-1->L+2 (80%)
10	34545.53	289.473	0.0021	Singlet-A	H-6->LUMO (11%), H-3->LUMO (26%), HOMO->L+5 (37%)
11	34706.84	288.1276	0.054	Singlet-A	H-3->L+1 (10%), H-2->L+2 (48%), H-1->L+3 (27%)
12	34819.76	287.1932	0.0489	Singlet-A	H-3->LUMO (46%), HOMO->L+3 (13%), HOMO->L+5 (23%)

Figure A.18. *m*[10]CPP Calculated absorption (red lines) compared to experimental absorption (black trace) results and table of calculated transitions.

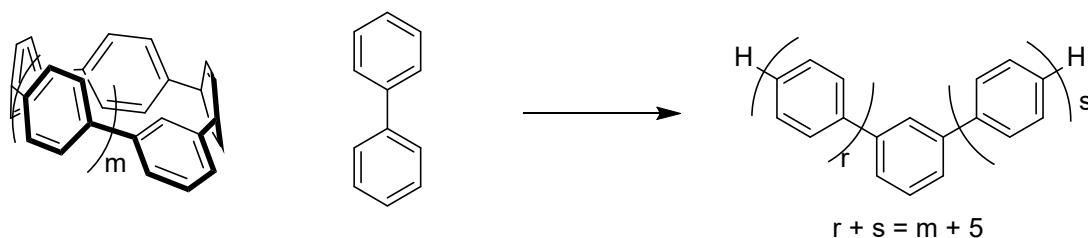


No.	Energy (cm-1)	Wavelength (nm)	Osc. Strength	Symmetry	Major contribs
1	26136.4	382.6082	0.2811	Singlet-A	H-1->L+1 (10%), HOMO->LUMO (86%)
2	28658.49	348.9367	2.1502	Singlet-A	H-1->LUMO (30%), HOMO->L+1 (67%)
3	29285.99	341.4602	0.0886	Singlet-A	H-1->LUMO (66%), HOMO->L+1 (30%)
4	29996.57	333.3715	0.647	Singlet-A	H-1->L+1 (74%), HOMO->LUMO (10%)
5	30553.89	327.2905	0.2915	Singlet-A	H-2->LUMO (88%)
6	31134.61	321.1859	0.3285	Singlet-A	HOMO->L+2 (92%)
7	31779.86	314.6647	0.0906	Singlet-A	H-2->L+1 (91%)
8	32568.67	307.0436	0.0951	Singlet-A	H-3->LUMO (18%), HOMO->L+3 (70%)
9	32750.95	305.3347	0.2706	Singlet-A	H-1->L+2 (82%)
10	33423.62	299.1897	0.031	Singlet-A	H-2->L+2 (64%), H-1->L+3 (21%)
11	33493.79	298.5628	0.0572	Singlet-A	H-3->LUMO (73%), HOMO->L+3 (23%)
12	33971.27	294.3664	0.3944	Singlet-A	H-3->L+1 (34%), H-2->L+2 (23%), H-1->L+3 (32%)

Figure A.19. *m*[12]CPP Calculated absorption (red lines) compared to experimental absorption (black trace) results and table of calculated transitions.

A.6. Inherent Strain Calculation

Strain calculated by comparison of single point energy of optimized geometries of the molecules in the theoretical homodesmotic reaction shown below. Geometries optimized using Gaussian 09⁸⁸ with B3LYP/6-31G(d,p).



$m[n]$ CPP	m	r	s	Nanohoop	biphenyl	Linear product	Strain (hartrees)	Strain (kcal/mol)
5	1	3	3	-1155.146	-463.3164	-1618.625	0.162858	102.2
6	2	4	3	-1386.234	-463.3164	-1849.674	0.123644	77.6
7	3	4	4	-1617.313	-463.3164	-2080.735	0.105867	66.4
8	4	5	4	-1848.389	-463.3164	-2311.795	0.090321	56.7
10	6	6	5	-2310.563	-463.3164	-2773.961	0.081901	51.4
12	8	7	6	-2772.704	-463.3164	-3236.089	0.068955	43.3

Table A.8. Single point energies of compounds used in homodesmotic reactions and calculated strain.


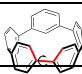
$m[n]$ CPP	Strain energy (kcal/mol)	Strain per aryl ring (kcal/mol)	Phenylene ipso carbon deviation from planarity (°)		Dihedral angle (°) 
5	102 (119)	20 (24)	17.0 (15.8)		23
6	78 (97)	13 (16)	14.1 (12.6)		25
7	66 (84)	9 (12)	12.0 (10.9)		28
8	57 (72)	7 (9)	10.6 (9.3)		30
10	51 (58)	5 (6)	8.4 (7.7)		31
12	43 (48)	4 (4)	7.0 (6.2)		34

Table A.9. Calculated strain energy in $m[n]$ CPPs, ipso carbon deviation, and dihedral angle. $[n]$ CPP values in brackets.³⁹ Strain per aryl ring values are not perfectly

comparable due to the *meta*-phenylene in *m[n]*CPPs. *ipso* carbon deviations are for phenylenes opposite to the *meta* phenylene in the nanohoop.

A.7. X-ray Crystallography.

Diffraction intensities were collected at 173 K on a Bruker Apex2 Duo CCD diffractometer with a micro-focus Incoatec *I μ S* Cu source, CuK α radiation, $\lambda = 1.54178$ Å. Absorption correction was applied by SADABS.¹³⁹ Space group was determined based on systematic absences. Structure was solved by direct methods and Fourier techniques and refined on F^2 using full matrix least-squares procedures. All non-H atoms were refined with anisotropic thermal parameters. H atoms were found on the residual density map and refined with isotropic thermal parameters. The Flack parameter is 0.016(7). All calculations were performed by the Bruker SHELXL-2014/7 package.¹⁴⁰

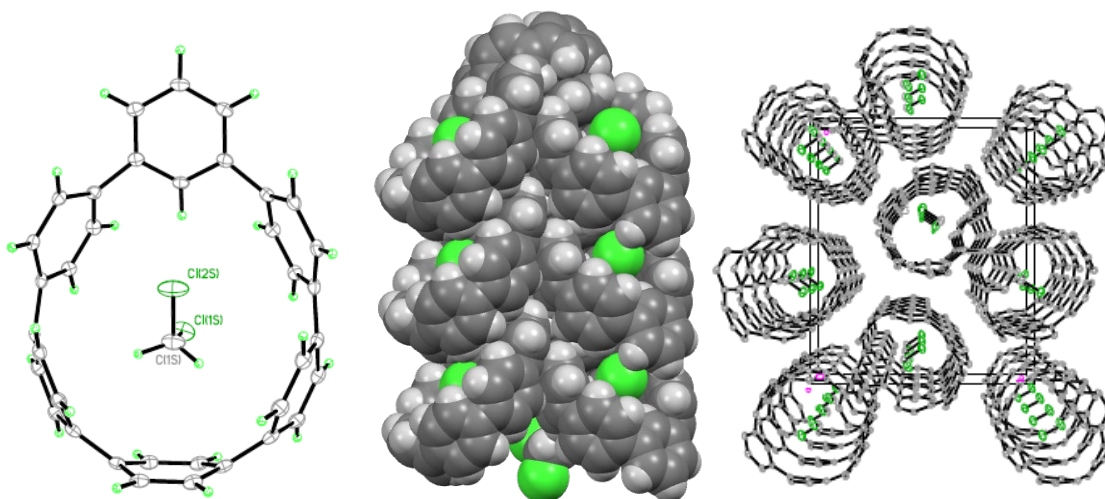


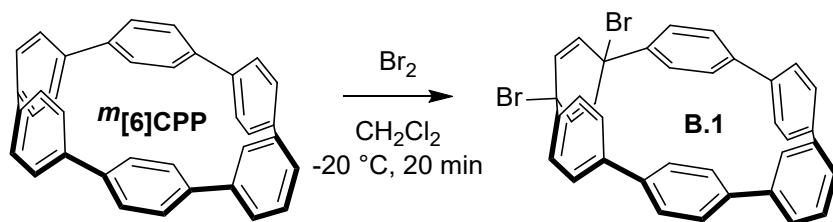
Figure A.20. ORTEP representation (thermal ellipsoids shown at 30% probability), space-filling model showing herringbone packing, and ORTEP representation showing columnar packing for *m*[6]CPP. One chlorine atom from a dichloromethane solvent molecule is located in the center of each hoop.

APPENDIX B

SUPPLEMENTARY INFORMATION FOR CHAPTER III

B.1. Experimental details

All glassware was flame dried and cooled under an inert atmosphere of nitrogen unless otherwise noted. Moisture sensitive reactions were carried out under nitrogen atmosphere using Schlenk and standard syringe/septa techniques. Dichloromethane was dried by filtration through alumina according to the methods describes by Grubbs.¹³⁶ ^1H NMR spectra were recorded at 500 MHz on a Bruker Advance-III-HD NMR spectrometer. ^{13}C NMR spectra were recorded at 125 MHz on a Bruker Advance-III-HD NMR spectrometer. All ^1H NMR spectra were taken in chloroform-*d* (referenced to TMS, δ 0.00 ppm). All ^{13}C NMR spectra were taken in chloroform-*d* (referenced to chloroform, δ 77.16 ppm). All reagents were obtained commercially unless otherwise noted. Mass spectra were obtained from the University of Illinois at Urbana-Champaign Mass Spectrometry Lab using ESI on a Micromass 70-VSE.



B.1. Freshly synthesized *m*[6]CPP³⁶ (8 mg, 17.5 nmol, 1 eq) was added to a flame dried 25 mL round bottom flask. The contents were evacuated and backfilled with nitrogen three times. Dichloromethane (6 mL) was added to the flask. This was cooled to $-20\text{ }^\circ\text{C}$. A 50 mM solution of Br_2 (64.0 μL) in methylene chloride (50 mL) was prepared in a flame dried 100 mL pear shaped flask. The bromine solution (385 μL , 19.3 nmol, 1.1 eq)

was added dropwise and the mixture was stirred at -20 °C for 20 min. The contents of the flask were passed through an Aura MT 0.45 µm PTFE syringe filter and evaporated under reduced pressure to obtain **B.1** as an orange-red solid (8.7 mg, 81%). ¹H NMR (500 MHz, Chloroform-*d*) δ 7.49 – 7.40 (m, 3H), 7.36 (d, *J* = 8.5 Hz, 4H), 7.33 (d, *J* = 8.4 Hz, 4H), 7.18 (d, *J* = 8.5 Hz, 4H), 7.11 (d, *J* = 8.4 Hz, 4H), 6.38 (s, 4H), 4.65 (t, *J* = 1.7 Hz, 1H). ¹³C NMR (126 MHz, CDCl₃) δ 143.35, 142.82, 142.69, 141.66, 140.34, 139.15, 130.35, 130.27, 129.08, 127.32, 126.78, 121.81, 56.44, 1.17. HRMS (ESI-TOF) (*m/z*): [M-HBr]⁺ calculated for C₃₆H₂₃Br, 534.09831; found, 534.09804.

B.2. Comments on calculations

Throughout the development of this program when fragments were clearly able to relax into perfectly flat aromatic hydrocarbons (fragments of CPPs or cyclophenacenes) the program worked best. This appears to be due to a clear and obvious trajectory on a potential energy surface between the strained and unstrained states and a finite end with a single conformation. When the trajectory is not so clear, as in the case of fragments with little strain (~10 kcal/mol or less) or alkyl chains (cyclophanes), more oversight by the user is required to acquire accurate results. There are two optimization errors that often lead to poor quality results. Non-converging optimizations where small changes in energy add up over many non-convergent cycles and instances where the algorithm takes a step into a high energy state. The program alerts the user if problems like this occur. This led to the use of the quasi-Newton rational function optimization algorithm for optimization, however, using this algorithm does not always solve these issues. When necessary,

calculating frequencies at each step does solve this problem in every instance tested, however, at a higher computational expense.

B.3. Instructions for running StrainViz

All details for running calculations can be found at

<https://github.com/CurtisColwell/StrainViz>

The following is an excerpt from the README.md file that details running a calculation

Use the following block diagram as a reference for the instructions below. All manual steps are shown in green, all automated steps are shown in red, and all intermediate files are shown in blue. The proton optimization files are deleted after being used.

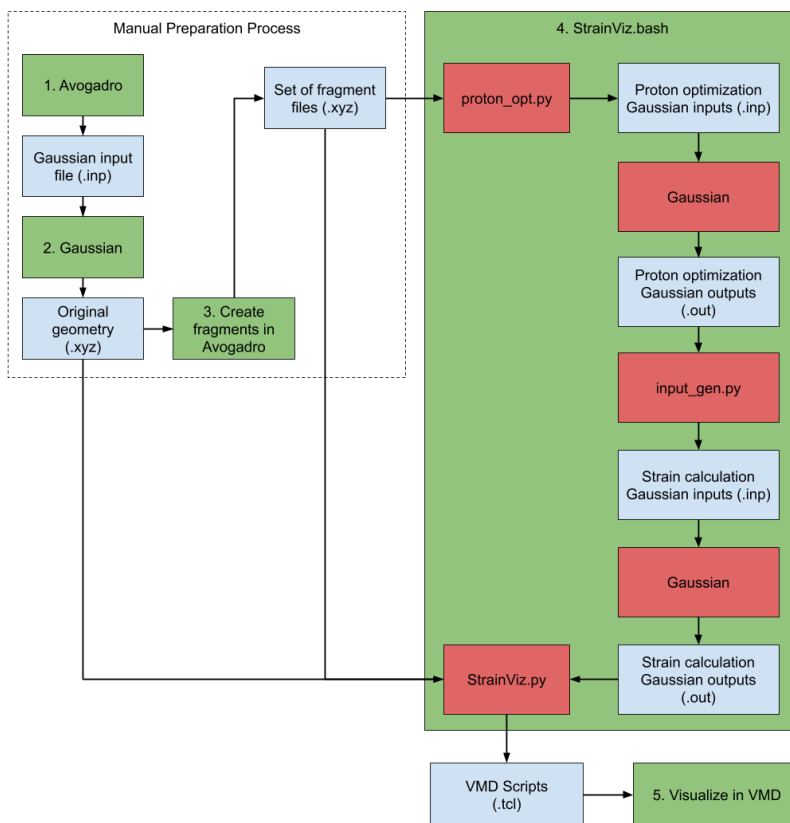


Figure B.1. Workflow diagram for StrainViz method.

1. Model the strained compound in Avogadro and create a Gaussian input file to optimize the geometry.
2. Use Gaussian to create an optimized geometry output file. Open this file in Avogadro and save it in the input/ directory with the .xyz file extension. Create a directory with the same name.
3. Create fragments by symmetrically deleting portions of the molecule that will allow the molecule to release its strain in Avogadro and save them as .xyz files in the directory named after the original molecule. Make sure that when a piece of the molecule is removed, protons are added to the empty bonding sites by drawing them at every severed bond. For an example, see the input/ folder where example-molecule.xyz is **[5]CPP** and five fragment .xyz files are in the related folder.
4. Run StrainViz to run multiple Gaussian jobs on each fragment and analyze the results. Specify the variable "molecule-name" so that it matches the geometry .xyz file and fragment folder, "processors-for-Gaussian" to be the number of processor for the Gaussian jobs, "level-of-theory" as a string that is the level of theory and basis set. This script creates .tcl files for the bond, angle and dihedral strain for each fragment and the combination of the fragments.

```
bash StrainViz.bash molecule-name processors-for-Gaussian level-of-theory
```

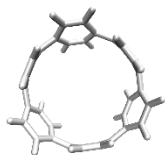
5. In VMD, open the "Tk Console" found under "Extensions", navigate to the output/molecule-name/ folder, and visualize the strain using the following

command while replacing "example.tcl" for the .tcl file you would like to visualize:

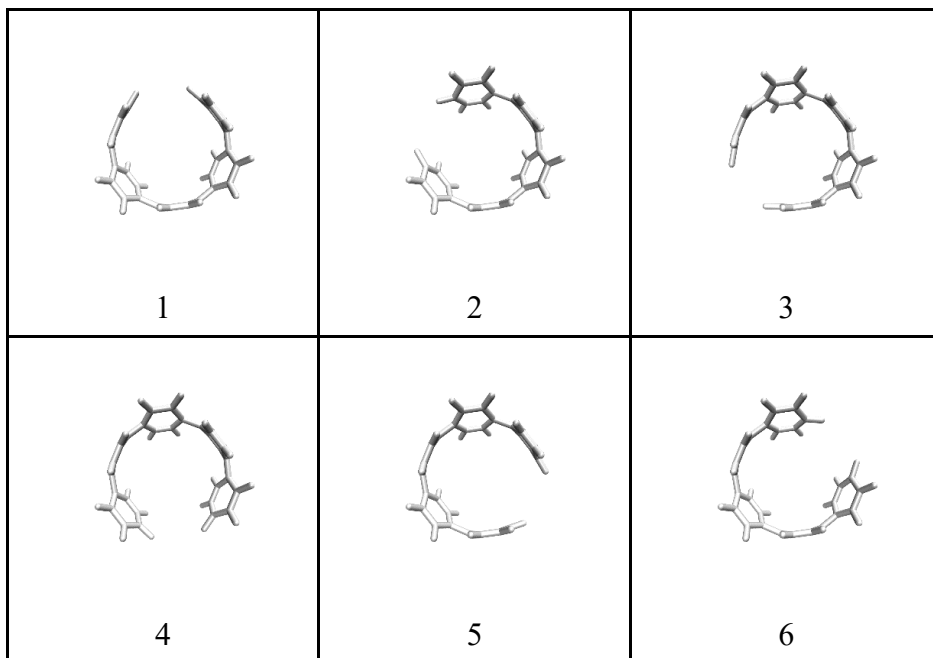
```
source example.tcl
```

B.4. Specific Example

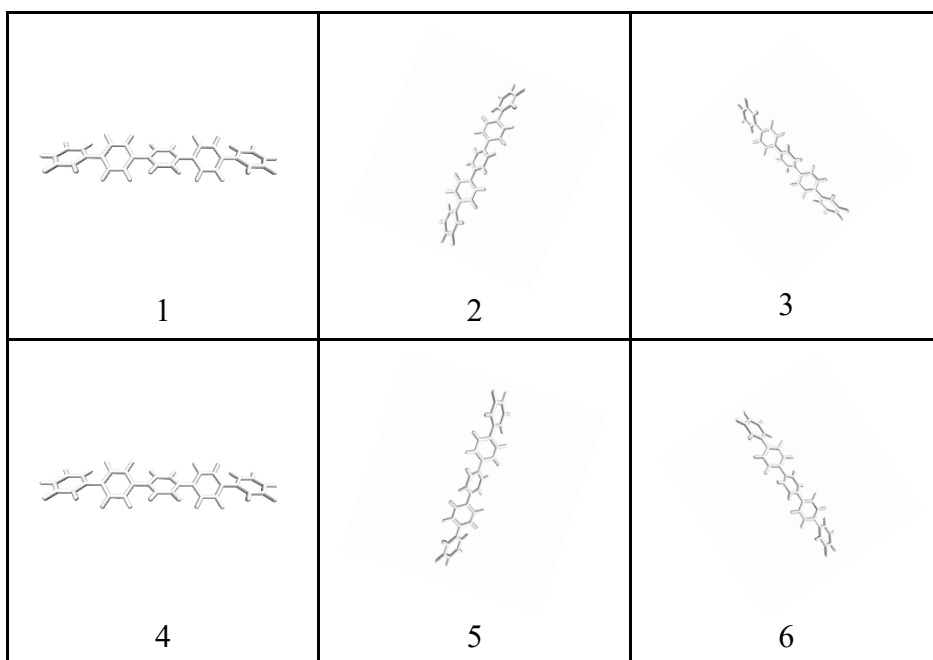
Below is a worked through example using [6]CPP. All files are from the attached Computational Results. First, the molecule is optimized using Gaussian to generate an optimized geometry for the molecule.



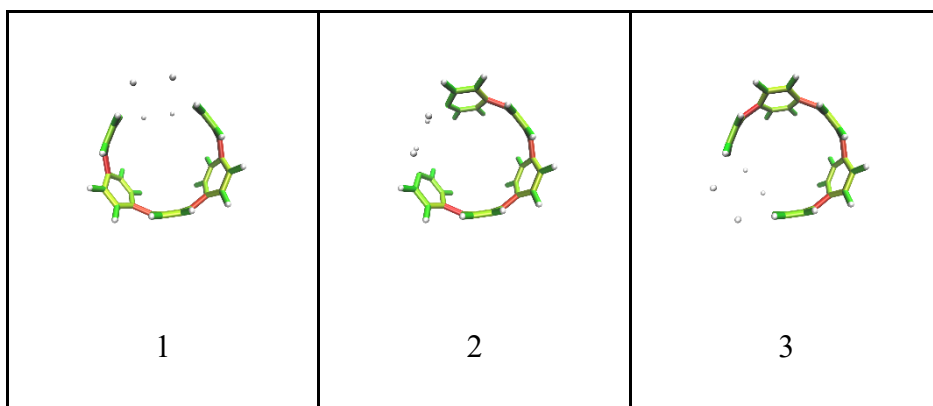
Then the molecule is split into six fragments.

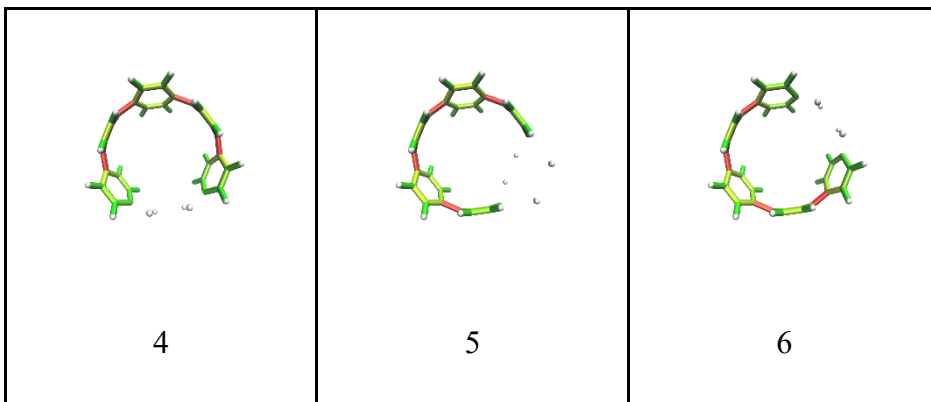


These six geometries are then submitted to StrainViz where they are optimized to find the following geometries and the strain released is determined.

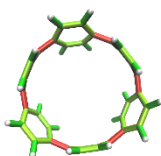


This strain is then mapped back on to the original geometry. In the output folder, there are three files generated per fragment: an angle, bond, and dihedral strain map. The dihedral map is shown here.





Finally, the strain is averaged over all fragments by the script and combined into a total picture for the entire molecule. This appears in the output folder as `total_force.tcl`



The scale bar can then be generated by opening `total_force.tcl` in a text editor. The first two lines are the minimum and maximum energies in kcal/mol.

B.5. Fragments used for strain calculations

All input files, fragment geometries, and output files are available for download. Fragment geometries are shown below and in .xyz format.

B.5.1. Fragments use for Figure III.4

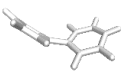
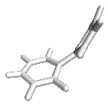
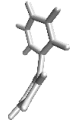
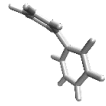
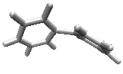
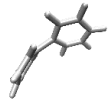
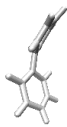
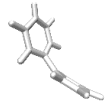
			
1	2	3	4
			
5	6	7	8

Table B.1. Fragments used for Figure III.4. Fragment size 2.

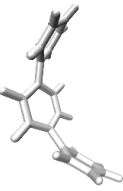
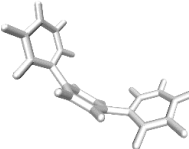
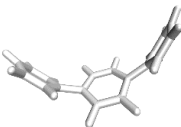
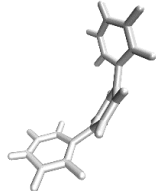
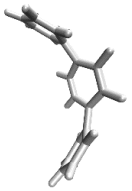
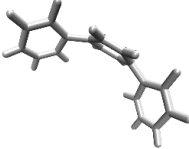
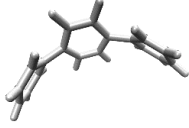
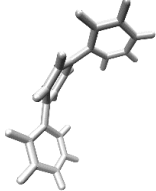
			
1	2	3	4
			
5	6	7	8

Table B.2. Fragments used for Figure III.4. Fragment size 3.

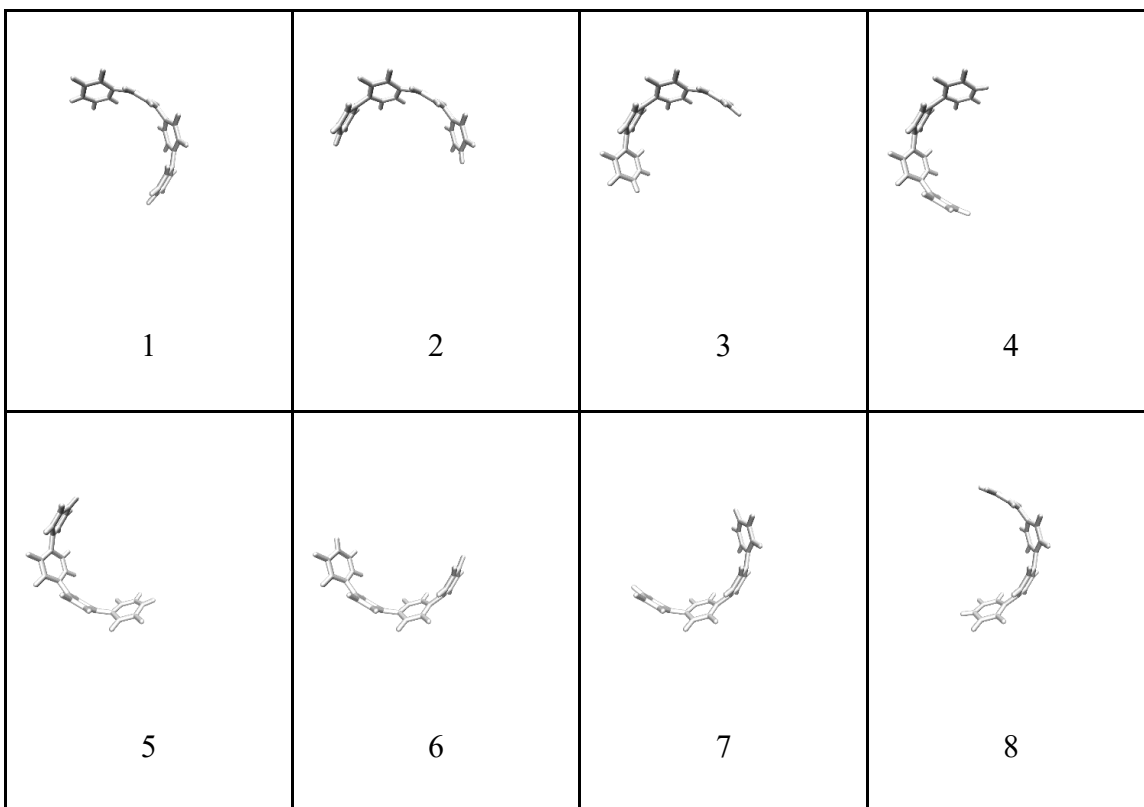


Table B.3. Fragments used for Figure III.4. Fragment size 4.

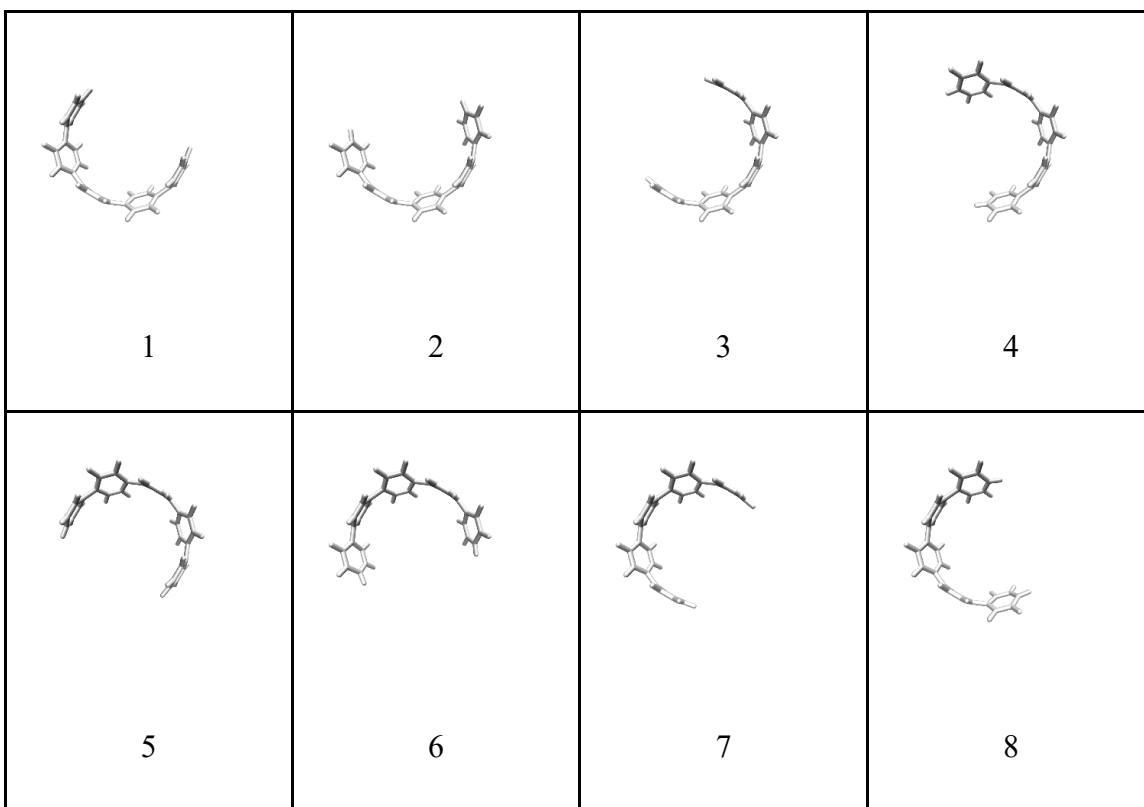


Table B.4. Fragments used for Figure III.4. Fragment size 5.

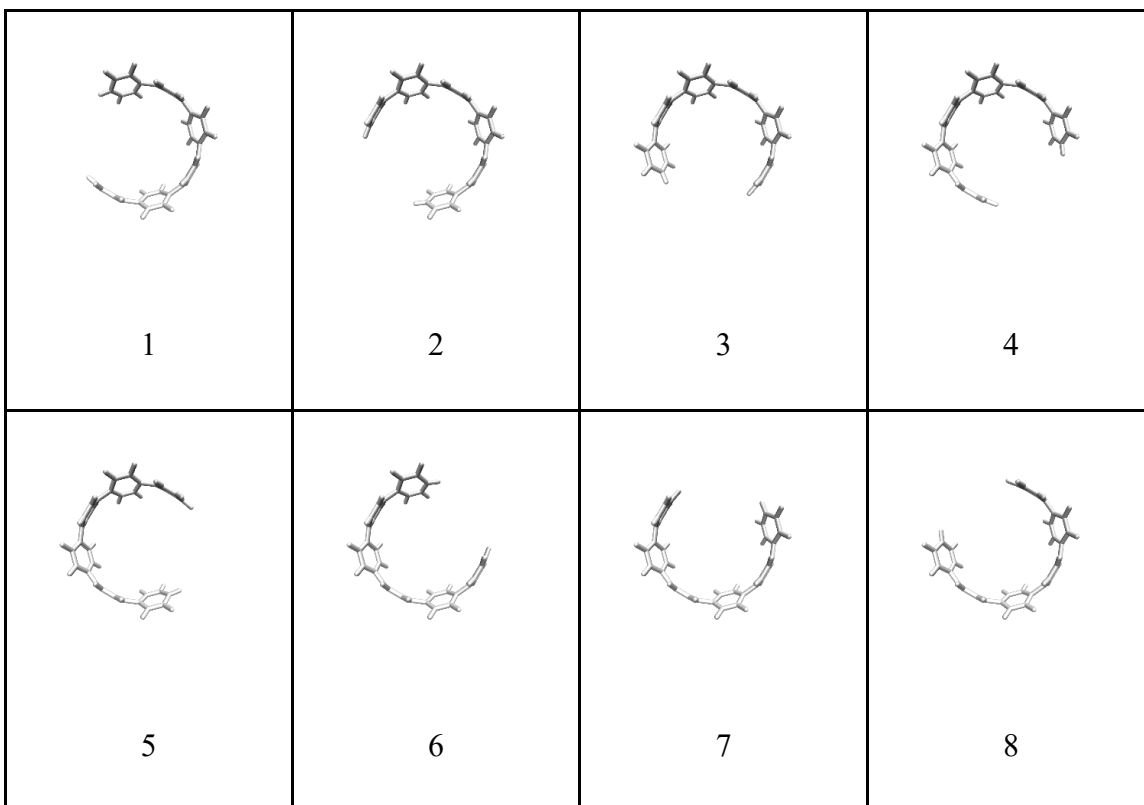


Table B.5. Fragments used for Figure III.4. Fragment size 6.

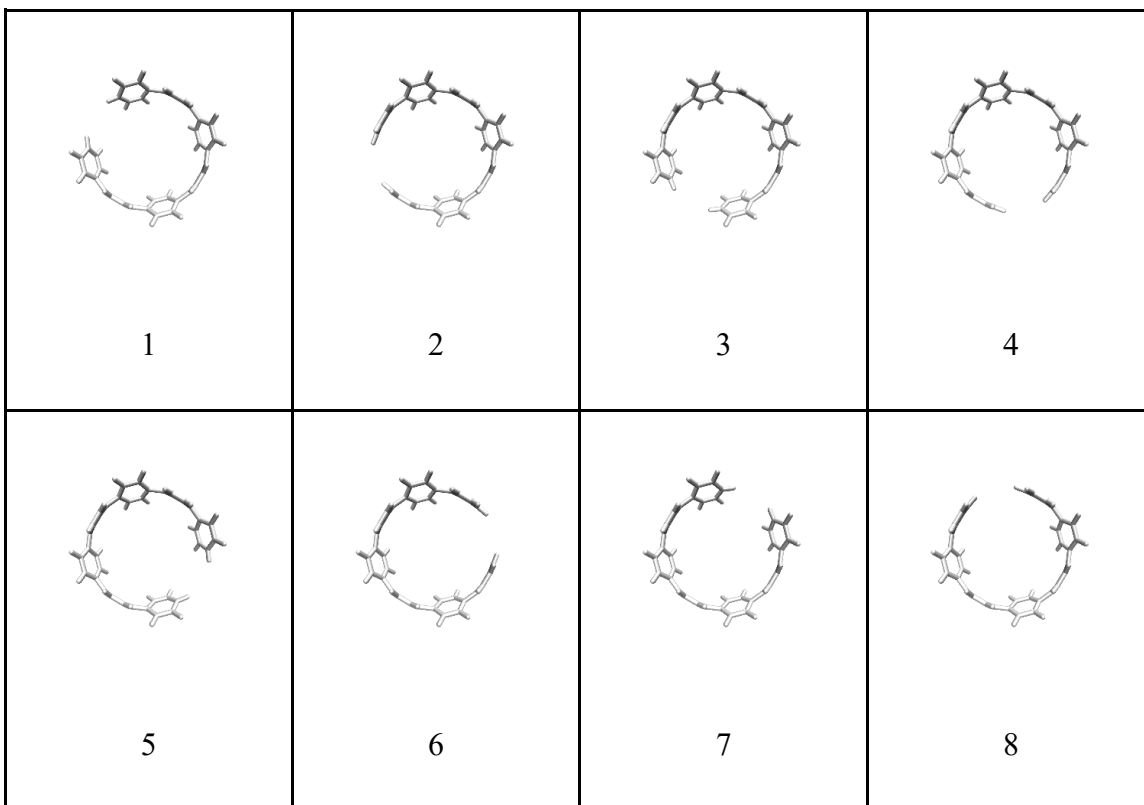


Table B.6. Fragments used for Figure III.4. Fragment size 7.

B.5.2. Fragments used for Figure III.5

[10]CPP

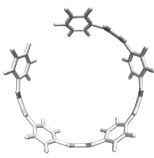
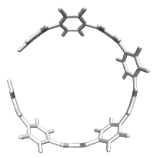
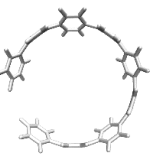
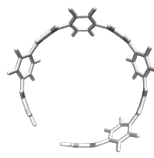
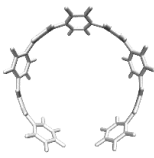
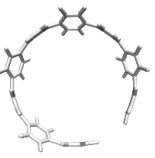
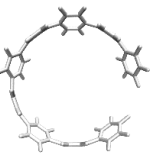
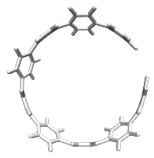
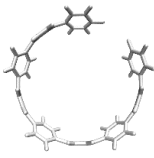

 1	 2	 3	 4
 5	 6	 7	 8
 9	 10		

Table B.7. Fragments used for [10]CPP.

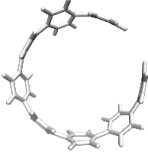
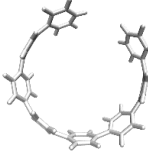
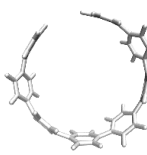
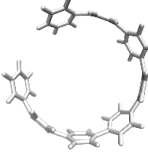
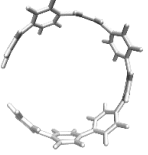
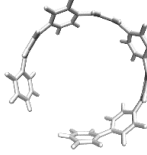
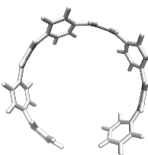
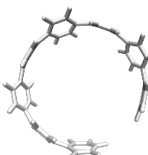
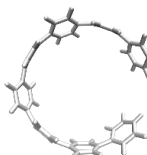
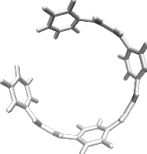
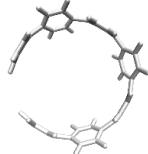
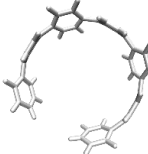
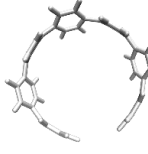
		
1	2	3
		
4	5	6
		
7	8	9

Table B.8. Fragments used for [9]CPP.

			
1	2	3	4

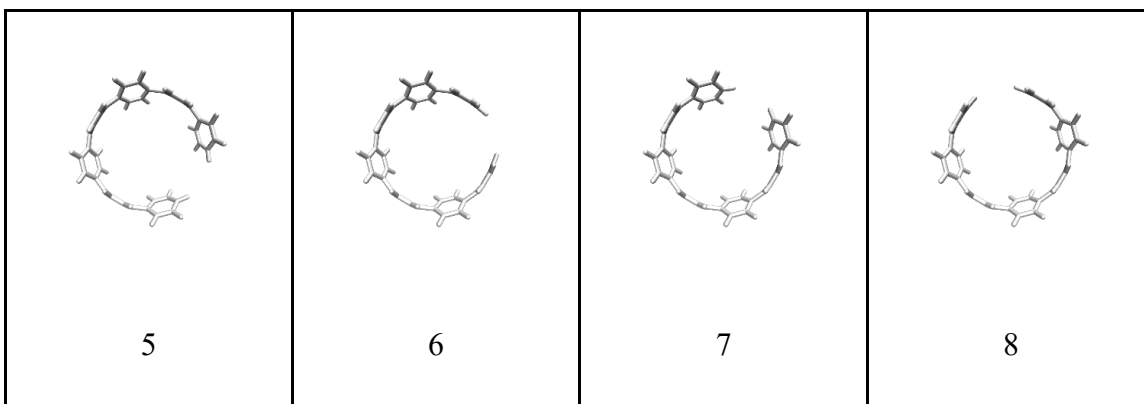


Table B.9. Fragments used for [8]CPP.

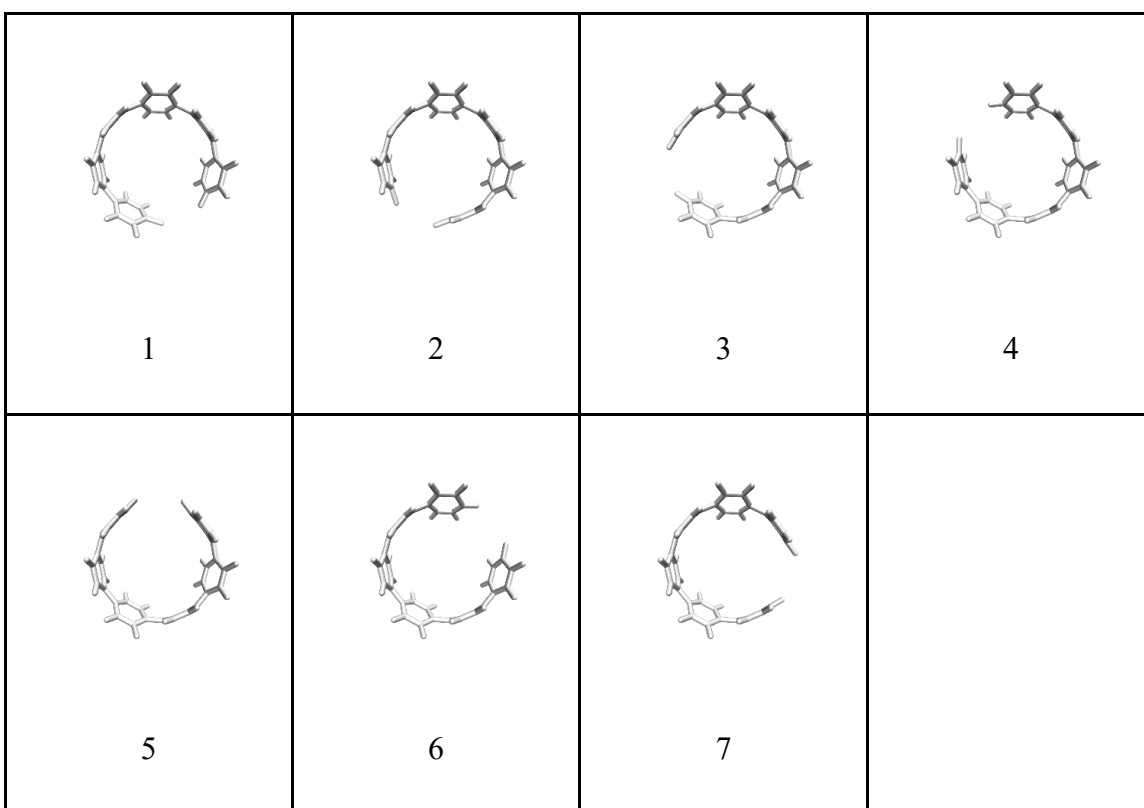


Table B.10. Fragments used for [7]CPP.

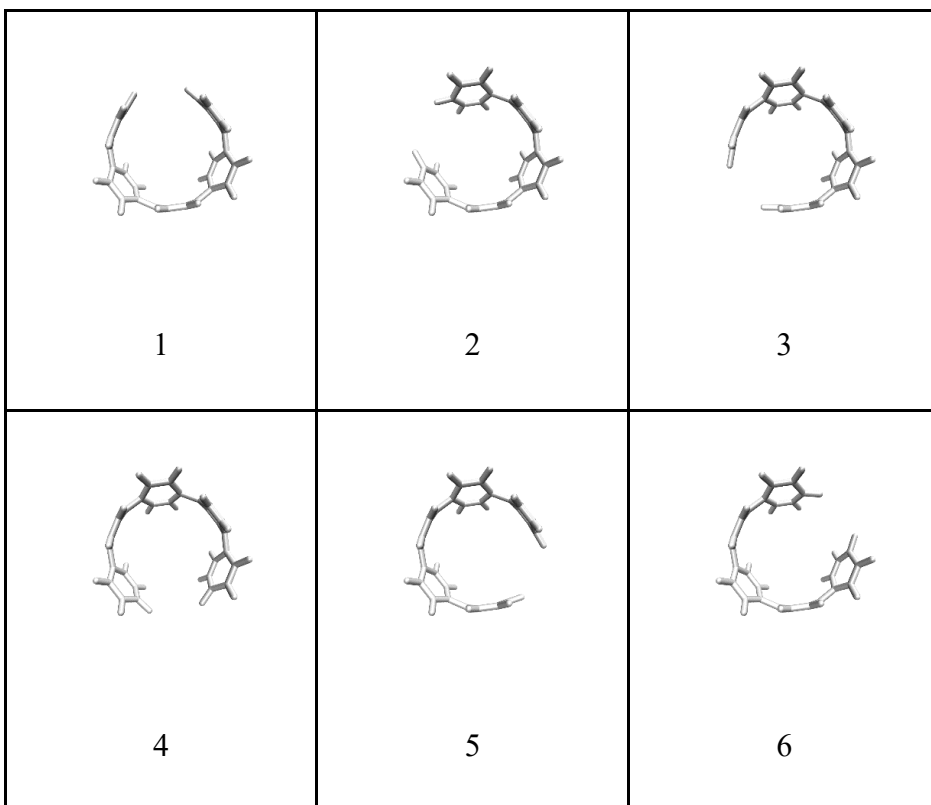


Table B.11. Fragments used for [6]CPP.

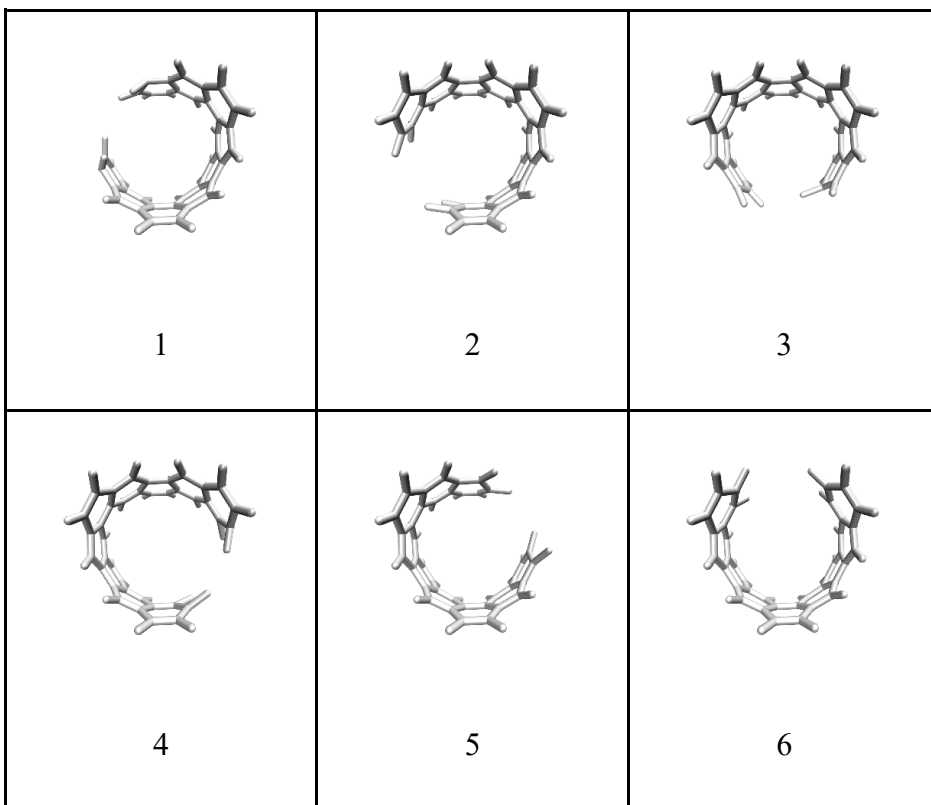


Table B.12. Fragments used for [6]cyclophenacene.

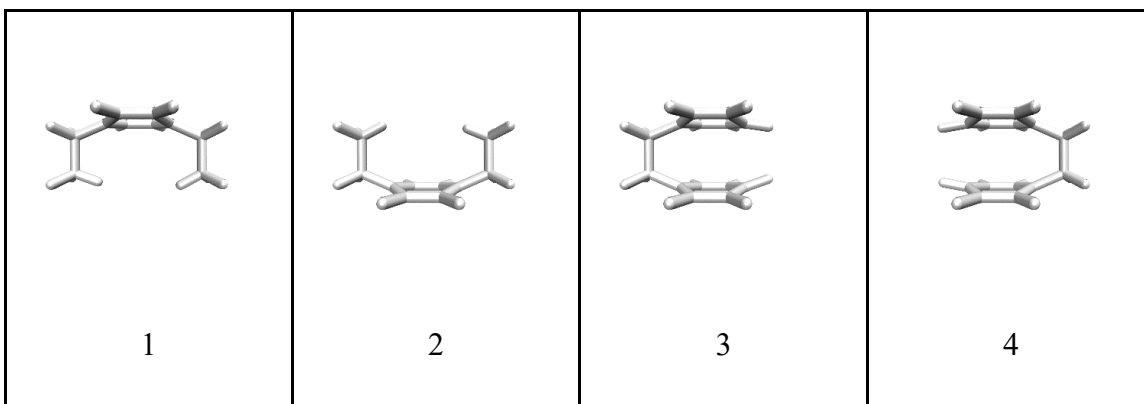


Table B.13. Fragments used for [2.2]paracyclophane.

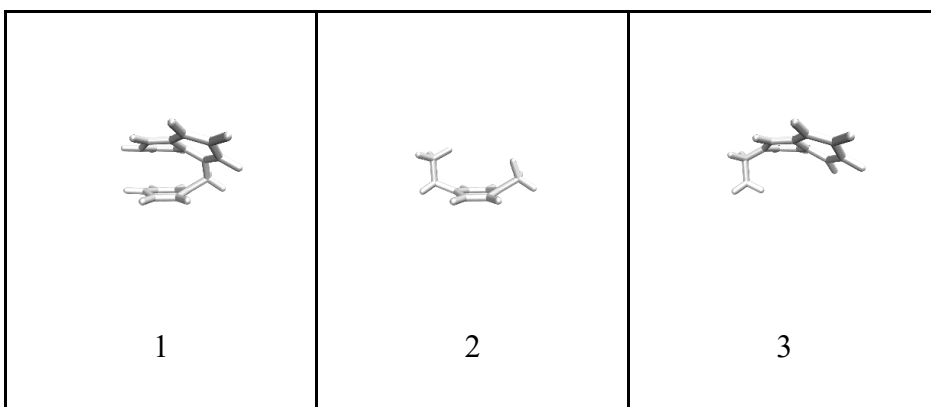


Table B.14. Fragments used for [2](6,1)naphthaleno[1]paracyclophane.

B.5.3. Fragments used for Figure III.6

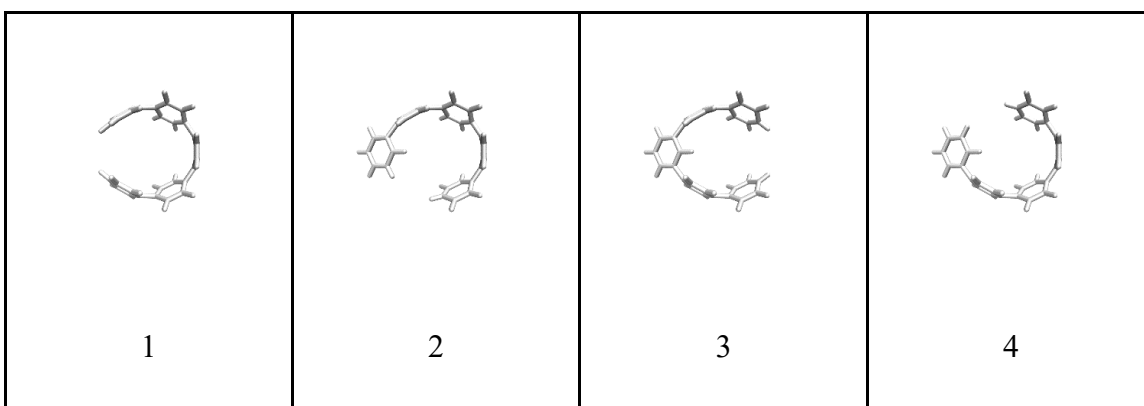


Table B.15. Fragments used for $m[6]CPP$.

B.5.4. Fragments used for Figure III.7

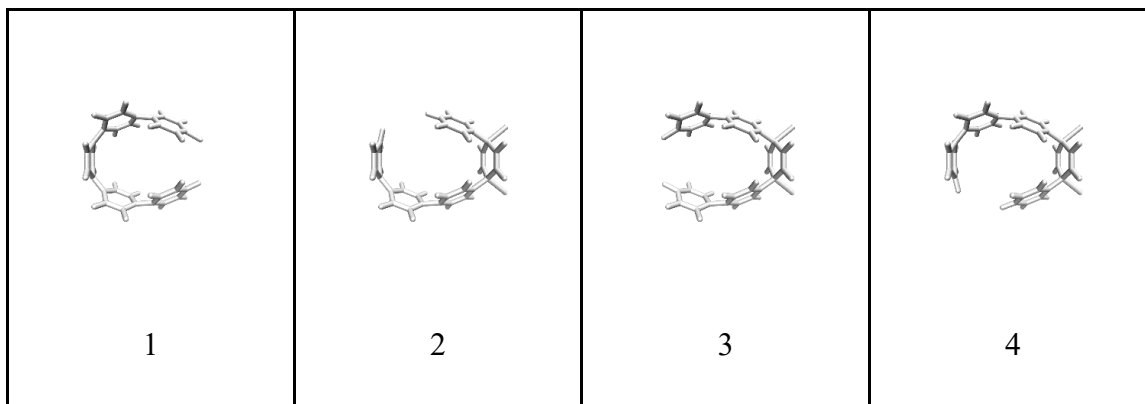


Table B.16. Fragments used for dibromo[6]CPP.

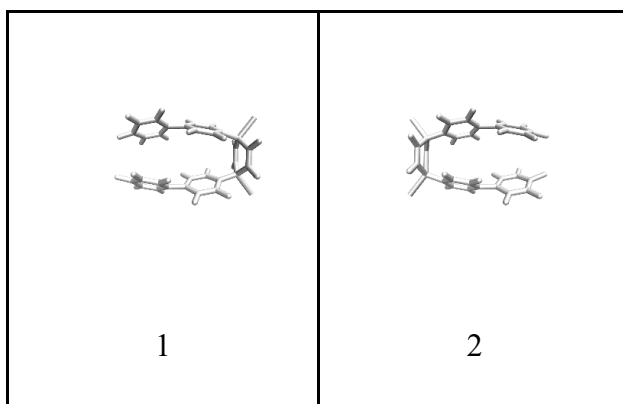


Table B.17. Fragments used for tetrabromo[6]CPP.

B.5.5. Fragments used for Figure III.8

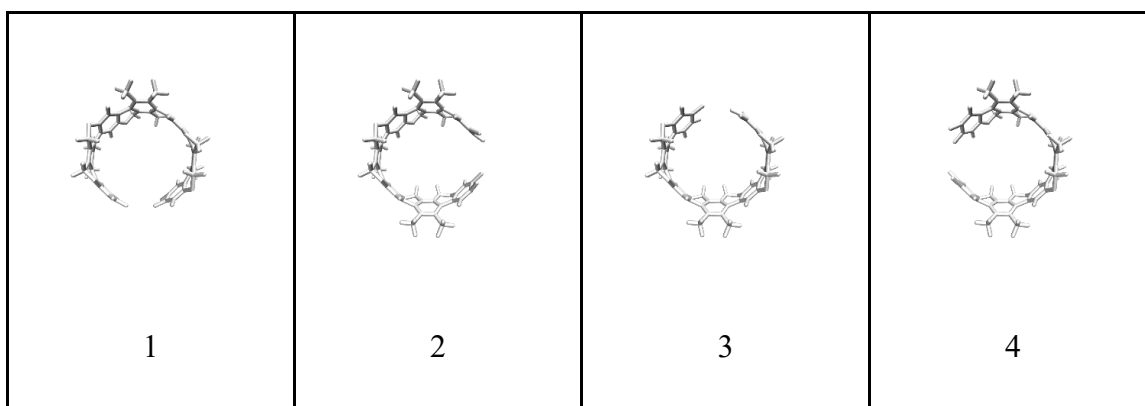


Table B.18. Fragments used for the Tanaka belt.

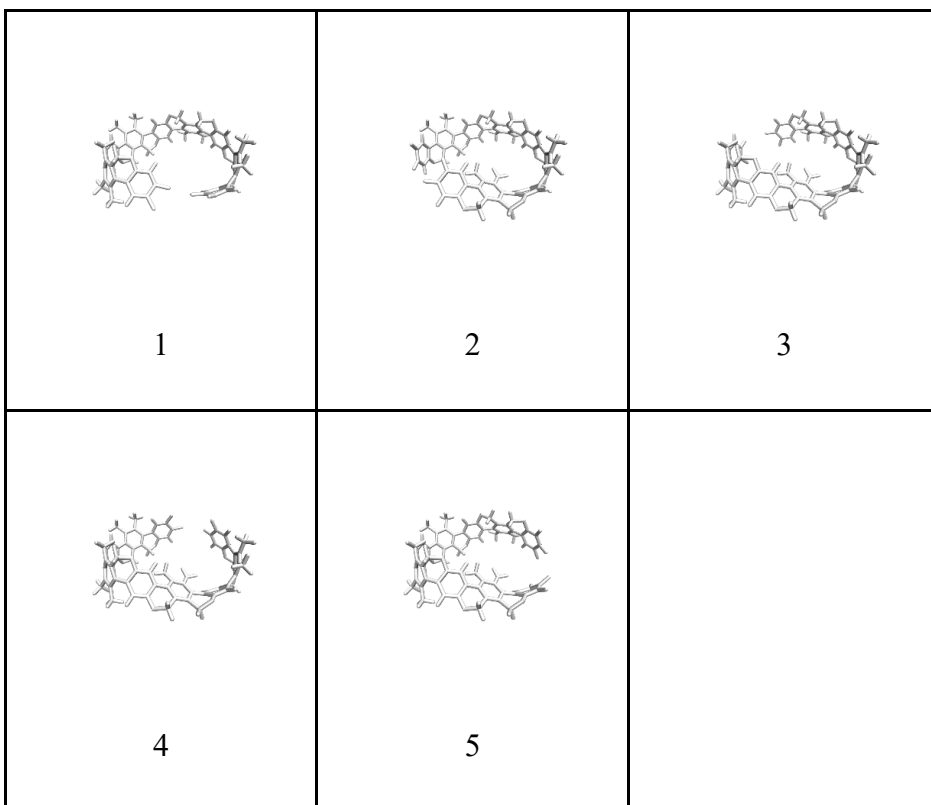


Table B.19. Fragments used for the Möbius Tanaka belt.

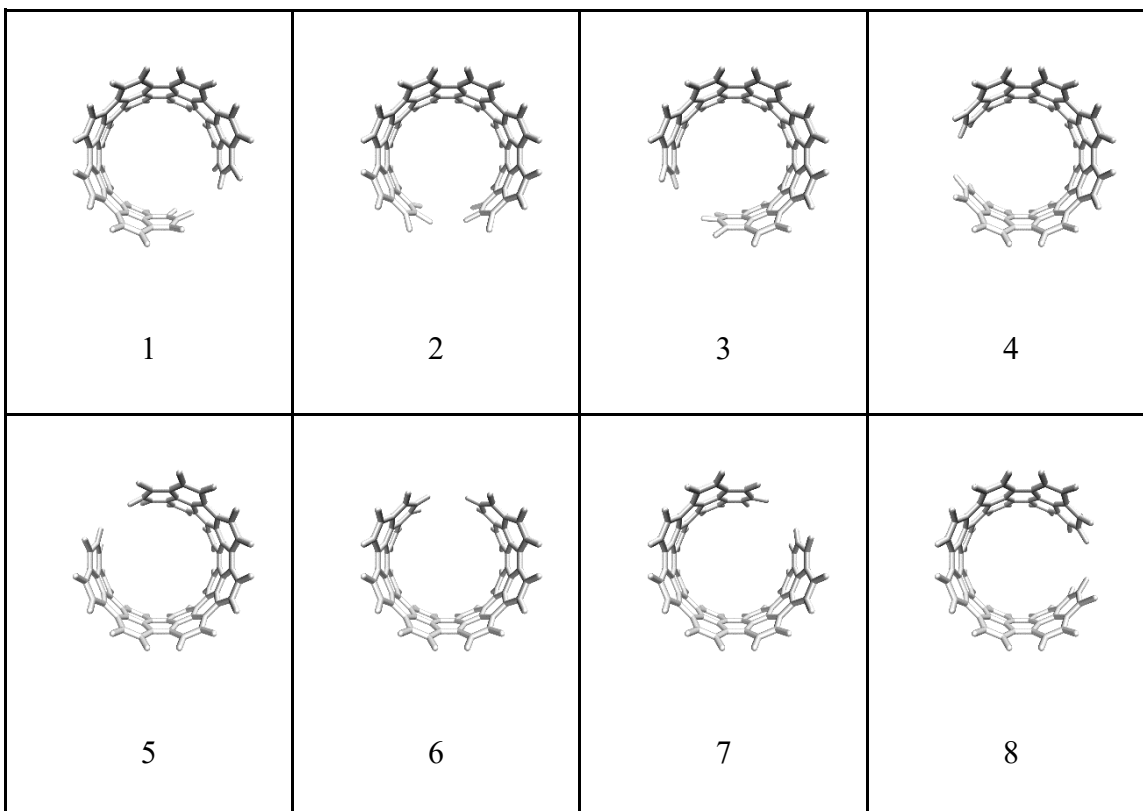


Table B.20. Fragments used for the Vögtle belt.

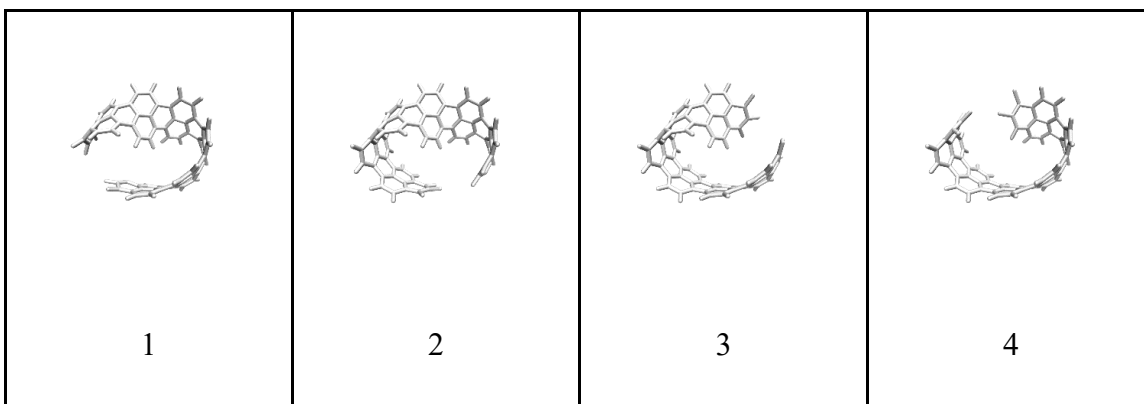


Table B.21. Fragments used for the Möbius Vögtle belt.

B.5.6. Fragments used for Figure III.9

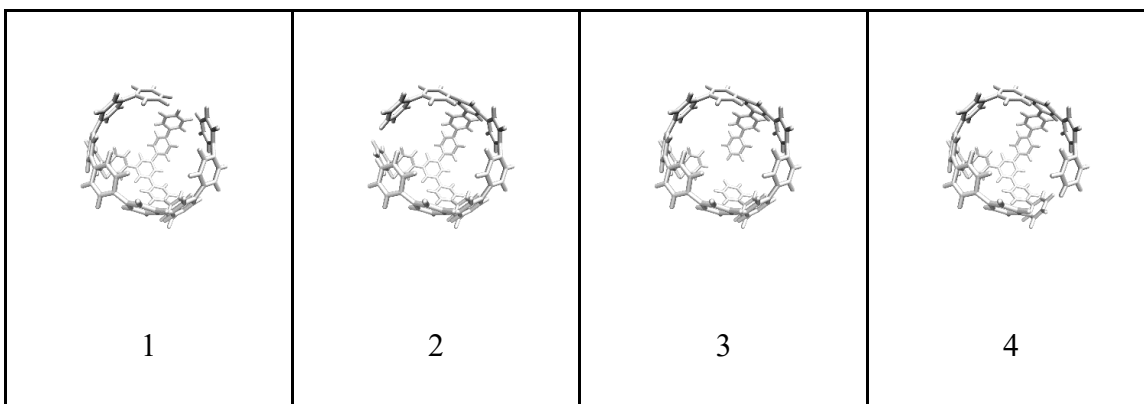


Table B.22. Fragments used for the Yamago ball.

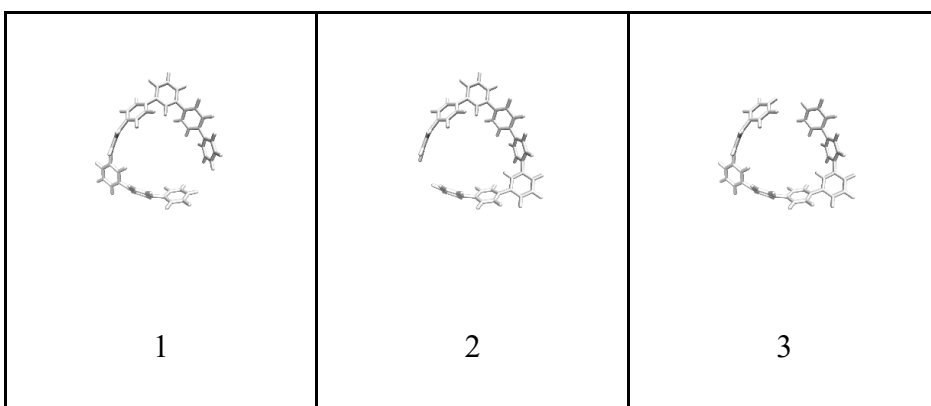


Table B.23. Fragments used for the Yamago ball panel.

B.5.7. Fragments used for Figure III.10

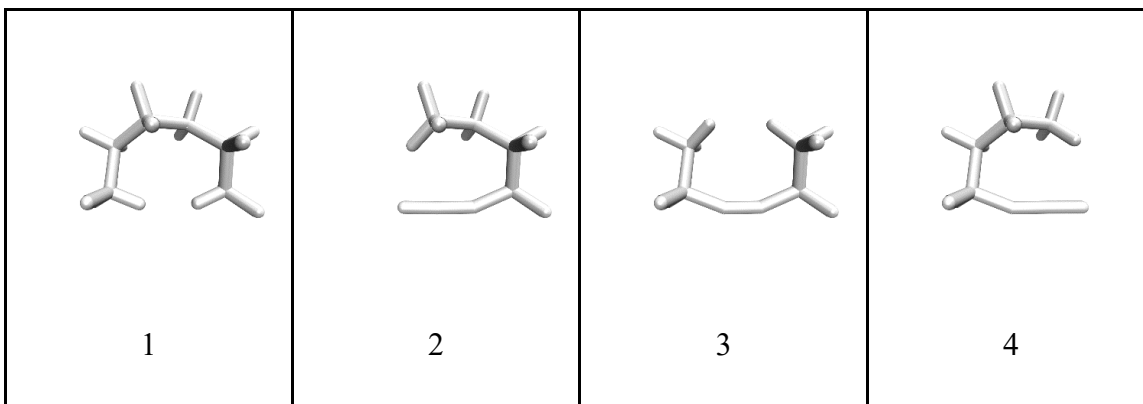


Table B.24. Fragments used for cyclooctyne.

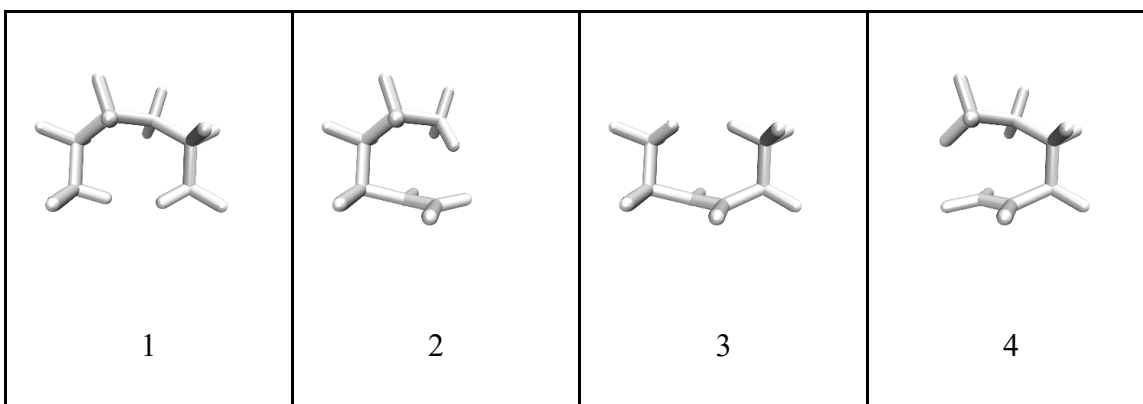


Table B.25. Fragments used for *trans*-cyclooctene.

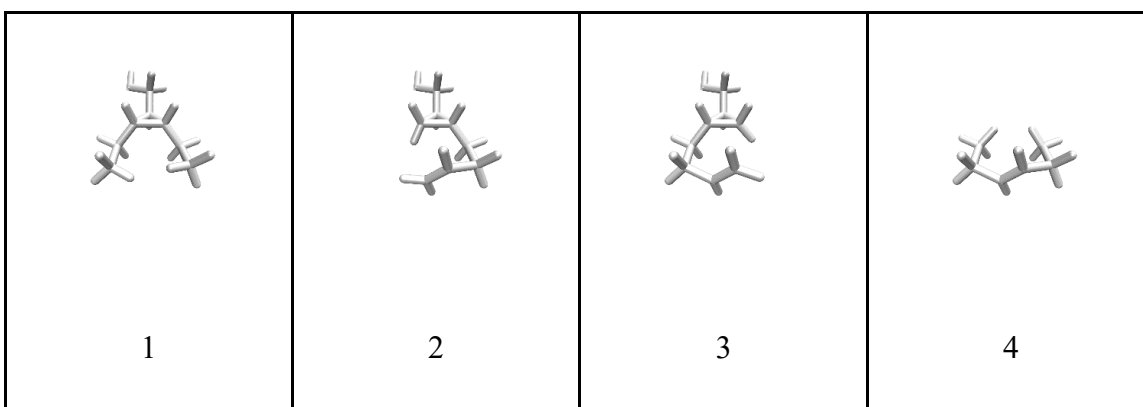


Table B.26. Fragments used for *trans*-bicyclo[6.1.0]nonene.

APPENDIX C

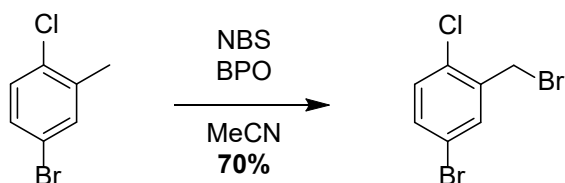
SUPPLEMENTARY INFORMATION FOR CHAPTER IV

The synthesis of molecules **IV.19** and **IV.20** is worked performed by Prof. Matthew Golder and the experimental details are published in the *Journal of the American Chemical Society* and in his doctoral thesis.

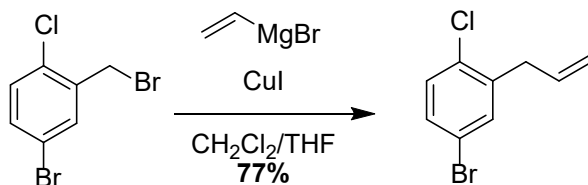
C.1. Experimental Details:

All glassware was flame dried and cooled under an inert atmosphere of nitrogen unless otherwise noted. Moisture sensitive reactions were carried out under an inert atmosphere of nitrogen with Schlenk line using standard syringe/septa techniques. Tetrahydrofuran, dichloromethane, 1,4-dioxane, and dimethylformamide were dried by filtration through alumina according to the methods described by Grubbs (JC Meyer).¹ Silica column chromatography was conducted with Zeochem Zeoprep 60 Eco 40-63 μm silica gel. Thin Layer Chromatography (TLC) was performed using Sorbent Technologies Silica Gel XHT TLC plates. Developed plates were visualized using UV light at wavelengths of 254 and 365 nm. ^1H NMR spectra were recorded at 600 MHz on a Bruker Avance-III, 500 MHz on a Bruker Avance-III, 500 MHz on a Varian INOVA or 300 MHz on a Varian INOVA. ^{13}C NMR spectra were recorded at 151 MHz on a Bruker Avance-III, 126 MHz on a Bruker Avance-III or 126 MHz on a Varian INOVA. All ^1H NMR spectra were taken in CDCl_3 (referenced to TMS, δ 0.00 ppm) or acetone-*d*₆ (referenced to residual acetone, δ 2.05 ppm). All ^{13}C NMR spectra were taken in CDCl_3 (referenced to chloroform, δ 77.16 ppm). Recycling gel permeation chromatography (GPC) was performed using a Japan Analytical Industry LC-9101 preparative HPLC with JAIGEL-1H/JAIGEL-2H columns in series using CHCl_3 . Automated flash chromatography was

performed using a Biotage Isolera One. All reagents were obtained commercially unless otherwise noted.

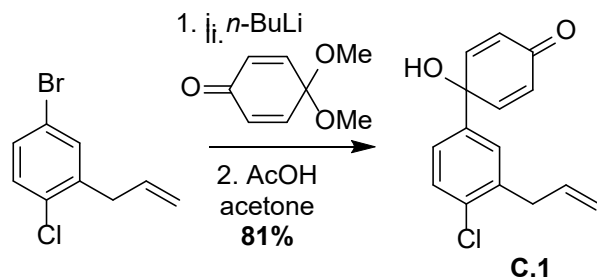


4-bromo-2-(bromomethyl)-1-chlorobenzene. 5-bromo-2-chlorotoluene (13.3 mL, 20.55 g, 100 mmol) was dissolved in acetonitrile (500 mL) in a 1 L flask open to the atmosphere. *N*-bromosuccinimide (19.6 g, 110 mmol) and benzoyl peroxide (0.5 g, 2 mmol) were added and the reaction was refluxed overnight. The next morning, the reaction was quenched by adding solid sodium sulfite (4 g). The mixture was concentrated and dissolved in dichloromethane. This was washed with water and brine. The solvent was then removed to yield a solid. The solid was recrystallized using methanol (30 mL) and washed with small amounts of cold methanol to yield 4-bromo-2-(bromomethyl)-1-chlorobenzene, a white crystalline solid (20.0 g, 70%). ¹H NMR (300 MHz, CDCl₃) δ(ppm) 7.58(d, *J* = 2.4 Hz, 1H), 7.38(dd, *J* = 8.5, 2.5 Hz, 1H), 7.26(d, *J* = 8.5 Hz, 1H), 4.52(s, 2H); ¹³C NMR (151 MHz, CDCl₃) δ(ppm) 137.07, 133.71, 132.99, 132.69, 131.17, 120.35, 29.09; IR (neat) 1903, 1770, 1643, 1464, 1215, 1082, 1049 cm⁻¹; HRMS (CI) (*m/z*): [M]⁺ calcd for C₇H₅Br₂Cl, 281.8446; found, 281.8447.



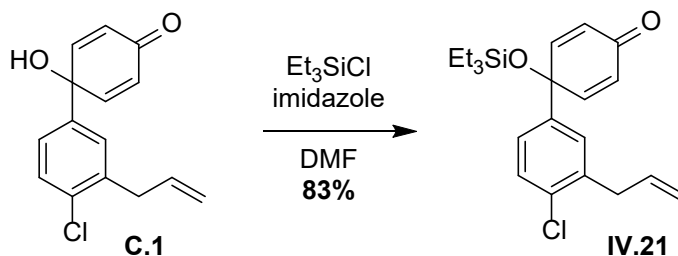
2-allyl-4-bromo-1-chlorobenzene. 4-bromo-2-(bromomethyl)-1-chlorobenzene (14.6 g, 51.3 mmol) and copper (I) bromide (4.89 g, 25.7 mmol) was suspended in

dichloromethane (260 mL) and cooled to -78 °C. A 430 mM solution of vinyl magnesium bromide in tetrahydrofuran (250 mL, 107.8 mmol) was then added as a slow stream to the mixture. The reaction was stirred for 3 h at -78 °C and warmed to room temperature by allowing the cooling bath to expire. The mixture was then quenched by adding saturated ammonium chloride solution (100 mL). The biphasic solution was filtered through celite. It was then extracted into ethyl acetate (2 x 200 mL), washed with brine (100 mL) and dried over anhydrous sodium sulfate. Solvent was removed to yield a white solid under an oil. The oil was decanted off and the solid was washed with ethyl acetate (100 mL). This solution was then concentrated and purified by vacuum distillation at 200 mTorr and 120 °C. Anhydrous sodium sulfate was then added to the distillate and it was filtered washing with ethyl acetate to remove contaminating water. This solution was concentrated to yield 2-allyl-4-bromo-1-chlorobenzene, a clear colorless oil (9.19 g, 77%). ¹H NMR (300 MHz, CDCl₃) δ(ppm) 7.36(d, *J* = 2.4 Hz, 1H), 7.29(dd, *J* = 8.5, 2.5 Hz, 1H), 7.22(d, *J* = 8.5 Hz, 1H), 5.93(ddt, *J* = 16.8, 10.1, 6.5 Hz, 1H), 5.15(dd, *J* = 10.1, 1.6 Hz, 1H), 5.09(dd, *J* = 16.8, 1.6 Hz, 1H), 3.46(d, *J* = 6.5 Hz, 2H); ¹³C NMR (126 MHz, CDCl₃) δ(ppm) 139.87, 134.55, 133.15, 130.79, 120.42, 117.32, 37.41; IR (neat) 1638, 1582, 1463, 1081, 1041 917, 807 cm⁻¹; HRMS (CI) *m/z* calcd for C₉H₈BrCl [M]⁺ 229.9498, found 229.9497.

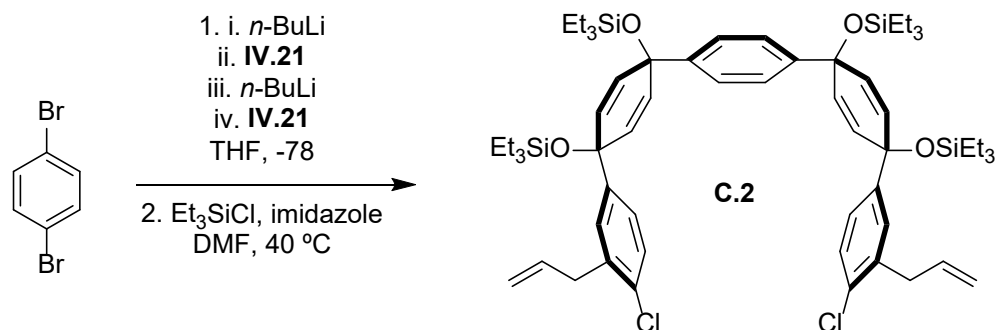


C.1. 2-allyl-4-bromo-1-chlorobenzene (5.2 g, 22.5 mmol) was stirred under vacuum to remove dissolved gases. Tetrahydrofuran (40 mL) was added and the solution was cooled to -78 °C. A 2.5 M solution of *n*-butyl lithium in hexanes (8.6 mL, 21.4 mmol) was added slowly. The solution was then stirred for 5 min and quinone monoketal (2.74 mL, 3.15 g, 20.4 mmol) was added slowly. The reaction was stirred at -78 °C for 30 min. It was then quenched with water (50 mL) and warmed to room temperature. The mixture was extracted with ethyl acetate (2 x 50 mL). The extract was washed with brine (40 mL) and dried over anhydrous sodium sulfate. Solvent was then removed to yield a yellow oil. This oil was dissolved in acetone (25 mL) and to the solution was added 10% aqueous acetic acid solution (25 mL). This mixture was stirred for 1 h at room temperature. It was then quenched with saturated sodium bicarbonate solution (25 mL) and extracted into ethyl acetate (2 x 30 mL). The extract was washed with saturated sodium bicarbonate solution (25 mL), water (25 mL) and brine (15 mL). It was dried of anhydrous sodium sulfate and solvent was removed to yield a brown oil. This oil was loaded onto silica and subjected to column chromatography (1:4 – 1:2 ethyl acetate/hexanes) to yield **C.1**, a yellow solid (4.32 g, 81%). ¹H NMR (300 MHz, CDCl₃) δ(ppm) 7.38(m, 1H), 7.37(m, 1H), 7.27(m, 1H), 6.87(d, *J* = 9.8 Hz, 2H), 6.25(d, *J* = 9.8 Hz, 2H), 5.96(ddt, *J* = 16.8, 10.1, 6.5 Hz, 1H), 5.13(dd, *J* = 10.0, 1.6 Hz, 1H), 5.09(dd, *J* = 16.9, 1.7 Hz, 1H), 3.53(d, *J* = 6.5 Hz, 2H), 2.47(s, 1H); ¹³C NMR (151 MHz, CDCl₃) δ(ppm) 185.71, 150.73,

138.26, 137.25, 134.79, 133.97, 129.68, 127.08, 126.62, 124.44, 116.67, 70.38, 37.56; IR (neat) 3500-3300 (br), 1661, 1622, 1473, 1390, 1039 cm^{-1} ; HRMS (CI) m/z calcd for $\text{C}_{15}\text{H}_{13}\text{ClO}_2$ $[\text{M}]^+$ 260.0604, found 260.0597.

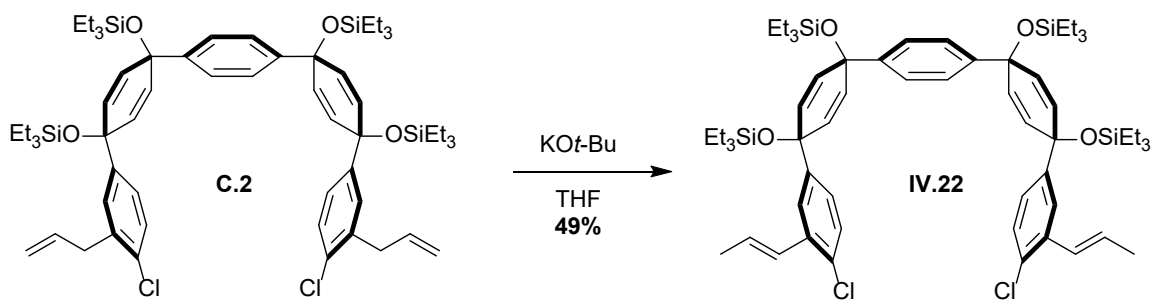


IV.21. **C.1** (4.64 g, 17.8 mmol) and imidazole (2.42 g, 35.6 mmol) was dissolved in dimethylformamide (90 mL). To this was added triethylsilyl chloride (4.48 mL, 4.02 g, 26.7 mmol). The reaction was stirred overnight at 40 °C. The next morning, the reaction was quenched with water (60 mL) and extracted using ethyl acetate (2 x 80 mL). The extract was then washed with brine (40 mL) and dried over anhydrous sodium sulfate. Solvent was removed to yield an oil. Purified by column chromatography (0 – 10% ethyl acetate/hexanes) to yield **IV.21**, a yellow oil (5.52 g, 83%). ^1H NMR (500 MHz, CDCl_3) δ (ppm) 7.33(m, 1H), 7.32(d, $J = 8.3$ Hz, 1H), 7.21(dd, $J = 8.4, 2.3$ Hz, 1H), 6.79(d, $J = 10.0$ Hz, 2H), 6.22(d, $J = 10.0$ Hz, 2H), 5.92(ddt, $J = 16.8, 10.1, 6.6$ Hz, 1H), 5.11(dd, $J = 10.1, 1.5$ Hz, 1H), 5.06(dd, $J = 17.0, 1.7$ Hz, 1H), 3.48(d, $J = 6.6$ Hz, 2H), 0.97(t, $J = 7.9, 9\text{H}$), 0.65(q, $J = 7.9, 6\text{H}$); ^{13}C NMR (126 MHz, CDCl_3) δ (ppm) 185.64, 151.56, 138.80, 138.13, 135.04, 133.66, 129.60, 127.29, 126.63, 124.60, 116.80, 72.72, 37.68, 6.86, 6.23; IR (neat) 1671, 1094, 1041, 1001 cm^{-1} ; HRMS (CI) m/z calcd for $\text{C}_{21}\text{H}_{27}\text{ClO}_2\text{Si}$ $[\text{M}]^+$ 374.1469, found 374.1482.



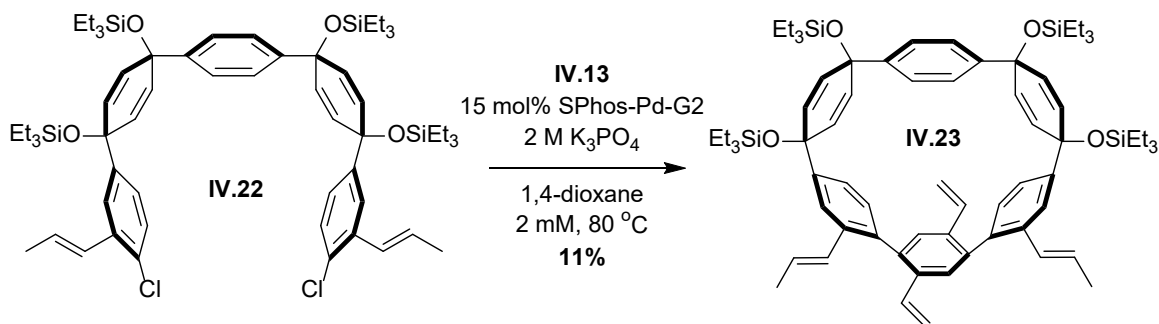
C.2. Dibromobenzene (324 mg, 1.37 mmol) was dissolved in tetrahydrofuran (14 mL) and cooled to -78 °C. A 2.36 M solution of *n*-butyl lithium in hexanes (580 μL, 1.37 mmol) was added and immediately after [2]ketone-chloride TES (500 μL, 515 mg, 1.37 mmol) was added. The reaction was stirred for 30 min and 2.36 M solution of *n*-butyl lithium in hexanes (580 μL, 1.37 mmol) and [2]ketone-chloride TES (500 μL, 515 mg, 1.37 mmol) was added again. The reaction was stirred for 30 min and quenched with water (20 mL). The mixture was warmed to room temperature and extracted with ethyl acetate (2 x 20 mL). The extract was washed with brine (20 mL) and dried over anhydrous sodium sulfate. Solvent was removed to yield an oil. The oil was added to a flask with imidazole (375 mg, 5.51 mmol) and put under nitrogen. Dimethylformamide (7 mL) was added followed by triethylsilyl chloride (690 μL, 622 mg, 4.13 mmol). The reaction was then stirred overnight at 40 °C. The next morning, the reaction was quenched with water (10 mL) and extracted using ethyl acetate (2 x 10 mL). The extract was then washed with brine (5 mL) and dried over anhydrous sodium sulfate. Solvent was removed to yield an oil. Purified by column chromatography (0 – 10% ethyl acetate/hexanes) to yield **C.2**, a yellow oil (1.14 g, 78%). In the case of a scaled up procedure, material was often isolated impure and used as is for next reaction. ¹H NMR (300 MHz, CDCl₃) δ(ppm) 7.22(s, 4H), 7.22(d, *J* = 8.2 Hz, 2H), 7.16(d, *J* = 2.2, 2H),

7.11(dd, $J = 8.3, 2.3$ Hz, 2H), 5.97(d, $J = 10.3$ Hz, 4H), 5.91(d, $J = 10.2$ Hz, 4H), 5.84(m, 2H), 4.96(m, 4H), 3.37(d, $J = 6.6$ Hz, 4H), 0.92(m, 36H), 0.59(m, 24H). ^{13}C NMR (151 MHz, CDCl_3) δ (ppm) 144.76, 144.75, 137.10, 135.16, 132.57, 131.53, 130.98, 128.86, 127.76, 125.50, 124.91, 116.21, 71.03, 71.01, 37.51, 6.87, 6.29; IR (neat) 2953, 2875, 1698, 1532 cm^{-1} ; LRMS (MALDI-TOF) m/z calcd for $\text{C}_{60}\text{H}_{88}\text{Cl}_2\text{O}_4\text{Si}_4[\text{M} + \text{Na}]^+$ 1077.50, found 1077.4.



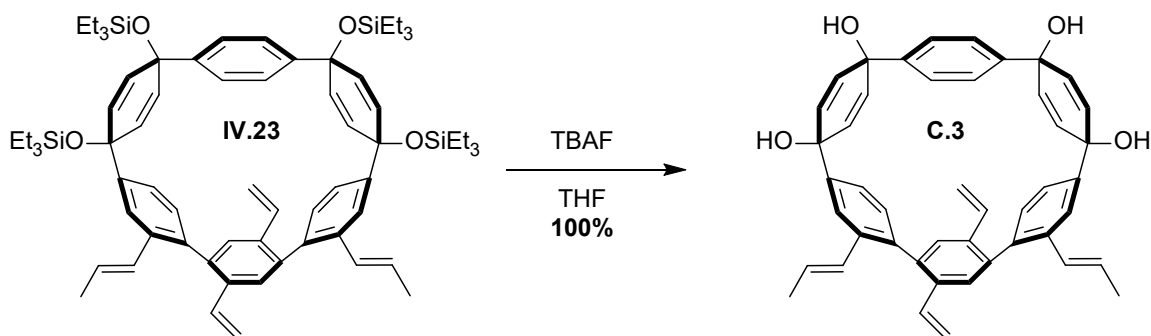
IV.22. **C.2** (1.14 g, 1.08 mmol) was stirred under vacuum to remove dissolved gases and dissolved in tetrahydrofuran (80 mL). Potassium *tert*-butoxide (266 mg, 2.38 mmol) was then added and the reaction was stirred for 5 min at room temperature. The reaction was then quenched with water (80 mL) and extracted in to ethyl acetate (2 x 60 mL). The extract was washed with brine (40 mL) and dried over anhydrous sodium sulfate. Solvent was removed to yield a yellow oil. Purified by column chromatography (10% dichloromethane/hexanes) to yield **IV.22**, a clear colorless oil (560 mg, 49%). ^1H NMR (300 MHz, CDCl_3) δ (ppm) 7.45(d, $J = 2.2$, 2H) 7.25(s, 4H), 7.20(d, $J = 8.4$ Hz, 2H), 7.09(dd, $J = 8.4, 2.2$ Hz, 2H), 6.71(dq, $J = 15.7, 1.7$ Hz, 2H), 6.00(m, 2H), 5.98(d, $J = 10.3$ Hz, 4H), 5.91(d, $J = 10.3$ Hz, 4H), 1.82(dd, $J = 6.7, 1.8$ Hz, 6H), 0.92(m, 36H), 0.59(m, 24H); ^{13}C NMR (126 MHz, CDCl_3) δ (ppm) 144.99, 144.76, 135.37, 131.73, 131.13, 129.24, 128.44, 127.29, 125.66, 125.34, 123.94, 71.19, 71.16, 18.75, 7.05, 7.03, 6.45; IR (neat) 2953, 2875, 1465, 1073 cm^{-1} ; LRMS (MALDI-TOF) m/z calcd for

$C_{60}H_{88}Cl_2O_4Si_4[M + Na]^+$ 1077.50, found 1077.3.



IV.23. **IV.13** (197 mg, 517 μ mol) and SPhos Pd G2 (56 mg, 78 μ mol) were placed in a round bottom flask. The flask was evacuated and refilled with nitrogen. **IV.22** (546 mg, 517 μ mol) was dissolved in dioxane (50 mL), purged with nitrogen, and added to the flask. Additional dioxane (183 mL) was added and the mixture was warmed to 80 °C. A 2 M aqueous solution of potassium phosphate tribasic (25 mL) was then added. The reaction was stirred for 3 h. It was then opened to the air, filtered through celite and extracted into ethyl acetate (2 x 100 mL). The extract was washed with brine (60 mL) and dried over anhydrous sodium sulfate. Solvent was removed to yield a brown oil. Purified by column chromatography (10% ethyl acetate/hexanes) to yield a golden oil. This golden oil was purified by gel permeation chromatography (chloroform) to yield **IV.23**, a yellow oil (65 mg, 11%). ¹H NMR (500 MHz, CDCl₃) δ (ppm) 7.80(d, J = 1.9 Hz, 2H) 7.44(s, 2H), 6.99(dd, J = 15.8, 1.9 Hz, 2H), 6.95(s, 4H), 6.92(m, 2H), 6.64(dd, J = 8.4, 1.9 Hz, 2H), 6.50(dq, J = 15.6, 6.6 Hz, 2H), 6.12(d, J = 8.3 Hz, 2H), 6.00(dd, J = 10.2, 2.4 Hz, 2H), 5.95(dd, J = 10.2, 2.4 Hz, 2H), 5.77(dd, J = 10.0, 2.4 Hz, 2H), 5.66(dd, J = 17.5, 1.2 Hz, 2H), 5.52(dd, J = 10.0, 2.3 Hz, 2H), 5.20(d, J = 10.8 Hz, 2H), 2.00(dd, J = 6.7, 1.7 Hz, 6H), 0.99(t, J = 7.9 Hz, 18H), 0.93(t, J = 7.9 Hz, 18H), 0.66(q, J = 7.9 Hz, 12H), 0.62(q, J = 7.9 Hz, 12H). ¹³C NMR (126 MHz, CDCl₃) δ (ppm) 144.85, 143.54, 142.10, 140.26, 135.84, 135.68, 135.55, 135.02, 134.41, 133.94, 131.44, 131.35, 131.23,

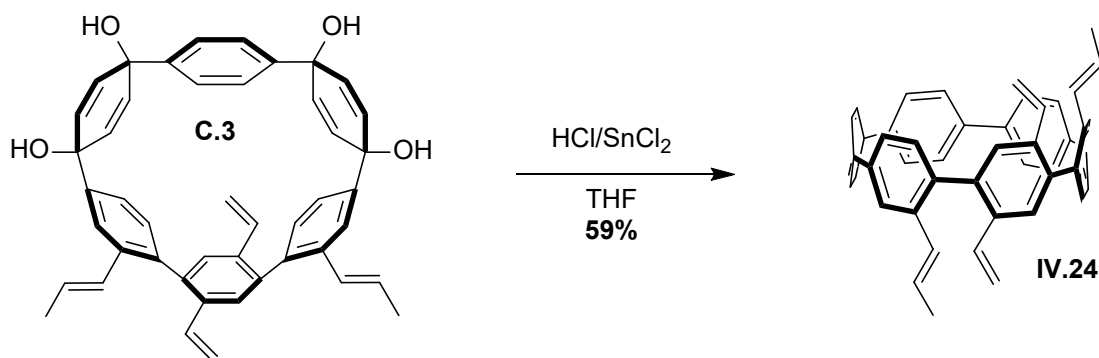
130.98, 129.99, 128.79, 128.29, 127.77, 127.58, 127.54, 127.22, 125.57, 123.65, 123.32, 115.36, 71.83, 71.14, 18.91, 7.11, 7.06, 6.59, 6.41; LRMS (MALDI) m/z calcd for $C_{70}H_{96}O_4Si_4(M)^+$ 1112.64, found 1112.61; IR (neat) 2954, 2875, 1076 cm^{-1} .



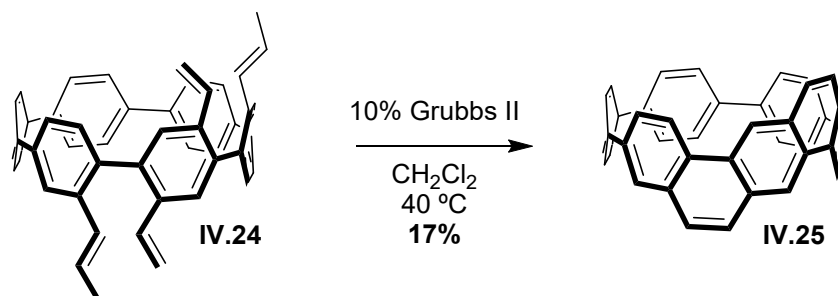
C.3. **IV.23** (65 mg, 58 μ mol) was dissolved in tetrahydrofuran (500 μ L). A 1 M solution of tetrabutylammonium fluoride in tetrahydrofuran (250 μ L) was added and the reaction was stirred for 1 h. It was then quenched with water (1 mL) and the tetrahydrofuran was evaporated under reduced pressure. This caused a brown solid to crash out of solution.

The solid was filtered and washed with water (1 mL) and dichloromethane (2 mL). Dried under vacuum to yield **C.3**, an orange brown solid (38 mg) used as is for next reaction.

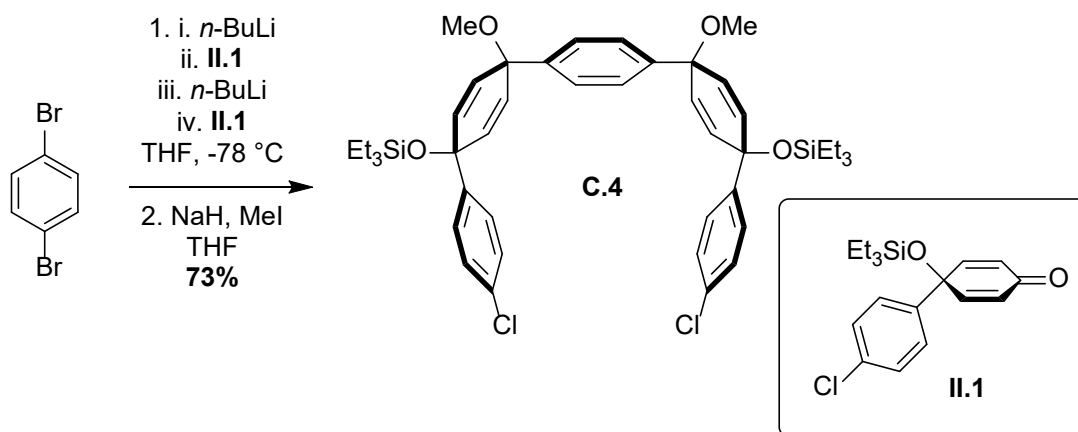
1H NMR (300 MHz, DMSO- d_6) δ (ppm) 7.86 (s, 2H), 7.39 (s, 2H), 6.97 (m, 2H), 6.93 (s, 4H), 6.84 (dd, $J = 17.5, 10.8$ Hz, 2H), 6.67 (d, $J = 8.3$ Hz, 2H), 6.55 (dd, $J = 15.7, 6.8$ Hz, 2H), 5.98 (d, $J = 8.3$ Hz, 2H), 5.86 (m, 2H), 5.76 (s, 2H), 5.74 (m, 2H), 5.59 (d, $J = 17.5$ Hz, 2H), 5.46 (dd, $J = 10.1, 2.2$ Hz, 2H), 5.25 (d, $J = 10.9$ Hz, 2H), 3.16 (s, 4H), 1.97 (d, $J = 6.1$ Hz, 6H); ^{13}C NMR (126 MHz, Acetone- d_6) δ (ppm) 145.05, 144.55, 143.05, 140.90, 136.93, 136.50, 136.20, 135.09, 134.92, 134.75, 132.02, 130.76, 130.42, 130.08, 128.77, 126.39, 124.94, 124.26, 116.34, 70.30, 69.53, 18.87; IR (neat) 3550-3100 (br), 1264, 1026 cm^{-1} .



IV.24. To a flask containing **C.3** (38 mg, 58 μmol) was added a solution of tin(II) chloride dihydrate (31 mg, 139 μmol), 12 M hydrochloric acid (23 μL) and tetrahydrofuran (4.8 mL). The reaction was stirred for 1 h. It was quenched with aqueous 1 M sodium hydroxide (1 mL) and extracted into ethyl acetate (2 x 2 mL). The extract was washed with brine (1 mL) and dried over anhydrous sodium sulfate. Solvent was removed to yield an orange-yellow solid. Purified by column chromatography (20% dichloromethane/hexanes) to yield **IV.24**, a yellow solid (20 mg, 59%). ^1H NMR (500 MHz, CDCl_3) δ (ppm) 7.63 (s, 2H), 7.48 (s, 8H), 7.35 (br, 2H), 7.18 (br, 2H), 6.77 (d, J = 8.5 Hz, 4H), 6.71 – 6.60 (m, 4H), 6.29 (dq, J = 13.8, 6.6 Hz, 2H), 5.38 (s, 2H), 5.15 (d, J = 10.8 Hz, 2H), 1.79 (d, J = 6.3 Hz, 6H); ^{13}C NMR (151 MHz, CDCl_3) δ (ppm) 137.64, 136.32, 136.00, 133.56, 131.71, 130.74, 128.97, 127.36, 121.08, 117.48, 115.63, 115.11, 69.46, 29.70, 18.65; IR (neat) 2978, 2931, 1360, 1088 cm^{-1} ; LRMS (MALDI-TOF) m/z calcd for $\text{C}_{46}\text{H}_{36}[\text{M}]^+$ 588.28, found 588.2.

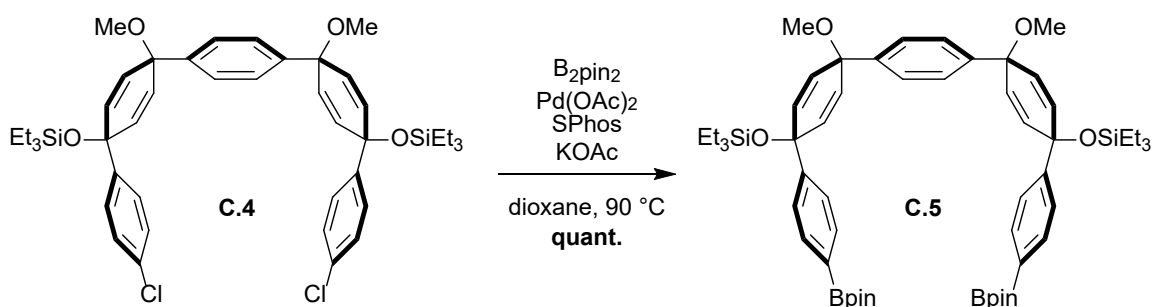


IV.25. **IV.24** (7 mg, 12 μmol) and Grubbs II catalyst (2 mg, 2.4 μmol) were dissolved in dichloromethane (1 mL). The solution was refluxed overnight. The next morning, solvent was removed and the solid was purified by column chromatography (20% dichloromethane/hexanes) to yield a red solid. This was further purified by gel permeation chromatography (chloroform) to yield **IV.25**, a red solid (1 mg, 17%). ^1H NMR (500 MHz, CDCl_3) δ (ppm) 8.54 (s, 2H), 8.26 (d, $J = 9.4$ Hz, 2H), 7.86 (d, $J = 10.1$ Hz, 2H), 7.79 (s, 2H), 7.75 (d, $J = 9.4$ Hz, 2H), 7.65 (d, $J = 9.2$ Hz, 2H), 7.59-7.63 (m, 6H), 7.50-7.57 (m, 6H); ^{13}C NMR (126 MHz, CDCl_3) δ (ppm) 134.51, 134.13, 133.86, 132.43, 132.35, 132.20, 129.04, 128.66, 128.22, 128.15, 127.37, 127.10, 126.93, 126.78, 126.43, 126.38, 126.26, 125.75, 125.57, 123.54, 122.49; IR (neat) 3045, 2925, 1570, 1480, 1259 cm^{-1} ; LRMS (MALDI-TOF) m/z calcd for $\text{C}_{40}\text{H}_{24}[\text{M}]^+$ 504.19, found 504.1.



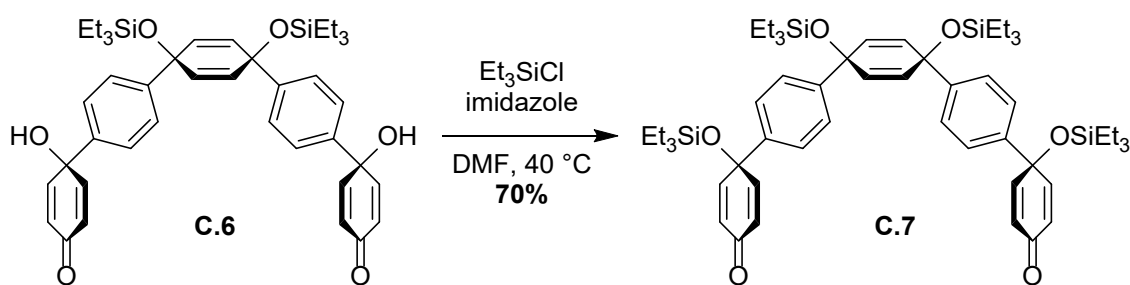
C.4. 1,4-dibromobenzene (609 mg, 2.58 mmol, 1 eq) was dissolved in tetrahydrofuran (26 mL, 0.1 M) and cooled to -78 $^{\circ}\text{C}$. A 2.5 M solution of *n*-BuLi in hexanes (1.03 mL,

2.58 mmol, 1 eq) was added followed by ketone **II.1** (800 μL , 864 mg, 2.58 mmol, 1 eq). This was stirred for an hour then a 2.5 M solution of *n*-BuLi in hexanes (1.03 mL, 2.58 mmol, 1 eq) was again added followed by ketone **II.1** (800 μL , 864 mg, 2.58 mmol, 1 eq). This was stirred for an additional hour and the reaction was quenched with water and extracted in EtOAc (2 x 30 mL). It was washed with brine (20 mL) and dried over sodium sulfate. Solvent was removed to yield a clear colorless oil. This oil was dissolved in tetrahydrofuran (26 mL, 0.1 M) and sodium hydride (310 mg, 7.74 mmol, 3 eq) was added carefully. Methyl iodide (642 μL , 1.46 g, 10.3 mmol, 4 eq) was added and the reaction was stirred overnight. The reaction was quenched with water and extracted in EtOAc (2 x 30 mL). It was washed with brine (20 mL) and dried over sodium sulfate. Solvent was removed to yield a brown solid. Washed with methanol to yield a white solid **C.4** (1.46 g, 73%). ^1H NMR (300 MHz, CDCl_3) δ 7.31 (s, 4H), 7.25 (d, $J = 8.7$ Hz, 4H), 7.20 (d, $J = 8.7$ Hz, 4H), 6.12 (d, $J = 10.1$ Hz, 4H), 5.96 (d, $J = 10.1$ Hz, 4H), 3.36 (s, 6H), 0.96 (t, $J = 7.9$ Hz, 18H), 0.66 (q, $J = 7.9$ Hz, 12H).

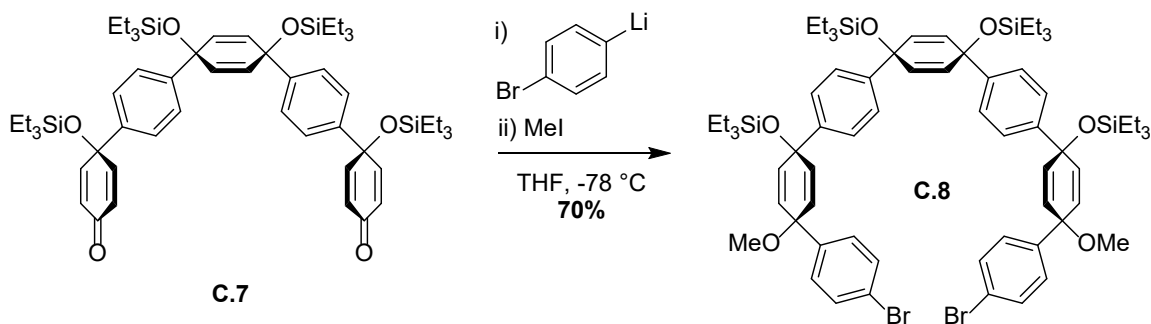


C.5. KOAc (1.17 g, 11.9 mmol, 6.6 eq) was added to a rounded bottom flask under vacuum and flame dried. Upon cooling, dichloride **C.4** (1.40 g, 1.80 mmol, 1 eq), $\text{Pd}(\text{OAc})_2$ (20 mg, 90 μmol , 0.05 eq), SPhos (92 mg, 230 μmol , 0.125 eq) and bis(pinacolato)diboron (1.83 g, 7.22 mmol, 4 eq) were added. The vessel was fitted with a rubber septum and evacuated/backfilled with nitrogen. Dioxane (6.0 mL, 0.3 M) was

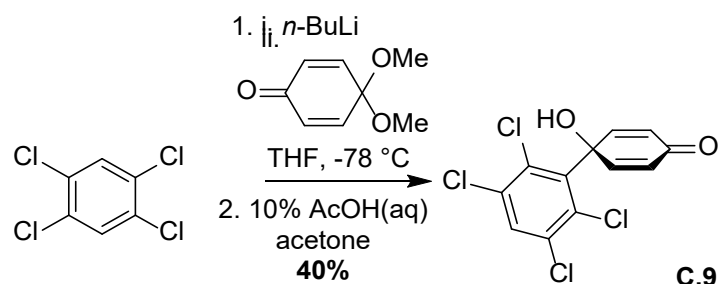
added and the reaction was warmed from room temperature to 90 °C. The reaction was stirred at this temperature overnight. In the morning, it was filtered through Celite, washing with EtOAc, and the solvent of the filtrate was removed under reduced pressure. The resulting residue was washed with EtOH to yield a white solid **C.5** (1.73 g, 100%). ¹H NMR (500 MHz, CDCl₃) δ 7.70 (d, J = 8.2 Hz, 4H), 7.35 (d, J = 8.2 Hz, 4H), 7.32 (s, 4H), 6.15 (d, J = 10.2 Hz, 4H), 5.93 (d, J = 10.1 Hz, 4H), 3.36 (s, 6H), 1.32 (s, 24H), 0.95 (t, J = 7.9 Hz, 18H), 0.65 (q, J = 7.9 Hz, 12H).



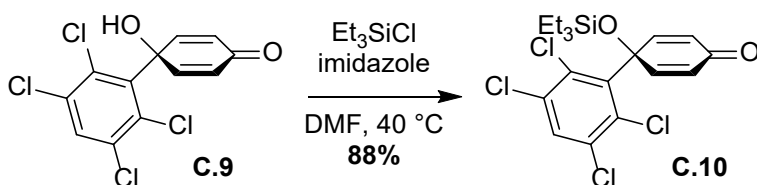
C.7. **C.6**² (2.80 g, 3.95 mmol, 1 eq) and imidazole (1.08 g, 15.8 mmol, 4 eq) were added to a flask and dissolved in dry DMF (20 mL, 200 mM). To the solution was added triethylsilyl chloride (1.99 mL, 1.79 g, 11.8 mmol, 3 eq) and the reaction was stirred overnight at 40 °C. In the morning, the reaction was quenched with a saturated solution of sodium bicarbonate and extracted with EtOAc (3 x 20 mL). The combined organic fraction was washed with a 5% aqueous solution of LiCl (3 x 10 mL) and brine (10 mL). Solvent was removed under reduced pressure to yield an oil. The oil was purified by column chromatography on silica (0 to 10% EtOAc in hexanes) to yield a solid **C.7** (2.6 g, 70%). ¹H NMR (500 MHz, Chloroform-d) δ 7.33 (d, J = 8.7 Hz, 4H), 7.30 (d, J = 8.7 Hz, 4H), 6.81 (d, J = 10.0 Hz, 4H), 6.20 (d, J = 10.0 Hz, 4H), 5.95 (s, 4H), 0.97 (t, J = 7.9 Hz, 18H), 0.91 (t, J = 8.0 Hz, 18H), 0.65 (q, J = 7.9 Hz, 12H), 0.58 (q, J = 7.9 Hz, 12H).



C.8. **C.7** (2.6 g, 2.8 mmol, 1 eq) and 1,4-dibromobenzene (1.44 g, 6.16 mmol, 2.2 eq) were each dissolved in tetrahydrofuran (15 mL, 200 mM) in separate flasks and cooled to $-78\text{ }^{\circ}\text{C}$. To the solution containing 1,4-dibromobenzene was added a 2.5 M solution of *n*-BuLi in hexanes (2.3 mL, 5.88 mmol, 2.1 eq). This mixture was then quickly transferred to the solution containing diketone **C.7** via cannula. The reaction was stirred for 1 h. MeI (600 μL , 1.4 g, 9.6 mmol, 3.5 eq) was added and the reaction was warmed to room temperature and left overnight. In the morning, the reaction was quenched with water. The mixture was extracted with EtOAc (2 x 30 mL) and the combined extracts were washed with brine (30 mL). The solution was dried over sodium sulfate and the solvent was removed to yield an oil. Purification by column chromatography on silica (0 to 10% EtOAc in hexanes) yielded a clear colorless oil **C.8** (2.63, 75%). $^1\text{H NMR}$ (500 MHz, CDCl_3) δ 7.38 (d, $J = 8.7\text{ Hz}$, 4H), 7.18-7.25 (m, 12H), 6.19 (d, $J = 10.0\text{ Hz}$, 4H), 5.96 (s, 4H), 5.85 (d, $J = 10.1\text{ Hz}$, 4H), 3.36 (s, 6H), 0.92 (t, $J = 7.9\text{ Hz}$, 36H), 0.61 (q, $J = 8.1\text{ Hz}$, 12H), 0.59 (q, $J = 8.1\text{ Hz}$, 12H).

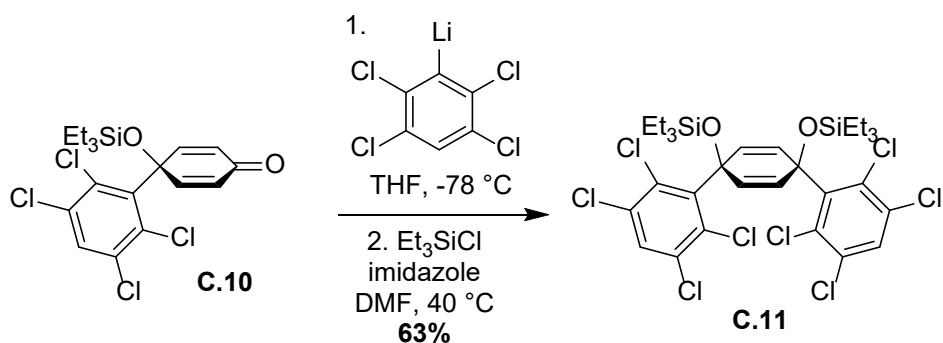


C.9. 1,2,4,5-tetrachlorobenzene (20.0 g, 92.6 mmol, 1.1 eq) was dissolved in tetrahydrofuran (280 mL, 300 mM) and cooled to -78 °C. A 2.5 M solution of *n*-BuLi in hexanes (35 mL, 88 mmol, 1.05 eq) was added followed by benzoquinone monomethyl ketal (11.3 mL, 13.0 g, 84.2 mmol, 1 eq). The solution was stirred at -78 °C for 1 h and quenched with water. The mixture was warmed to room temperature and extracted with EtOAc (3 x 100 mL). The combined organic extracts were washed with brine (50 mL) and dried over anhydrous sodium sulfate. Solvent was removed under reduced pressure to yield an off white solid. The solid was dissolved in acetone (200 mL) and a solution of 10% AcOH in water (100 mL) was added. The reaction was stirred for 1 h at room temperature and quenched with an aqueous saturated solution of sodium bicarbonate. The mixture was filtered washing with water and dichloromethane to yield a yellow solid **C.9** (10.8 g, 40%). ¹H NMR (500 MHz, Acetone-*d*₆) δ 7.94 (s, 1H), 7.29 (d, *J* = 10.1 Hz, 2H), 6.21 (d, *J* = 10.1 Hz, 2H), 5.72 (s, 1H).



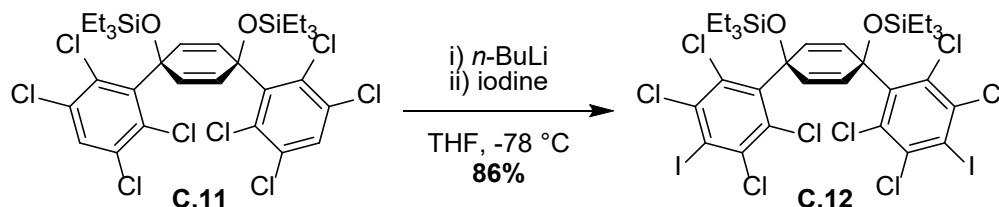
C.10. **C.9** (15.0 g, 46.3 mmol, 1 eq) and imidazole (4.73 g, 69.4 mmol, 1.5 eq) were added to a flask and dissolved in dry DMF (230 mL, 200 mM). To the solution was added TESCl (9.7 mL, 8.7 g, 58 mmol, 1.25 eq) and the reaction was stirred overnight at

40 °C. In the morning, the reaction was quenched with a saturated solution of sodium bicarbonate and extracted with EtOAc (3 x 100 mL). The combined organic fraction was washed with a 5% aqueous solution of LiCl (3 x 50 mL) and brine (50 mL). Solvent was removed under reduced pressure to yield an oil. The oil was purified by column chromatography on silica (0 to 40% EtOAc in hexanes) to yield a yellow solid **C.10** (17.9 g, 88%). ¹H NMR (500 MHz, Chloroform-d) δ 7.65 (s, 1H), 7.21 (d, J = 10.1 Hz, 2H), 6.30 (d, J = 10.0 Hz, 2H), 0.91 (t, J = 7.9 Hz, 9H), 0.63 (q, J = 7.9 Hz, 6H).

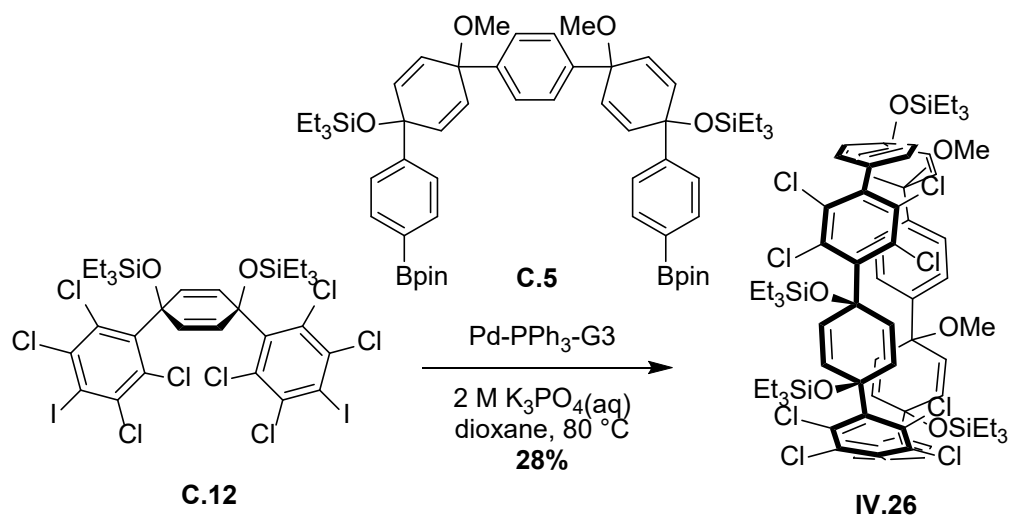


C.11. 1,2,4,5-tetrachlorobenzene (2.71 g, 12.6 mmol, 1.1 eq) was dissolved in tetrahydrofuran (38 mL, 300 mM) and cooled to -78 °C. A 2.5 M solution of *n*-BuLi in hexanes (4.8 mL, 12 mmol, 1.05 eq) was added followed by ketone **C.10** (5.00 g, 11.4 mmol, 1 eq). The solution was stirred at -78 °C for 1 h and quenched with water. The mixture was warmed to room temperature and extracted with EtOAc (3 x 30 mL). The combined organic extracts were washed with brine (20 mL) and dried over anhydrous sodium sulfate. Solvent was removed under reduced pressure to yield a solid. The solid was transferred to a flask with imidazole (1.16 g, 17.1 mmol, 1.5 eq) and dissolved in dry DMF (57 mL, 200 mM). To the solution was added triethylsilyl chloride (2.4 mL, 2.1 g, 14 mmol, 1.25 eq) and the reaction was stirred overnight at 40 °C. In the morning, the reaction was quenched with a saturated solution of sodium bicarbonate and extracted with

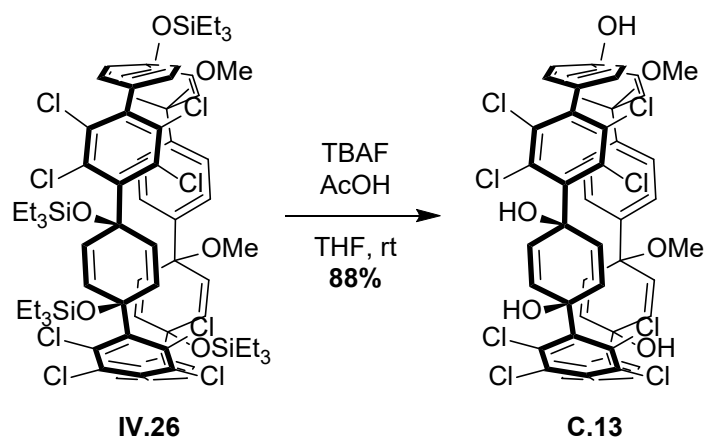
EtOAc (3 x 50 mL). The combined organic fraction was washed with a 5% aqueous solution of LiCl (3 x 30 mL) and brine (30 mL). Solvent was removed under reduced pressure to yield a solid. The solid was purified by column chromatography on silica (0 to 10% dichloromethane in hexanes) to yield a solid **C.11** (5.5 g, 63%). ¹H NMR (500 MHz, CDCl₃) δ 7.51 (s, 2H), 6.62 (s, 4H), 0.91 (t, J = 7.9 Hz, 18H), 0.62 (q, J = 7.9 Hz, 12H).



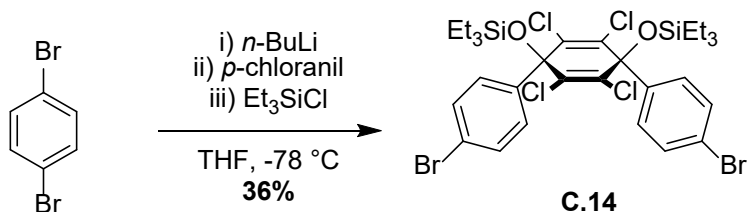
C.12. **C.11** (1.45 g, 1.89 mmol, 1 eq) was dissolved in tetrahydrofuran (19 mL, 100 mM) and cooled to -78 °C. A 2.5 M solution of *n*-BuLi in hexanes (1.7 mL, 4.2 mmol, 2.2 eq) was added dropwise and immediately followed by iodine (1.15 g, 4.53 mmol, 2.4 eq). The reaction was warmed to room temperature and quenched with a saturated aqueous solution of sodium bisulfite. The mixture was then extracted with EtOAc (3 x 10 mL) and the combined extracts were washed with a saturated aqueous solution of sodium bicarbonate (10 mL) and brine (10 mL). The solution was dried over anhydrous sodium sulfate and the solvent was removed under reduced pressure to yield a white solid **C.12** (1.66 g, 86%). ¹H NMR (300 MHz, CDCl₃) δ 6.65 (s, 4H), 0.92 (t, J = 7.9 Hz, 18H), 0.61 (q, J = 8.2, 7.6 Hz, 12H).



IV.26. **C.5** (250 mg, 261 μmol , 1 eq), **C.12** (266 mg, 261 μmol , 1 eq) and PPh_3 Pd G3 (33 mg, 26 μmol , 0.1 eq) were dissolved in dioxane (130 mL, 2 mM) and the mixture was warmed to 80 °C. A 2 M aqueous solution of potassium phosphate tribasic (13 mL) was then added. The reaction was stirred overnight. It was then opened to the air, filtered through celite and extracted into ethyl acetate (2 x 80 mL). The extract was washed with brine (60 mL) and dried over anhydrous sodium sulfate. Solvent was removed to yield a solid. The solid was purified by gel permeation chromatography (chloroform) to yield a white solid **IV.26** (100 mg, 28%). $^1\text{H NMR}$ (500 MHz, CDCl_3) δ 7.59 – 7.40 (br, 4H), 7.37 (s, 4H), 7.08 (d, $J = 8.8$ Hz, 4H), 6.93 (s, 4H), 6.24 (d, $J = 10.2$ Hz, 4H), 5.85 (d, $J = 10.2$ Hz, 4H), 3.37 (s, 6H), 0.98 (t, $J = 7.9$ Hz, 18H), 0.90 (t, $J = 7.9$ Hz, 18H), 0.69 (q, $J = 7.9$ Hz, 12H), 0.58 (q, $J = 7.9$ Hz, 12H). $^{13}\text{C NMR}$ (126 MHz, CDCl_3) δ 146.61, 142.83, 141.09, 140.80, 137.23, 135.22, 134.61, 134.12, 132.40, 129.56, 125.93, 76.22, 74.40, 71.01, 51.85, 7.05, 6.57, 6.46.

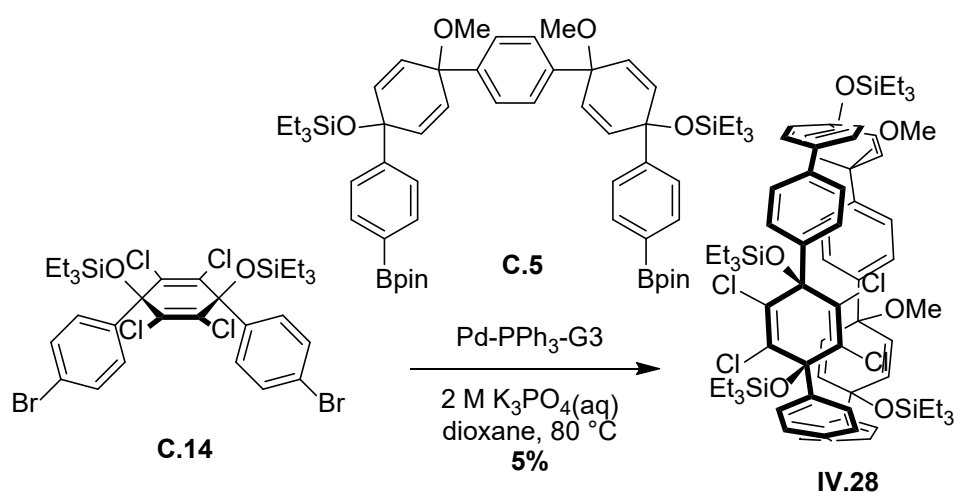


C.13. **IV.26** (210 mg, 148 μmol , 1 eq) was dissolved in tetrahydrofuran (6.2 mL, 24 mM) and AcOH (250 μL , 270 mg, 4.4 mmol, 30 eq). A 1 M solution of tetrabutylammonium fluoride in tetrahydrofuran (1.5 mL, 1.5 mmol, 10 eq) was added. The reaction was stirred for 4 h and quenched with water. This mixture was extracted with EtOAc (3 x 5 mL) and the combined extracts were dried over anhydrous sodium sulfate. Solvent was removed under reduced pressure to yield a solid **C.13** (132 mg, 88%). ^1H NMR (500 MHz, Acetone- d_6) δ 7.67 (br, 4H), 7.39 (s, 4H), 7.22 (d, $J = 8.8$ Hz, 4H), 6.98 (s, 4H), 6.29 (d, $J = 10.0$ Hz, 4H), 5.73 (d, $J = 10.1$ Hz, 4H), 3.37 (s, 6H).



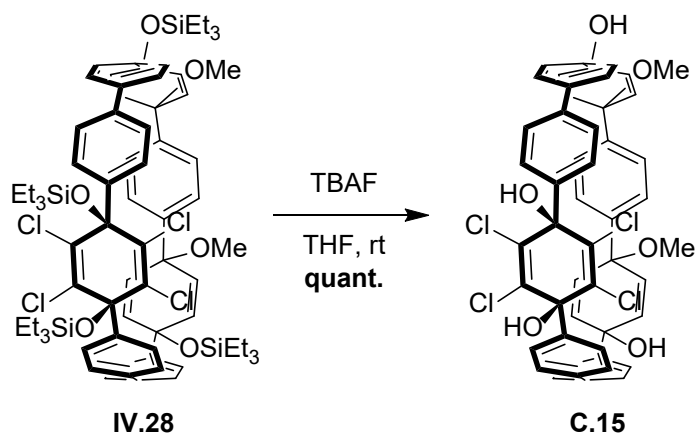
C.14. 1,4-dibromobenzene (6.00 g, 25.4 mmol, 2.4 eq) was dissolved in tetrahydrofuran (53 mL, 200 mM) and cooled to -78 $^\circ\text{C}$. A 2.5 M solution of $n\text{-BuLi}$ in hexanes (9.3 mL, 23 mmol, 2.2 eq) was added followed by chloranil (2.61 g, 10.6 mmol, 1 eq). The solution was stirred at -78 $^\circ\text{C}$ for 1 h and triethylsilyl chloride (5.3 mL, 4.8 g, 32 mmol, 3 eq) was added. The mixture was warmed to room temperature and stirred overnight. In

the morning, it was quenched with water and extracted with EtOAc (3 x 50 mL). The combined organic extracts were washed with brine (40 mL) and dried over anhydrous sodium sulfate. Solvent was removed under reduced pressure to yield a 2:1 mixture of both possible isomers as an oil. The mixture was purified by column chromatography on silica (hexanes) to yield an oil that crystallized into a white solid **C.14** (3.0 g, 36%). ¹H NMR (500 MHz, CDCl₃) δ 7.49 (d, J = 8.7 Hz, 4H), 7.28 (d, J = 8.7 Hz, 4H), 1.02 (t, J = 7.9 Hz, 18H), 0.78 (q, J = 7.9 Hz, 12H).

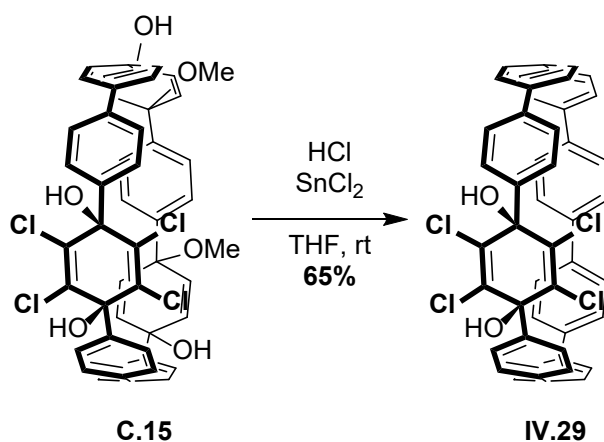


IV.28. **C.5** (500 mg, 521 μmol , 1 eq), dibromide **C.14** (411 mg, 521 μmol , 1 eq) and SPhos Pd G2 (38 mg, 52 μmol , 0.1 eq) were dissolved in dioxane (260 mL, 2 mM) and the mixture was warmed to 80 °C. A 2 M aqueous solution of potassium phosphate tribasic (26 mL) was then added. The reaction was stirred overnight. It was then opened to the air, filtered through celite and extracted into ethyl acetate (2 x 120 mL). The extract was washed with brine (100 mL) and dried over anhydrous sodium sulfate. Solvent was removed to yield a brown oil. The solid was purified by column chromatography (0 to 20% EtOAc in hexanes) to yield a golden oil. Acetone added and filtered to yield a white solid **IV.28** (35 mg, 5%). ¹H NMR (500 MHz, CDCl₃) δ 7.55 (s, 4H), 7.51 (d, J = 8.5 Hz,

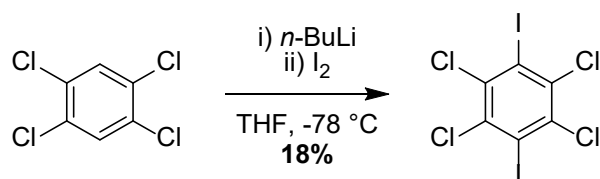
4H), 7.47 (d, $J = 8.9$ Hz, 4H), 7.45 (d, $J = 8.4$ Hz, 4H), 7.21 (d, $J = 8.6$ Hz, 4H), 6.12 (d, $J = 10.2$ Hz, 4H), 6.03 (d, $J = 10.2$ Hz, 4H), 3.30 (s, 6H), 1.05 (t, $J = 7.9$ Hz, 18H), 1.01 (t, $J = 8.0$ Hz, 18H), 0.83 (q, $J = 7.9$ Hz, 12H), 0.73 (q, $J = 7.9$ Hz, 12H).



C.15. **IV.28** (30 mg, 23 μmol , 1 eq) was dissolved in tetrahydrofuran (1.0 mL, 24 mM) and a 1 M solution of tetrabutylammonium fluoride in tetrahydrofuran (230 μL , 230 μmol , 10 eq) was added. The reaction was stirred for 1 h and quenched with water. Solvent was removed under reduced pressure to result in a white suspension. This mixture was filtered and washed with dichloromethane to yield a white solid **C.15** (20 mg, 100%). ^1H NMR (500 MHz, Acetone- d_6) δ 7.74 (d, $J = 8.3$ Hz, 4H), 7.63 (d, $J = 7.9$ Hz, 4H), 7.61 (d, $J = 8.2$ Hz, 4H) 7.57 (s, 4H), 7.43 (d, $J = 8.3$ Hz, 4H), 6.21 (d, $J = 10.1$ Hz, 4H), 5.80 (d, $J = 10.0$ Hz, 4H), 3.34 (s, 6H).



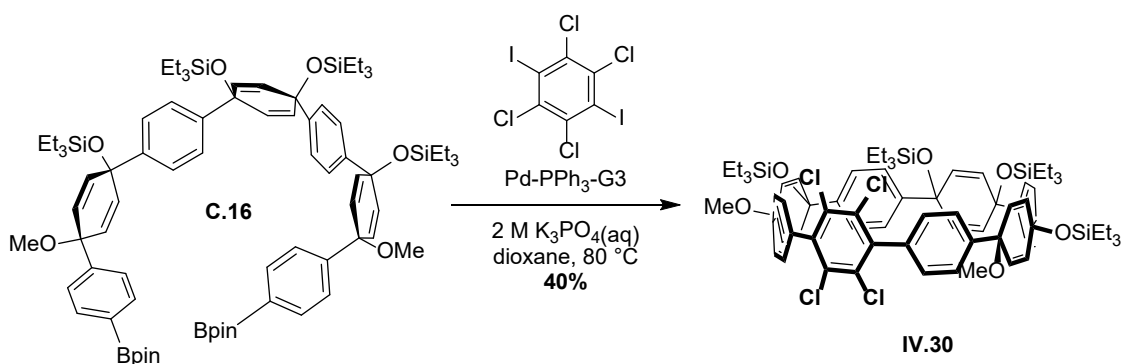
IV.29. **C.15** (10 mg, 11 μmol , 1 eq) was dissolved in minimal tetrahydrofuran. A solution of $\text{SnCl}_2 \cdot 2\text{H}_2\text{O}$ (8.5 mg, 38 μmol , 3.3 eq) and 12 M HCl (6.3 μL , 75 μmol , 6.6 eq) in tetrahydrofuran (0.5 mL) was added and the reaction was stirred for 1 h. The reaction was then quenched with a 1 M aqueous solution of NaOH and extracted with dichloromethane (3 x 3 mL). The combined extracts were dried over anhydrous sodium sulfate and solvent was removed under reduced pressure to yield a fluorescent solid. Purified by column chromatography on silica (0 to 30% EtOAc in dichloromethane) to yield solid **IV.29** (5.5 mg, 65%). ^1H NMR (600 MHz, CDCl_3) δ 7.55 (s, 4H), 7.53 (m, 8H), 7.50 (d, $J = 8.4$ Hz, 4H), 7.34 (d, $J = 8.4$ Hz, 4H), 7.31 (d, $J = 8.4$ Hz, 4H), 7.20 (d, $J = 8.5$ Hz, 4H), 3.17 (s, 2H). ^{13}C NMR (151 MHz, CDCl_3) δ 142.89, 139.33, 139.23, 138.24, 137.12, 137.00, 136.73, 134.06, 128.43, 127.87, 127.77, 127.51, 127.26, 127.22, 77.95.



1,2,4,5-tetrachloro-3,6-diiodobenzene. 1,2,4,5-tetrachlorobenzene (1.00 g, 4.63 mmol, 1 eq) was dissolved in tetrahydrofuran (22 mL, 500 mM) and cooled to -78 $^{\circ}\text{C}$. A 2.5 M solution of *n*-BuLi in hexanes (4.1 mL, 10 mmol, 2.2 eq) was added dropwise and stirred

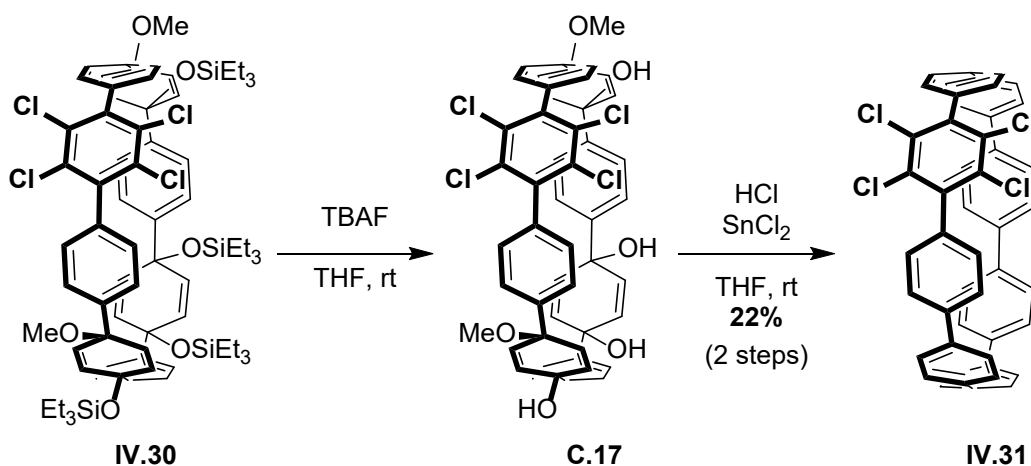
for 30 min. Iodine (2.82 g, 11.1 mmol, 2.4 eq) was added and the reaction was warmed to room temperature. It was then quenched with a saturated aqueous solution of sodium bisulfite. The mixture was then extracted with EtOAc (3 x 10 mL) and the combined extracts were washed with a saturated aqueous solution of sodium bicarbonate (10 mL) and brine (10 mL). The solution was dried over anhydrous sodium sulfate and the solvent was removed under reduced pressure to yield a yellow solid. This solid was recrystallized in EtOH to yield a yellow solid 1,2,4,5-tetrachloro-3,6-diiodobenzene (386 mg, 18%).

^{13}C NMR (151 MHz, CDCl_3) $\delta(\text{ppm})$ 136.39, 105.26.



IV.30. **C.16** (180 mg, 131 μmol , 1 eq), 1,2,4,5-tetrachloro-3,6-diiodobenzene (61 mg, 131 μmol , 1 eq) and PPh_3 Pd G3 (8.3 mg, 13 μmol , 0.1 eq) were dissolved in dioxane (66 mL, 2 mM) and the mixture was warmed to 80 °C. A 2 M aqueous solution of potassium phosphate tribasic (6.6 mL) was then added. The reaction was stirred overnight. It was then opened to the air, filtered through celite and extracted into ethyl acetate (2 x 40 mL). The extract was washed with brine (60 mL) and dried over anhydrous sodium sulfate. Solvent was removed to yield a yellow oil. The solid was purified by gel permeation chromatography (chloroform) to yield a solid **IV.30** (70 mg, 40%). ^1H NMR (500 MHz, Chloroform- d) δ 7.37 (d, $J = 8.5$ Hz, 4H), 7.34 (d, $J = 8.4$ Hz, 4H), 7.24 (d, $J = 8.8$ Hz, 4H), 6.98 (d, $J = 8.4$ Hz, 4H), 6.27 (d, $J = 10.1$ Hz, 4H), 6.24 (s, 4H), 5.97 (d, $J = 10.1$

Hz, 4H), 3.49 (s, 6H), 0.93 (t, J = 7.9 Hz, 18H), 0.84 (t, J = 7.9 Hz, 18H), 0.59 (q, J = 7.9 Hz, 12H), 0.42 (q, J = 8.0 Hz, 12H).



IV.31. **IV.30** (70 mg, 53 μmol , 1 eq) was dissolved in tetrahydrofuran (2.2 mL, 24 mM) and a 1 M solution of tetrabutylammonium fluoride in tetrahydrofuran (315 μL , 315 μmol , 6 eq) was added. The reaction was stirred for 1 h and quenched with water. This mixture was extracted with EtOAc (3 x 3 mL) and the combined extracts were dried over anhydrous sodium sulfate. Solvent was removed under reduced pressure to yield a solid. This solid was purified by column chromatography (EtOAc) to yield a mixture containing **C.17**. This solid was dissolved in minimal tetrahydrofuran. A solution of $\text{SnCl}_2 \cdot 2\text{H}_2\text{O}$ (27 mg, 120 μmol , 3.3 eq) and 12 M HCl (20 μL , 240 μmol , 6.6 eq) in tetrahydrofuran (1.5 mL) was added and the reaction was stirred for 1.5 h. The reaction was then quenched with a 1M aqueous solution of NaOH and extracted with dichloromethane (3 x 3 mL). The combined extracts were dried over anhydrous sodium sulfate and solvent was removed under reduced pressure to yield a fluorescent solid. Purified by column chromatography on silica (dichloromethane) to yield a solid. This solid was further purified by prep plate (25% dichloromethane in hexanes) to yield pure cycloparaphenylene **IV.31** as a solid (6 mg, 22%). $^1\text{H NMR}$ (600 MHz, CDCl_3) δ 7.56 (d,

$J = 8.7$ Hz, 4H), 7.52 (d, $J = 8.8$ Hz, 4H), 7.44 (d, $J = 8.2$ Hz, 4H), 7.44 (s, 4H), 7.34 (d, $J = 8.7$ Hz, 4H), 7.31 (d, $J = 8.5$ Hz, 4H), 7.21 (d, $J = 8.6$ Hz, 4H). ^{13}C NMR (151 MHz, CDCl_3) δ 142.17, 140.42, 139.22, 138.06, 137.94, 137.86, 137.33, 134.70, 132.45, 132.41, 128.58, 127.57, 127.54, 127.29, 127.25.

C.2. X-ray Crystallography.

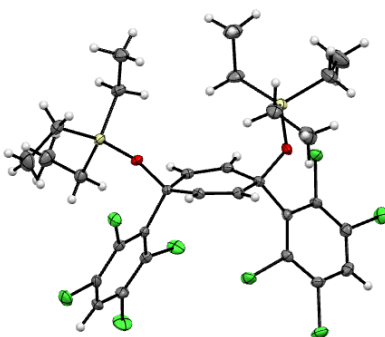


Figure C.1. ORTEP representation of **C.11** (thermal ellipsoids shown at 50% probability) verifying *cis* geometry.

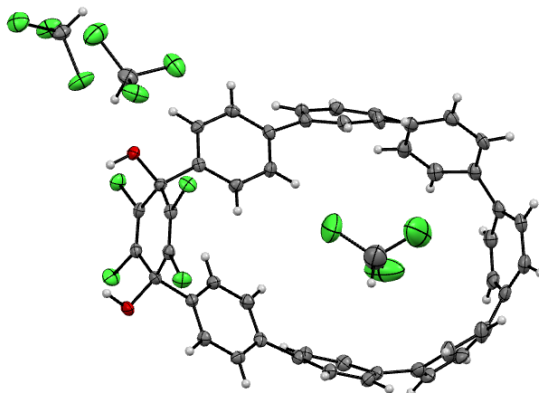


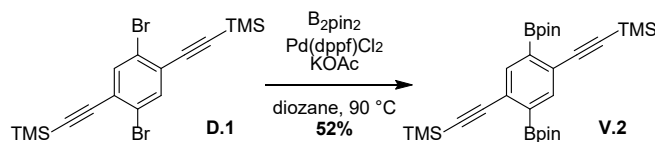
Figure C.2. ORTEP representation of partially aromatized **IV.29** (thermal ellipsoids shown at 50% probability).

APPENDIX D

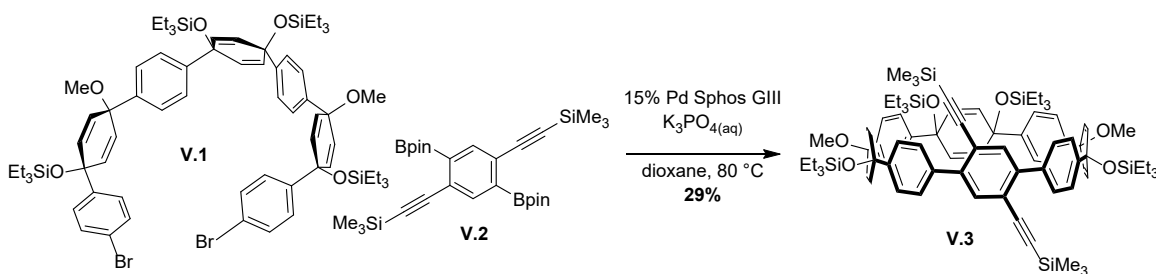
SUPPLEMENTARY INFORMATION FOR CHAPTER V

D.1. Experimental Details

All glassware was flame dried and cooled under an inert atmosphere of nitrogen unless otherwise noted. Moisture sensitive reactions were carried out under nitrogen atmosphere using Schlenk and standard syringe/septa techniques. Tetrahydrofuran, CH₂Cl₂, DMF, and dioxane were dried by filtration through alumina according to the methods describes by Grubbs.¹³⁶ Column chromatography was conducted with Zeochem Zeoprep 60 Eco 40-63 μm silica gel. Automated flash chromatography was performed using a Biotage Isolera One. Recycling gel permeation chromatography (GPC) was performed using a Japan Analytical Industry LC-9101 preparative HPLC with JAIGEL-1H/JAIGEL-2H columns in series using CHCl₃. Thin Layer Chromatography (TLC) was performed using Sorbent Technologies Silica Gel XHT TLC plates. Developed plates were visualized using UV light at wavelengths of 254 and 365 nm. ¹H NMR spectra were recorded at 500 MHz or 600 MHz on a Bruker Advance-III-HD NMR spectrometer. ¹³C NMR spectra were recorded 150 MHz on a Bruker Advance-III-HD NMR spectrometer. All ¹H NMR spectra were taken in CDCl₃ (referenced to TMS, δ 0.00 ppm) or DMSO-*d*₆ (referenced to residual DMSO, δ 2.50 ppm). All ¹³C NMR spectra were taken in CDCl₃ (referenced to TMS, δ 0.00 ppm) or DMSO-*d*₆ (referenced to DMSO, δ 39.52 ppm). Absorbance and fluorescence spectra were obtained in a 1 cm Quartz cuvette with dichloromethane using an Agilent Cary 100 UV-Vis spectrometer and a Horiba Jobin Yvon Fluoromax-4 Fluorimeter. All reagents were obtained commercially unless otherwise noted. Compounds X, Y, and Z were prepared according to literature procedure.

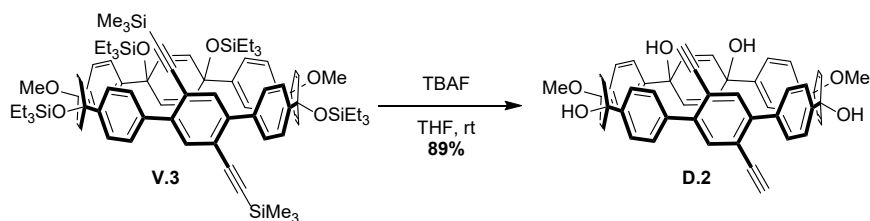


V.2. KOAc (6.05 g, 61.6 mmol, 6.6 eq) was added to a rounded bottom flask under vacuum and flame dried. Upon cooling, **D.1** (4.00 g, 9.34 mmol, 1 eq), Pd(dppf)₂Cl₂ (229 mg, 280 μmol, 0.03 eq) and bis(pinacolato)diboron (5.69 g, 22.4 mmol, 2.4 eq) were added. The vessel was fitted with a rubber septum and evacuated/backfilled with nitrogen. Dioxane was added, the reaction was warmed from room temperature to 90 °C and stirred at this temperature overnight. In the morning, it was filtered through Celite, washing with EtOAc, and the solvent of the filtrate was removed under reduced pressure. The resulting residue was recrystallized in EtOH to yield **V.2** as brown crystals (2.54 g, 52%). IR (neat) 2981, 2154, 1372, 1324, 1249 cm⁻¹; ¹H NMR (500 MHz, Chloroform-*d*) δ 7.82 (s, 2H), 1.36 (s, 24H), 0.25 (s, 18H). ¹³C NMR (126 MHz, CDCl₃) δ 139.43, 126.71, 105.37, 97.71, 84.17, 24.99. HRMS (ASAP) (m/z): [M+H]⁺ calculated for C₂₈H₄₅B₂O₄Si₂, 523.3042; found, 523.3091.



V.3. **V.1** (1.8 g, 1.4 mmol, 1 eq), **V.2** (882 mg, 1.7 μmol, 1.2 eq), and SPhos Pd G3 (110 mg, 140 μmol, 0.1 eq) were dissolved in dioxane (280 mL, 5 mM) and purged with nitrogen while heating to 80 °C. An aqueous solution of K₃PO₄ (28 mL) was added and

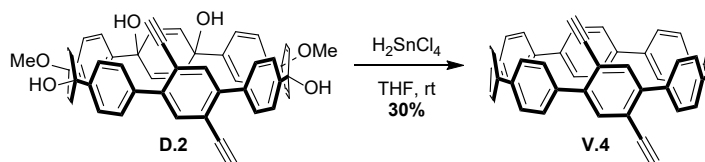
the mixture was stirred for 18 h. The mixture was then filtered through Celite and dried over anhydrous sodium sulfate. Solvent was removed under reduced pressure to yield a brown solid. The solid was purified by column chromatography on silica (0 to 100% dichloromethane in hexanes) to yield **V.3** as an orange solid (558 mg, 29%). IR (neat) 2953, 2875, 2155, 1477, 1409, 1249 cm^{-1} ; ^1H NMR (600 MHz, Chloroform-*d*) δ 7.46 (s, 2H), 7.39 (d, $J = 8.4$ Hz, 4H), 7.32 (d, $J = 8.4$ Hz, 4H), 7.29 (d, $J = 8.4$ Hz, 4H), 7.18 (d, $J = 8.6$ Hz, 4H), 6.19 (dd, $J = 10.1, 2.5$ Hz, 2H), 6.16 (dd, $J = 10.1, 2.4$ Hz, 2H), 6.12 (m, 4H), 5.95 (dd, $J = 10.2, 2.5$ Hz, 2H), 5.90 (dd, $J = 10.1, 2.5$ Hz, 2H), 3.31 (s, 6H), 1.01 (t, $J = 7.9$ Hz, 18H), 0.86 (t, $J = 8.0$ Hz, 18H), 0.71 (q, $J = 7.8$ Hz, 12H), 0.49 (q, $J = 7.7$ Hz, 12H), 0.13 (s, 12H). ^{13}C NMR (126 MHz, CDCl_3) δ 146.87, 144.83, 142.87, 142.26, 138.70, 136.43, 135.84, 135.02, 134.90, 133.50, 129.65, 126.63, 126.32, 125.28, 104.73, 99.59, 74.80, 72.68, 69.75, 52.04, 7.53, 7.42, 7.02, 6.89. HRMS (ASAP) (m/z): $[\text{M}]^+$ calculated for $\text{C}_{84}\text{H}_{114}\text{O}_6\text{Si}_6$, 1386.7231; found, 1386.7169.



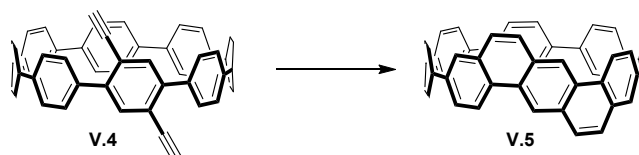
D.2. **V.3** (558 mg, 402 μmol , 1 eq) was dissolved in tetrahydrofuran (2 mL, 200 mM) and a 1 M solution of tetrabutylammonium fluoride in tetrahydrofuran (3.2 mL, 3.2 mmol, 8 eq) was added. The reaction was stirred for 1 h and quenched with water.

Tetrahydrofuran was removed under reduced pressure to yield a suspension that was filtered washing with water and dichloromethane to yield an off white solid **D.2** (283 mg, 89%). IR (neat) 3293, 2958, 1477, 1409 cm^{-1} ; ^1H NMR (500 MHz, Acetone-*d*₆) δ 7.57 (s, 4H), 7.56 (d, $J = 8.8$ Hz, 4H), 7.50 (d, $J = 8.2$ Hz, 4H), 7.36 (d, $J = 8.8$ Hz, 4H), 7.21 (d,

$J = 8.4$ Hz, 4H), 6.27 (d, $J = 10.1$ Hz, 4H), 5.95 (s, 4H), 5.84 (d, $J = 10.1$ Hz, 4H), 3.79 (s, 2H), 3.29 (s, 6H). ^{13}C NMR (126 MHz, Acetone) δ 144.83, 142.55, 142.18, 138.02, 135.65, 135.35, 134.66, 129.20, 129.02, 125.92, 125.74, 125.46, 120.61, 83.33, 82.19, 74.70, 66.67, 50.68.

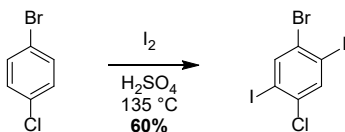


V.4. **D.2** (100 mg, 127 μmol , 1 eq) was dissolved in tetrahydrofuran (3 mL, 40 mM). A solution of $\text{SnCl}_2 \cdot 2\text{H}_2\text{O}$ (95 mg, 420 μmol , 3.3 eq) and 12 M HCl (67 μL , 800 μmol , 6.3 eq) in tetrahydrofuran (3.2 mL) was added and the reaction was stirred for 1 h. The reaction was then quenched with a 1 M aqueous solution of NaOH and extracted with dichloromethane (3 x 5 mL). The combined extracts were dried over anhydrous sodium sulfate and solvent was removed under reduced pressure to yield a yellow solid. Purified by column chromatography on silica (40% to 100% dichloromethane in hexanes) to yield a yellow solid CPP **V.4** (25 mg, 30%). ^1H NMR (500 MHz, Chloroform-*d*) δ 7.62 (d, $J = 8.7$ Hz, 4H), 7.54 – 7.49 (m, 8H), 7.48 – 7.44 (m, 14H), 7.42 (d, $J = 8.8$ Hz, 4H), 3.26 (s, 2H). ^{13}C NMR (126 MHz, CDCl_3) δ 140.78, 139.53, 138.15, 137.88, 137.87, 137.82, 137.54, 136.18, 135.56, 129.75, 127.91, 127.56, 127.54, 127.43, 127.27, 120.39, 83.02, 82.56. LRMS (MALDI) (m/z): $[\text{M}]^+$ calculated for $\text{C}_{52}\text{H}_{32}$, 656.250; found, 656.257.



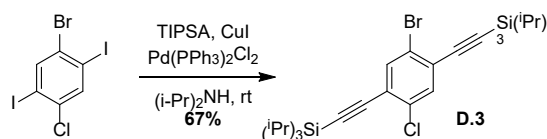
V.5. **V.4**, $\text{TpRu}(\text{PPh}_3)(\text{MeCN})_2\text{SbF}_6$ (1.0 mg, 1.2 μmol , 0.2 eq) and dimethylsulfone (7.2 mg, 77 μmol) were dissolved in TCE-*d*2 (600 μL , 10 mM) in an NMR tube. The starting

mass of CPP **4** was determined to be 3.5 mg based on dimethylsulfone as the internal standard. The reaction was then heated to 100 °C for 6 h. The reaction was determined to be complete by NMR indicated by complete disappearance of starting material peaks and appearance of product peaks. Yield was determined using the dimethylsulfone internal standard (2.8 mg, 80%). The product could be isolated by evaporating the solvent and purification by column chromatography on silica (dichloromethane) to yield a yellow solid CPP **6**. ¹H NMR (500 MHz, CDCl₃) δ 8.56 (s, 2H), 8.36 (d, J = 9.1 Hz, 2H), 7.82 (dd, J = 9.1, 2.1 Hz, 2H), 7.79 (d, J = 2.0 Hz, 2H), 7.66 (d, J = 9.0 Hz, 2H), 7.59 (d, J = 8.5 Hz, 4H), 7.53 – 7.38 (m, 18H). ¹³C NMR (126 MHz, CDCl₃) δ 137.68, 137.47, 136.56, 135.46, 132.70, 131.99, 129.46, 128.93, 127.59, 127.53, 127.38, 127.31, 127.26, 127.14, 127.04, 126.55, 126.28, 125.19, 123.70, 122.58.

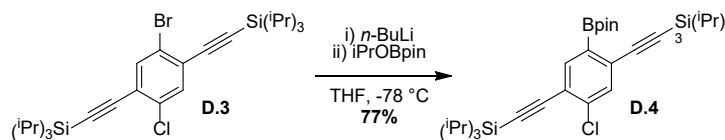


1-bromo-4-chloro-2,5-diiodobenzene. 1-bromo-4-chlorobenzene (32 g, 104 mmol, 1 eq) was suspended in concentrated sulfuric acid (500 mL, 330 mM). Iodine (85 g, 230 mmol, 2 eq) was added and the reaction was heated to 135 °C for two days. The reaction was then cooled to room temperature and poured into 300 mL of ice. A large chunk remained in the flask. The acidic mixture was extracted three times with dichloromethane (3 x 100 mL) and washed with 1 M aqueous NaOH to remove excess iodine. The large chunk remaining in the round bottom was washed with 1 M aqueous NaOH and dissolved in dichloromethane by sonicating and refluxing. This solution was washed with 1 M aqueous NaOH and combined with the previous extracts. Half a part of MeOH was added to promote crystallization and the mixture was cooled in a refrigerator overnight.

Filtration and washing with MeOH yielded white crystalline 1-bromo-4-chloro-2,5-diiodobenzene (44.4 g, 60%). ^1H NMR (500 MHz, Chloroform-*d*) δ 8.04 (s, 1H), 7.88 (s, 1H). ^{13}C NMR (126 MHz, CDCl_3) δ 142.14, 139.24, 138.24, 128.53, 100.97, 98.14. HRMS (EI) (m/z): $[\text{M}]^+$ calculated for $\text{C}_6\text{H}_2\text{BrClI}_2$, 441.7105; found, 441.7118.

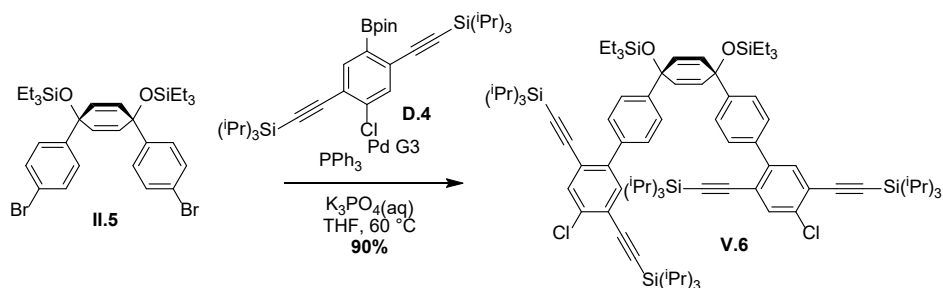


D.3. 1-bromo-4-chloro-2,5-diiodobenzene (20 g, 45 mmol, 1 eq), copper(I) iodide (430 mg, 2.26 mmol, 0.05 eq), and $\text{Pd}(\text{PPh}_3)_2\text{Cl}_2$ (317 mg, 451 μmol , 0.01 eq) were dissolved in diisopropylamine (450 mL, 100 mM) and purged with nitrogen for 10 min. Purging was stopped and triisopropylsilylacetylene (20.6 mL, 16.8 g, 92.0 mmol, 2.04 eq) was added. The reaction was stirred overnight. The next morning, a saturated aqueous solution of ammonium chloride (200 mL) was added and the mixture was extracted with ether (3 x 200 mL). The combined extracts were washed with brine, dried over anhydrous Na_2SO_4 and evaporated to yield a yellow solid. The solid was recrystallized in *i*PrOH to yield **D.3** as white crystals (16.6 g, 67%). ^1H NMR (300 MHz, Chloroform-*d*) δ 7.68 (s, 1H), 7.50 (s, 1H), 1.14 (m, 42H). ^{13}C NMR (151 MHz, Chloroform-*d*) δ 136.51, 134.82, 133.48, 126.41, 124.41, 122.95, 103.35, 101.50, 100.39, 99.69, 18.64, 18.62, 11.25, 11.23. HRMS (EI) (m/z): $[\text{M}]^+$ calculated for $\text{C}_{28}\text{H}_{44}\text{BrClSi}_2$, 550.1872; found, 550.1853.



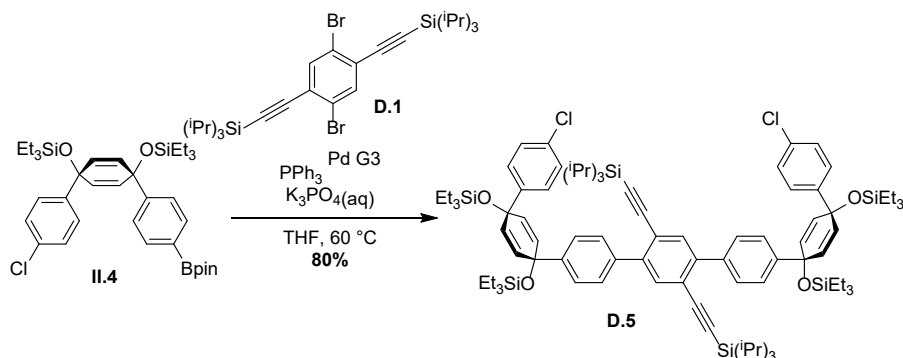
D.4. **D.3** (2.5 g, 4.5 mmol, 1 eq) was dissolved in tetrahydrofuran (23 mL, 200 mM) and cooled to $-78\text{ }^\circ\text{C}$. A 2.5 M solution of *n*-BuLi in hexanes (2.2 mL, 5.4 mmol, 1.2 eq) was added followed by 2-isopropoxy-4,4,5,5-tetramethyl-1,3,2-dioxaborolane (1.2 mL, 1.1 g,

5.9 mmol, 1.3 eq). The reaction was then warmed to room temperature and quenched with water (10 mL). The mixture was extracted with EtOAc (2 x 20 mL) and the extracts were dried over anhydrous Na₂SO₄ and evaporated to yield a brown sticky syrup. Purified by chromatography (0 to 25% EtOAc in hexanes) to yield **D.4** as a clear colorless oil (2.1 g, 77%). IR (neat) 2942, 2865, 2159, 1469, 1386 cm⁻¹; ¹H NMR (500 MHz, Chloroform-*d*) δ 7.85 (d, *J* = 2.4 Hz, 1H), 7.52 (d, *J* = 2.4 Hz, 1H), 1.34 (d, *J* = 2.4 Hz, 12H), 1.15 (s, 42H). ¹³C NMR (151 MHz, Chloroform-*d*) δ 140.38, 138.32, 134.08, 129.13, 122.54, 105.94, 102.78, 98.50, 96.21, 84.16, 24.80, 18.77, 18.67, 11.36, 11.31. HRMS (ASAP) (*m/z*): [M+H]⁺ calculated for C₃₄H₅₇BClO₂Si₂, 599.3679; found, 599.3668.

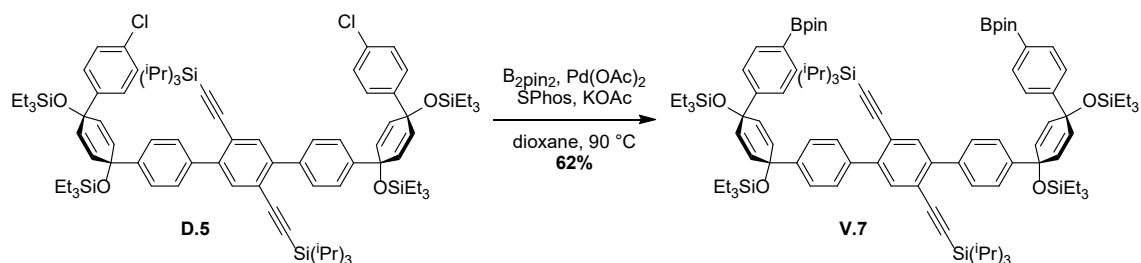


V.6. **II.5** (880 mg, 1.35 mmol, 1 eq), **D.4** (1.70 g, 2.84 mmol, 2.1 eq) and PPh₃ Pd G3 (26 mg, 41 μmol, 0.03 eq) dissolved in tetrahydrofuran (27 mL, 50 mM) and warmed to 60 °C. A 2 M aqueous solution of K₃PO₄ (5 mL) was added and the reaction was left overnight. In the morning the reaction was filtered through celite, dried over Na₂SO₄ and the solvent was removed under reduced pressure to yield an oil. Purified by chromatography (hexanes to 1:9 CH₂Cl₂/hexanes) to yield **V.6** as a clear colorless oil (1.74 g, 90%). ¹H NMR (500 MHz, Chloroform-*d*) δ 7.57 (d, *J* = 1.7 Hz, 2H), 7.48 – 7.42 (m, 6H), 7.37 (d, *J* = 8.3 Hz, 4H), 5.98 (s, 4H), 1.12 (s, *J* = 42H), 1.00 – 0.93 (m, 60H), 0.64 (q, *J* = 7.9 Hz, 12H). ¹³C NMR (126 MHz, CDCl₃) δ 145.59, 142.09, 137.64, 134.45, 134.22, 133.72, 131.47, 128.91, 125.57, 123.27, 122.85, 104.69, 102.78, 98.70,

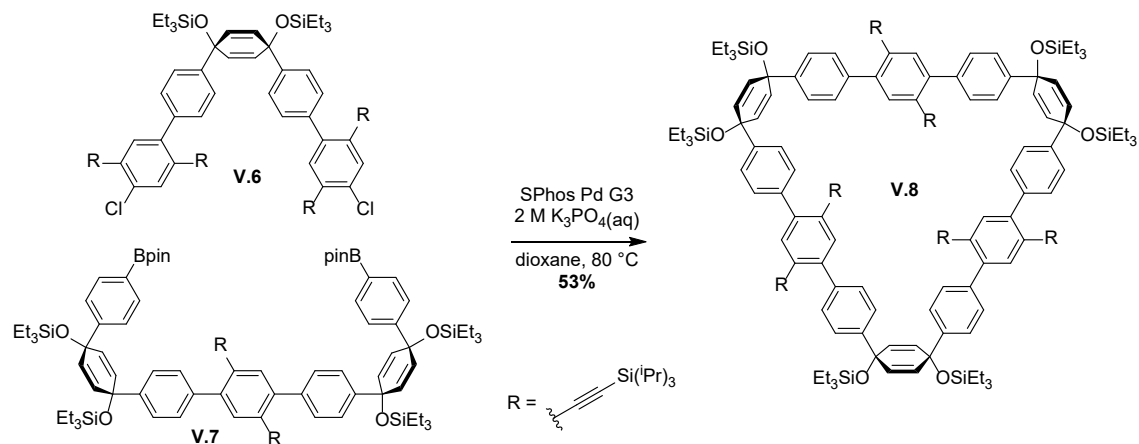
97.22, 71.28, 18.63, 18.56, 11.27, 11.21, 7.08, 6.47. LRMS (MALDI) (m/z): [M]⁺
calculated for C₈₆H₁₃₀Cl₂O₂Si₆, 1435.81; found, 1435.84.



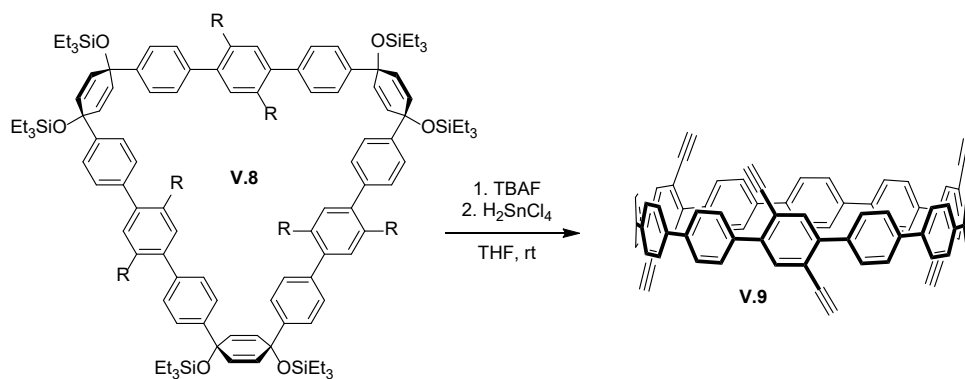
D.5. **D.1** (1.00 g, 1.68 mmol, 1 eq), **II.4** (2.30 g, 3.52 mmol, 2.1 eq) and PPh₃ Pd G3 (32 mg, 50 μmol, 0.03 eq) dissolved in tetrahydrofuran (8.4 mL, 200 mM) and warmed to 60 °C. A 2 M aqueous solution of K₃PO₄ (1.7 mL) was added and the reaction was left overnight. In the morning the reaction was filtered through celite, dried over Na₂SO₄ and the solvent was removed under reduced pressure to yield an oil. Purified by chromatography (hexanes to 25% CH₂Cl₂/hexanes) to yield **D.5** as white solid (2.0 g, 80%). IR (neat) 2954, 2874, 2160, 1465, 1077 cm⁻¹; ¹H NMR (500 MHz, Chloroform-*d*) δ 7.53 (s, 2H), 7.51 (d, *J* = 8.3 Hz, 4H), 7.32 (d, *J* = 8.8 Hz, 8H), 7.24 (d, *J* = 8.4 Hz, 4H), 5.98 (s, 8H), 0.97 (s, 42H), 0.97 (t, *J* = 8.0 Hz, 18H), (t, *J* = 7.9 Hz, 18H), 0.65 (q, *J* = 8.0 Hz, 12H), 0.59 (q, *J* = 7.9 Hz, 12H). ¹³C NMR (126 MHz, CDCl₃) δ 145.02, 144.74, 142.31, 138.33, 134.47, 133.07, 132.03, 130.90, 129.02, 128.27, 127.41, 125.36, 121.90, 105.88, 95.92, 71.36, 71.02, 18.57, 11.25, 7.07, 7.03, 6.45. HRMS (ASAP) (m/z): [M]⁺ calculated for C₈₈H₁₂₈Cl₂O₄Si₆, 1486.7805; found, 1486.7798.



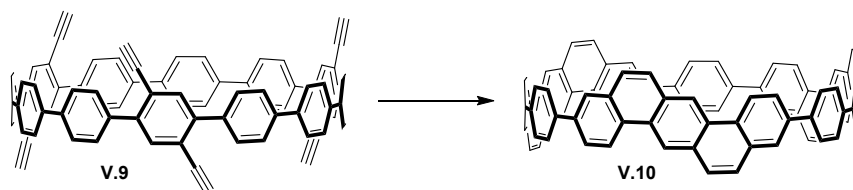
V.7. **D.5** (206 mg, 138 μmol , 1 eq), KOAc (90 mg, 910 μmol , 6.6 eq), B_2pin_2 (140 mg, 553 μmol , 4 eq), Pd(OAc)_2 (1.6 mg, 6.9 μmol , 0.05 eq), and SPhos (7.1 mg, 17 μmol , 0.125 eq) were dissolved in dioxane (1.4 mL, 100 mM) and heated to 90 $^\circ\text{C}$ overnight. The next morning, it was filtered through celite and the solvent was removed under reduced pressure to yield an oil. Purified by chromatography on silica (10 to 50% CH_2Cl_2 /hexanes) to yield **V.7** as a clear colorless oil (143 mg, 62%). IR (neat) 2952, 2875, 2153, 1361 cm^{-1} ; ^1H NMR (500 MHz, Chloroform-*d*) δ 7.73 (d, $J = 7.7$ Hz, 4H), 7.53 (s, 2H), 7.49 (d, $J = 7.9$ Hz, 4H), 7.42 (d, $J = 7.7$ Hz, 4H), 7.34 (d, $J = 7.9$ Hz, 4H), 6.03 (d, $J = 9.7$ Hz, 4H), 5.94 (d, $J = 9.8$ Hz, 4H), 1.33 (s, 24zH), 1.01 – 0.94 (m, 60H), 0.91 (t, $J = 7.9$ Hz, 18H), 0.67 (q, $J = 7.9$ Hz, 12H), 0.56 (q, $J = 7.9$ Hz, 12H). ^{13}C NMR (126 MHz, CDCl_3) δ 149.20, 145.20, 142.43, 138.22, 134.72, 134.37, 131.83, 131.06, 128.97, 125.36, 125.31, 121.89, 105.92, 95.76, 83.71, 71.44, 71.38, 24.88, 18.58, 11.24, 7.09, 7.05, 6.46, 6.43. HRMS (ASAP) (m/z): $[\text{M}]^+$ calculated for $\text{C}_{100}\text{H}_{152}\text{B}_2\text{O}_8\text{Si}_6$, 1671.0289; found, 1671.0256.



V.8. **V.7**, **V.6**, and SPhos Pd G3 dissolved in dioxane and warmed to 80 °C. A 2 M aqueous solution of potassium phosphate tribasic was then added and the reaction was stirred for two hours. It was then filtered through celite and dried over anhydrous sodium sulfate. Solvent was removed to yield a brown solid. The solid was purified by column chromatography on silica (0 to 25% EtOAc in hexanes) to yield a golden oil. To the oil was added a small amount of acetone and a white solid precipitated. The solid was collected by filtration and the filtrate was purified by gel permeation chromatography (chloroform) to isolate additional **V.8** (120 mg, 53%). IR (neat) 2942, 2865, 2160, 1461, 1073 cm^{-1} ; ^1H NMR (600 MHz, Chloroform-*d*) δ 7.52 (s, 6H), 7.51 (d, $J = 8.4$ Hz, 12H), 7.39 (d, $J = 8.3$ Hz, 12H), 5.99 (s, 12H), 1.02 – 0.91 (m, 180H), 0.65 (q, $J = 7.9$ Hz, 36H). ^{13}C NMR (151 MHz, CDCl_3) δ 145.09, 142.12, 138.14, 134.26, 131.22, 128.81, 125.28, 121.68, 105.71, 95.50, 71.23, 18.37, 11.03, 6.89, 6.28.

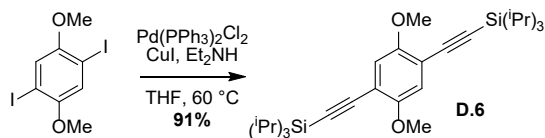


V.9. **V.8** (50 mg, 43 μmol , 1 eq) was dissolved in tetrahydrofuran (2 mL, 20 mM). A solution of $\text{SnCl}_2 \cdot 2\text{H}_2\text{O}$ (32 mg, 140 μmol , 3.3 eq) and 12 M HCl (23 μL , 270 μmol , 6.3 eq) in tetrahydrofuran (2.2 mL) was added and the reaction was stirred for 1 h. The reaction was then quenched with a 1 M aqueous solution of NaOH and extracted with dichloromethane (3 x 5 mL). The combined extracts were dried over anhydrous sodium sulfate and solvent was removed under reduced pressure to yield a yellow solid. Purified by column chromatography on silica (20 to 80% dichloromethane in hexanes) to yield a yellow solid **V.9** (10 mg, 22%). IR (neat) 3292, 2953, 2873, 2162, 1475 cm^{-1} ; ^1H NMR (500 MHz, Chloroform-*d*) δ 7.68 (d, $J = 8.6$ Hz, 12H), 7.63 (s, 12H), 7.60 (d, $J = 8.7$ Hz, 12H), 7.57 (s, 6H), 3.20 (s, 6H). ^{13}C NMR (126 MHz, CDCl_3) δ 141.57, 139.64, 138.87, 137.12, 135.55, 129.81, 127.57, 126.84, 120.69, 82.78, 82.12.

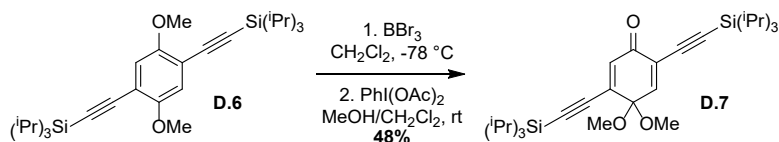


V.10. **V.9** (9.0 mg, 8.5 μmol , 1 eq), $(\text{Ph}_3\text{P})\text{Ru}(\text{cymene})\text{Cl}_2$ (2.9 mg, 5.1 μmol , 60%), and NH_4PF_6 (1.7 mg, 10 μmol , 1.2 eq) were dissolved in DCE (400 μL , 20 mM) and heated to 100 $^\circ\text{C}$ in a microwave vessel for 12 h. The reaction was cooled, filtered through a 1 μm filter, and purified by gel permeation chromatography (chloroform) to yield **V.10**, a

white solid (1.0 mg, 11%). ¹H NMR (600 MHz, CDCl₃) δ 8.82 (s, 6H), 8.64 – 8.56 (m, 6H), 7.96 – 7.75 (m, 24H), 7.66 (s, 12H), 7.64 – 7.57 (m, 6H).

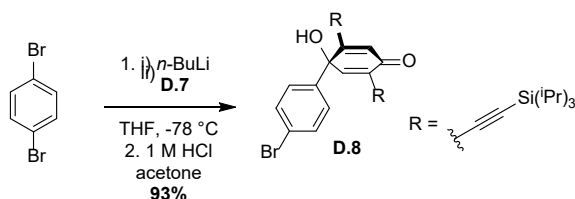


D.6. 1,4-diiodo-2,5-dimethoxybenzene (27.4 g, 70.3 mmol, 1 eq), copper(I) iodide (669 mg, 3.51 mmol, 0.05 eq), and Pd(PPh₃)₂Cl₂ (148 mg, 211 μmol, 0.003 eq) were dissolved in tetrahydrofuran (70 mL, 1M) and diisopropylamine (70 mL). The mixture was purged with nitrogen for 15 min and triisopropylsilylacetylene (33 mL, 27 g, 150 mmol, 2.1 eq) was added. The solution became dark red and it was heated to 60 °C for 24 h with vigorous stirring. The reaction was quenched with an aqueous saturated solution of NH₄Cl and extracted with ether (3 x 100 mL). The combined extracts were dried over anhydrous Na₂SO₄ and solvent was removed to yield a yellow solid. Recrystallization in iPrOH yielded **D.6** as white crystals (31.9 g, 91%). IR (neat) 2943, 2864, 2147, 1495, 1460, 1389 cm⁻¹; ¹H NMR (300 MHz, Chloroform-*d*) δ 6.88 (s, 2H), 3.81 (s, 6H), 1.14 (s, 42H). ¹³C NMR (151 MHz, CDCl₃) δ 154.73, 116.42, 114.02, 102.88, 96.89, 56.68, 18.67, 11.37. HRMS (ASAP) (m/z): [M]⁺ calculated for C₃₀H₅₀O₂Si₂, 498.3349; found, 498.3351.



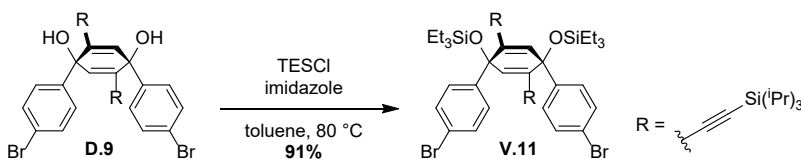
D.7. **D.6** (10 g, 20.0 mmol, 1 eq) was dissolved in dichloromethane (160 mL, 125 mM) and cooled to -78 °C. Boron tribromide (2.1 mL, 5.5 g, 22 mmol, 1.1 eq) was carefully added dropwise and the cooling bath was removed to slowly warm the reaction to room

temperature over 1.5 h. Then, water (40 mL) was added to quench and the mixture was stirred for 30 min. This mixture was extracted with dichloromethane (3 x 40 mL), dried over anhydrous Na₂SO₄, and the solvent was removed to yield an orange solid. The solid was purified by column chromatography on silica (0 to 25% dichloromethane in hexanes) to yield a white solid (8 g). This solid was dissolved in dichloromethane (40 mL) and MeOH (40 mL) and cooled to 0 °C. Phenyliodonium diacetate (5.85 g, 18.1 mmol, 1.1 eq) was added and the reaction was warmed to room temperature overnight. The next day, the reaction was quenched with an aqueous saturated solution of NaHCO₃ and the mixture was extracted with dichloromethane (3 x 30 mL). The combined extracts were washed with 1 M NaOH (a white precipitate formed and was ignored), dried over anhydrous Na₂SO₄, and solvent was removed to yield an orange oil. This oil was purified by vacuum distillation (70 °C, ~1 mTorr) to remove iodobenzene and column chromatography on alumina (0 to 20% dichloromethane in hexanes) to yield **D.7** as an orange oil (5.0 g, 48%). IR (neat) 2943, 2865, 2149, 1663, 1463 cm⁻¹; ¹H NMR (500 MHz, Chloroform-*d*) δ 6.87 (s, 1H), 6.52 (s, 1H), 3.38 (s, 6H), 1.12 (s, 42H). ¹³C NMR (151 MHz, CDCl₃) δ 181.11, 146.34, 139.41, 134.59, 126.82, 107.15, 101.61, 98.81, 98.70, 94.32, 77.22, 77.01, 76.80, 51.43, 18.60, 18.54, 11.21, 11.16. HRMS (ASAP) (m/z): [M+H]⁺ calculated for C₃₀H₅₁O₃Si₂, 515.3377; found, 515.3346.



D.8 1,4-dibromobenzene (2.54 g, 10.8 mmol, 1.2 eq) was dissolved in tetrahydrofuran (54 mL, 200 mM) and cooled to -78 °C. A 2.5 M solution of *n*-BuLi in hexanes (4.0 mL,

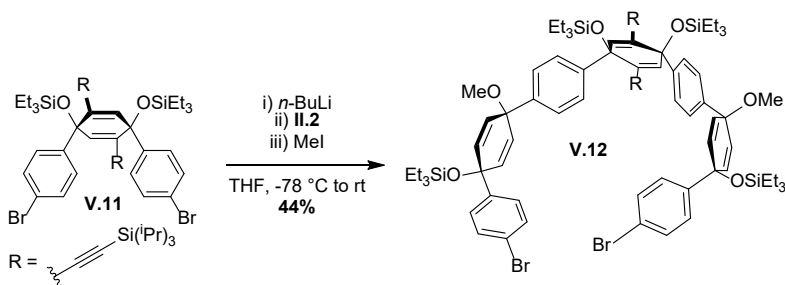
bromophenyl lithiate in tetrahydrofuran was cannulated at -78 °C into the flask containing bromoketone. This mixture was stirred for 1 h, quenched with water (10 mL), warmed to room temperature, and extracted with EtOAc (3 x 10 mL). The combined extracts were washed with brine (10 mL), dried over Na₂SO₄, and solvent was removed under reduced pressure. The residue was purified by column chromatography on silica (30 to 100% CH₂Cl₂/hexanes) to yield **D.9** as a white solid (570 mg, 95%). IR (neat) 3490, 2942, 2864, 2147, 1462, 1406 cm⁻¹; ¹H NMR (600 MHz, Chloroform-*d*) δ 7.46 (d, *J* = 8.5 Hz, 4H), 7.29 (d, *J* = 8.5 Hz, 4H), 6.37 (s, 2H), 2.63 (s, 2H), 0.91 – 0.90 (m, 42H). ¹³C NMR (151 MHz, CDCl₃) δ 141.77, 137.71, 131.55, 127.86, 124.17, 122.10, 102.54, 96.47, 71.39, 18.41,* 18.40,* 11.00. *diastereotopic HRMS (ASAP) (*m/z*): [M]⁺ calculated for C₄₀H₅₄Br₂O₂Si₂, 780.2029; found, 780.1968.



V.11. **D.9** (3.00 g, 3.83 mmol, 1 eq) and imidazole (1.04 g, 15.3 mmol, 4 eq) were dissolved in toluene (19 mL, 200 mM). Triethylsilyl chloride (1.93 mL, 1.73 g, 11.5 mmol, 3 eq) was added and the reaction was heated to 80 °C overnight. The next day, the reaction was quenched with water (20 mL) and extracted with CH₂Cl₂ (3 x 20 mL). The combined extracts were dried over anhydrous Na₂SO₄ and solvent was removed under reduced pressure. The crude residue was purified by column chromatography on silica (hexanes) to yield **V.11** as a white solid (3.12 g, 91%). IR (neat) 2943, 2866, 2162, 1484, 1462 cm⁻¹; ¹H NMR (500 MHz, Chloroform-*d*) δ 7.40 (d, *J* = 8.7 Hz, 4H), 7.32 (d, *J* = 8.7 Hz, 3H), 6.14 (s, 2H), 1.05 (s, 42H), 0.94 (t, *J* = 7.9 Hz, 19H), 0.64 (q, *J* = 8.2 Hz, 12H). ¹³C NMR (126 MHz, CDCl₃) δ 143.02, 136.49, 130.86, 128.38, 128.05, 121.74,

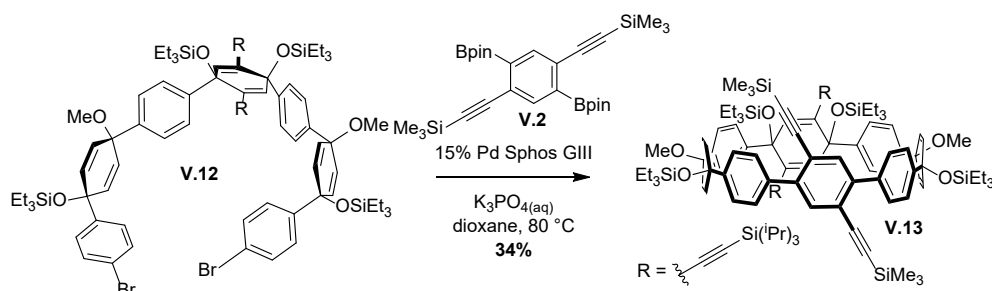
104.01, 94.31, 72.36, 18.55,* 18.54,* 11.30, 7.06, 6.46. *diastereotopic HRMS (ASAP)

(m/z): $[M]^+$ calculated for $C_{52}H_{82}Br_2O_2Si_4$, 1008.3759; found, 1008.3734.

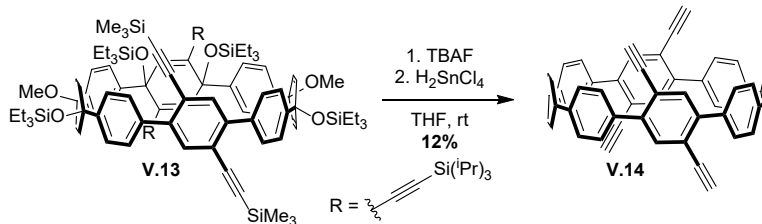


V.12 **V.11** (1.00 g, 1.54 mmol, 1 eq) was dissolved in tetrahydrofuran (60 mL, 50 mM) and cooled to $-78\text{ }^{\circ}\text{C}$. A 2 M solution of *n*-BuLi in hexanes (1.2 mL, 3.1 mmol, 2 eq) was added quickly followed by **II.2** (930 μL , 1.2 g, 3.1 mmol, 2 eq). The reaction was stirred for 1 h at $-78\text{ }^{\circ}\text{C}$, quenched with MeI (380 μL , 870 mg, 6.1 mmol, 4 eq), warmed to room temperature, and stirred overnight. Water (50 mL) was added and the mixture was extracted with EtOAc (3 x 50 mL). The combined extracts were dried over sodium sulfate and the solvent was removed under reduced pressure. The crude material was purified by column chromatography on silica (0 to 40% dichloromethane in hexanes) to yield **V.12** as a white solid (860 mg, 44%). IR (neat) 2952, 2875, 2149, 1462, 1406 cm^{-1} ; ^1H NMR (600 MHz, Chloroform-*d*) δ 7.45 (d, $J = 8.5$ Hz, 4H), 7.34 (d, $J = 8.6$ Hz, 4H), 7.29 (d, $J = 8.4$ Hz, 4H), 7.18 (d, $J = 8.6$ Hz, 4H), 6.17 (s, 2H), 6.12 (dd, $J = 10.1, 2.3$ Hz, 2H), 6.05 (dd, $J = 10.1, 2.2$ Hz, 2H), 6.02 (dd, $J = 10.0, 2.2$ Hz, 2H), 5.99 (dd, $J = 10.1, 2.3$ Hz, 2H), 3.33 (s, 6H), 1.04 – 0.99 (m, 42H), 0.97 (t, $J = 7.9$ Hz, 18H), 0.95 (t, $J = 7.9$ Hz, 18H), 0.67 (q, $J = 7.9$ Hz, 12H), 0.66 (q, $J = 7.7$ Hz, 12H). ^{13}C NMR (151 MHz, CDCl_3) δ 144.99, 143.70, 142.20, 137.08, 135.45, 134.42, 131.12, 129.88, 128.80, 127.62, 127.53, 126.80, 125.69, 121.06, 104.60, 93.43, 74.21, 72.60, 71.68, 51.98, 18.58,

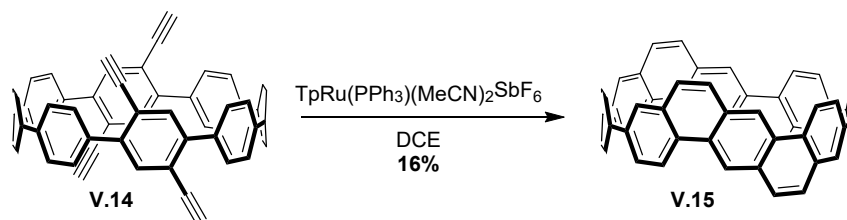
11.28, 7.12, 7.07, 6.51, 6.48. HRMS (ASAP) (m/z): $[M]^+$ calculated for $C_{90}H_{134}Br_2O_6Si_6$, 1636.7163; found, 1636.7216.



V.13. **V.12** (850 mg, 518 μ mol, 1 eq), **V.2** (271 mg, 518 μ mol, 1 eq), and SPhos Pd G3 (40 mg, 52 μ mol, 0.1 eq) were dissolved in dioxane (260 mL, 2 mM) and purged with nitrogen while heating to 80 $^{\circ}$ C. An aqueous solution of K_3PO_4 (26 mL) was added and the mixture was stirred for 18 h. The mixture was then filtered through Celite and dried over anhydrous sodium sulfate. Solvent was removed under reduced pressure to yield a brown solid. The solid was purified by column chromatography on silica (0 to 20% EtOAc in hexanes) and then gel permeation chromatography (chloroform) to yield **V.13** as an orange solid (305 mg, 34%). IR (neat) 2953, 2874, 2155, 1462, 1409 cm^{-1} ; 1H NMR (500 MHz, Chloroform-*d*) δ 7.49 – 7.45 (m, 6H), 7.36 (d, J = 8.2 Hz, 4H), 7.33 (d, J = 8.3 Hz, 4H), 7.10 (d, J = 8.3 Hz, 4H), 6.34 (s, 2H), 6.32 (dd, J = 10.4, 2.5 Hz, 3H), 6.09 (dd, J = 10.1, 2.4 Hz, 2H), 5.84 (dd, J = 10.2, 2.4 Hz, 2H), 5.74 (dd, J = 10.1, 2.4 Hz, 2H), 3.33 (s, 6H), 1.00 (d, J = 7.9 Hz, 18H), 0.96 (s, 42H), 0.87 (t, J = 7.9 Hz, 18H), 0.70 (q, J = 7.9 Hz, 12H), 0.56 (q, J = 8.0 Hz, 12H), 0.14 (s, 18H). ^{13}C NMR (126 MHz, $CDCl_3$) δ 144.71, 143.69, 142.73, 142.08, 138.99, 138.63, 136.28, 134.39, 134.36, 131.68, 129.90, 129.53, 128.26, 127.17, 125.40, 125.03, 121.57, 105.21, 104.40, 99.19, 94.88, 74.64, 72.05, 71.79, 51.62, 18.61, 18.58, 11.20, 7.20, 7.07, 6.80, 6.56, -0.31. HRMS (ASAP) (m/z): $[M]^+$ calculated for $C_{106}H_{154}O_6Si_8$, 1746.9900; found, 1746.9906.

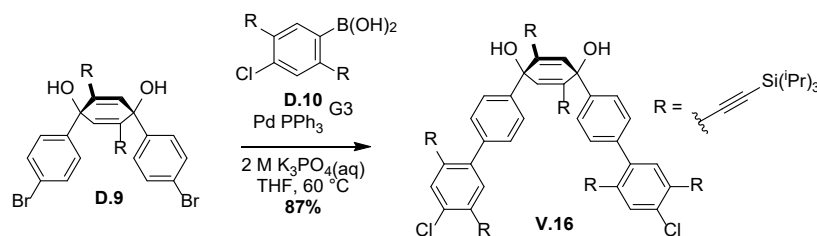


V.14. **V.13** (19 mg, 23 μmol , 1 eq) was dissolved in tetrahydrofuran (600 μL , 40 mM). A solution of $\text{SnCl}_2 \cdot 2\text{H}_2\text{O}$ (17 mg, 75 μmol , 3.3 eq) and 12 M aqueous HCl (12 μL , 140 μmol , 6.3 eq) in tetrahydrofuran (600 μL , 40 mM) was added and the reaction was stirred for 1 h. The reaction was then quenched with a 1M aqueous solution of NaOH (1 mL) and extracted with dichloromethane (3 x 5 mL). The combined extracts were dried over anhydrous sodium sulfate and solvent was removed under reduced pressure to yield a yellow solid. Purified by preparatory plate on silica (50% dichloromethane in hexanes) to yield **V.14**, a yellow solid (2.0 mg, 12%). IR (neat) 2952, 2874, 2154, 1749, 1461 cm^{-1} ; ^1H NMR (500 MHz, Chloroform-*d*) δ 7.60 (d, $J = 8.5$ Hz, 8H), 7.47 (s, 8H), 7.43 (d, $J = 8.5$ Hz, 8H), 7.43 (s, 4H).

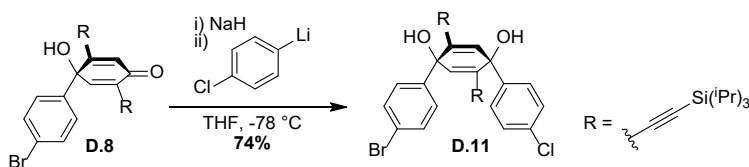


V.15. **V.14** (2.0 mg, 2.8 μmol , 1 eq), $\text{TpRu}(\text{PPh}_3)(\text{MeCN})_2\text{SbF}_6$ (1.0 mg, 1.1 μmol , 0.4 eq), and a dimethylsulfone NMR standard were dissolved in CD_2Cl_4 (600 μL , 5 mM) and heated to 100 $^\circ\text{C}$ for 12 h. The reaction was then cooled, the solvent was removed, and the residue was purified by gel permeation chromatography (chloroform) to yield **V.15** (300 μg , 16%). ^1H NMR (600 MHz, Chloroform-*d*) δ 8.51 (s, 4H), 8.32 (d, $J = 9.2$ Hz, 4H), 7.79 – 7.75

(m, 4H), 7.73 (d, $J = 9.1$ Hz, 4H), 7.71 (d, $J = 7.8$ Hz, 4H), 7.61 (d, $J = 9.1$ Hz, 4H), 7.56 (s, 8H).

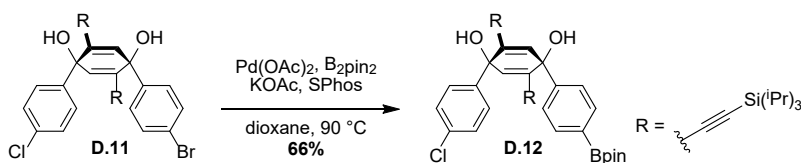


V.16. **D.9** (105 mg, 134 μ mol, 1 eq), **D.4** (153 mg, 295 μ mol, 2.2 eq), and Pd PPh₃ G3 (4.2 mg, 6.7 μ mol, 0.05 eq) were dissolved in tetrahydrofuran (2.7 mL, 50 mM) and heated to 60 °C. A 2 M aqueous solution of K₃PO₄ (540 μ L) was added to initiate the reaction and the reaction was stirred for 18 h. The mixture was then filtered through Celite and dried over anhydrous sodium sulfate. Solvent was removed under reduced pressure to yield a brown solid. The solid was purified by column chromatography on silica (0 to 20% EtOAc in hexanes) and then gel permeation chromatography (chloroform) to yield **V.13** as an orange solid (183 mg, 87%). ¹H NMR (600 MHz, Chloroform-*d*) δ 7.59 (s, 2H), 7.48 (q, $J = 8.5$ Hz, 8H), 7.34 (s, 2H), 6.38 (s, 2H), 2.64 (s, 2H), 1.13 (s, 42H), 0.98 (s, 42H), 0.90 (s, 42H).

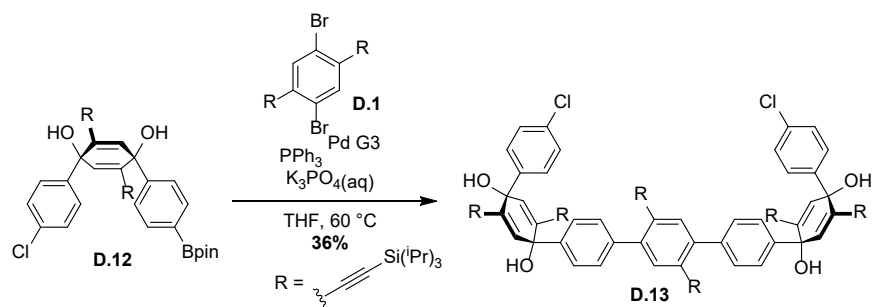


D.11. **D.8** (2.40 g, 8.8 mmol, 1 eq) was dissolved in tetrahydrofuran (38 mL, 100 mM) and cooled to -78 °C. NaH (199 mg, 5.0 mmol, 1.3 eq) was added and the mixture was stirred for 30 min. In a second flask, 1-bromo-4-chlorobenzene (1.69 g, 8.82 mmol, 2.3 eq) was dissolved in tetrahydrofuran (38 mL) and cooled to -78 °C. A 2.5 M solution of

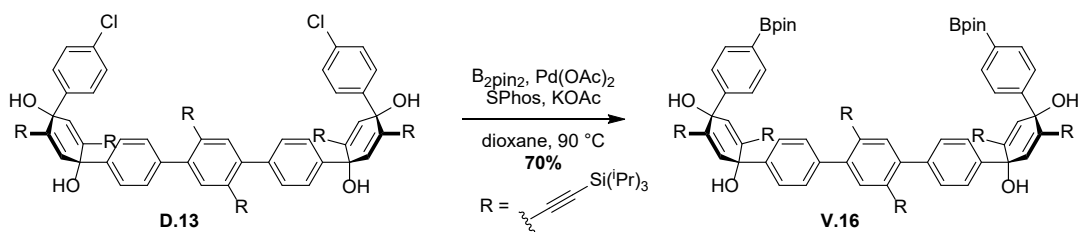
n-BuLi in hexanes (2.4 mL, 8.4 mmol, 2.2 eq) was added and the resulting solution of 4-chlorophenyl lithiate in tetrahydrofuran was cannulated at -78 °C into the flask containing bromoketone. This mixture was stirred for 1 h, quenched with water (30 mL), warmed to room temperature, and extracted with EtOAc (3 x 30 mL). The combined extracts were washed with brine (30 mL), dried over Na₂SO₄, and solvent was removed under reduced pressure. The residue was purified by column chromatography on silica (30 to 100% CH₂Cl₂/hexanes) to yield **D.11** as a white solid (2.10 mg, 74%). ¹H NMR (600 MHz, Chloroform-*d*) δ 7.46 (d, *J* = 8.5 Hz, 2H), 7.36 (d, *J* = 8.6 Hz, 2H), 7.32 – 7.28 (m, 4H), 6.38 (s, 1H), 6.37 (s, 1H), 2.65 (s, 2H), 0.90 (d, *J* = 4.4 Hz, 42H).



D.12. KOAc (87.8 mg, 894 μmol, 6.6 eq) was added to a rounded bottom flask under vacuum and flame dried. Upon cooling, **D.11** (100 mg, 135 μmol, 1 eq), Pd(dppf)₂Cl₂ (11.1 mg, 13.5 μmol, 0.1 eq) and bis(pinacolato)diboron (41.3 mg, 163 μmol, 1.2 eq) were added. The vessel was fitted with a rubber septum and evacuated/backfilled with nitrogen. Dioxane (1.4 mL, 100 mM) was added, the reaction was warmed from room temperature to 90 °C and stirred at this temperature overnight. In the morning, it was filtered through Celite, washing with EtOAc, and the solvent of the filtrate was removed under reduced pressure. The resulting residue was purified by column chromatography on silica (0 to 100% dichloromethane in hexanes) to yield **D.12** (70 mg, 66%). ¹H NMR (500 MHz, Chloroform-*d*) δ 7.78 (d, *J* = 7.8 Hz, 2H), 7.42 (d, *J* = 7.8 Hz, 2H), 7.36 (d, *J* = 8.1 Hz, 2H), 7.26 (d, *J* = 8.1 Hz, 2H), 6.40 (s, 1H), 6.39 (s, 1H), 2.68 (s, 1H), 2.62 (s, 1H), 1.35 (s, 12H), 0.89 (s, 42H).

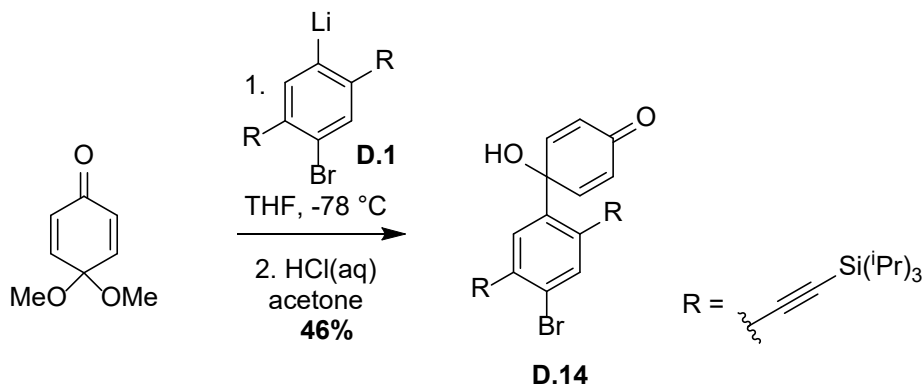


D.13. **D.1** (25 mg, 42 μmol , 1 eq), **D.12** (70 mg, 89 μmol , 2.1 eq) and PPh_3 Pd G3 (1.3 mg, 2.1 μmol , 0.05 eq) dissolved in tetrahydrofuran (1.8 mL, 50 mM) and warmed to 60 °C. A 2 M aqueous solution of K_3PO_4 (360 μL) was added and the reaction was left overnight. In the morning the reaction was filtered through celite, dried over Na_2SO_4 and the solvent was removed under reduced pressure to yield an oil. Purified by chromatography (0 to 100% CH_2Cl_2 /hexanes) to yield **D.13** as a white solid (27 mg, 36%). ^1H NMR (500 MHz, Chloroform-*d*) δ 7.58 (d, $J = 7.7$ Hz, 4H), 7.47 (d, $J = 7.0$ Hz, 6H), 7.43 (d, $J = 7.7$ Hz, 4H), 7.30 (d, $J = 7.5$ Hz, 4H), 6.42 (s, 2H), 6.38 (s, 2H), 2.70 (s, 2H), 2.69 (s, 2H), 1.29 – 1.24 (m, 42H), 0.92 (s, 84H).

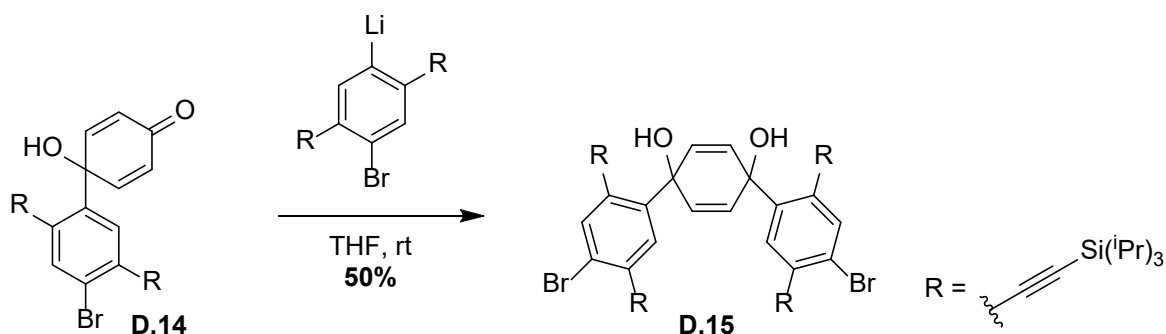


V.16. **D.13** (27 mg, 15 μmol , 1 eq), KOAc (10 mg, 100 μmol , 6.6 eq), B_2pin_2 (16 mg, 62 μmol , 4 eq), $\text{Pd}(\text{OAc})_2$ (1.0 mg, 4.6 μmol , 0.3 eq), and SPhos (4.7 mg, 12 μmol , 0.75 eq) were dissolved in dioxane (1.0 mL, 15 mM) and heated to 90 °C overnight. The next morning, it was filtered through celite and the solvent was removed under reduced pressure to yield an oil. Purified by chromatography on silica (0 to 40% EtOAc in hexanes) to yield **V.16** as a clear colorless oil (21 mg, 70%). ^1H NMR (600 MHz, Chloroform-*d*) δ 7.79

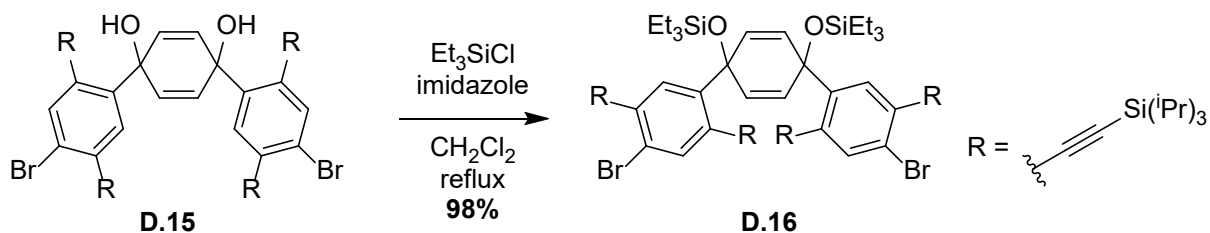
(d, $J = 7.9$ Hz, 4H), 7.62 (d, $J = 8.2$ Hz, 4H), 7.54 (s, 2H), 7.50 (d, $J = 5.1$ Hz, 8H), 6.46 (s, 2H), 6.43 (s, 2H), 2.69 (s, 4H), 1.34 (s, 24H), 1.26 (s, 42H), 0.95 – 0.86 (m, 84H).



D.14. D.1 (8.5 g, 14.2 mmol, 1 eq) was dissolved in tetrahydrofuran (70 mL, 200 mM) and cooled to -78 C at 2:20. A 2.5 M solution of *n*-BuLi in hexanes (5.7 mL, 14.2 mmol, 1 eq) was added dropwise followed by benzoquinone monomethyl ketal (1.91 mL, 2.20 g, 14.2 mmol, 1 eq) added dropwise. The reaction was stirred at -78 °C for 1 h, warmed up to room temperature, quenched with water (35 mL) and extracted with EtOAc (3 x 35 mL). The combined extracts were washed with brine (35 mL), dried over anhydrous Na_2SO_4 , and the solvent was removed under reduced pressure. The crude material was dissolved in acetone (50 mL) and a 10% aqueous solution of acetic acid (50 mL) was added. The reaction was stirred for 18 h at room temperature and quenched with a saturated solution of Na_2CO_3 (50 mL). This mixture was then filtered to recover the crude product. Purification by column chromatography on silica (0 to 40% EtOAc in hexanes) yielded **D.14** as a solid (4.07 g, 46%). ^1H NMR (500 MHz, Chloroform-*d*) δ 7.74 (s, 1H), 7.46 (s, 1H), 7.12 (d, $J = 9.8$ Hz, 2H), 6.31 (d, $J = 9.7$ Hz, 2H), 4.38 (s, 1H), 1.14 (s, 45H).

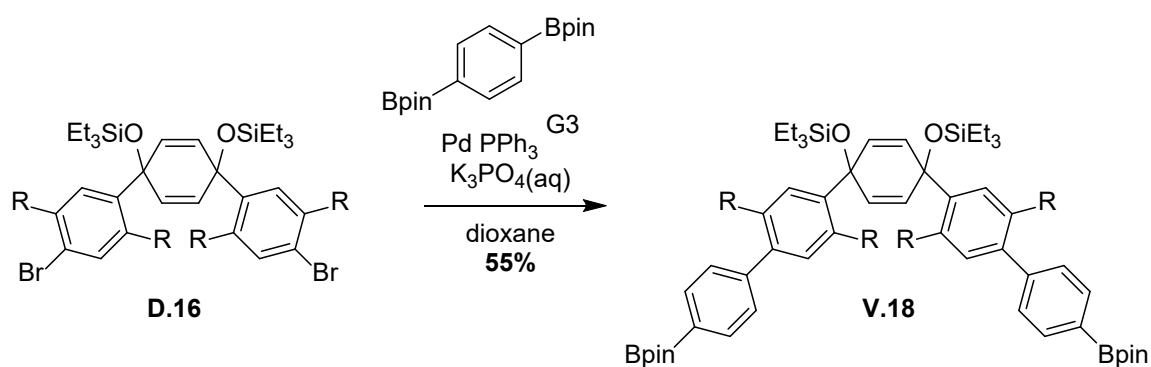


D.15. **D.14** (2.00 g, 3.20 mmol, 1 eq) was dissolved in tetrahydrofuran (80 mL, 40 mM). In a second flask, **D.1** (4.58 g, 4.58 mmol, 2.4 eq) was dissolved in tetrahydrofuran (80 mL) and cooled to -78°C . A 2.5 M solution of *n*-BuLi in hexanes (3.1 mL, 7.7 mmol, 2.4 eq) was added and the resulting lithiate solution in tetrahydrofuran was cannulated at -78°C into the flask containing **D.14** at room temperature. This mixture was stirred for 1 h at room temperature, quenched with water (80 mL), and extracted with EtOAc (3 x 80 mL). The combined extracts were washed with brine (80 mL), dried over Na_2SO_4 , and solvent was removed under reduced pressure to yield a mixture of *cis* and *trans* isomers. The residue was purified by column chromatography on silica (20 to 60% CH_2Cl_2 /hexanes) to separate the isomers and yield the desired *cis* isomer **D.15** (1.83 g, 50%). ^1H NMR (500 MHz, Chloroform-*d*) δ 7.72 (s, 2H), 6.93 (s, 2H), 6.49 (s, 4H), 4.47 (s, 2H), 1.21 – 1.18 (m, 42H), 1.09 – 1.06 (m, 42H).

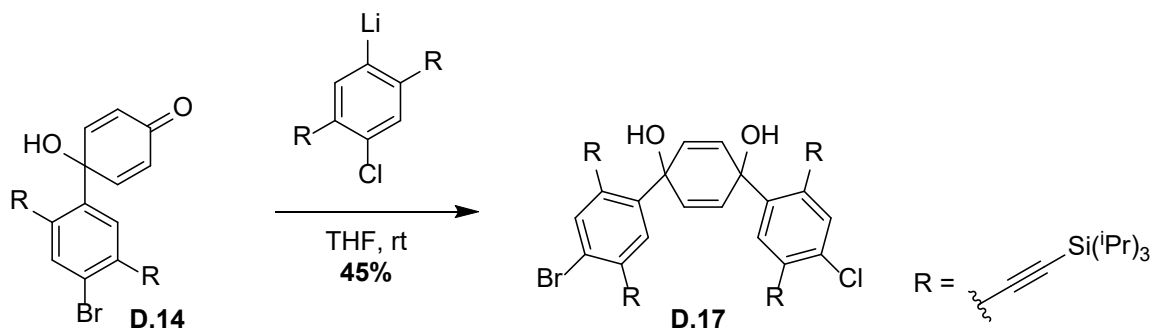


D.16. **D.15** (450 mg, 394 μmol , 1 eq) and imidazole (107 mg, 1.57 mmol, 4 eq) were dissolved in CH_2Cl_2 (10 mL, 40 mM). Triethylsilyl chloride (200 μL , 180 mg, 1.2 mmol,

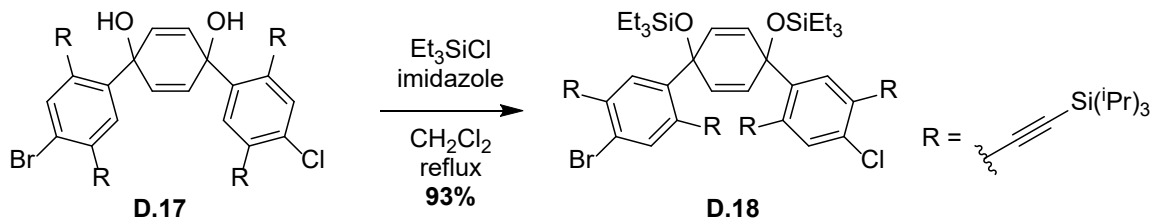
3 eq) was added and the reaction was refluxed for 18 h. The reaction was quenched with water (20 mL) and extracted with CH₂Cl₂ (3 x 20 mL). The combined extracts were dried over anhydrous Na₂SO₄ and solvent was removed under reduced pressure. The crude residue was purified by column chromatography on silica (10% EtOAc in hexanes) to yield **D.16** as a white solid (530 mg, 98%). ¹H NMR (600 MHz, Chloroform-*d*) δ 7.63 (s, 2H), 6.93 (s, 2H), 6.54 (s, 4H), 1.16 (s, 42H), 1.06 (s, 42H), 0.88 (t, *J* = 7.9 Hz, 18H), 0.57 (q, *J* = 7.9 Hz, 12H).



V.18. **D.16** (635 mg, 463 μmol, 1 eq), 1,4-benzene diboronic acid pinacol ester (764 mg, 2.31 mmol, 5 eq) and PPh₃ Pd G3 (115 mg, 23 μmol, 0.05 eq) dissolved in tetrahydrofuran (9 mL, 50 mM) and warmed to 60 °C. A 2 M aqueous solution of K₃PO₄ (1.2 mL) was added and the reaction was stirred at 60 °C for 18 h. The reaction was filtered through celite, dried over Na₂SO₄, and the solvent was removed under reduced pressure to yield an oil. Purified by chromatography (0 to 60% CH₂Cl₂/hexanes) to yield **V.18** as a white solid (410 mg, 55%). ¹H NMR (600 MHz, Chloroform-*d*) δ 7.79 (d, *J* = 7.7 Hz, 4H), 7.54 (d, *J* = 7.8 Hz, 4H), 7.48 (s, 2H), 7.23 (s, 2H), 6.65 (s, 4H), 1.35 (s, 24H), 1.15 (s, 42H), 0.93 (t, *J* = 8.0 Hz, 18H), 0.90 – 0.84 (m, 42H), 0.52 (q, *J* = 7.9 Hz, 12H).

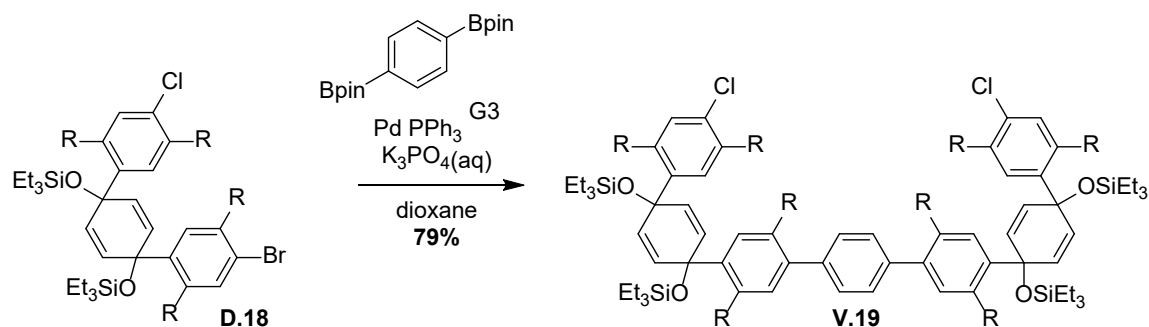


D.17. **D.14** (1.20 g, 1.92 mmol, 1 eq) was dissolved in tetrahydrofuran (20 mL, 100 mM). In a second flask, **D.4** (2.54 g, 4.60 mmol, 2.4 eq) was dissolved in tetrahydrofuran (27 mL) and cooled to $-78\text{ }^{\circ}\text{C}$. A 2.5 M solution of *n*-BuLi in hexanes (1.8 mL, 4.6 mmol, 2.4 eq) was added and the resulting lithiate solution in tetrahydrofuran was cannulated at $-78\text{ }^{\circ}\text{C}$ into the flask containing **D.14** at room temperature. This mixture was stirred for 1 h at room temperature, quenched with water (20 mL), and extracted with EtOAc (3 x 20 mL). The combined extracts were washed with brine (20 mL), dried over Na_2SO_4 , and solvent was removed under reduced pressure to yield a mixture of *cis* and *trans* isomers. The residue was purified by column chromatography on silica (20 to 60% CH_2Cl_2 /hexanes) to separate the isomers and yield the desired *cis* isomer **D.17** (940 mg, 45%). ^1H NMR (500 MHz, Chloroform-*d*) δ 7.69 (s, 1H), 7.51 (s, 1H), 6.91 (s, 1H), 6.89 (s, 1H), 6.47 (d, $J = 2.0$ Hz, 4H), 4.46 (s, 1H), 4.43 (s, 1H), 1.17 (s, 42H), 1.05 (s, 42H).

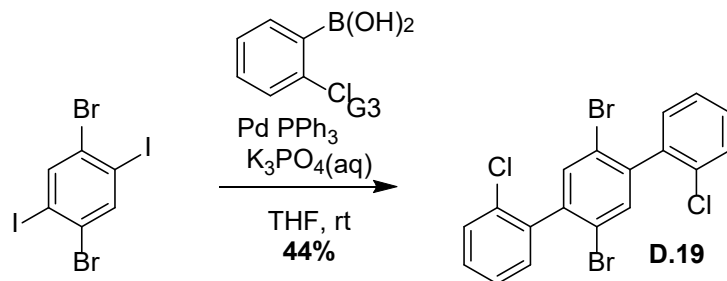


D.18. **D.17** (500 mg, 455 μmol , 1 eq) and imidazole (124 mg, 1.82 mmol, 4 eq) were dissolved in CH_2Cl_2 (11 mL, 40 mM). Triethylsilyl chloride (190 μL , 170 mg, 1.1 mmol, 2.5 eq) was added and the reaction was refluxed for 18 h. The reaction was quenched with

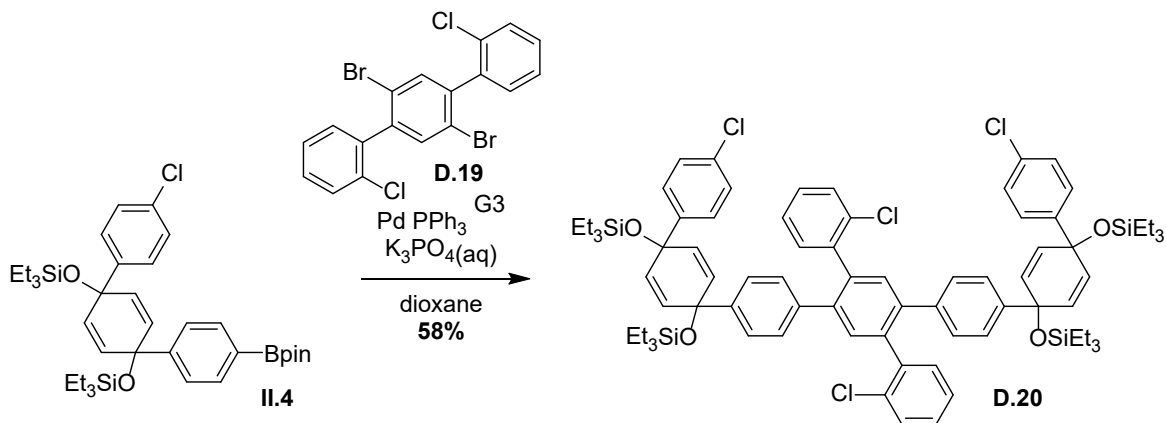
water (10 mL) and extracted with CH₂Cl₂ (3 x 10 mL). The combined extracts were dried over anhydrous Na₂SO₄ and solvent was removed under reduced pressure. The crude residue was purified by column chromatography on silica (0 to 20% EtOAc in hexanes) to yield **D.18** as a white solid (560 mg, 93%). ¹H NMR (500 MHz, Chloroform-*d*) δ 7.63 (s, 1H), 7.45 (s, 1H), 6.93 (s, 1H), 6.91 (s, 1H), 6.55 (d, *J* = 2.0 Hz, 4H), 1.16 (s, 42H), 1.06 (s, 42H), 0.86 (t, *J* = 7.9 Hz, 18H), 0.57 (q, *J* = 7.7 Hz, 12H).



V.19. **D.18** (470 mg, 354 μmol, 2 eq), 1,4-benzene diboronic acid pinacol ester (58 mg, 180 μmol, 1 eq) and PPh₃ Pd G3 (5.6 mg, 8.9 μmol, 0.05 eq) dissolved in tetrahydrofuran (7.1 mL, 50 mM) and warmed to 60 °C. A 2 M aqueous solution of K₃PO₄ (1.8 mL) was added and the reaction was stirred at 60 °C for 18 h. The reaction was filtered through celite, dried over Na₂SO₄, and the solvent was removed under reduced pressure to yield an oil. Purified by chromatography (0 to 20% CH₂Cl₂/hexanes) to yield **V.19** as a white solid (360 mg, 79%). ¹H NMR (600 MHz, Chloroform-*d*) δ 7.50 (s, 4H), 7.47 (s, 2H), 7.46 (s, 2H), 7.11 (s, 2H), 7.10 (s, 2H), 6.61 (s, 8H), 1.16 (d, *J* = 4.2 Hz, 84H), 1.01 (d, *J* = 5.0 Hz, 42H), 0.94 (d, *J* = 2.7 Hz, 42H), 0.87 (t, *J* = 7.4 Hz, 36H), 0.62 (q, *J* = 8.2 Hz, 12H), 0.58 (q, *J* = 8.1 Hz, 12H).

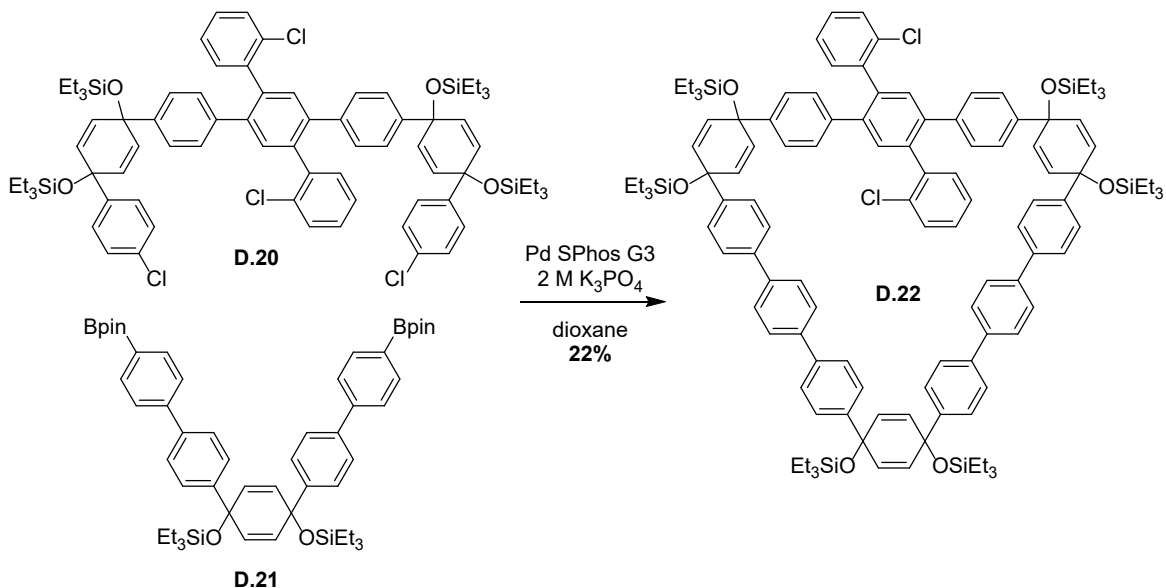


D.19. 1,4-dibromo-2,5-diiodobenzene (1.00 g, 2.05 mmol, 1 eq), 2-chlorobenzene boronic acid (1.28 g, 8.20 mmol, 1 eq) and PPh₃ Pd G3 (65 mg, 100 μmol, 0.05 eq) dissolved in tetrahydrofuran (21 mL, 100 mM) and warmed to 60 °C. A saturated aqueous solution of K₂CO₃ (2.1 mL) was added and the reaction was stirred at 60 °C for 18 h. The reaction was filtered through celite, dried over Na₂SO₄, and the solvent was removed under reduced pressure to yield an oil. Purified by chromatography (0 to 5% EtOAc in hexanes) to yield **D.19** as a white solid (410 mg, 44%). ¹H NMR (300 MHz, Chloroform-*d*) δ 7.58 (s, 2H), 7.53 – 7.48 (m, 2H), 7.42 – 7.32 (m, 4H).

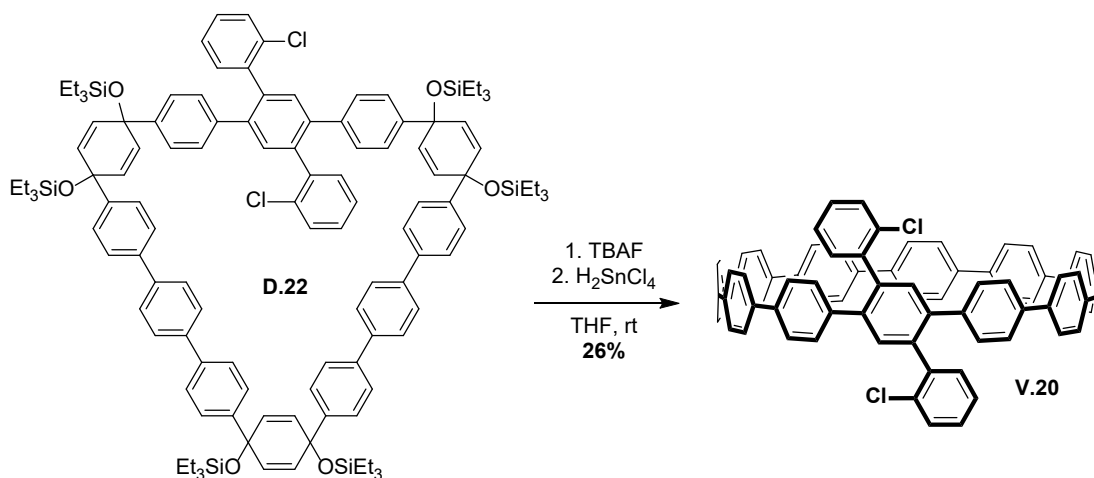


D.20. **D.19** (70 mg, 153 μmol, 1 eq), **II.4** (200 mg, 306 μmol, 2 eq) and PPh₃ Pd G3 (4.8 mg, 7.7 μmol, 0.05 eq) dissolved in tetrahydrofuran (6.1 mL, 50 mM) and warmed to 60 °C. A 2M aqueous solution of K₃PO₄ (1.5 mL) was added and the reaction was stirred at 60 °C for 2 days. The reaction was filtered through celite, dried over Na₂SO₄, and the solvent was removed under reduced pressure to yield an oil. Purified by chromatography

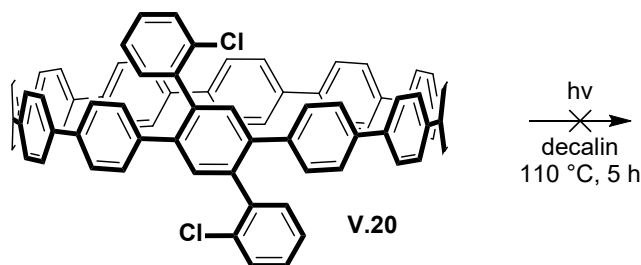
(0 to 20% EtOAc in hexanes) to yield **D.20** as a white solid (120 mg, 58%). ¹H NMR (500 MHz, Chloroform-*d*) δ 7.45 (d, $J = 7.0$ Hz, 2H), 7.39 – 7.30 (m, 4H), 7.23 (d, $J = 8.0$ Hz, 2H), 7.18 (d, $J = 8.3$ Hz, 4H), 7.14 (d, $J = 8.3$ Hz, 4H), 7.14 (s, 8H) 6.01 (d, $J = 10.1$ Hz, 4H), 5.87 – 5.81 (m, 4H), 0.95 (t, $J = 7.9$ Hz, 18H), 0.87 (t, $J = 7.9$ Hz, 18H), 0.64 (q, $J = 7.9$ Hz, 12H), 0.48 (q, $J = 7.9$ Hz, 12H).



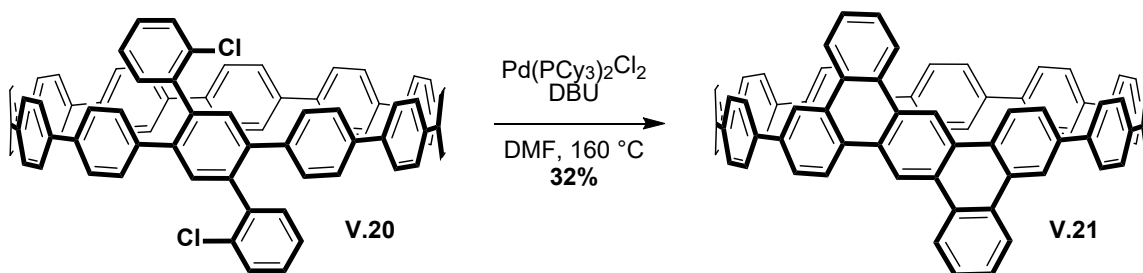
D.22. **D.20** (120 mg, 89 μmol , 1 eq), **D.21** (80 mg, 89 μmol , 1 eq) and PPh₃ Pd G3 (6.9 mg, 8.9 μmol , 0.1 eq) dissolved in dioxane (44 mL, 2 mM) and warmed to 80 °C. A 2M aqueous solution of K₃PO₄ (4.4 mL) was added and the reaction was stirred at 80 °C for 18 h. The reaction was filtered through celite, dried over Na₂SO₄, and the solvent was removed under reduced pressure to yield an oil. Purified by chromatography (0 to 20% EtOAc in hexanes) to yield a yellow solid that was further purified by gel permeation chromatography (chloroform) to yield **D.22** as a white solid (38 mg, 22%). ¹H NMR (600 MHz, Chloroform-*d*) δ 7.74 – 7.10 (m, 42H), 6.09 – 6.00 (m, 8H), 5.96 – 5.87 (m, 4H), 1.04 – 0.92 (m, 54H), 0.74 – 0.59 (m, 36H).



V.20. **D.22** (38 mg, 20 μmol , 1 eq) was dissolved in tetrahydrofuran (500 μL , 40 mM) and a 1 M solution of tetrabutylammonium fluoride in tetrahydrofuran (140 μL , 140 μmol , 7 eq) was added. The reaction was stirred for 1 h and quenched with water. tetrahydrofuran was removed under reduced pressure to yield a suspension that was filtered washing with water and dichloromethane to yield an off white solid. This solid was dissolved in tetrahydrofuran (1.0 mL, 20 mM). A solution of $\text{SnCl}_2 \cdot 2\text{H}_2\text{O}$ (15 mg, 67 μmol , 3.3 eq) and a 12 M aqueous solution of HCl (67 μL , 130 μmol , 6.3 eq) in tetrahydrofuran (1.0 mL) was added and the reaction was stirred for 1 h. The reaction was then quenched with a 1 M aqueous solution of NaOH (1.0 mL) and extracted with dichloromethane (3 x 2.0 mL). The combined extracts were dried over anhydrous sodium sulfate and solvent was removed under reduced pressure to yield a yellow solid. Purified by column chromatography on silica (50% dichloromethane in hexanes) to yield a yellow solid **V.20** (6.0 mg, 26%). ^1H NMR (600 MHz, Chloroform-*d*) δ 7.64 – 7.57 (m, 44H), 7.45 (d, $J = 8.3$ Hz, 4H), 7.32 (d, $J = 8.2$ Hz, 4H), 7.14 (d, $J = 8.2$ Hz, 2H).

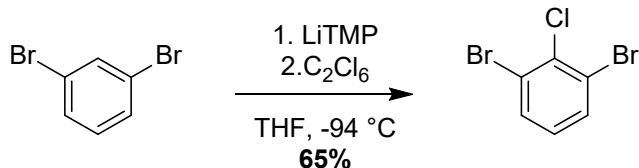


Unsuccessful synthesis of V.21. V.20 (1.5 mg, 1.3 μmol) dissolved in decalin (5 mL, 200 μM) in a pyrex round bottom and purged with N_2 . Irradiated with UV light without cooling in order to reach a temperature of 110 $^\circ\text{C}$. Irradiation continued for 5 h. Solvent removed under reduced pressure and analyzed by NMR.

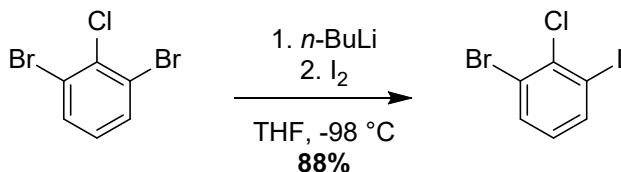


V.21. V.20 (1 mg, 900 nmol, 1 eq), $\text{Pd}(\text{PCy}_3)_2\text{Cl}_2$ (1 mg, 1.4 μmol , 1.6 eq) and one drop DBU were dissolved in DMF (440 μL , 2 mM) and purged with nitrogen in a microwave tube. The tube was then sealed and heated to 160 $^\circ\text{C}$ for 12 h. Quenched with a 10% aqueous solution of LiCl (1 mL) and extracted with dichloromethane (3 x 1 mL). The extracts were then combined and the solvent was removed under reduced pressure. The resulting residue was purified by gel permeation chromatography (chloroform) to yield V.21 as a white solid (300 μg , 32%). ^1H NMR (600 MHz, Chloroform-*d*) δ 9.34 (s, 2H), 8.68 – 8.63 (m, 4H), 8.57 (s, 2H), 8.54 (d, $J = 7.3$ Hz, 2H), 7.91 (d, $J = 8.9$ Hz, 2H), 7.78 (d, $J = 8.5$ Hz, 6H), 7.75 (d, $J = 7.0$ Hz, 2H), 7.64 (d, $J = 8.3$ Hz, 4H), 7.63 – 7.58 (m, 28H).

The following four reactions were performed and developed by Prof. Tobias Schaub.

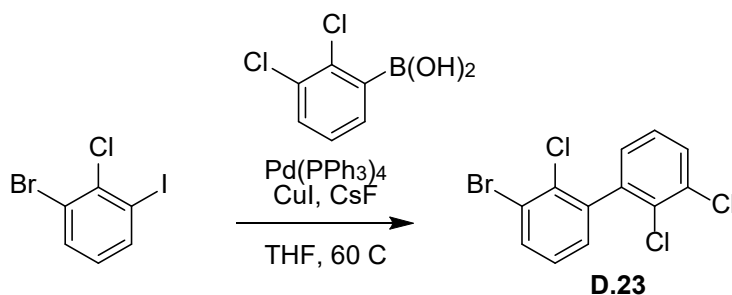


1,3-dibromo-2-chlorobenzene. A 2.5 M solution of *n*-BuLi in hexanes (51 mL, 130 mmol, 1 eq) was added to tetrahydrofuran (250 mL, 500 mM) at -78 °C. To this solution was added 2,2,6,6-tetramethylpiperidine (21 mL, 18 g, 130 mmol, 1 eq) followed by 1,3-dibromobenzene (15 mL, 30 g, 130 mmol, 1 eq). The reaction was stirred for 30 min at -78 °C. Hexachloroethane (31.6 g, 136 mmol, 1.05 eq) was added and the mixture was allowed to warm to room temperature. Water was added (100 mL) and the mixture was extracted with EtOAc (2 x 100 mL). The combined extracts were washed with a 10% aqueous solution of HCl (2 x 100 mL), water (100 mL), and brine (60 mL). The organic phase was then dried over Na₂SO₄ and the solvent was removed under reduced pressure. The resulting residue was recrystallized in MeOH to yield 1,3-dibromo-2-chlorobenzene as a white crystalline solid (22.4 g, 65%). ¹H NMR (500 MHz, Chloroform-*d*) δ 7.62 (d, *J* = 8.1 Hz, 2H), 7.01 (t, *J* = 8.0 Hz, 1H).



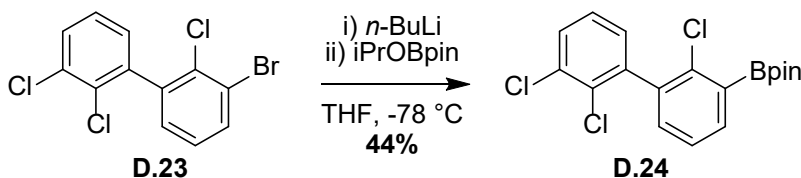
1-bromo-2-chloro-3-iodobenzene. 1,3-dibromo-2-chlorobenzene (19.3 g, 71.2 mmol, 1 eq) was dissolved in Et₂O (400 mL, 170 mM) and cooled to -98 °C. A 2.5 M solution of *n*-BuLi in hexanes (29 mL, 73 mmol, 1.03 eq) was added dropwise and the reaction was stirred for 20 min. Iodine (27.1 g, 214 mmol, 3 eq) was added and the reaction was allowed to warm to room temperature over 30 min. Water (200 mL) was added and the mixture was

extracted with EtOAc (3 x 200 mL). The combined extracts were washed with a saturated aqueous solution of Na₂S₂O₃ (200 mL) and brine (150 mL). The organic phase was dried over Na₂SO₄ and solvent was removed under reduced pressure to yield 1-bromo-2-chloro-3-iodobenzene as a tan crystalline solid (19.9 g, 88%). ¹H NMR (500 MHz, Chloroform-*d*) δ 7.83 (dd, *J* = 8.0, 1.5 Hz, 1H), 7.63 (dd, *J* = 8.0, 1.4 Hz, 1H), 6.82 (t, *J* = 8.0 Hz, 1H). ¹³C NMR (126 MHz, cdcl₃) δ 139.39, 133.82, 132.82, 128.98, 122.06, 98.94.

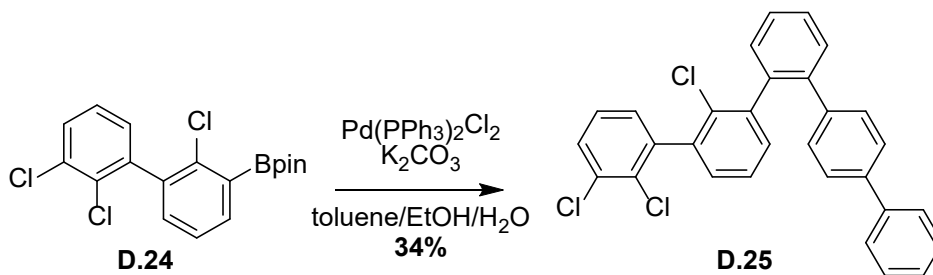


D.23. 1-bromo-2-chloro-3-iodobenzene (379 mg, 1.19 mmol, 1.1 eq), 2,3-dichlorobenzene boronic acid (296 mg, 1.08 mmol, 1 eq), copper (I) iodide (21 mg, 108 μmol, 0.1 eq), and anhydrous cesium fluoride (329 mg, 2.17 mmol, 2 eq) were dissolved in dioxane (6 mL, 200 mM) and purged with nitrogen for 5 min. Pd(PPh₃)₄ (63 mg, 54.2 μmol, 0.05 eq) was added and the reaction was sealed and heated to 60 °C for 24 h. Water (6 mL) was added and the mixture was extracted with EtOAc (3 x 5 mL). The combined extracts were washed with water (10 mL) and brine (5 mL) and dried over anhydrous Na₂SO₄. The solvent was removed under reduced pressure to yield an oil that was purified by column chromatography on silica (0 to 10% EtOAc in hexanes) yielding **D.23** as a white crystalline solid (220 mg, 60%). ¹H NMR (500 MHz, Chloroform-*d*) δ 7.69 (dd, *J* = 5.9, 3.6 Hz, 1H), 7.52 (dt, *J* = 8.0, 1.8 Hz, 1H), 7.27 (td, *J* = 7.9, 1.3 Hz, 1H), 7.22 – 7.17 (m,

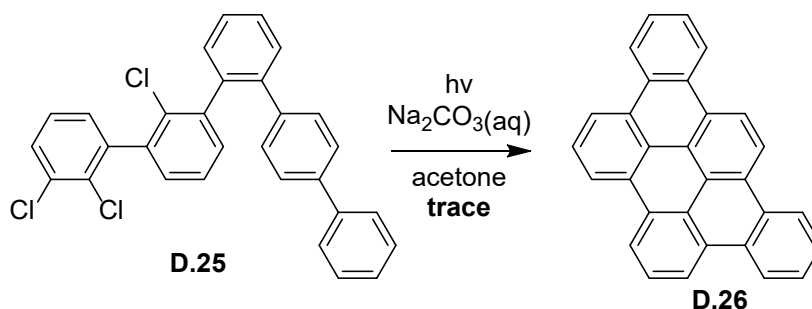
2H), 7.14 (dd, $J = 7.7, 1.6$ Hz, 1H). ^{13}C NMR (126 MHz, cdCl_3) δ 140.47, 140.12, 133.67, 133.41, 131.93, 130.31, 129.71, 129.03, 129.00, 127.51, 127.19, 123.51.



D.24. **D.23** (100 mg, 297 μmol , 1 eq) was dissolved in tetrahydrofuran (2 mL, 250 mM) and cooled to $-78\text{ }^\circ\text{C}$. A 2.5 M solution of *n*-BuLi in hexanes (120 μL , 297 μmol , 1 eq) was added dropwise and the reaction was stirred for 10 min. *i*PrOBpin (182 μL , 166 mg, 892 μmol , 3 eq) was added and the reaction was allowed to warm to room temperature over 30 min. Water (2 mL) was added and the mixture was extracted with EtOAc (3 x 2 mL). The combined extracts were washed with water (2 mL) and brine (2 mL). The organic phase was dried over Na_2SO_4 and solvent was removed under reduced pressure. This crude material was recrystallized in EtOH to yield **D.24** as a white crystalline solid (50 mg, 44%). ^1H NMR (500 MHz, Chloroform-*d*) δ 7.71 (d, $J = 7.2$ Hz, 1H), 7.49 (d, $J = 8.1$ Hz, 1H), 7.31 (t, $J = 7.5$ Hz, 1H), 7.27 (d, $J = 8.9$ Hz, 1H), 7.23 (d, $J = 7.8$ Hz, 1H), 7.13 (d, $J = 7.6$ Hz, 1H), 1.38 (s, 12H). ^{13}C NMR (126 MHz, CDCl_3) δ 141.15, 138.57, 138.09, 136.16, 133.31, 133.09, 132.26, 130.00, 129.52, 127.08, 126.01, 84.49, 24.97, 24.93.



D.25. D.24 (50 mg, 132 μmol , 1.1 eq), 2-bromoterphenyl (37 mg, 120 μmol , 1 eq), and potassium carbonate (74 mg, 538 μmol , 4.5 eq) were dissolved in a mixture of toluene (500 μL), EtOH (120 μL), and water (240 μL). This mixture was purged with nitrogen for 5 min. $\text{Pd}(\text{PPh}_3)_2\text{Cl}_2$ (4.2 mg, 6.0 μmol , 0.05 eq) was added and the reaction was sealed and heated to 90 $^\circ\text{C}$ for 18 h. The mixture was filtered through Celite and dried over anhydrous Na_2SO_4 . The solvent was removed under reduced pressure to yield a residue that was purified by column chromatography on silica (0 to 30% dichloromethane in hexanes) yielding **D.23** as a white solid (20 mg, 34%). ^1H NMR (600 MHz, Chloroform- d) δ 7.60 – 7.08 (m, 19H).



D.26. V.25 (7.0 mg, 1.4 μmol) dissolved in acetone (4.8 mL, 3 mM) and a 1 M aqueous solution of Na_2CO_3 (480 μL) was added in a pyrex round bottom and purged with N_2 . Irradiated with UV light with cooling in order to maintain a temperature near room temperature. Irradiation continued for 5 h. Solvent removed under reduced pressure and analyzed by NMR to identify literature known tribenzo[*b,n,pqr*]perylene **D.26**.¹⁴¹

D.2. X-ray Crystallography.

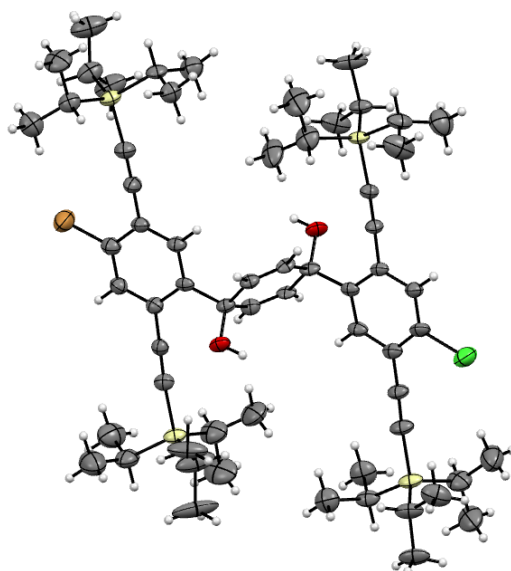


Figure D.1. ORTEP representation of *trans* isomer of **D.17** (thermal ellipsoids shown at 50% probability) verifying *cis* geometry of **D.17**.

REFERENCES CITED

- (1) Segawa, Y.; Omachi, H.; Itami, K. *Org. Lett.* **2010**, *12*, 2262–2265.
- (2) Adamska, L.; Nayyar, I.; Chen, H.; Swan, A. K.; Oldani, N.; Fernandez-Alberti, S.; Golder, M. R.; Jasti, R.; Doorn, S. K.; Tretiak, S. *Nano Lett.* **2014**, *14*, 6539–6546.
- (3) Darzi, E. R.; Jasti, R. *Chem. Soc. Rev.* **2015**, *44*, 6401–6410.
- (4) Iwamoto, T.; Watanabe, Y.; Sadahiro, T.; Haino, T.; Yamago, S. *Angew. Chem. Int. Ed.* **2011**, *50*, 8342–8344.
- (5) Xia, J.; Bacon, J. W.; Jasti, R. *Chem. Sci.* **2012**, *3*, 3018.
- (6) Li, P.; Zakharov, L. N.; Jasti, R. *Angew. Chem. Int. Ed.* **2017**, *56*, 5237–5241.
- (7) Mun, J.; Kang, J.; Zheng, Y.; Luo, S.; Wu, H. C.; Matsuhisa, N.; Xu, J.; Wang, G. J. N.; Yun, Y.; Xue, G.; et al. *Adv. Mater.* **2019**, *31*, 1903912.
- (8) Schaub, T. A.; Prantl, E. A.; Kohn, J.; Bursch, M.; Marshall, C. R.; Leonhardt, E. J.; Lovell, T. C.; Zakharov, L. N.; Brozek, C. K.; Waldvogel, S. R.; et al. *J. Am. Chem. Soc.* **2020**, *142*, 8763–8775.
- (9) Jasti, R.; Bhattacharjee, J.; Neaton, J. B.; Bertozzi, C. R. *J. Am. Chem. Soc.* **2008**, *130*, 17646–17647.
- (10) Takaba, H.; Omachi, H.; Yamamoto, Y.; Bouffard, J.; Itami, K. *Angew. Chem. Int. Ed.* **2009**, *48*, 6112–6116.
- (11) Yamago, S.; Watanabe, Y.; Iwamoto, T. *Angew. Chem. Int. Ed.* **2010**, *49*, 757–759.
- (12) Iwamoto, T.; Watanabe, Y.; Sakamoto, Y.; Suzuki, T.; Yamago, S. *J. Am. Chem. Soc.* **2011**, *133*, 8354–8361.

- (13) Darzi, E. R.; Sisto, T. J.; Jasti, R. *J. Org. Chem.* **2012**, *77*, 6624–6628.
- (14) Sisto, T. J.; Golder, M. R.; Hirst, E. S.; Jasti, R. *J. Am. Chem. Soc.* **2011**, *133*, 15800–15802.
- (15) Xia, J.; Jasti, R. *Angew. Chem. Int. Ed. Engl.* **2012**, *51*, 2474–2476.
- (16) Evans, P. J.; Darzi, E. R.; Jasti, R. *Nat. Chem.* **2014**, *6*, 404–408.
- (17) Sisto, T. J.; Tian, X.; Jasti, R. *J. Org. Chem.* **2012**, *77*, 5857–5860.
- (18) Sisto, T. J.; Zakharov, L. N.; White, B. M.; Jasti, R. *Chem. Sci.* **2016**, *7*, 3681–3688.
- (19) Xia, J.; Golder, M. R.; Foster, M. E.; Wong, B. M.; Jasti, R. *J. Am. Chem. Soc.* **2012**, *134*, 19709–19715.
- (20) Darzi, E. R.; Hirst, E. S.; Weber, C. D.; Zakharov, L. N.; Lonergan, M. C.; Jasti, R. *ACS Cent. Sci.* **2015**, *1*, 335–342.
- (21) Van Raden, J. M.; Darzi, E. R.; Zakharov, L. N.; Jasti, R.; Yamago, S.; Sasamori, T.; Tokitoh, N.; Itami, K.; Doorn, S. K.; Tretiak, S.; et al. *Org. Biomol. Chem.* **2016**, *14*, 5721–5727.
- (22) Hayase, N.; Miyauchi, Y.; Aida, Y.; Sugiyama, H.; Uekusa, H.; Shibata, Y.; Tanaka, K. *Org. Lett.* **2017**, *19*, 2993–2996.
- (23) Li, S.; Huang, C.; Thakellapalli, H.; Farajidizaji, B.; Popp, B. V.; Petersen, J. L.; Wang, K. K. *Org. Lett.* **2016**, *18*, 2268–2271.
- (24) Kayahara, E.; Patel, V. K.; Yamago, S. *J. Am. Chem. Soc.* **2014**, *136*, 2284–2287.
- (25) Patel, V. K.; Kayahara, E.; Yamago, S. *Chem. Eur. J.* **2015**, *21*, 5742–5749.
- (26) Golder, M. R.; Zakharov, L. N.; Jasti, R. *Pure Appl. Chem.* **2017**, *89*, 1603–1617.

- (27) Golder, M. R.; Colwell, C. E.; Wong, B. M.; Zakharov, L. N.; Zhen, J.; Jasti, R. *J. Am. Chem. Soc.* **2016**, *138*, 6577–6582.
- (28) White, B. M.; Zhao, Y.; Kawashima, T. E.; Branchaud, B. P.; Pluth, M. D.; Jasti, R. *ACS Cent. Sci.* **2018**, *4*, 1173–1178.
- (29) Van Raden, J. M.; Leonhardt, E. J.; Zakharov, L. N.; Pérez-Guardiola, A.; Pérez-Jiménez, A. J.; Marshall, C. R.; Brozek, C. K.; Sancho-García, J. C.; Jasti, R. *J. Org. Chem.* **2019**, acs.joc.9b02340.
- (30) Leonhardt, E. J.; Van Raden, J. M.; Miller, D.; Zakharov, L. N.; Alemán, B.; Jasti, R. *Nano Lett.* **2018**, *18*, 7991–7997.
- (31) Schaub, T. A.; Margraf, J. T.; Zakharov, L.; Reuter, K.; Jasti, R. *Angew. Chem. Int. Ed.* **2018**, *57*, 16348–16353.
- (32) Lee, S.; Chénard, E.; Gray, D. L.; Moore, J. S. *J. Am. Chem. Soc.* **2016**, *138*, 13814–13817.
- (33) Jackson, E. P.; Sisto, T. J.; Darzi, E. R.; Jasti, R. *Tetrahedron* **2016**, *72*, 3754–3758.
- (34) Van Raden, J. M.; White, B. M.; Zakharov, L. N.; Jasti, R. *Angew. Chem. Int. Ed.* **2019**, *58*, 7341–7345.
- (35) Leonhardt, E. J.; Jasti, R. *Nat. Rev. Chem.* **2019**, *3*, 672–686.
- (36) Lovell, T. C.; Colwell, C. E.; Zakharov, L. N.; Jasti, R. *Chem. Sci.* **2019**, *10*, 3786–3790.
- (37) Colwell, C. E.; Price, T. W.; Stauch, T.; Jasti, R. *Chem. Sci.* **2020**, *11*, 3923–3930.
- (38) Peters, G. M.; Grover, G.; Maust, R. L.; Colwell, C. E.; Bates, H.; Edgell, W. A.; Jasti, R.; Kertesz, M.; Tovar, J. D. *J. Am. Chem. Soc.* **2020**, *142*, 2293–2300.

- (39) Darzi, E. R.; Jasti, R. *Chem. Soc. Rev.* **2015**, *44*, 6401–6410.
- (40) Evans, P. J.; Darzi, E. R.; Jasti, R. *Nat. Chem.* **2014**, *6*, 404–408.
- (41) Kayahara, E.; Patel, V. K.; Yamago, S. *J. Am. Chem. Soc.* **2014**, *136*, 2284–2287.
- (42) Xia, J.; Jasti, R. *Angew. Chem. Int. Ed.* **2012**, *51*, 2474–2476.
- (43) Iwamoto, T.; Watanabe, Y.; Sakamoto, Y.; Suzuki, T.; Yamago, S. *J. Am. Chem. Soc.* **2011**, *133*, 8354–8361.
- (44) Segawa, Y.; Fukazawa, A.; Matsuura, S.; Omachi, H.; Yamaguchi, S.; Irle, S.; Itami, K. *Org. Biomol. Chem.* **2012**, *10*, 5979–5984.
- (45) Franklin-Mergarejo, R.; Alvarez, D. O.; Tretiak, S.; Fernandez-Alberti, S. *Sci. Rep.* **2016**, *6*, 31253.
- (46) White, B. M.; Zhao, Y.; Kawashima, T. E.; Branchaud, B. P.; Pluth, M. D.; Jasti, R. *ACS Cent. Sci.* **2018**, *4*, 1173–1178.
- (47) Della Sala, P.; Talotta, C.; Capobianco, A.; Soriente, A.; De Rosa, M.; Neri, P.; Gaeta, C. *Organic Letters*. UTC 2018, p 37.
- (48) Della Sala, P.; Talotta, C.; Caruso, T.; De Rosa, M.; Soriente, A.; Neri, P.; Gaeta, C. *J. Org. Chem.* **2017**, *82*, 9885–9889.
- (49) Iwamoto, T.; Watanabe, Y.; Sadahiro, T.; Haino, T.; Yamago, S. *Angew. Chem. Int. Ed.* **2011**, *50*, 8342–8344.
- (50) Ball, M.; Zhong, Y.; Fowler, B.; Zhang, B.; Li, P.; Etkin, G.; Paley, D. W.; Decatur, J.; Dalsania, A. K.; Li, H.; et al. *J. Am. Chem. Soc.* **2016**, *138*, 12861–12867.
- (51) Kayahara, E.; Sun, L.; Onishi, H.; Suzuki, K.; Fukushima, T.; Sawada, A.; Kaji, H.; Yamago, S. *J. Am. Chem. Soc.* **2017**, *139*, 18480–18483.

- (52) Darzi, E. R.; White, B. M.; Loventhal, L. K.; Zakharov, L. N.; Jasti, R. *J. Am. Chem. Soc.* **2017**, *139*, 3106–3114.
- (53) Jackson, E. P.; Sisto, T. J.; Darzi, E. R.; Jasti, R. *Tetrahedron* **2016**, *72*, 3754–3758.
- (54) Darzi, E. R.; Sisto, T. J.; Jasti, R. *J. Org. Chem.* **2012**, *77*, 6624–6628.
- (55) Kayahara, E.; Qu, R.; Yamago, S. *Angew. Chem. Int. Ed.* **2017**, *56*, 10428–10432.
- (56) Kayahara, E.; Hayashi, T.; Takeuchi, K.; Ozawa, F.; Ashida, K.; Ogoshi, S.; Yamago, S. *Angew. Chem. Int. Ed.* **2018**, *57*, 11418–11421.
- (57) Segawa, Y.; Omachi, H.; Itami, K. *Angew. Chem. Int. Ed.* **2010**, *12*, 2262–2265.
- (58) Li, P.; Sisto, T. J.; Darzi, E. R.; Jasti, R. *Org. Lett.* **2014**, *16*, 182–185.
- (59) Lai, R. Y.; Fleming, J. J.; Merner, B. L.; Vermeij, R. J.; Bodwell, G. J.; Bard, A. J. *J. Phys. Chem. A* **2004**, *108*, 376–383.
- (60) Haugland, R. P. *Handbook of Fluorescent Probes and Research Chemicals*; Molecular Probes: Eugene, 1992.
- (61) Cosa, G.; Focsaneanu, K.-S.; McLean, J. R. N.; McNamee, J. P.; Scaiano, J. C. *Photochem. Photobiol.* **2001**, *73*, 585.
- (62) Hard, T.; Fan, P.; Kearns, D. R. *Photochem. Photobiol.* **1990**, *51*, 77–86.
- (63) Johnson, I. *Histochem. J.* **1998**, *30*, 123–140.
- (64) Lavis, L. D.; Chao, T.-Y.; Raines, R. T. *ACS Chem. Biol.* **2006**, *1*, 252–260.
- (65) Kubin, R. F.; Fletcher, A. N. *J. Lumin.* **1982**, *27*, 455–462.
- (66) Agard, N. J.; Prescher, J. A.; Bertozzi, C. R. *J. Am. Chem. Soc.* **2004**, *126*, 15046–15047.

- (67) Baskin, J. M.; Prescher, J. A.; Laughlin, S. T.; Agard, N. J.; Chang, P. V; Miller, I. A.; Lo, A.; Codelli, J. A.; Bertozzi, C. R. *Proc. Natl. Acad. Sci. U.S.A.* **2007**, *104*, 16793–16797.
- (68) Bielawski, C. W.; Grubbs, R. H. *Prog. Polym. Sci.* **2007**, *32*, 1–29.
- (69) Walker, R.; Conrad, R. M.; Grubbs, R. H. *Macromolecules* **2009**, *42*, 599–605.
- (70) Kayahara, E.; Cheng, Y.; Yamago, S. *Chem. Lett.* **2018**, *47*, 1108–1111.
- (71) Kayahara, E.; Qu, R.; Yamago, S. *Angew. Chem. Int. Ed.* **2017**, *56*, 10428–10432.
- (72) Kayahara, E.; Hayashi, T.; Takeuchi, K.; Ozawa, F.; Ashida, K.; Ogoshi, S.; Yamago, S. *Angew. Chem. Int. Ed.* **2018**, *57*, 11418–11421.
- (73) Miki, K.; Ohe, K. *Chem. – A Eur. J.* **2019**, 10.1002/chem.20190411.
- (74) Darzi, E. R.; White, B. M.; Loventhal, L. K.; Zakharov, L. N.; Jasti, R. *J. Am. Chem. Soc.* **2017**, *139*, 3106–3114.
- (75) Bachrach, S. M. *Computational Organic Chemistry*, 2nd Editio.; John Wiley & Sons, Inc.: Hoboken, NJ, USA, 2007.
- (76) Daoust, K. J.; Hernandez, S. M.; Konrad, K. M.; Mackie, I. D.; Winstanley, J.; Johnson, R. P. *J. Org. Chem.* **2006**, *71*, 5708–5714.
- (77) Roux, M. V.; Dávalos, J. Z.; Jiménez, P.; Notario, R.; Castaño, O.; Chickos, J. S.; Hanshaw, W.; Zhao, H.; Rath, N.; Liebman, J. F.; et al. *J. Org. Chem.* **2005**, *70*, 5461–5470.
- (78) De Meijere, A.; Kozhushkov, S. I.; Rauch, K.; Schill, H.; Verevkin, S. P.; Kümmerlin, M.; Beckhaus, H. D.; Rüdhardt, C.; Yufit, D. S. *J. Am. Chem. Soc.* **2003**, *125*, 15110–15113.
- (79) Haddon, R. C.; Scott, L. T. *Pure Appl. Chem.* **1986**, *58*, 137–142.

- (80) Haddon, R. C. *Science* (80-.). **1993**, *261*, 1545–1550.
- (81) Stauch, T.; Dreuw, A. *Acc. Chem. Res.* **2017**, *50*, 1041–1048.
- (82) Stauch, T.; Günther, B.; Dreuw, A. *J. Phys. Chem. A* **2016**, *120*, 7198–7204.
- (83) Slavov, C.; Yang, C.; Heindl, A. H.; Stauch, T.; Wegner, H. A.; Dreuw, A.; Wachtveitl, J. *J. Phys. Chem. Lett.* **2018**, *9*, 4776–4781.
- (84) Colwell, C. E. StrainViz github.com/CurtisColwell/StrainViz/.
- (85) Bachrach, S. M. *J. Chem. Educ.* **1990**, *67*, 907–908.
- (86) Wheeler, S. E.; Houk, K. N.; Schleyer, P. v. R.; Allen, W. D. *J. Am. Chem. Soc.* **2009**, *131*, 2547–2560.
- (87) Rio, J.; Erbahar, D.; Rayson, M.; Briddon, P.; Ewels, C. P.; Sato, S.; Kono, H.; Fukuzumi, S.; Isobe, H.; Baonza, V. G.; et al. *Phys. Chem. Chem. Phys.* **2016**, *18*, 23257–23263.
- (88) Frisch, M. J.; Trucks, G. W.; Schlegel, H. B.; Scuseria, G. E.; Robb, M. A.; Cheeseman, J. R.; Scalmani, G.; Barone, V.; Mennucci, B.; Petersson, G. A.; et al. Gaussian, Inc.: Wallingford CT, 2013.
- (89) Li, X.; Frisch, M. J. *J. Chem. Theory Comput.* **2006**, *2*, 835–839.
- (90) Neese, F. *Wiley Interdiscip. Rev. Comput. Mol. Sci.* **2012**, *2*, 73–78.
- (91) Neese, F. *Wiley Interdiscip. Rev. Comput. Mol. Sci.* **2018**, *8*, e1327.
- (92) Avdoshenko, S. M.; Konda, S. S. M.; Makarov, D. E. *J. Chem. Phys.* **2014**, *141*, 134115.
- (93) Stauch, T.; Dreuw, A. *Chem. Sci.* **2017**, *8*, 5567–5575.
- (94) Bachrach, S. M.; Stück, D. *J. Org. Chem.* **2010**, *75*, 6595–6604.

- (95) Povie, G.; Segawa, Y.; Nishihara, T.; Miyauchi, Y.; Itami, K. *Science* (80-.). **2017**, *356*, 172–175.
- (96) Biswas, S.; Qiu, C. S.; Dawe, L. N.; Zhao, Y.; Bodwell, G. J. *Angew. Chem. Int. Ed.* **2019**, *58*, 9166–9170.
- (97) Bachrach, S. M. *J. Phys. Chem. A* **2011**, *115*, 2396–2401.
- (98) Nishigaki, S.; Shibata, Y.; Nakajima, A.; Okajima, H.; Masumoto, Y.; Osawa, T.; Muranaka, A.; Sugiyama, H.; Horikawa, A.; Uekusa, H.; et al. *J. Am. Chem. Soc.* **2019**, *141*, 14955–14960.
- (99) Saitta, A. M.; Soper, P. D.; Wasserman, E.; Klein, M. L. *Nature* **1999**, *399*, 46–48.
- (100) Stauch, T.; Dreuw, A. *Angew. Chem. Int. Ed.* **2016**, *55*, 811–814.
- (101) Vögtle, F.; Schröder, A.; Karbach, D. *Angew. Chem. Int. Ed.* **1991**, *30*, 575–577.
- (102) Herges, R. *Chem. Rev.* **2006**, *106*, 4820–4842.
- (103) Kayahara, E.; Iwamoto, T.; Takaya, H.; Suzuki, T.; Fujitsuka, M.; Majima, T.; Yasuda, N.; Matsuyama, N.; Seki, S.; Yamago, S. *Nat. Commun.* **2013**, *4*, 2694.
- (104) Liu, F.; Liang, Y.; Houk, K. N. *J. Am. Chem. Soc.* **2014**, *136*, 11483–11493.
- (105) Bickelhaupt, F. M.; Houk, K. N. *Angewandte Chemie - International Edition*. John Wiley & Sons, Ltd August 14, 2017, pp 10070–10086.
- (106) Taylor, M. T.; Blackman, M. L.; Dmitrenko, O.; Fox, J. M. *J. Am. Chem. Soc.* **2011**, *133*, 9646–9649.
- (107) Liu, J.; Wang, C.; Tu, X.; Liu, B.; Chen, L.; Zheng, M.; Zhou, C. *Nat. Commun.* **2012**, *3*, 1199.
- (108) Omachi, H.; Nakayama, T.; Takahashi, E.; Segawa, Y.; Itami, K. *Nat. Chem.* **2013**, *5*, 572–576.

- (109) Liu, B.; Liu, J.; Li, H. B.; Bhola, R.; Jackson, E. A.; Scott, L. T.; Page, A.; Irle, S.; Morokuma, K.; Zhou, C. *Nano Lett.* **2015**, *15*, 586–595.
- (110) Sanchez-Valencia, J. R.; Dienel, T.; Gröning, O.; Shorubalko, I.; Mueller, A.; Jansen, M.; Amsharov, K.; Ruffieux, P.; Fasel, R. *Nature* **2014**, *512*, 61–64.
- (111) Povie, G.; Segawa, Y.; Nishihara, T.; Miyauchi, Y.; Itami, K. *J. Am. Chem. Soc.* **2018**, *140*, 10054–10059.
- (112) Cheung, K. Y.; Gui, S.; Deng, C.; Liang, H.; Xia, Z.; Liu, Z.; Chi, L.; Miao, Q. *Chem* **2019**, *0*, 1–10.
- (113) Golling, F. E.; Osella, S.; Quernheim, M.; Wagner, M.; Beljonne, D.; Müllen, K. *Chem. Sci.* **2015**, *6*, 7072–7078.
- (114) Golling, F. E.; Osella, S.; Quernheim, M.; Wagner, M.; Beljonne, D.; Ullen, K. .
- (115) Merner, B. L.; Dawe, L. N.; Bodwell, G. J. *Angew. Chem. Int. Ed.* **2009**, *48*, 5487–5491.
- (116) Hashimoto, S.; Kayahara, E.; Mizuhata, Y.; Tokitoh, N.; Takeuchi, K.; Ozawa, F.; Yamago, S. *Org. Lett.* **2018**, *20*, 5973–5976.
- (117) Li, S.; Aljhdli, M.; Thakellapalli, H.; Farajidizaji, B.; Zhang, Y.; Akhmedov, N. G.; Milsman, C.; Popp, B. V.; Wang, K. K. *Org. Lett.* **2017**, *19*, 4078–4081.
- (118) Fürstner, A.; Mamane, V. *J. Org. Chem.* **2002**, *67*, 6264–6267.
- (119) Merlic, C. A.; Pauly, M. E. *J. Am. Chem. Soc.* **1996**, *118*, 11319–11320.
- (120) Shen, H. C.; Tang, J. M.; Chang, H. K.; Yang, C. W.; Liu, R. S. *J. Org. Chem.* **2005**, *70*, 10113–10116.
- (121) Chen, T. A.; Lee, T. J.; Lin, M. Y.; Sohel, S. M. A.; Diau, E. W. G.; Lush, S. F.; Liu, R. S. *Chem. Eur. J.* **2010**, *16*, 1826–1833.

- (122) Daigle, M.; Picard-Lafond, A.; Soligo, E.; Morin, J. F. *Angew. Chem. Int. Ed.* **2016**, *55*, 2042–2047.
- (123) Daigle, M.; Miao, D.; Lucotti, A.; Tommasini, M.; Morin, J.-F. *Angew. Chem. Int. Ed.* **2017**, *56*, 6213–6217.
- (124) Sletten, E. M.; Bertozzi, C. R. **2011**.
- (125) Spicer, C. D.; Pashuck, E. T.; Stevens, M. M. **2018**.
- (126) Sletten, E. M.; Bertozzi, C. R. *Angew. Chem. Int. Ed.* **2009**, *48*, 6974–6998.
- (127) Kolb, H. C.; Finn, M. G.; Sharpless, K. B. *Angew. Chem. Int. Ed.* **2001**, *40*, 2004–2021.
- (128) Hein, C. D.; Liu, X. M.; Wang, D. *Pharmaceutical Research*. Springer October 29, 2008, pp 2216–2230.
- (129) Pang, Y.; Li, J.; Hu, B.; Karasz, F. E. *Macromolecules* **1998**, *31*, 6730–6732.
- (130) Liu, J.; Lam, J. W. Y.; Tang, B. Z. *Chem. Rev.* **2009**, *109*, 5799–5867.
- (131) Ito, S.; Wehmeier, M.; Brand, J. D.; Kübel, C.; Epsch, R.; Rabe, J. P.; Müllen, K. *Chem. Eur. J.* **2000**, *6*, 4327–4342.
- (132) Simpson, C. D.; Brand, J. D.; Berresheim, A. J.; Przybilla, L.; Räder, H. J.; Müllen, K. *Chem. Eur. J.* **2002**, *8*, 1424–1429.
- (133) Müller, M.; Kübel, C.; Müllen, K. *Chemistry - A European Journal*. John Wiley & Sons, Ltd November 2, 1998, pp 2099–2109.
- (134) Trost, B. M.; Weiss, A. H. *Adv. Synth. Catal.* **2009**, *351*, 963–983.
- (135) Huang, Q.; Zhuang, G.; Zhang, M.; Wang, J.; Wang, S.; Wu, Y.; Yang, S.; Du, P. *J. Am. Chem. Soc.* **2019**, *141*, 18938–18943.

- (136) Pangborn, A. B.; Giardello, M. A.; Grubbs, R. H.; Rosen, R. K.; Timmers, F. J. *Organometallics* **1996**, *15*, 1518–1520.
- (137) Pelter, A.; Elgendy, S. *Tetrahedron Lett.* **1988**, *29*, 677–680.
- (138) Bruno, N. C.; Tudge, M. T.; Buchwald, S. L. *Chem. Sci.* **2013**, *4*, 916–920.
- (139) Sheldrick, G. M. Bruker AXS: Madison, WI 1998.
- (140) Sheldrick, G. M. *Acta Cryst. C* **2015**, *71*, 3–8.
- (141) Steiner, A. K.; Amsharov, K. Y. *Angew. Chem. Int. Ed.* **2017**, *56*, 14732–14736.